
Effects of Gradation and Cohesion on Bridge Scour, Vol. 5. Effect of Cohesion Bridge Abutment Scour

PUBLICATION NO. FHWA-RD-99-187

DECEMBER 1999

PB2000-103274



U.S. Department of Transportation
Federal Highway Administration

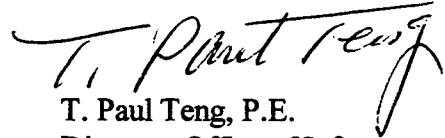
Research, Development, and Technology
Turner-Fairbank Highway Research Center
6300 Georgetown Pike
McLean, VA 22101-2296

REPRODUCED BY: **NTIS**
U.S. Department of Commerce
National Technical Information Service
Springfield, Virginia 22161



FOREWORD

This report is volume 5 of a six volume series describing detailed laboratory experiments conducted at Colorado State University for the Federal Highway Administration as part of a study entitled "Effects of Sediment Gradation and Cohesion on Bridge Scour". Volume 5 describes the effects of cohesion on local abutment scour. This six volume series will be distributed to NTIS only and will not be printed by FHWA. A separate summary report which describes the key results from the six volume series will be published by FHWA and distributed to the FHWA Division Offices.



T. Paul Teng, P.E.
Director, Office of Infrastructure
Research and Development

NOTICE

This document is disseminated under the sponsorship of the Department of Transportation in the interest of information exchange. The United States Government assumes no liability for the contents or use thereof. This report does not constitute a standard, specification, or regulation.

The United States Government does not endorse products or manufacturers. Trade and manufacturers names appear in this report only because they are considered essential to the object of the document.

PROTECTED UNDER INTERNATIONAL COPYRIGHT
ALL RIGHTS RESERVED
NATIONAL TECHNICAL INFORMATION SERVICE
U.S. DEPARTMENT OF COMMERCE

Reproduced from
best available copy.



1. Report No. FHWA-RD-99-187		2. C PB2000-103274 		3. Recipient's Catalog No.	
4. Title and Subtitle EFFECTS OF GRADATION AND COHESION ON BRIDGE SCOUR Vol. 5. Effect of Cohesion on Bridge Abutment Scour				5. Report Date December 1999	
				6. Performing Organization Code	
7. Author(s) Albert Molinas and Nagy Y. Reiad				8. Performing Organization Report No.	
9. Performance Organization Name and Address Colorado State University Engineering Research Center Fort Collins, Colorado				10. Work Unit No. (TRAIS) NCP# 3D3C1-582	
				11. Contract or Grant No. DTFH61-91-C-00004	
12. Sponsoring Agency and Address Office of Engineering Research and Development Federal Highway Administration 6300 Georgetown Pike MxclLean, Va 22101				13. Type of Report and Period Covered Laboratory Final Report Jan 1991 - Jan 1996	
				14. Sponsoring Agency Code	
15. Supplementary Notes Contracting Officer's Technical Representative: J. Sterling Jones HNR-10					
16. Abstract <p>The effects of cohesion on abutment scour was investigated experimentally using four-foot- and eight-foot-wide test flumes at the Engineering Research Center, Colorado State University. In the first part of experiments, clayey-sand mixtures with varying amounts of clay were subjected to different approach flow conditions. The abutment scour resulting from these experiments were normalized with pure sand scour experiments. For Montmorillonitic clay mixtures, experimental results show that for sandy clays, increasing the clay content up to 30 percent may reduce scour by up to 40 percent. For Kaolinitic clay mixtures the results are more dramatic, scour reduction is up to 80 percent of that observed in pure sands.</p> <p>Beyond a certain percentage of clay content (30-40 percent for the present mixture) parameters such as compaction, initial water content, degree of saturation, shear strength, etc. dominate the abutment scour. In the second part of experiments, these effects were investigated for flow conditions with Froude numbers ranging form 0.2 to 0.6. Regression equations relating flow and selected cohesive soil parameters to abutment scour were developed for the particular abutment and flow conditions that were used in the experiments. These experiments showed that abutment scour in cohesion material can be expressed in terms of cohesive soil parameters which can be determined in the field.</p> <p>The equations derived from this study do not attempt to relate effects due to abutment geometry, flow depth, gradation of sand in clay-sand mixtures, etc. and therefore are not intended for general application. These relationships are derived to explain the variability of abutment scour with cohesion properties.</p> <p>This publication is the fifth volume of a six volume series. The other volumes are as follows: Vol. 1. Effect of Sediment Gradation and Coarse Material Fraction on Clear Water Scour Around Bridge Piers Vol. 2. Experimental Study of Sediment Gradation and Flow Hydrograph Effects on Clear Water Scour Around Circular Piers Vol. 3. Abutment Scour for Nonuniform Mixtures Vol. 4. Experimental Study of Scour Around Circular Piers in Cohesive Soils Vol. 6. Abutment Scour in Uniform and Stratified Sand Mixtures</p>					
17. Key Words Bridge Scour, Pier Scour, Abutment Scour, Gradation, Coarse Sediment, Cohesion, Clay Scour			18. Distribution Statement No restrictions. This document is available to the public through the National Technical Information Service, Springfield, Va. 22161		
19. Security Classif. (of this report) Unclassified		20. Security Classif. (of this page) Unclassified		21. No. of Pages 250	22. Price

SI* (MODERN METRIC) CONVERSION FACTORS

APPROXIMATE CONVERSIONS TO SI UNITS

Symbol	When You Know	Multiply By	To Find	Symbol	When You Know	Multiply By	To Find	Symbol
LENGTH								
in	inches	25.4	millimeters	mm	millimeters	0.039	inches	in
ft	feet	0.305	meters	m	meters	3.28	feet	ft
yd	yards	0.914	kilometers	m	meters	1.09	yards	yd
mi	miles	1.61		km	kilometers	0.621	miles	mi
AREA								
in ²	square inches	645.2	square millimeters	mm ²	square millimeters	0.0016	square inches	in ²
ft ²	square feet	0.093	square meters	m ²	square meters	10.764	square feet	ft ²
yd ²	square yards	0.836	square meters	m ²	square meters	1.195	square yards	yd ²
ac	acres	0.405	hectares	ha	hectares	2.47	acres	ac
mi ²	square miles	2.59	square kilometers	km ²	square kilometers	0.386	square miles	mi ²
VOLUME								
fl oz	fluid ounces	29.57	milliliters	mL	milliliters	0.034	fluid ounces	fl oz
gal	gallons	3.785	liters	L	liters	0.264	gallons	gal
ft ³	cubic feet	0.028	cubic meters	m ³	cubic meters	35.71	cubic feet	ft ³
yd ³	cubic yards	0.765	cubic meters	m ³	cubic meters	1.307	cubic yards	yd ³
NOTE: Volumes greater than 1000 l shall be shown in m ³ .								
MASS								
oz	ounces	28.35	grams	g	grams	0.035	ounces	oz
lb	pounds	0.454	kilograms	kg	kilograms	2.202	pounds	lb
T	short tons (2000 lb)	0.907	megagrams (or "metric ton")	Mg (or "t")	megagrams (or "metric ton")	1.103	short tons (2000 lb)	T
TEMPERATURE (exact)								
°F	Fahrenheit temperature	5(F-32)/9 or (F-32)/1.8	Celsius temperature	°C	Celsius temperature	1.8C + 32	Fahrenheit temperature	°F
ILLUMINATION								
fc	foot-candles	10.76	lux	lx	lux	0.0929	foot-candles	fc
fl	foot-Lamberts	3.426	candela/m ²	cd/m ²	candela/m ²	0.2919	foot-Lamberts	fl
FORCE and PRESSURE or STRESS								
lbf	poundforce	4.45	newtons	N	newtons	0.225	poundforce	lbf
lb/in ²	poundforce per square inch	6.89	kilopascals	kPa	kilopascals	0.145	poundforce per square inch	lb/in ²

(Revised September 1983)

* SI is the symbol for the International System of Units. Appropriate rounding should be made to comply with Section 4 of ASTM E380.

EFFECTS OF GRADATION AND COHESION ON BRIDGE SCOUR

VOLUME V

TABLE OF CONTENTS

CHAPTER 1 INTRODUCTION	1
CHAPTER 2 LITERATURE REVIEW	8
2.1 Introduction	8
2.2 Local Scour at Bridge Abutments	8
2.3 Mechanics of Clear Water Scour at Bridge Abutments	9
2.4 Abutment Scour Equations for Non-Cohesive Materials	17
2.5 Clay Erosion Studies	21
2.5.1 Alaeddin Shaikh, 1986	22
2.5.2 Steven Abt, 1980 "Scour at Culvert Outlets"	28
2.5.3 Kandiah Arulanandan, 1980	30
CHAPTER 3 COHESIVE MATERIAL PROPERTIES	33
3.1 The Structure of Compacted Clay	33
3.1.1 Aggregation and Dispersion of Soil Particles	34
3.1.2 Arrangement of Soil Particles	38
3.1.3 Nature of Water in Clay	39
3.1.4 Theory of Compaction	40
3.1.5 Changes in Soil Structures	43

3.2	Engineering Properties of Compacted Clay	45
3.2.1	Permeability of Compacted Clay	46
3.2.2	Compression of Compacted Clay	48
3.2.3	Shear Strength of Compacted Clay	49
3.2.4	Effect of Compaction Conditions on Strength	52
3.2.4.1	Molded Strength	52
3.2.4.2	Strength of Saturated Samples	52
3.2.5	Atterberg Limits	55
CHAPTER 4 EXPERIMENTAL EQUIPMENT AND PROCEDURES		57
4.1	Introduction	57
4.2	Equipment	57
4.2.1	Test Flumes	57
4.2.2	Abutments	59
4.2.3	Currentmeter	59
4.2.4	Torvane Gauge	61
4.2.5	Point Gauge	61
4.3	Materials	61
4.3.1	Bed Material Proposed	61
4.3.2	Compaction Tests	62
4.3.3	Atterberg limits, Chemical, and X-Ray Diffraction Tests	62
4.3.4	Grain Size Analysis-Mechanical and Hydrometer Methods	73

4.4	Procedures	76
4.4.1	Preparation of the Soil	76
4.4.2	Running the Experiments	78
4.4.3	Individual Measurements	80
	Flow Discharge	81
	Flow depth	81
	Velocity	82
	Slope	82
	Flow Temperature	84
	Time Rate of Scour	84
	Initial and Final Bed Topographies around Abutments	84
	Volume of Scour Hole	85
	Water Content in Clay	85
CHAPTER 5 ANALYSIS OF RESULTS		86
5.1	Introduction	86
5.2	Dimensional Analysis	87
5.3	Geometry of Scour Hole	101
5.4	Montmorillonite Clay Experiments	102
5.4.1	Effect of Initial Water Content on the Clay Mixture	102
	5.4.1.1 Variation of Scour Depth with Approach Flow	
	Conditions	105
	5.4.1.2 Cross-Sectional Profile of the Scour Holes	108

5.4.1.3	Longitudinal Slope of the Scour Holes	116
5.4.1.4	Effect of Initial Water Content on Time Rate of Scour	122
5.4.2	Effect of Clay Compaction on the Clay Mixture	130
5.4.2.1	Variation of Scour Depth with Approach Flow Conditions	130
5.4.2.2	Cross-Sectional Profile of the Scour Holes	134
5.4.2.3	Longitudinal Slope of the Scour Holes	139
5.4.2.4	Effect of Clay Compaction on Time Rate of Scour	142
5.4.3	Effect of Clay Content on Clay Mixture	142
5.4.3.1	Variation of Scour Depth with Approach Flow Conditions	145
5.4.3.2	Cross-Sectional Profile of the Scour Holes	148
5.4.3.3	Longitudinal Slope of the Scour Holes	148
5.4.3.4	Effect of Clay Content on Time Rate of Scour	159
5.4.4	Comparison between Compaction and Torvane Shear Strength . .	163
5.5	Kaolinite Clay Experiments	165
5.5.1	Effect of Initial Water Content on the Clay Mixture	165
5.5.1.1	Variation of Scour Depth with Approach Flow Conditions	166
5.5.1.2	Cross-Sectional Profile of the Scour Holes	170

5.5.1.3	Longitudinal Slope of the Scour Holes	174
5.5.1.4	Effect of Water Content on Time Rate of Scour	174
5.5.2	Effect of Clay Content on Clay Mixture	182
5.5.2.1	Variation of Scour Depth with Approach Flow Conditions	182
5.5.2.2	Cross-Sectional Profile of the Scour Holes	184
5.5.2.3	Longitudinal Slope of the Scour Holes	193
5.5.2.4	Effect of Clay Content on Time Rate of Scour	193
5.5.3	Comparison between Compaction and Torvane shear stress	200
5.6	Abutment Scour Prediction Equations for Cohesive Materials	202
5.6.1	Montmorillonite Clay Equations	203
5.6.2	Kaolinite Clay Equations	210
CHAPTER 6	SUMMARY, CONCLUSIONS, AND RECOMMENDATIONS	218
6.1	Summary	218
6.2	Conclusion	219
6.3	Recommendations for Future Research	223
REFERENCES	225

EFFECTS OF GRADATION AND COHESION ON BRIDGE SCOUR

VOLUME V

LIST OF FIGURES

Figure

2.1	Abutment Flow Structure (After Kwan, 1988)	10
2.2	Downflow with Associated Primary Vortex (After Kwan, 1988)	12
2.3	Primary Vortex in Relation to Scour Hole (After Kwan, 1988)	12
2.4	Conceptualized Model of Secondary Vortex Formation (After Kwan, 1988)	15
2.5	Flow Separation and Wake Vortices (After Kwan, 1988)	15
2.6	Shear Stress Amplification at Abutment (After Rajaratnam and Nwachukwu, 1983)	16
2.7	Coefficient of Erosion Rate versus Clay Content (After Shaikh, 1986) .	25
2.8	Coefficient of Erosion Rate as a Function of SAR (After Shaikh, 1986)	26
2.9	Coefficient of Erosion Rate versus Torvane Shear Strength (After Shaikh, 1986)	27
2.10	Critical Shear Stress versus SAR for Different Salt Concentrations (After Heinzen, 1977)	32
3.1	Sediment Structure	37
3.2	Effects of Compaction on Sediment Structure	41
3.3	Compaction-Permeability Test	47
3.4	Effect of One-Dimensional Compression	50

Figure

3.5	Cone Index and Dry Density versus Water Content	53
3.6	Shear Strength versus Water Content at Failure	54
4.1	Measured and Calculated Velocities from Orifice Equation for 8-foot Wide Flume (Abdou, 1993)	60
4.2	Moisture Content -Specific Weight Relationship from Compaction Test for 100 % Montmorillonite Clay	63
4.3	Moisture Content -Specific Weight Relationship from Compaction Test for 15 % Montmorillonite Clay	64
4.4	Moisture Content -Specific Weight Relationship from Compaction Test for 30 % Montmorillonite Clay	65
4.5	Moisture Content -Specific Weight Relationship from Compaction Test for 40 % Montmorillonite Clay	66
4.6	Moisture Content -Specific Weight Relationship from Compaction Test for 10 % Kaolinite Clay	67
4.7	Moisture Content -Specific Weight Relationship from Compaction Test for 20 % Kaolinite Clay	68
4.8	Moisture Content -Specific Weight Relationship from Compaction Test for 30 % Kaolinite Clay	69
4.9	Moisture Content -Specific Weight Relationship from Compaction Test for 50 % Kaolinite Clay	70
4.10	Grain Size Distribution for Montmorillonite Clay	74

Figure

4.11 Grain Size Distribution for Medium Sand ($D_{50}=0.81$ mm, $\sigma_g=2.41$) . . .	75
4.12 Locations of Measured Approach Velocity for the 0.36 feet Wide Abutment in the 8 feet Flume	83
5.1 Cross-Section along the Abutment Scour Hole in the Upstream Direction for Run No.30-A	103
5.2a Three Dimensional View of Abutment Scour Hole Geometry for Run No. 30-A	104
5.2b Photograph of Abutment Scour Hole Geometry for Run No. 30-A	104
5.3 Variation of Dimensionless Abutment Scour Depth with Froude Number for Montmorillonite Clay	106
5.4 Variation of Dimensionless Abutment Scour Depth with Froude Number for the Medium Sand Bed ($D_{50}= 0.81$ mm)	107
5.5 Effect of Initial Water Content on Dimensionless Abutment Scour Depth for Montmorillonite Clay	109
5.6 Variation of Normalized Scour Depth with Initial Water Content for Montmorillonite Clay	110
5.7 The Locations of Cross-Sectional and Longitudinal Profiles of the Abutment Scour Hole	111
5.8 Effect of Initial Water Content on the Scour Hole Geometry at the Upstream Abutment Face	112

Figure

5.9 Effect of Initial Water Content on the Scour Hole Geometry at the
Upstream Abutment Face 113

5.10 Effect of Initial Water Content on the Scour Hole Geometry at the
Upstream Abutment Face 114

5.11 Effect of Initial Water Content on the Scour Hole Geometry at the
Upstream Abutment Face 115

5.12 View of the Abutment Scour Hole Geometry for Initial Water Contents
of 11 %, 20 %, 35 %, and 46 % 117

5.13 Longitudinal Profile of the Scour Hole for 12 % Initial Water Content . . 119

5.14 Longitudinal Profile of the Scour Hole for 20 % Initial Water Content . . 119

5.15 Longitudinal Profile of the Scour Hole for 28 % Initial Water Content . . 120

5.16 Longitudinal Profile of the Scour Hole for 35 % Initial Water Content . . 120

5.17 Longitudinal Profile of the Scour Hole for 45 % Initial Water Content . . 121

5.18 Variation of Longitudinal Slope Angles with Different Initial Water Content 123

5.19 Time Rate of Scour for Initial Water Content of 11 % and 20 %
(Runs 4-50 and 4-42) 125

5.20 Time Rate of Scour for Initial Water Content of 17 % and 38 %
(Runs 8-35-A and 8-29-B) 126

5.21 Time Rate of Scour for Initial Water Content of 37 % and 45 %
(Runs 8-38-A and 8-37-B) 127

Figure

5.22 Time Rate of Normalized Scour for Different Flow Conditions (Runs 8-27-B and 8-35-B)	129
5.23 Variation of Dimensionless Abutment Scour Depth with Froude Number for Montmorillonite Clay	131
5.24 Effect of Compaction on Dimensionless Abutment Scour Depth for Montmorillonite Clay with 12 % IWC	132
5.25 Effect of Compaction on Dimensionless Abutment Scour Depth for Montmorillonite Clay with 20 % IWC	133
5.26 Variation of Normalized Scour Depth with Compaction for Montmorillonite Clay with 12 %, and 20 % IWC	135
5.27 Effect of Compaction on the Scour Hole Geometry at the Upstream Abutment Face (IWC=12 %)	126
5.28 Effect of Compaction on the Scour Hole Geometry at the Upstream Abutment Face (IWC=20 %)	137
5.29 View of the Abutment Scour Hole Geometry for Compaction Ratios of 79 %, and 66 %	138
5.30 Longitudinal Profile of the Scour Hole for Low Compaction (IWC=20 %)	140
5.31 Variation of Longitudinal Slope Angles with Compactions of 63 %, and 77 %	141
5.32 Time Rate of Scour for Compaction Ratios of 73 % and 64 % with 13 % IWC (Runs 8-27-B and 8-31-B)	143

Figure

5.33 Time Rate of Scour for Compaction Ratios of 75 % and 58 % with 20 % IWC (Runs 8-30-B and 8-31-A)	144
5.34 Effect of Clay Content on Dimensionless Abutment Scour Depth for Montmorillonite Clay	146
5.35 Variation of Normalized Scour Depth with Clay Content for Montmorillonite Clay	147
5.36 Effect of Clay Content on the Scour Hole Geometry at the Upstream Abutment Face ($Fr=0.19$)	149
5.37 Effect of Clay Content on the Scour Hole Geometry at the Upstream Abutment Face ($Fr=0.24$)	150
5.38 Effect of Clay Content on the Scour Hole Geometry at the Upstream Abutment Face ($Fr=0.35$)	151
5.39 Effect of Clay Content on the Scour Hole Geometry at the Upstream Abutment Face ($Fr=0.46$)	152
5.40 Longitudinal Profile of the Scour Hole for Medium Sand ($D_{50}=0.81$ mm)	154
5.41 Longitudinal Profile of the Scour Hole for 15 % Clay Content	155
5.42 Longitudinal Profile of the Scour Hole for 30 % Clay Content	156
5.43 Longitudinal Profile of the Scour Hole for 40 % Clay Content	157
5.44 Variation of Longitudinal Slope Angles with Different Clay Contents . .	158
5.45 Variation of Time Rate of Scour with Clay Content ($Fr=0.24$, Runs 8-82-A ,B ,C , and D)	160

Figure

5.46 Variation of Time Rate of Scour with Clay Content ($Fr=0.19$, Runs 8-83-A ,B ,C , and D)	161
5.47 Variation of Time Rate of Scour with Clay Content ($Fr=0.35$, Runs 8-81-A ,B ,C , and D)	162
5.48 Relationship between Compaction and Torvane Shear Strength for Montmorillonite Clay	164
5.49 Variation of Dimensionless Abutment Scour Depth with Froude Number for Kaolinite Clay	167
5.50 Variation of Dimensionless Abutment Scour Depth with Initial Water Content for Different Froude Numbers	168
5.51 Variation of Normalized Scour Depth with Initial Water Content for Kaolinite Clay	169
5.52 Effect of Initial Water Content on the Scour Hole Geometry at the Upstream Abutment Face ($Fr=0.604$)	171
5.53 Effect of Initial Water Content on the Scour Hole Geometry at the Upstream Abutment Face ($Fr=0.36$)	172
5.54 Effect of Initial Water Content on the Scour Hole Geometry at the Upstream Abutment Face ($Fr=0.56$)	173
5.55 Longitudinal Profile of the Scour Hole for 15 % Initial Water Content . .	175
5.56 Longitudinal Profile of the Scour Hole for 20 % Initial Water Content . .	176
5.57 Longitudinal Profile of the Scour Hole for 25 % Initial Water Content . .	177

Figure

5.58 Longitudinal Profile of the Scour Hole for 30 % Initial Water Content . . 178

5.59 Variation of Longitudinal Slope Angles with Different Initial Water Content 179

5.60 Time Rate of Scour for Initial Water Content of 15 %, 22, and 25 %
(Runs 8-72-A and 8-76-A, B) 180

5.61 Time Rate of Scour for Initial Water Content of 18 % and 23 %
(Runs 8-74-A, B) 181

5.62 Time Rate of Normalized Scour for Different Flow Conditions
(Runs 8-71-A and 8-72-A) 183

5.63 Effect of Clay Content on Dimensionless Abutment Scour Depth
for Kaolinite Clay 185

5.64 Variation of Normalized Scour Depth with Clay Content for Kaolinite Clay 186

5.65 Effect of Clay Content on the Scour Hole Geometry at the Upstream
Abutment Face ($Fr=0.40$) 188

5.66 Effect of Clay Content on the Scour Hole Geometry at the Upstream
Abutment Face ($Fr=0.53$) 189

5.67 Effect of Clay Content on the Scour Hole Geometry at the Upstream
Abutment Face ($Fr=0.18$) 190

5.68 View of the Abutment Scour Hole Geometry for Clay Contents of 10 %, 20 %, 30 %, and 50 % 191

5.69 Longitudinal Profile of the Scour Hole for 10 % Clay Content 194

5.70 Longitudinal Profile of the Scour Hole for 20 % Clay Content 195

Figure

5.71 Longitudinal Profile of the Scour Hole for 50 % Clay Content	196
5.72 Variation of Longitudinal Slope Angles with Different Clay Contents . .	197
5.73 Variation of Time Rate of Scour with Clay Content (Fr=0.40, Runs 8-81-A , 8-78-A, 8-79-B, and 8-80-C)	198
5.74 Variation of Time Rate of Scour with Clay Content (Fr=0.53, Runs 8-84-A , 8-79-A, 8-80-B, and 8-72-A)	199
5.75 Relationship between Compaction and Torvane Shear for Kaolinite Clay	201
5.76 Comparison between Measured and Predicted Normalized Scour Depth using Equations 5.8 and 5.9 for Montmorillonite Clays	207
5.77 Comparison of Prediction Equations for Normalized Scour Depth for Montmorillonite Clay with Actual Data	208
5.78 Effect of Compaction on Maximum Scour Depth for Kaolinite Clay . .	211
5.79 Effect of Initial Water Content on Normalized Scour Depth for Kaolinite Clay	212
5.80 Variation of Normalized Scour Depth with Froude Number for Kaolinite Clay	214
5.81 Effect of Clay Type on Normalized Scour Depth for Different Clay Contents	217

EFFECTS OF GRADATION AND COHESION ON BRIDGE SCOUR

VOLUME V

LIST OF TABLES

Table

5.1	Set No.1 Experiments Utilizing Montmorillonite Clay in the 8-foot Flume with 0.72 feet Abutment Width (39 Runs)	88
5.2	Set No.2 Experiments Utilizing Montmorillonite Clay in the 4 and 8 feet Flumes with 0.36 feet Abutment Width (49 Runs)	90
5.3	Set No.3 Experiments Utilizing Kaolinite Clay in the 8-foot Flume with 0.36 feet Abutment Width (33 Runs)	92
5.4	Set No.1 Experiments for Normalized Scour Depth (39 Runs)	94
5.5	Set No.2 Experiments for Normalized Scour Depth (49 Runs)	95
5.6	Set No.3 Experiments for Normalized Scour Depth (39 Runs)	96
5.7	Effect of Initial Water Content on Scour Geometry for Montmorillonite Clay	116
5.8	Effect of Initial Water Content on Time Rate of Scour for Montmorillonite Clay	128
5.9	Effect of Compaction on the Scour Geometry for Montmorillonite Clay	139
5.10	Effect of Compaction on Time Rate of Scour for Montmorillonite Clay .	142
5.11	Effect of Clay Content on Scour Geometry for Montmorillonite Clay . .	153
5.12	Effect of Clay Content on Time Rate of Scour for Montmorillonite Clay	163

5.13 Effect of Initial Water Content on Scour Geometry for Kaolinite Clay . .	170
5.14 Effect of Initial Water Content on Time Rate of Scour for Kaolinite Clay	182
5.15 Effect of Clay Content on Scour Geometry for Kaolinite Clay	187
5.16 Effect of Clay Content on Time Rate of Scour for Kaolinite Clay	200
5.17 Interpolated Values of Normalized Depth of Scour for Different Percentages of Montmorillonite Clay Content	209
5.18 Interpolated Values of Normalized Depth of Scour for Different Percentages of Kaolinite Clay Content	215

LIST OF SYMBOLS

d_c	Depth of maximum clay scour (ft)
d_s	Depth of maximum sand scour (ft)
y	Flow depth (ft)
a	Width of abutment (ft)
L	Length of abutment (ft)
U	Mean approach velocity (ft/s)
WC	Initial water content of clay (%)
CC	Sample clay content (%)
C	Sample compaction related to the optimum compaction (%)
T	Torvane shear stress (lb/ft ²)
t	Total time of running the experiment
g	Gravity acceleration (ft/s ²)
α	Angle of attack
ϕ	Shape factor
ρ	Water density (lb/ft ³)
ν	Kinematic viscosity (ft ² /s)

CHAPTER 1

INTRODUCTION

Scour is the enlargement of a flow section by the removal of material composing the boundary through the action of the fluid. The flow in a channel exerts shear forces on particles composing the boundary and forces them to move. The capacity of flow determines the depth and shape of the resulting scour. Even if the flow is constant, the change in the shape of scour alters the boundary conditions which in return results in unsteady conditions (time dependent). The enlargement of the scour hole reduces the velocity along the scour boundary and decreases the rate of scour.

There are three types of phenomena due to changes in bed levels at abutment locations: local scour, general scour, and degradation or aggradation. Local scour is caused by local disturbances in the flow such as vortices and eddies. Local scour occurs around piers, abutments, and other structures (man-made or natural) obstructing the flow. General scour is scour due to increased velocities across the channel because of reduced flow area. This type of scour is encountered at channel constrictions (narrower channels). Degradation or Aggradation is caused by the changes in control structures (such as dams) which cause changes in the sediment contents and river geomorphology. Different scour phenomena can occur simultaneously, such as local scour with degradation or local scour with general scour.

Within the frame of our knowledge of physical phenomena the general characteristics of scour can be formulated only for a narrow range of conditions. But for a closer look with more detail of scour features, the need rises for experimentation. The sediment properties are very important quantifying the scour process. These properties are even more pronounced in the case of cohesive sediments where the erosion resistance of cohesive materials plays a highly significant effect on the rate of scour. Non cohesive materials have been studied extensively in the previous local abutment scour experiments. Even with limited variability of non-cohesive material properties (size, shape and gradation), the reliability of local abutment scour using various prediction equations vary significantly. Bridge abutments are placed in cohesive materials at a number of sites. Unfortunately, there are no systematic experimental studies devoted to predict the maximum depth of scour and the geometry of bridge abutment scour in cohesive soils. Early investigations results devoted to the study of erosion in cohesive soils in general identified some of the clay characteristics that could affect local abutment scour. These characteristics along with other parameters is used in this study to investigate the maximum depth of scour and geometry of bridge abutment in cohesive soils. For abutments placed in cohesive soils, the current engineering practice is to use the non-cohesive prediction equation to estimate the local abutment scour. These equations, even though results in conservative design criteria, in some instances are not realistic and may result in non-economical design. This factor is more important especially, in estimating the scour susceptibility of existing structures for a limited life expectancy.

In this study, one hundred-twenty six abutment scour experiments were conducted

in the hydraulics laboratory. The abutment used is a vertical wall with rectangular cross-section with two to one length to width ratio and no change of the outside shape. Two abutment sizes are used, one with 0.36 feet width and the second with 0.72 feet width. The types of clay that were used are natural Montmorillonite clay from local farm site and pure 100 % Kaolinite from Kaolin company. In the experiments, for Montmorillonite clay, initial water content, clay content and compaction are varied. In Kaolinite clay, initial water content and clay content are varied. For Montmorillonite clay, initial Water Content values are 12 %, 20 %, 28 %, 35 %, and 45 %. Clay content values are concrete sand with 0 % clay, 15 %, 30 %, and 40 % clay content. The compaction ranges are low compaction and high compaction. For Kaolinite clay, the Initial Water Contents are 15 %, 20 %, 25 %, and 30 %, and the clay contents are 10 %, 20 %, 30 %, and 50 %. The experiments are conducted in two flumes, the 8 feet width flume with 200 feet length and 4 feet depth and the other one is the 4 feet width flume with 35 ft length and 2 feet depth. In the experiments, a wide range of discharges are used depending on the erodability criteria of each mixture. Many geotechnical and chemical tests were conducted on the clays to determine its properties and investigate some of its behaviors. Some of these test are Torvane gauge for shear measurements for each experiment, Atterberg limits (liquid limit and plastic limit), the standard compaction test for each clay mixture. Also, X-ray diffraction test to define the clay mineralogy, chemical tests (to determine sodium adsorption ratio, sodium, calcium, magnesium, soil pH), and grain size analysis (mechanical and hydrometer methods). The discharge is measured using a calibrated orifice meter. The velocity is measured at two cross-sections

upstream of the abutment at four locations of each cross-section and each location have 10 vertical measurements. The average approach velocity of the abutment is calculated from these measurements. The depth of scour is measured with time during the run by reading a meter installed on the inside side of the abutment plexiglass. At each experiment, the initial and final water contents along with the mixture compaction are measured. Also, the temperature is measured in each experiment. The volume of each scour hole is measured to know the amount of clay that is eroded.

The objective of this study is construct a physical model of the vertical wall abutment in the hydraulics laboratory flume and place two types of clay (Montmorillonite and Kaolinite) around the abutment site with different Initial Water Content, clay content and compaction. Then run the flume with different mean flow velocities and fix the rest of the hydraulic variables. From these runs, a set of experimental data will be collected and analyzed to relate maximum depth of scour to clay properties such as initial water content, clay content, and compaction and use the dimensional analysis along with SAS program to formulate prediction equations for maximum depth of scour. The cross-sectional profiles of the scour hole are compared to show the effect of clay properties on the shape and width of the scour holes. The longitudinal slopes of the scour holes, upstream and down-stream are calculated for each clay mixture and then compared to show the effect of increasing initial water content, clay content, and compaction on the longitudinal slope angles of the scour holes. Time rate of scour is compared for different clay properties by using an exponential equation form with a constant K to fit the data. As the K value increases, the time needed to reach maximum depth of scour decreases.

This criteria is used to compare the time needed to reach maximum depth of scour for different clay properties. Also, the effect of Froude number on the time needed to reach maximum depth of scour is investigated to see if the rate of scouring increase with the increase of Froude number. The Torvane shear is measured for each experiment and compared for different clay properties to find out if it is a reliable tool to predict maximum depth of scour. Notice, these experiments were performed under laboratory conditions and for short term runs only and the resulting curves and conclusions are based on that which are different than the field where results are influenced by climatic changes.

After this introduction section, chapter 2 is about literature review. The first part is devoted to local scour at bridge abutments and the mechanics of clear water scour at bridge abutments. This part is followed by a presentation of some of the abutment scour equations for non-cohesive materials. The following part in chapter 2 is devoted to the clay erosion studies where Alaeddin Shaikh in 1986 investigated the erosion characteristics of clay. The second study is done by Steven Abt in 1980 to study the scour at culvert for cohesive bed materials. The third study is a report by Kandiah Arulanandan in 1980 to describe the results of erosion and soil characterization tests performed on samples of cohesive soils.

Chapter 3 is handling the cohesive soil properties in two sections, the first section describes the structure of compacted clay where it presents aggregation and dispersion of soil particles, arrangement of soil particles, and the nature of water in clay. Also, the section includes the theory of compaction and the changes in soil structures. The second

section discuss the engineering properties of compacted clay such as permeability, compression, and shear strength of compacted clay.

Chapter 4 is explaining the experimental equipment and procedures that are performed on the clay. The explanation of the equipment include the flume, the abutment, the currentmeter, the Torvane gauge, and the point gauge. The second part give details of the materials used and the types of tests that are performed on the soil such as compaction test, Atterberg limits, chemical tests, X-ray diffraction test, and grain size analysis. The third part handles the procedures of the experiments such as how to run the flume, the preparation of the soil samples, and an explanation of how to take the individual measurements (velocity, flow depth, initial water content).

Chapter 5 is devoted to the analysis of the results beginning with the dimensional analysis then the geometry of the scour hole. After that, an analysis of each clay type in a separate section, the first section is the Montmorillonite clay experiments, and the second section is the Kaolinite clay. The first section have three subsections, effect of initial water content, effect of compaction, and effect of clay content. The second Kaolinite section is divided into two subsections, effect of initial water content, and effect of clay content. Each subsection includes scour depth as a function of Froude number, cross-sectional profile and longitudinal slope of the scour holes, and time rate of scour. Each section is ended by a comparison between compaction and Torvane shear strength for that type of soil. The final section is devoted for the development of prediction equations of maximum scour depth for both Montmorillonite and Kaolinite clays.

Chapter 6 present the summary of the investigation, the conclusion, and the recommendations for future studies.

CHAPTER 2

LITERATURE REVIEW

2.1 Introduction

This chapter presents a review of the literature on the mechanics of clear water scour at bridge abutments including some of the most commonly accepted equations for predicting abutment scour in alluvial channels. Since there are no previous studies for abutment scour in cohesive materials, following the non-cohesive abutment scour literature review, previous studies for clay erosion is presented. The aim of clay erosion literature review is focused on erosive properties of clays and on parameters effecting cohesive material scour in general.

2.2 Local Scour at Bridge Abutments

Local scour around abutments is defined as scour due to the change in local flow conditions by the presence of abutments. This change in the local flow patterns causes the removal of bed material from around the abutments. In the literature, there are two basic categories of abutment local scour in alluvial (non-cohesive) environments:

a. Clear Water Scour

Clear water abutment scour is the local scour in the absence of sediment transport

into the scour hole formed by the presence of an abutment. The sediment is removed only from the scour hole where the bed shear stress around the abutment is greater than the critical shear stress. As the size of the scour hole increases, the local flow around the abutments is modified and the rate of scouring is reduced until the equilibrium condition is reached where the maximum scour is accomplished (Kwan, 1984), Tey (1984), Wong (1982).

b. Live-Bed Scour

Live-bed abutment scour occurs in the case where general sediment transport into the abutment site is present and in cases where upstream sediment is continuously transported into the scour hole to replace some or all the removed material from the scour hole. In live bed scour, the bed shear stress is everywhere greater than the critical shear stress and its magnitude depends on the flow conditions. Bed forms such as ripples, dunes, antidunes, etc. may develop (Simons and Senturk, 1976) depending on alluvial river environment. Initially, the local scour develops rapidly and then oscillates as the bed form pass through the scour hole.

2.3 Mechanics of Scour at Bridge Abutment

The flow structure that cause abutment local scour is complex in detail and could be separated into (Kwan, 1988):

- a. Downflow
- b. Primary vortex

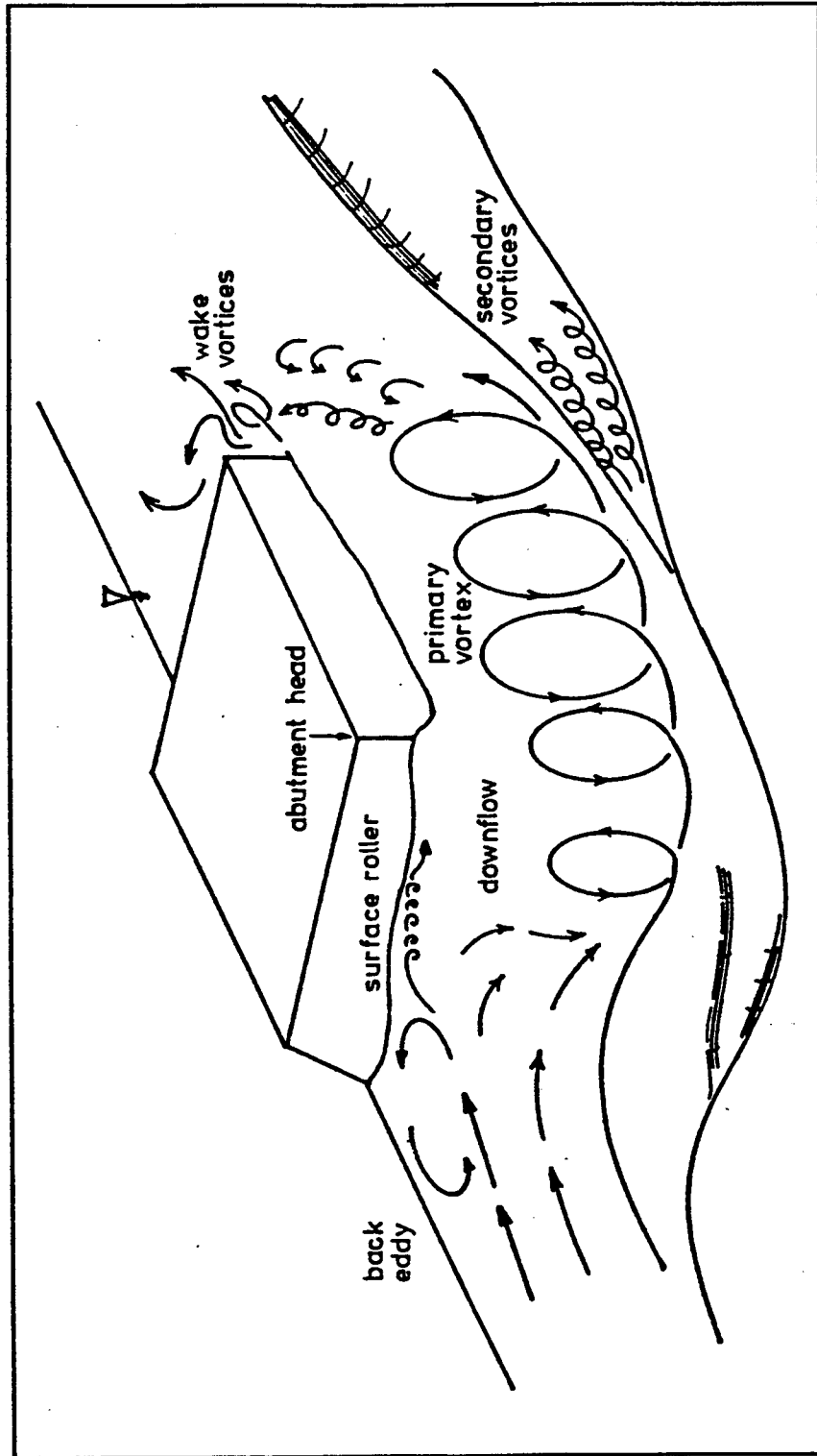


Figure (2.1) Abutment Flow Structure (After Kwan, 1988)

- c. Secondary vortex
- d. Wake vortices

This complex flow structure is conceptually shown in Figure 2.1.

a. Downflow

At abutment, approach flow faces a stagnation region which develops a vertical stagnation pressure gradient. This pressure gradient is developed because the approach velocity increases downward from the surface. Consequently the stagnation pressure decreases downward and a net downward force is created to drive the flow downward as shown in Figure 2.2 (Kwan, 1988). The jet created by the down flow pushes the bed causing it to erode sediment and then rolls up and become part of the primary vortex.

b. Primary Vortex

The primary vortex at abutment is identified by many researchers as the basic mechanism for scour (Wong, 1982), Kwan (1984), Tey (1984), and Kandasamy (1985). The primary vortex develops once the initial scour hole is formed and is responsible for the further development of the scour hole (Melville, 1975), Baker (1980), and Qadar (1981). The flow accelerates downward into the hole and outward around the abutment in a spiraling motion as shown in Figure 2.3. The primary vortex axis is aligned in the main flow direction and is deflected as it passes through the abutment. Facing downstream, for an abutment on the left bank along the primary vortex axis, the rotation is counterclockwise.

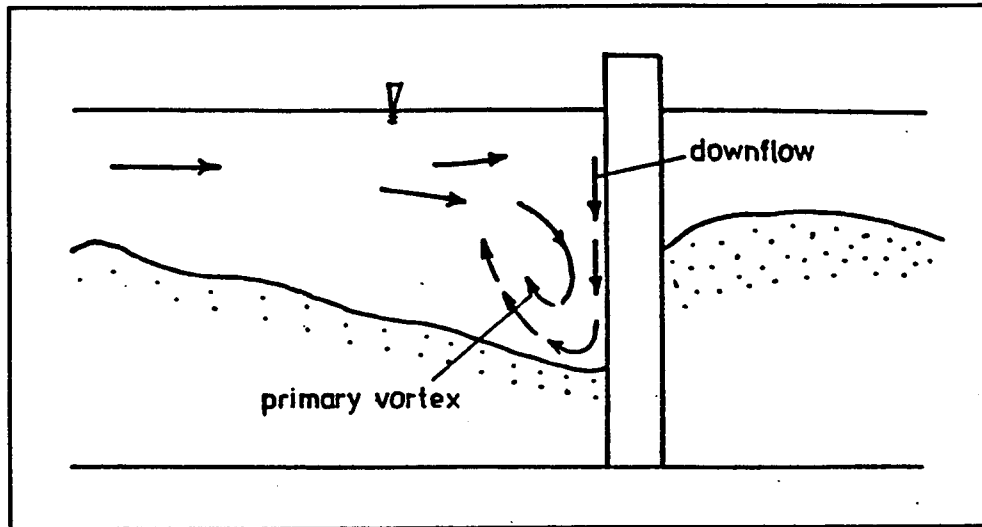


Figure (2.2) Downflow with Associated Primary Vortex (After Kwan, 1988)

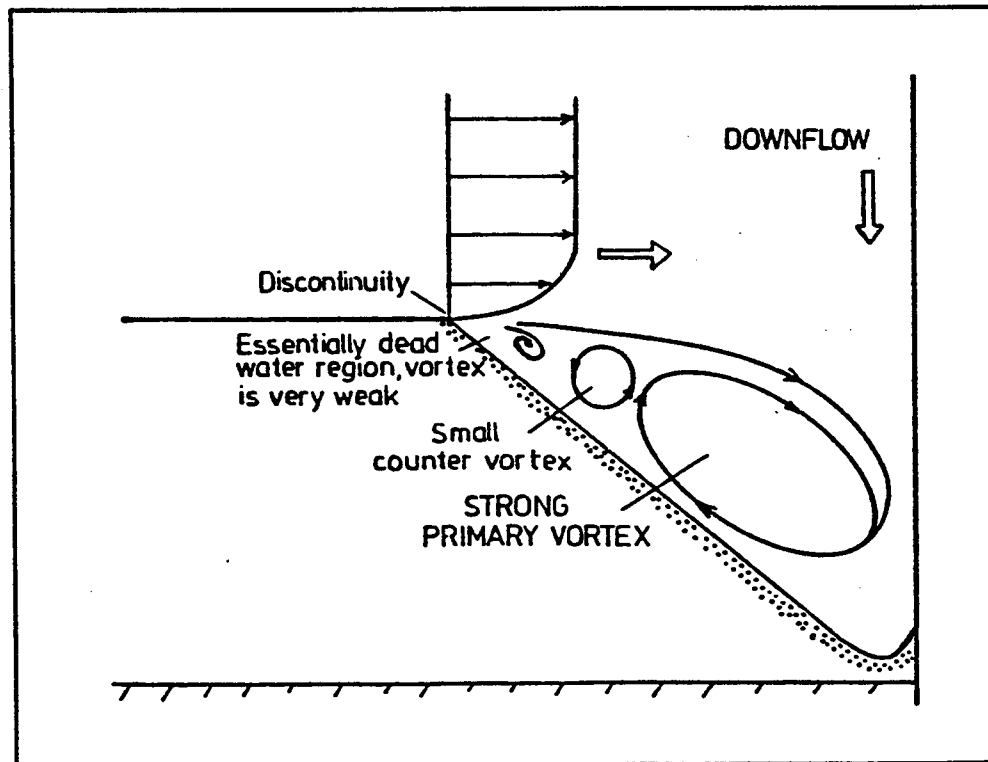


Figure (2.3) Primary Vortex in relation to Scour Hole (After Kwan, 1988)

C. Secondary Vortex

Most of the scour holes feature a series of grooves next to the primary scour which suggests that a secondary vortex is induced by the primary vortex with an opposite direction of rotation to the primary vortex as shown in Figure 2.4 (Kandasamy 1985), Kwan (1988).

d. Wake Vortices

The wake vortices is created by the separation of the flow by the upstream abutment corner. The unstable shear layers created by the flow separation roll up to form eddy structures known as wake vortices. The wake vortices are carried downstream by the mean flow and cause an erosion process acting like small tornadoes sucking up material from the bed. The wake vortices is very weak compared to the primary vortex. Very weak vortices are also observed at the interface of the dead water and main flow region at the upstream of the abutments as shown in Figure 2.5.

e. Development of Scour Hole and Primary Vortex System

When the flow is introduced into the abutment, the streamlines contract causing the flow to accelerate and increasing the local shear stresses by several orders of magnitude as shown in Figure 2.6. At the upstream corner of the abutment, the turbulent shear stress is greater than the critical shear stress for the bed material causing initiation of motion. The scour hole keeps getting deeper and larger, and as the slope of the scour hole sides exceeds the angle of repose, additional material slips and slides

into the scour hole.

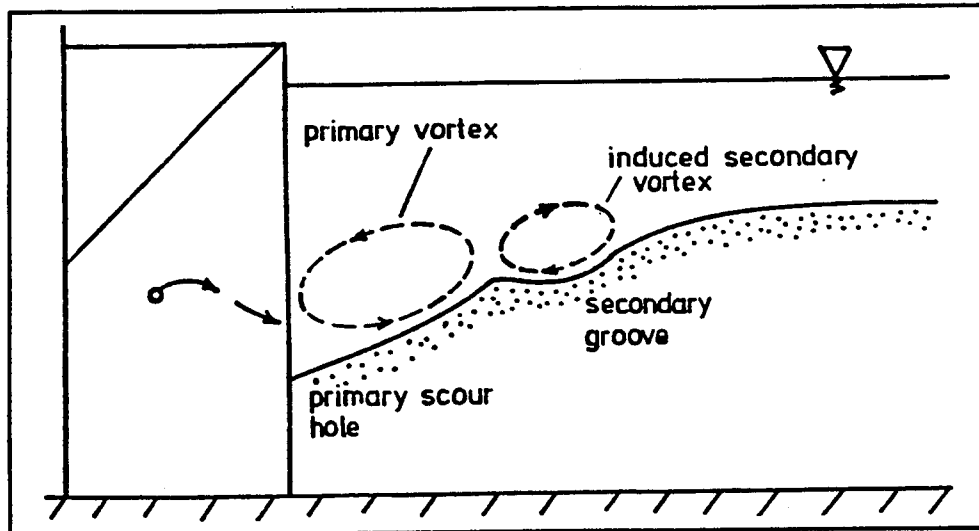


Figure (2.4) Conceptualised Model of Secondary Vortex Formation (After Kwan, 1988)

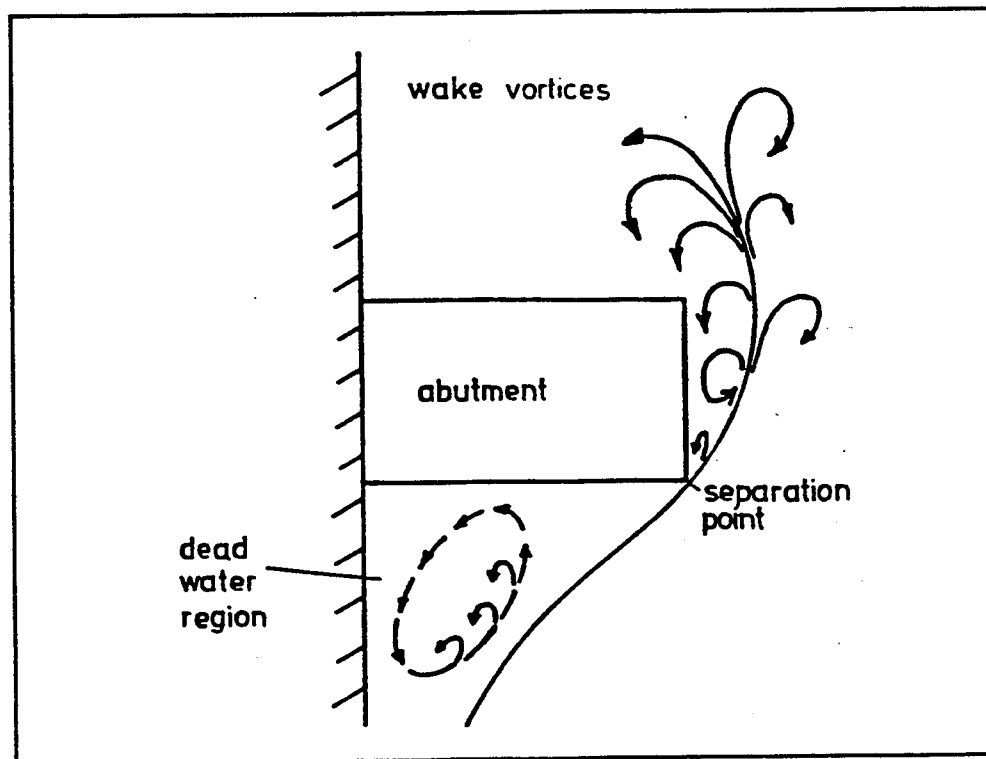


Figure (2.5) Flow Separation and Wake Vortices (After Kwan, 1988)

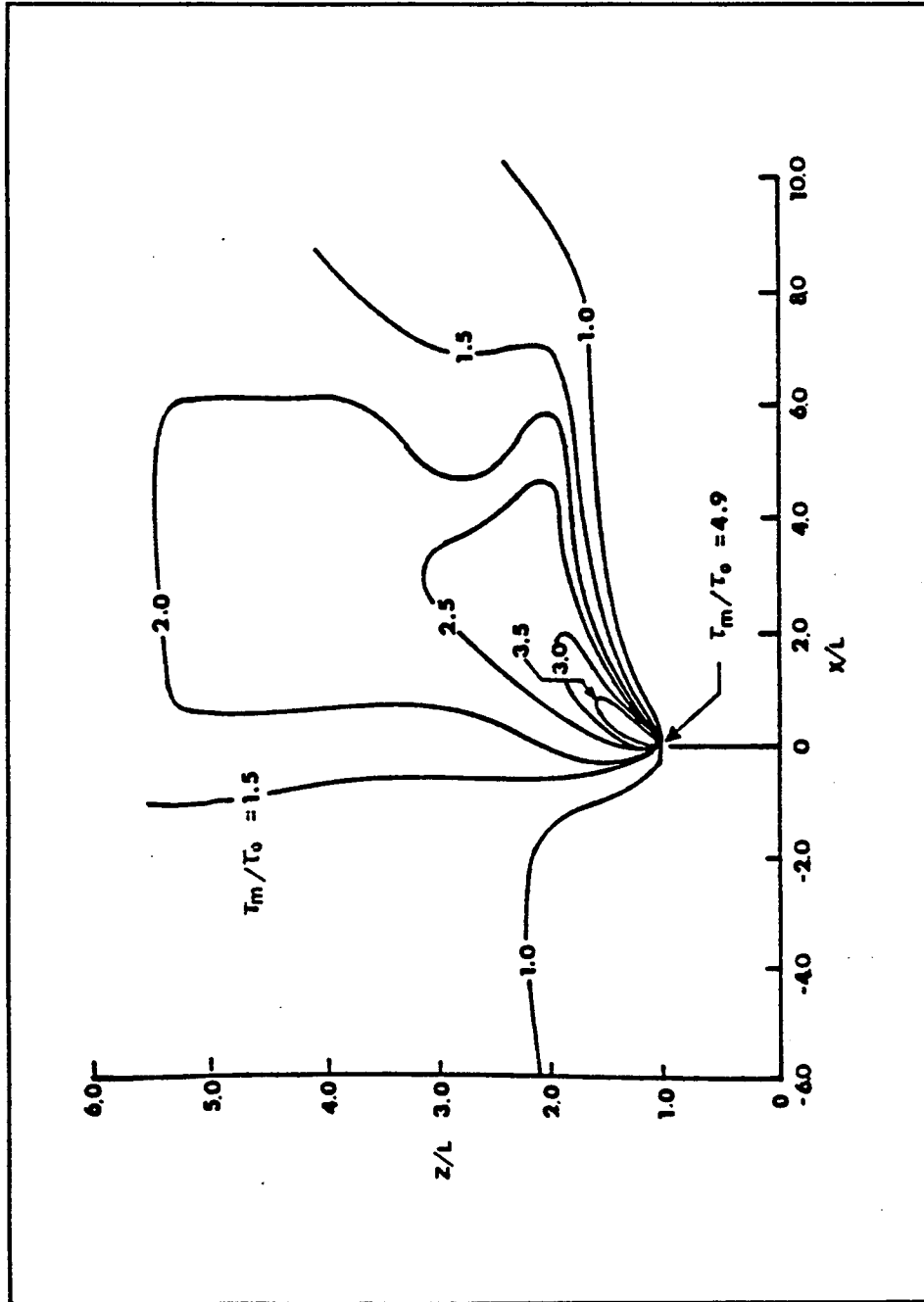


Figure (2.6) Shear Stress Amplification at Abutment (After Rajaratnam and Nwachukwu, 1983)

This material is carried downstream as suspended load and bed load. After this initial phase of scouring, the downflow pushes the flow into a strong spiralling flow which is due to the development of the primary vortex. As the strength of the primary vortex and downflow gets stronger, the size of the scour hole increases (Morton, 1983). The scour hole is enlarged until equilibrium is reached when the magnitude of the velocity and the shear stresses inside the scour hole can no longer move the sediment. The scour hole shape is of an inverted circular cone and features the secondary groove due to the secondary vortex. A longitudinal ridge separates primary scour hole from this secondary groove (Kwan, 1988).

2.4 Abutment Scour Equations for Non-Cohesive Materials

The following equations are the results of previous work done by Liu, et al (1961), Laursen (1980), and Froehlich (1989) to predict local abutment scour in sand and is presented in Hydraulic Engineering circular No. 18 (1991).

1. Liu, et al Equations, 1961

As a result of an extensive experimental study at CSU Hydraulics Laboratory, Liu et al. derived the following equations for live-bed and clear water conditions.

Live-Bed Scour at a Spill-Through Abutments

The equilibrium scour depth for local live-bed scour in sand at a stable spill-through slope with no over-bank flow when the flow is subcritical is determined by:

$$\frac{y_s}{y_1} = 1.1 \left(\frac{a}{y_1} \right)^{0.40} Fr_1^{0.33} \quad (2.1)$$

where:

y_s = Equilibrium depth of scour (measured from the mean bed level to the bottom of the scour hole);

y_1 = Average upstream flow depth in the main channel;

a = Abutment and embankment length (measured at the top of the water surface and normal to the side of the channel from where the top of the design flood hits the bank to the outer edge of the abutment);

Fr_1 = Upstream Froude number ($= V_1 / (g y_1)^{0.5}$);

V_1 = Upstream velocity.

Live-Bed Scour at a Vertical-Wall Abutments

When the abutment terminates at a vertical wall and the wall on the upstream side is also vertical, the scour hole in sand is twice the amount predicted by the spill-through abutment equation (Liu, et al (1961) and Gill (1972)). Liu, et al's equation for vertical wall abutment with no over bank flow when the flow is subcritical is :

$$\frac{y_s}{y_1} = 2.15 \left(\frac{a}{y_1} \right)^{0.40} Fr_1^{0.33} \quad (2.2)$$

where the definition of terms are given above

2. Laursen Equation, 1980

Live-Bed Scour at a Vertical Wall Abutment

For live bed scour, where the approach shear stress is greater than the critical shear stress, and for a vertical-wall abutment, the depth of scour can be obtained from:

$$\frac{a}{y_1} = 2.75 \frac{y_s}{y_1} \left[\left(\frac{y_s}{11.5y_1} + 1 \right)^{1.7} - 1 \right] \quad (2.3)$$

The simplified form of this equations:

$$\frac{y_s}{y_1} = 1.5 \left(\frac{a}{y_1} \right)^{0.48} \quad (2.4)$$

Clear Water Scour at a Vertical Wall Abutment

If the approach shear stress is less than the critical shear stress, the vertical-wall abutment equation developed by Laursen is:

$$\frac{a}{y_1} = 2.75 \frac{y_s}{y_1} \left[\frac{\left(\frac{y_s}{11.5y_1} + 1 \right)^{\frac{7}{6}}}{\left(\frac{\tau_1}{\tau_c} \right)^{0.5}} - 1 \right] \quad (2.5)$$

where

τ_1 = Approach shear stress;

τ_c = Critical shear stress for the D_{50} of the upstream bed material;

D_{50} = Grain size of the bed material for which 50 percent of the sediment is finer.

For other abutment types, Laursen suggested to correct this equation by a shape

factor. The shape factor for 45 degree wing wall is 0.9 and for spill-through abutment is 0.8

3. Froehlich's Equation, 1989

Live-Bed Scour at an Abutment

Froehlich analyzed the 170 live-bed scour measurements conducted by previous researchers in laboratory flumes by statistical methods and his regression analysis resulted in the following equation:

$$\frac{y_s}{y_1} = 2.27 K_1 K_2 \left(\frac{a'}{y_1}\right)^{0.43} Fr_c^{0.61} + 1 \quad (2.6)$$

where:

K_1 = Coefficient for abutment shape;

K_2 = Coefficient for angle of embankment to flow ($= (\theta / 90)^{0.13}$);

a' = Length of abutment projected normal to flow ($= A_c / y_1$);

A_c = Flow area of the approach cross-section obstructed by the embankment;

Fr_c = Froude number of the approach flow ($= V_c / (g y_c)^{0.5}$);

V_c = Q_c / A_c ;

Q_c = The flow obstructed by the abutment and approach embankment;

y_1 = Depth of flood plain flow at the abutment;

y_s = Scour depth.

For vertical-wall abutments, the value of K_1 is 1.0, for vertical-wall abutments

with wing walls, K_1 is 0.82, and for spill-through abutments, K_1 is 0.55.

If dunes are present in the main channel upstream of the abutment, Froehlich arbitrarily suggests that scour depth be increased by an additional $(y_1 / 6)$.

Clear Water Scour at an Abutment

The multiple regression analysis of 164 clear-water scour measurements in laboratory flumes, Froehlich developed the following equation:

$$\frac{y_2}{y_1} = 0.78 K_1 K_2 \left(\frac{a'}{y_1}\right)^{0.63} Fr_e^{1.16} \left(\frac{y_1}{D_{50}}\right)^{0.43} G^{-1.87} + 1 \quad (2.7)$$

where :

G = Geometric standard deviation of bed material ($= (D_{84} / D_{16})^{0.5}$);

D_{84} , D_{16} = Grain sizes of the bed material for which 84 and 16 percent of the sediment is finer by weight respectively.

The constant term unity (+1) is a safety factor in this equation to predict higher scour depth than what is measured in the laboratory flumes. This constant becomes a very conservative correction factor for larger depths of flow.

2.5 Clay Erosion Studies

The following clay erosion studies were selected from a large number of previous clay erosion studies since they concentrated on the behavior of clay and its engineering properties.

2.5.1 Alaeddin Shaikh (1986)

The rate of erosion for saturated and unsaturated soil differs because in unsaturated soils, water penetrates into the soil increasing the pore air pressure causing different erosion mechanism than the one in saturated soils. Shaikh deals with unsaturated, compacted earth structures such as dams & embankments. The result of his work is an empirical relationship for estimating the erosion rate as a function of tractive shear stress and soil properties. In Shaikh's experiments, two types of Montmorillonite clays were used (Na-montmorillonite and Ca-Montmorillonite) and one type of Kaolinite clay. Different percentages of clays were mixed with ground silica by weight (100 %, 70 %, 40 %, 10 %). Samples were compacted near optimum water content and tap water was used for eroding. The variables studied were clay type, clay content, pore water chemistry, and compaction water content and the SAR of the ca-montmorillonite was increased to examine the effect of salt concentration on the rate of erosion.

A small recirculated rectangular flume was used in the experiments and the sample was placed in a container and then was placed in the recirculating flume and was subject to the flow. A pitot-tube connected to a pressure transducer was used to measure velocity profiles. The velocity profiles were then used to estimate the tractive stresses on the flume bed. The erosion rate was determined by the difference in weight before and after the test.

The tractive force, which is the shear force generated by the flowing water on the bottom of the flume, is important in the study of erosion. For low flow depth and high slope, Shaikh used the following relationships to estimate the tractive stress:

$$\tau = \gamma R S \quad (2.8)$$

where:

τ = Average tractive stress;

γ = Unit weight of water;

R = Hydraulic radius;

S = The slope of the flume bed.

For a given slope and flow depth, the average value of V will be obtained from five measured velocity profiles along the flume using Prandtl-von Karman equation :

$$\frac{V}{V_*} = 5.5 + 5.75 \log \frac{V_* Y}{\nu} \quad (2.9)$$

where:

$V_* = \sqrt{\tau/\rho}$ = shear velocity, LT^{-1} ;

τ = tractive stress, FL^{-1} ;

ρ = density of water, ML^{-3} ;

ν = kinematic viscosity of water, L^2T^{-1} .

And from the shear velocity V_* , can calculate the tractive stress from:

$$\tau = \rho V_*^2 \quad (2.10)$$

The Torvane Gauge is used to measure the surface shear strength of each compacted sample to relate critical tractive stress and shear strength.

In Shaikh's experiments the properties of clay have been shown to have a major effect on the rate of erosion and the conclusions were:

1. Ca-Montmorillonite and kaolinite samples almost have the same chemical properties

of the saturation extract, therefore the difference in erosion rate could be related to their mineralogy. The erosion rate of Ca-Montmorillonite was larger than that of kaolinite which agrees with those reported by Grissinger (1966) and Alizadeh (1974).

2. For kaolinite clay as the compaction water content increases, the rate of erosion decreases. As reported by Hodek and Lovell (1979), that the compaction of kaolinite cause formation of aggregates for particles which slow down the erosion rate.

3. Na-Montmorillonite was mixed with ground silica to prepare the samples and the relation between coefficient of erosion rate, C, and the percentage of clay for Na-Montmorillonite is expressed as:

$$C = 4.14 (\% \text{ Clay})^{-0.91} \quad (3.11)$$

where C is the coefficient of erosion rate. The erosion rate $\dot{\epsilon}$ can be estimated for a given tractive stress, τ by :

$$\dot{\epsilon} = C \tau \quad (2.12)$$

In Figure 2.7, as the percentage of clay decreases, the coefficient of erosion rate increases because the increase of clay increases the amount of salts and consequently reduce the rate of erosion.

4. The change in erosion rate is related to the change in SAR where as the SAR increases, the coefficient of erosion rate, C, decreases as shown in Figure 2.8.

5. For Ca-Montmorillonite there is no relation between shear strength and coefficient of erosion where for the same shear strength gets different erosion rates. But there was a trend for Na-Montmorillonite mixed with ground silica to show a decrease in erosion rate with the increase of shear strength as shown in Figure 2.9.

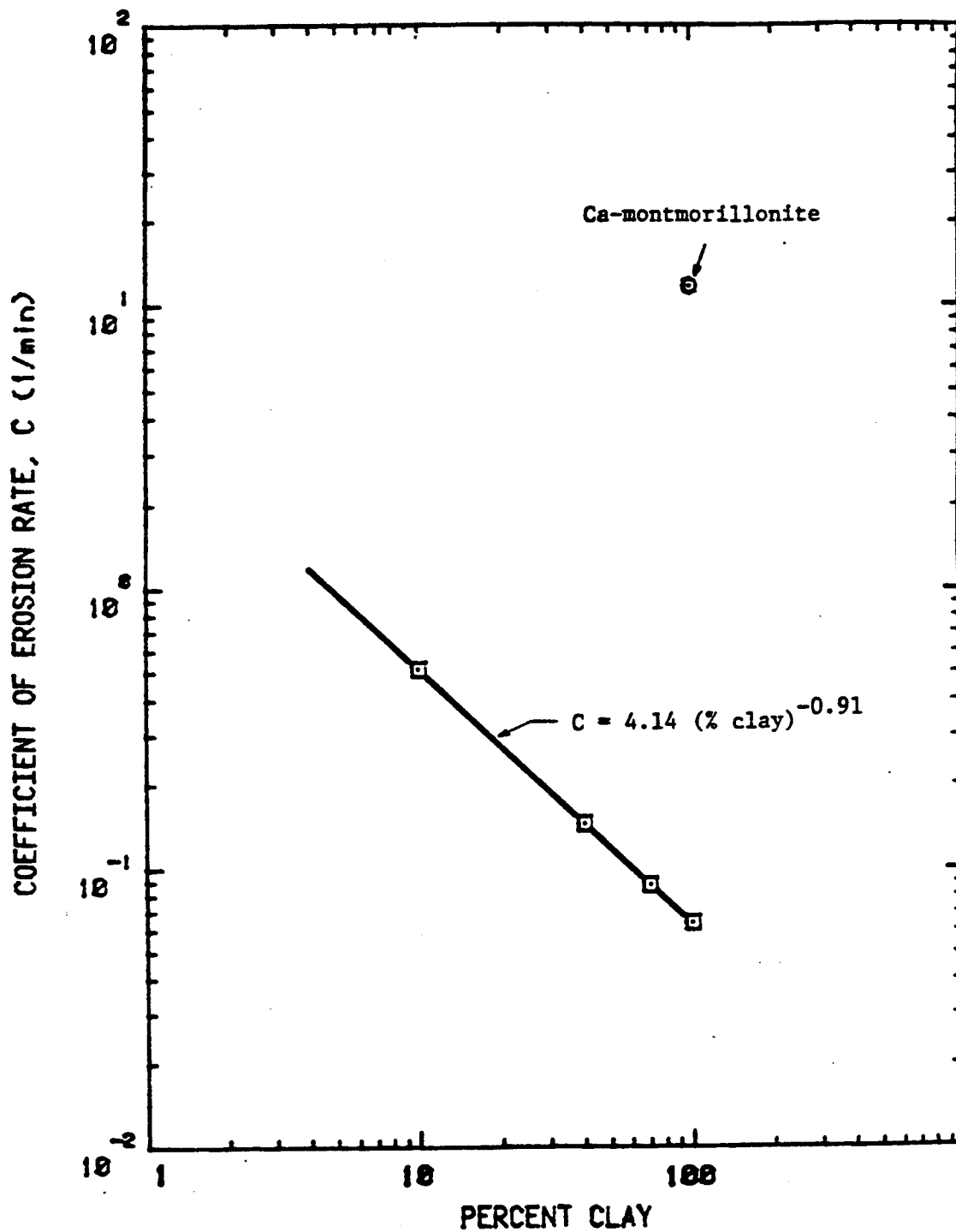


Figure (2.7) Coefficient of Erosion Rate versus Clay Content (After Shaikh, 1986)

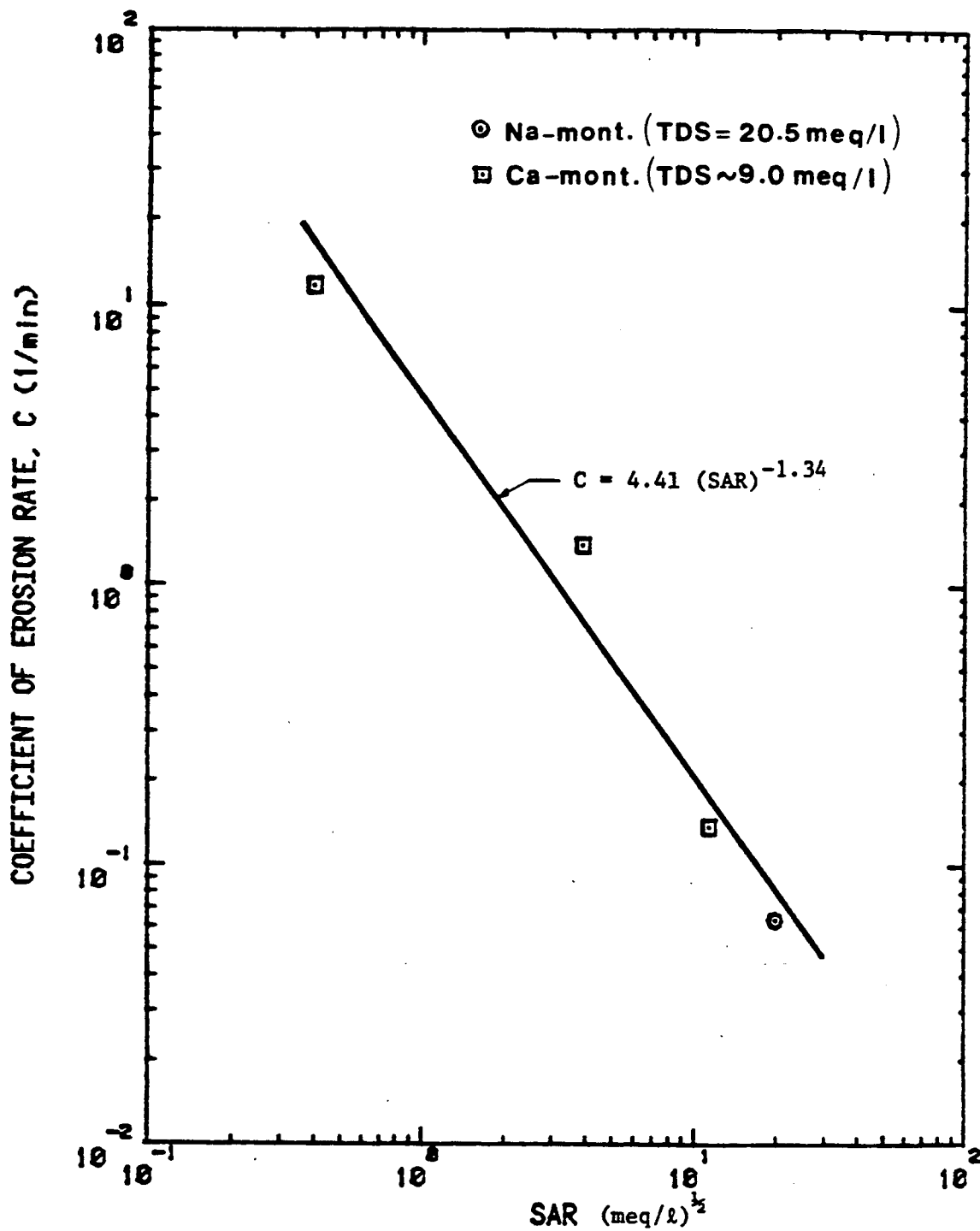


Figure (2.8) Coefficient of Erosion Rate as a Function of SAR (After Shaikh, 1986)

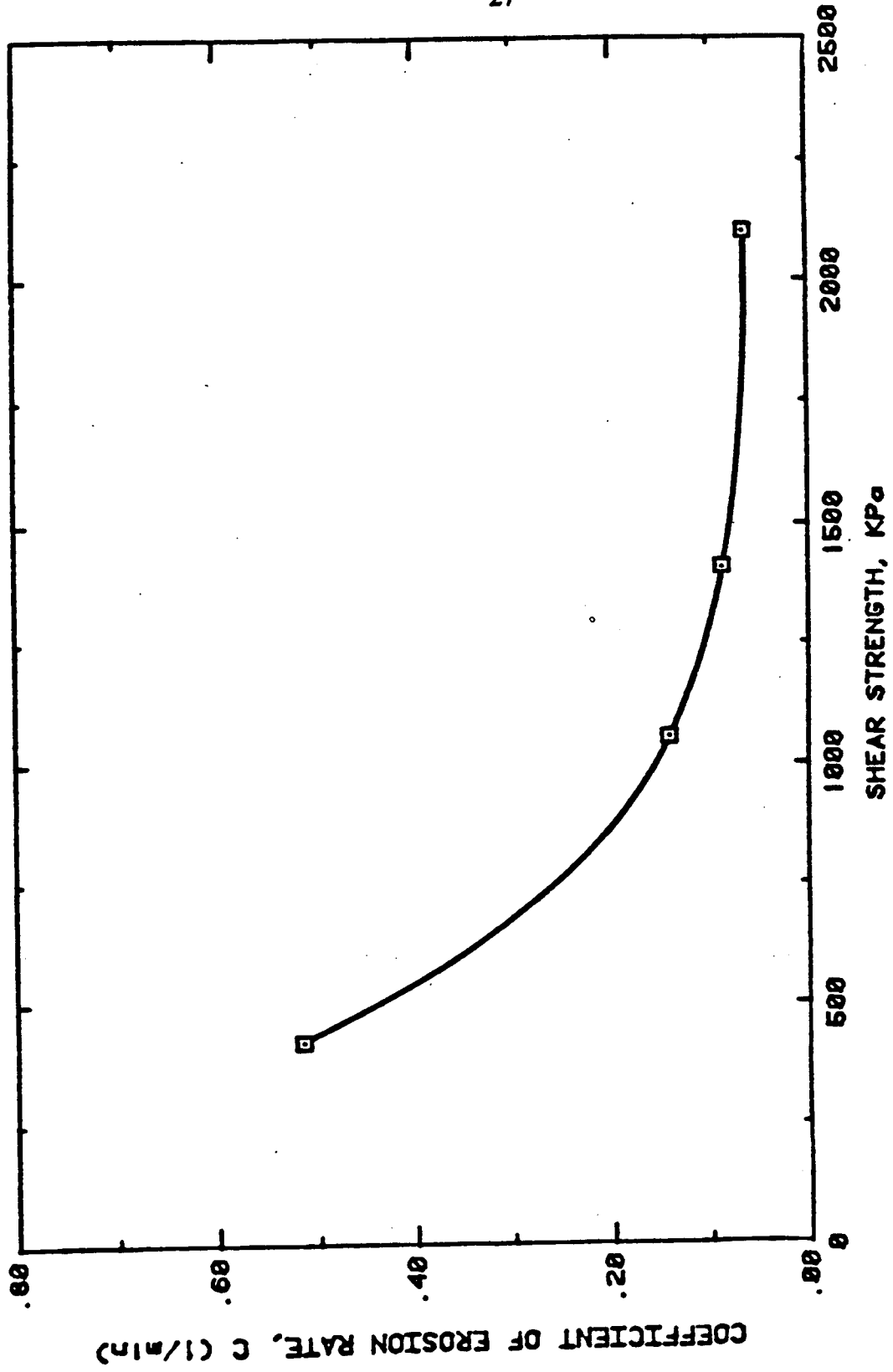


Figure (2.9) Coefficient of Erosion Rate versus Torvane Shear Strength (After Shaikh, 1986)

2.5.2 Steven Abt, 1980, "Scour at Culvert Outlets"

The study investigated scour at culvert outlets for cohesive bed material. The basic soil characteristics were determined such as plasticity index, grain size distribution, dispersion ratio, percent of clay, cation exchange capacity, density, ion type, moisture content and sodium absorption ratio. From the scour mechanism, it was noticed that erosion, entrainment and transport of cohesive material at culvert outlets is a very complex process. Through experimentation he related scour cavity characteristics to some of the erosion process parameters through performing a dimensional analysis. He found that discharge intensity and modified shear number are significant expressions in describing erosion. He also found that other important variables are time, scour depth, width, length and volume. The culvert diameter and the discharge. The soil used was SC cohesive soil according to the unified soil classification system with 58 % sand and 28 % clay. The density of the bed material was 90 % +/- 2 % of the optimum dry density. Discharge ranged from 1.9 to 29.1 cfs and the time duration for each one of his 12 experiments was 1000 minutes. The experiment was stopped to measure the scour dimensions at 31, 100, 316, and 1000 minutes. The scour cavities formed as a result of the jet discharging at the culvert outlet and impinging upon the cohesive bed. Relationships were developed to relate maximum depth of scour (d'), discharge intensity ($Qg^{-0.5}D^{-2.5}$), and modified shear number ($\tau_c \rho^{-1} V^{-2}$) to the dimensional cavity characteristics of depth, width, length, and volume of scour and also relate growth of scour to time. The conclusion of this study were:

1. Scour cavities were geometrically similar independent of discharge and culvert

diameter.

2. Seventy percent of max scour was formed during the initial thirty-one minutes of scouring.

3. There was a time related relation between time of scouring and volume of scour. Also it was observed that forty-five percent of total volume of scour occur in the initial thirty-one minutes of scouring.

4. Armoring did not occur within the scour cavity but rather around the cavity rim and along the mound.

5. there were three methods presented to describe the scour characteristics as follows:

A. relate (d/D) to the dimension of scour:

$$(V/D^3), (L/D) \text{ or } (W/D) = a(d/D)^b * (t_0/t)^c \quad (2.14)$$

Where a,b,c are constants estimated from tables to is peak flow duration less than 1000 minutes and t is 1000 minutes

B. relate scour dimension to culvert diameter and discharge using the discharge intensity relationships expressed as:

$$(d/D), (V/D^3), (L/D) \text{ or } (W/D) = a(Qg^{-0.5}D^{-2.5})^b * (t_0/t)^c \quad (2.15)$$

C. relate scour dimensions to material properties such as van shear strength, plasticity index and water content. Which will help to compute critical tractive from knowing the culvert outlet velocity, the modified shear number can be computed. Then, the modified shear number can be related to the scour dimensions as expressed by:

$$(d/D), (V/D^3), (L/D) \text{ or } (W/D) = a(\tau_c \rho^{-1} V^{-2} * 10^3)^b * (t_0/t)^c \quad (2.16)$$

2.5.3 Kandiah Arulanandan, 1980

The report describes the results of erosion and soil characterization tests performed on cohesive soils. Cohesive soils are controlled by physical and chemical surface phenomenon such as the structure and particle bonding of the soil and interaction with the pore and eroding fluids. Because erosion of cohesive soils is a surface phenomenon explains why some of the soil properties such as vane shear strength, unconfined compressive strength and dry unit weight have no effect on prediction of erosion and it is related to type and amount of clay, pore fluid salt concentration and sodium adsorption ratio SAR, soil paste PH, and organic matter content. Soil erodibility is measured in either a flume or rotating cylinder device. But it was noticed that the flume give good results for partially saturated soils, while rotating cylinder device was good to determine erodibility of saturated cohesive soils. The purpose of the study is to relate soil erodibility to soil composition and structure and eroding water composition for undisturbed cohesive soils of various stream banks across the united states. The samples were subjected to geotechnical and chemical tests to classify it and to determine the type and percentage of clay. The flume used for erosion tests was 8 feet long, 0.5 feet wide and 1.0 foot deep and the discharge was 0.127 cfs with water depth of 0.5 inch and velocity of 4 ft/sec. The sample is contained in 3 inch diameter, 3.9 inch long aluminum tube. The top of the tube is in the level of the bed. To begin the experiment, get an undisturbed sample directly from the ground using an aluminum tube and wet it then weight it. Insert the tube with the sample into the groove in the flume bed until the surface of the soil is leveled with the flume bed. Begin the run with low rate for the first

test and gradually increase the flow rate in the subsequent tests where each test run for 2.5 minutes. After the run, calculate the weight of soil lost from the sample which is equal the difference in weight before and after the experiment. Repeat from 5 to 10 times the erosion test for each sample with increased rate of discharge and plot the relation between shear stress and erosion rate for each sample. The conclusions of this report were:

- 1) Figure 2.10 shows predicted critical shear stress τ_c by giving sodium adsorption ratio (SAR), electrical conductivity, and total salt concentration. These was done by Heinzen (1977) using various artificial soil mixtures and distilled water as eroding fluid. Comparing τ_c predicted from these charts with the one measured in this study yield that predicted τ_c is less than the one measured in this study for both undisturbed and remolded soil because of the high concentration of salt in the eroding fluid which increase τ_c . So, Figure 2.10 give a reasonable estimate of τ_c for natural undisturbed soil subject to hydraulic shear stress from river (eroding) water. Also, the steel container may have served to increase the τ_c value of undisturbed soils.
- 2) For the remolded samples, as the salt concentration increases in the eroding fluid, the critical shear stress of the soil increases and the rate of erosion decreases.
- 5) For low τ_c will get a high rate of change of erosion rate and for high τ_c will get a low rate of erosion, so we can predicate τ_c if we know the rate of erosion and vise versa.

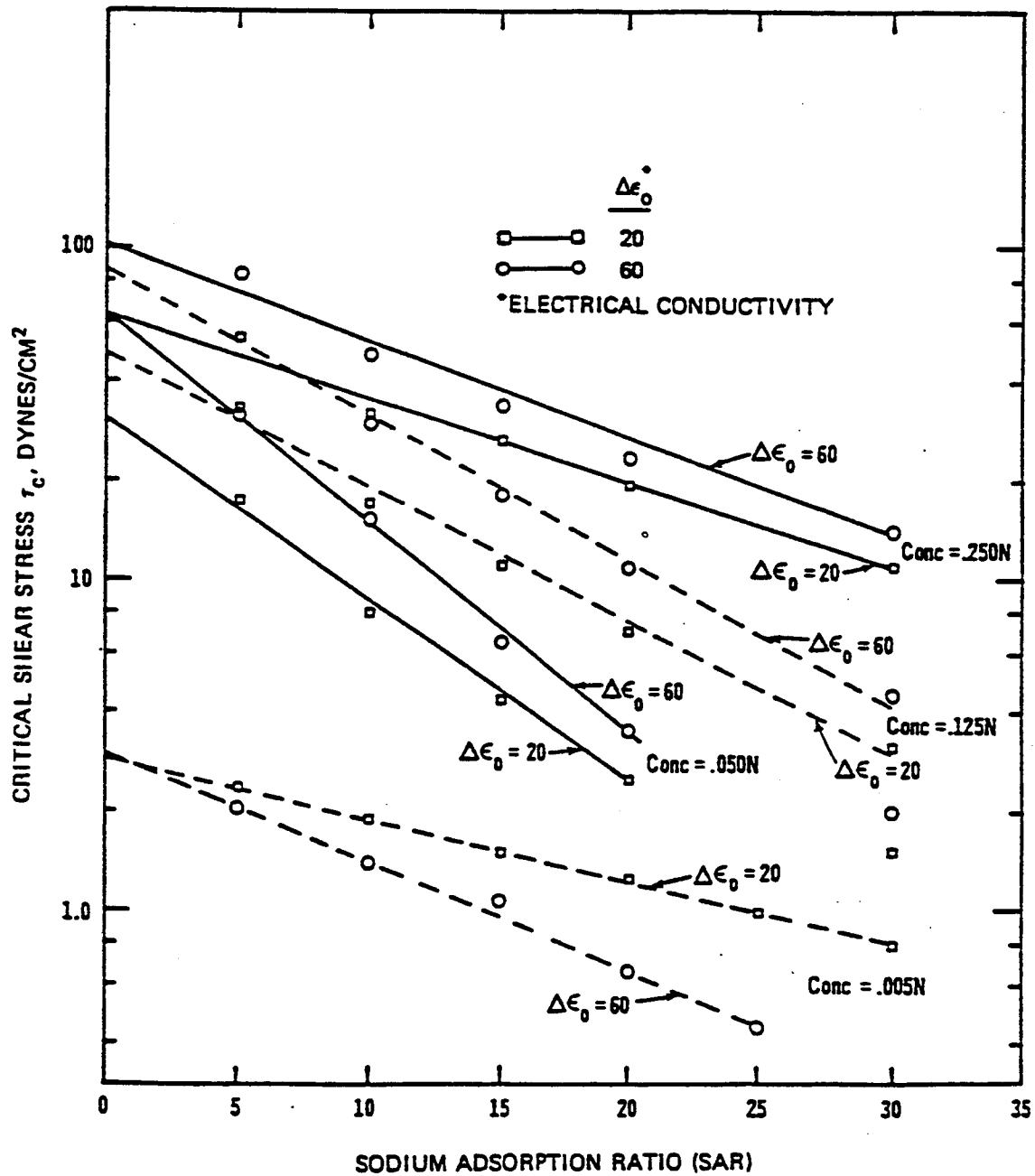


Figure (2.10) Critical Shear Stress versus SAR for Different Salt Concentrations (After Heinzen, 1977)

CHAPTER 3

COHESIVE MATERIAL PROPERTIES

This chapter include two parts; the structure of compacted clay and the engineering properties of compacted clay. The purpose of the first part is to give first a general description of clay structure where it explains the arrangement of soil particles and what forces affect this arrangement. Also, it explains the nature of water in clay and the theory of compaction (the process and the variables that could be changed during compaction). In the second part of this chapter, the engineering properties of compacted clay is presented. The basic theories and structure of clay introduced in the first part is used to explain some of the engineering properties of clay. This engineering properties of clay along with the clay structure will be used to derive some of the properties that explains the cause and the amount of abutment local scour in cohesive soils and to describe the behavior of the erosion process under the flow of water. The engineering properties includes the permeability, the compression, the shear strength, and the strength of saturated clay.

3.1 The Structure of Compacted Clay

Structure of clay is the arrangement of soil particles and the electrical forces acting between adjacent particles. This structure determines the clay properties. One

of the important questions for fine grained cohesive soils is whether to compact clay wet or dry of optimum moisture content. The study of compacted clays can improve our knowledge of natural clays since similarities exist between the structures of natural and compacted clays. In this section detailed discussion of the clay structure is presented which includes aggregation and dispersion of soil particles, arrangement of soil particles, nature of water in clay, theory of compaction, and the changes in soil structure.

3.1.1 Aggregation and Dispersion of Soil Particles

There are different variables and forces that act between the soil particles which will determine the soil strength and its erodability process which could shed some light on why some soils erode very rapidly and some do not erode at all.

The three electrical forces acting between atoms are: i) primary valence bonds; ii) hydrogen bonds; and iii) secondary valence forces. The strongest bond is the primary valence bonds that hold atoms together in the basic mineral units. There are also three types of minerals: i) the ionic (an exchange of electrons by the linked atoms); ii) the covalent (sharing of electrons by the linked atoms); and iii) the heteropolar (in effect, part ionic and part covalent, since it results from an unequal sharing of electrons by the linked atoms). The ionic and heteropolar mineral bonds act like magnets. The normal stresses which are applied to the soils do not brake the primary valence and hydrogen bonds. The secondary valence forces which are known as van der Waals forces are similar to the attraction between two short magnets. The secondary valence forces are the source of clay strength and the reason for the soils to hold water. These forces are therefore

important to the soils engineer. The electrostatic attraction or repulsion of electrically charged units of matter is another type of primary valence linkage and are greatly influenced by applied stresses and changes of the soil-water system and these in addition to the secondary valence forces are of the most concern to the soil engineer. When the specific surface of a particle is large enough to carry electrical forces bigger than the mass forces, it is called "colloid". Clay particles are usually in the colloidal range because the colloidal size range from one micron to one millimicron (10 A). Clay particles carry a net negative charge and the particle is neutralized by the exchangeable cations. For dry clay, the cations neutralize the particle surface. For clay placed in water, the cations swarm around the colloid and is called "double layer". For the quantitative description of ion distributions adjacent to charged surfaces, the Gouy-Chapman theory of the double layer (Gouy, 1910; Chapman, 1913) was the most accurate in describing the distribution of ions. This theory was proven to be accurate for low concentration of suspended particles (sposito, 1989). This theory provides a good basis to understand flocculation and dispersion process and the formation of soil structures. this also help to understand the process of clay compression, swelling, and erosion (Mitchell, 1993). Clay particles carry net negative charges and repel each other. But, the secondary valence attractive forces also act between particles and combining the repulsive and attractive forces gives the total potential energy which is related to the interparticle spacing (Kruyt, 1952; Bolt, 1955). When adjacent particles approach each other the potential energy is reduced and form the aggregate which is called "flocculate". When adjacent particles move apart, the potential energy increases and the particles will

disperse. Aggregation and dispersion form due to the changes in the variables of the colloidal system. Aggregation increases because of the increase of i) electrolyte concentration; ii) ion valence; and iii) temperature. Dispersion increases because of the increase of i) dielectric constant; ii) size of hydrated ion; iii) PH; and iv) anion adsorption.

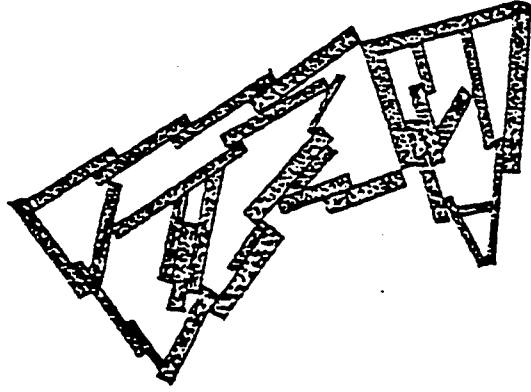
The decrease in the double layer thickness reduces the electrical repulsion which causes a tendency toward flocculation. As the hydrated ion gets smaller, as it can approach the colloidal surface and the smaller the double layer which cause more flocculation. High PH causes the increase of the net charge which expand the double layer and increase dispersion. As Figure (3.1) illustrates, there are three types of sediment structures:

1. Salt flocculation: where orientation approach parallelism.
2. Non-Salt flocculation: where orientation approach a perpendicular array.
3. Dispersion: where orientation is almost parallel.

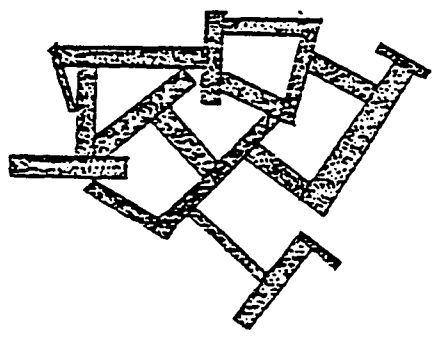
The addition of salt to the Kaolinite - water system increases the concentration of anions which gather at the edges of the particles. As a result, the particle is less able to cause flocculation and we will get the salt flocculation type.

Because the soil engineer is concerned with large masses of soil there are many factors neglected in colloidal theories explained as follows:

1. Particle Size and Shape: there are many types, sizes and shapes of soils in the nature which include more than one mineral and several impurities. Also include silt-size particles which affect the arrangements of the plate shaped particles.



a. Salt Flocculation



b. Non-Salt Flocculation



c. Dispersion

Figure (3.1) Sediment Structure.

2. **Soil Concentration:** The mineral concentration in the soil is very high which create physical and electrical interference among neighboring particles. This interference conflict with the theory of colloid interaction which simply consider two adjacent particles only.

3. **Inter-particle Spacing:** If the distance between two particles are less than 10 A, other forces not considered by the theory operate.

4. **Applied Forces:** Colloid theory consider only the forces arising from the nature of clay particles in dilute suspensions. However in large clay masses, there are external forces such as those which occur from overlaying structures or from moving water which of great importance in determining clay behavior.

Because of these previous factors, numerical equations based on colloidal theory met with failure. However the colloidal theory is useful to understand the fundamental behavior of fine grained soils.

3.1.2 Arrangement of Soil Particles

Clay mineralogists determined the sizes and shapes of clay mineral crystals using electron microscope and the common minerals include: Kaolinite, Halloysite, Montmorillonite, Nontronite, Illite, Attapulgite, Chlorite, and Vermiculite. In addition there are the rough - edged shapes approaching spheres such as quartz, feldspars, carbonates, and oxides. (Michell, 1956) described particle arrangement by:

1. Texture such as regularity and transition between Components.
2. Particle Orientation such as degree of parallism and clay around silt.

Preparation of clays for the X-ray and electron diffraction tests destroys the structure of natural soil such as drying treatment. Different atomic arrangements in clay crystals respond to X-ray with different diffraction patterns which identify the type of clay mineral crystal (Mitchell, 1993). In soil engineering the term "dispersion" is called "repulsion" because dispersed sediment implies interparticle electrical repulsion and "flocculation" is called "attraction" because flocculated sediment implies interparticle electrical attraction. During compaction for dispersed soil, the particles can slide past one another and give a very good arrangement and packing. On the other hand mechanical manipulation for flocculating particles is less effective in arranging particles because particles stick to one another when they approach each other. Particle arrangement in flocculated sediment are nonparallel but a parallel arrangement can result from one-dimensional consolidation under a very high pressure.

3.1.3 Nature of Water in Clay

Terzaghi (1925) pointed out that the effect of water on clay behavior is very important. The factors that is important to the soil engineer are: amount of water; nature of water, and stresses in the water. The nature of water in clay is not completely known even though many studies have been devoted to that subject. The force between water and clay particle decreases as the distance increases. There are two types of attraction forces, the first is a direct contact between the water and the soil. The other type is the attraction between the water and the particle through the double layer.

There are three types of water in clay depending on the type of force between the

water and the soil and they are adsorbed water, double layer water and free water. The adsorbed water is that which strongly held by the soil, the double layer water is all the water attracted to the soil; and free water is water which is not attracted to the soil at all. Adsorbed water is the inner part of the double layer water and sometimes they use "adsorbed" to describe both adsorbed and double layer water. The adsorbed layer is about 10 A thickness and the double layer is about 200 A to 400 A thickness ((Rosenqvist, 1957), (Michaels and Lin, 1955), and (Martin, 1957)) and the force required to pull this adsorbed water off the mineral surface is prodigious. As suggested by Lambe (1958), the mineral to mineral contact in clay occur when their double layers interact. When the interparticle spacing has been reduced to a distance of approximately 20 A, all of the water between the particles is tightly held. There is a widely held concept that the cohesion in a natural clay is due to "water bonds". The water-mineral link is strong and the water does contribute to soil strength where the double layer plays a very important role in determining the interparticle forces. But the water-bond concept are limited by the fact that the maximum cohesion a clay ever possesses occurs when the clay is dry. So, water has an important rule in determining the properties of clay. In most natural clay, all of the water is contained within the double layer.

3.1.4 Theory of Compaction

The concept of "water deficiency" recognizes that any given soil particle under any given state of stresses requires a certain amount of water to develop fully its double layer. The difference between this needed water and the existing water is deficient water

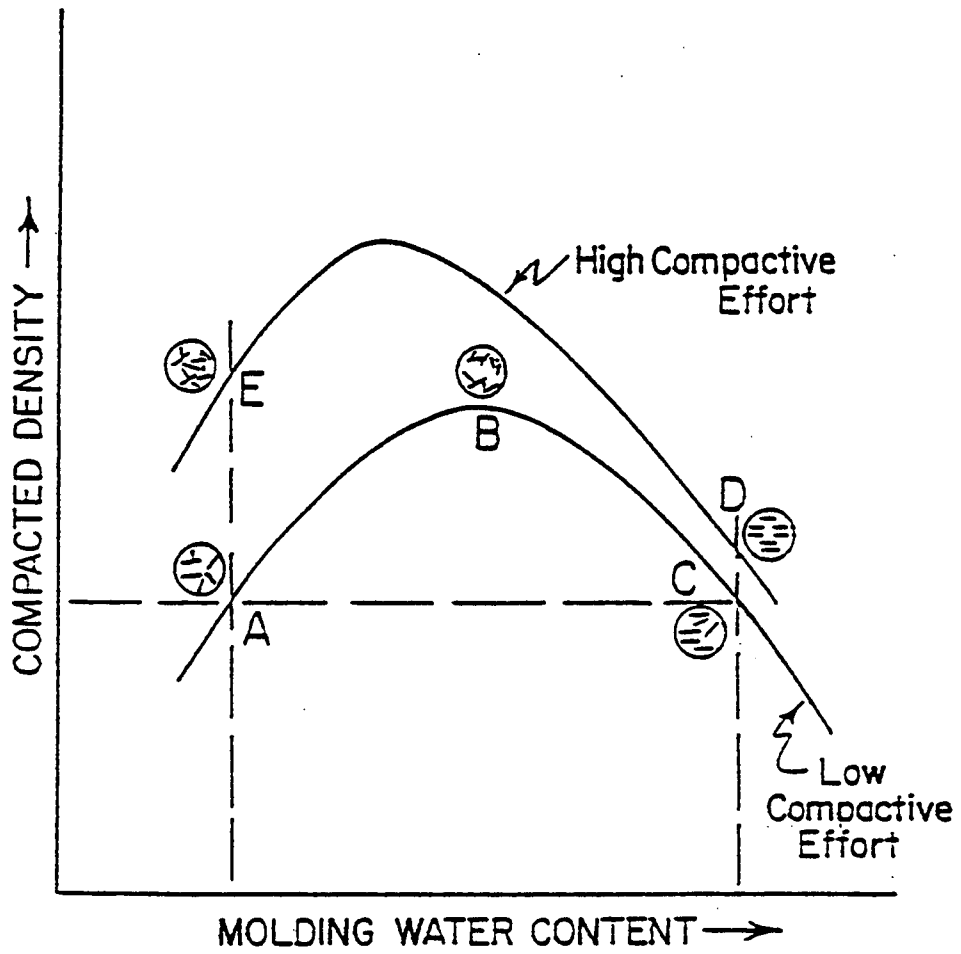


Figure (3.2) Effects of Compaction on Sediment Structure.

which the particle will try to attract. Figure 3.2 gives molding water content versus compacted density for low compaction and high compaction. At 'A' there is not sufficient water for the double layer to develop and this cause the tendency toward flocculation of the colloids which means a low degree of particle orientation and low density. Increasing the molding water from 'A' to 'B' expands the double layers around the soil particles which permits a more orderly arrangement of particles and higher density. A further increase of water from 'B' to 'C' results in a further expansion of the double layer and a continued reduction in the net attractive forces between particles. But the added water has diluted the concentration of soil particles per volume and resulted in low density. Also, Figure 3.2 illustrates the effect of more compactive effort which produce higher compacted density and more nearly parallel clay particles and closer together.

The variables that could be changed during compaction are:

1. Type of compaction: Dynamic compaction gives a different product from static compaction where time and area of contact between compacting element and soil are important variables in determining the effect of compaction (Seed, Lundgren and Chan, 1954).

2. Amount of Compaction: As the compactive work increases, the density increases for a given clay and water content. As it known, greater the compaction, greater the strength but it could give lower strength in some cases.

- 3 . Amount of Water: If the water amount added increases more than a certain limit, the water lubricates the soil and reduce the density and weaken the soil strength

as discussed before.

4. Additives: Dispersants act as additional water where they reduce optimum water content and increase maximum compacted density. Aggregants raise optimum water content and reduce the maximum compacted density. Dispersants permit a higher degree of particle orientation, while aggregants result in a more random array.

Pacey (1956) measured particle orientation as a function of molding water content on compacted Boston blue clay. His data agree with our theory where as the molding water increases, the density increases and the more nearly parallel are the clay particles. Direct measurements of particle orientations are difficult and simple methods are needed. one of the methods could be the amount of shrinkage upon drying where parallel particles will have less volume reduction than soil with particles of random array. Also notice that water gets into a dispersed soil at a slower rate than it does with flocculated soil because of the lower permeability of the dispersed sample. Another method is to measure the pressure required to prevent swelling of the clay when it is put in contact with water. Hvorsley (1938) dried samples which was subjected to different loading conditions and he found that the cracks were parallel to particle orientation. Haggarty (1957) found that a clay with oriented particles shrinks the most in a direction perpendicular to the plates and least parallel to the plates. Also, a clay with randomly oriented particles shrinks equally in all directions.

3.1.5 Changes in Soil Structure

There are different causes that affect on the structure of clay as follows:

A. Normal pressure and shear deformation tends to push particles together and decrease interparticle spacing which gives more aligned particles. One-dimensional compression is more effective in forcing particles into more parallel orientation than does three-dimensional compression.

B. Time is required for the adsorbed water to be extruded and also for the layers of adsorbed water of adjacent particles to slide in relation to each other. Seed (1958) showed that repetitive load applications increases the strength of a compacted silty clay.

C. Environmental changes such as increase of water in the soil-water system which expands the double layer tends to decrease soil strength where that increases interparticle repulsion. The increase in temperature causes an increase in the double layer thickness which decreases the shear strength of a clay (Mitchell, 1993). The shear strength also decreases with the increase of pH of the pore fluid.

D. Disturbance can change particle arrangement and interparticle forces (Mitchell, 1956) where remolding and shear strains arranges particles in a parallel array.

E. Strength loss with time, especially for soil compacted dry of optimum, can be caused by an increase in moisture due to changes in ground water which increases interparticle repulsion.

F. Loss of strength past peak strength is caused by changes in orientations and spacings of soil particles especially in soils sensitive to disturbance.

G. Organic materials are found in clay with different degrees of concentrations and the type of organics will determine there interaction with clay and the corresponding effect on shear strength of clay (Raussell-Colom and Serratosa, 1987).

3.1.6 Structure of Kaolinite and Montmorillonite

The structure of Kaolinite mineral consists of a single tetrahedral sheet and a single alumina octahedral sheet combined in one unit. One common layer consists of the tips of the silica tetrahedron and one of the layers of the octahedral sheet. A strong hydrogen bonds held together the successive Kaolin mineral layers. The hydrogen bonds prevent hydration and allow the layers to stack up forming a large crystal (Holtz and Kovacs, 1981).

Montmorillonite is a mineral consists of an octahedral sheet sandwiched between two silica sheets. All the tips of the tetrahedra point toward the center of the unit cell. The oxygens forming the tips of the tetrahedra are common to the octahedral sheet as well. The successive layers are bonded together by van der Waals forces and ionic bonds. The difference between Kaolinite and Montmorillonite clay minerals is the type of bonds. The hydrogen bonds of Kaolinite clay are much stronger than the van der Waals forces and ionic bonds of Montmorillonite clay. As a result, it is more easier for water to enter between the sheets of montmorillonite clay and separate into individual units.

3.2 Engineering Properties of Compacted Clay

In this section, the theoretical principles of clay structure, which was presented in the previous section, is used to explain the engineering behavior of compacted clay. The purpose of this section is to describe the behavior of clay which will help to explain the erosion process of abutment local scour in cohesive soils under a certain flow

conditions and different clay properties. The engineering properties of clay includes the permeability of compacted clay, compression of compacted clay, shear strength of compacted clay, effect of compaction conditions on strength, and strength of saturated samples. More detailed description are given in the following sections.

3.2.1 Permeability of Compacted Clay

Permeability is important in problems such as stability and seepage and also in the basic research of clay. The factors that affect on the permeability of clay are as follows (Lambe, 1958):

- A) Soil compaction
- B) Characteristics of permeant
- C) Void ratio
- D) Degree of saturation
- E) Structure

But the structure of the soil has a very large effect on its permeability. Permeability tests on samples of Jamaica sandy clay first compacted and then subject to flow until a steady-state has existed. The results Figure 3.3 shows that we will have a higher permeability for the soil that is compacted dry of optimum than the soil that is compacted wet of optimum. The reason for that is the random orientation of the samples compacted dry of optimum which means more large pores than the samples compacted wet of optimum that have more nearly parallel arrangement. The term $K_v S^2$ in the Kozeny-Carman equation is a good measure of soil structure or particle orientation.

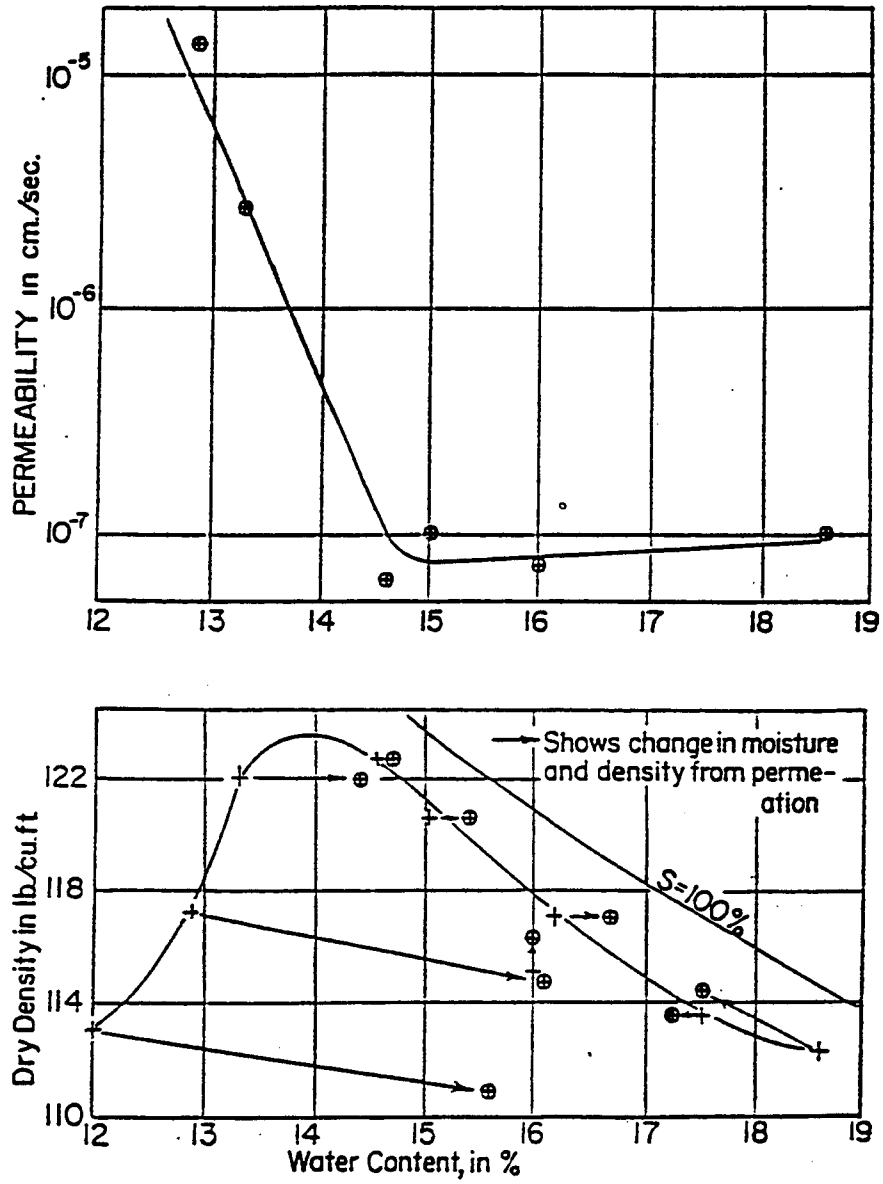


Figure (3.3) Compaction-Permeability Test.

The equation is

$$K_o S^2 = \frac{1}{K} \frac{e^3}{1+e} \quad (3.1)$$

where:

S = Specific surface.

K_o = Constant depend on pore shape and tortuosity of flow

K = absolute permeability

e = void ratio

So, for more particle orientation get less void and less permeability.

3.2.2 Compression of Compacted Clay

The clay compresses if subjected to pressure and the compression is due to:

1. change of volume and amount of gas
2. particle deformation and diminution
3. particle rearrangement
4. Decrease in the size of micelles

Because of compression, gas could cause decrease in soil volume because of increase in pressure or because of lower temperature. Also compression could cause the gas to go into solution in the pore water. Particle deformation and diminution are in significant in clays because the contact area is big enough so that the stresses applied is not enough to cause particle crushing or elastic deformation. The rearrangement of soil particles contribute to compression because of going from random array to a more

orderly array particles. There are data (Hvorslev, 1938; Mitchell, 1956) proof that one dimensional compression cause alignment of particles. Figure 3.4 illustrates the effect of one-dimensional compression on the clay structure. The orientations in the circles show that the load tends to align the particles in parallel array. For remolded or wet-side compacted clay where we have already parallel particles, the load merely brings them closer together. Volume decreases caused by arrangement of particles are nonrecoverable. Also, the decrease in the size of micells (which means soil mineral particle and double layer water) contribute to compression upon applying of pressure.

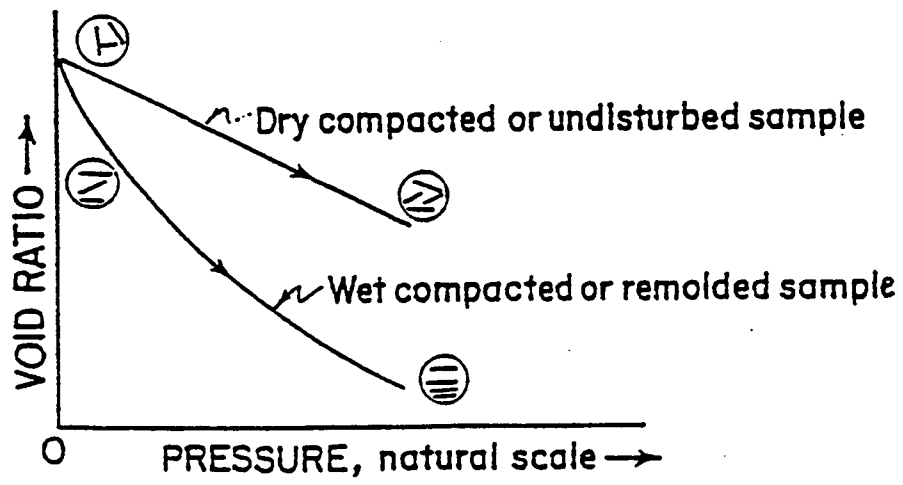
3.2.3 Shear Strength of Compacted Clay

The shear strength of a plastic clay is a colloidal-type strength. By considering the system of forces between particles, there will be four horizontal forces:

1. σ = The externally applied intergranular stress
2. A = The electrical attraction
3. R = The electrical repulsion
4. I = Contact pressure

The intergranular stress is equal to the total applied normal stress minus the pore water stress and the soil engineer could measure. Stress A is primarily came from van der Waals forces. Stress R is primarily from electrostatic repulsion between clay particles. Pressure I is a repulsive stress and it acts when adjacent particles are in contact. For dispersed particles get the equilibrium condition:

$$\sigma + A = R \quad (3.2)$$



a. LOW PRESSURE
CONSOLIDATION

Figure (3.4) Effect of One-Dimensional Compression.

for particles in contact get the equilibrium condition

$$\sigma + A = R + I \quad (3.3)$$

The electrical forces A, R, and I that determines the shear strength of clay depends also on particle spacing, particle orientation, externally applied stresses and characteristics of soil water system. These causes are explained as follows:

A) Electrical forces: this is function of particle displacement. The greater A and I, the greater is the shear strength; the greater R, the lower the shear strength.

B) Particle Spacing: electrical forces get greater as the clay particles get closer.

C) Particles orientation: the shear strength get weaker as the particles gets more nearly parallel.

D) Externally applied Stresses: The shear strength is affected by the externally applied intergranular pressure which in turn change the spacing and orientation of particles which alters the electrical forces between the particles.

E) Characteristics of the soil water system: any expansion of the double layers increases the electrical repulsive force between adjacent particles.

The shear strength could be described by cohesion and friction angle as (which is called " Coulomb equation "):

Strength = Cohesion + σ tangent of the friction angle

$$S = C + \sigma \tan \phi \quad (3.4)$$

3.2.4 Effect of Compaction Conditions on Strength

3.2.4.1 As Molded Strength

As presented in Figure 3.5 from (Pacey, 1956) for compaction and strength on boston blue clay, we can conclude the following :

- A) At dry of optimum, strength increases as the compaction increases.
- B) Increased compaction at wet of optimum could increase or decrease strength.
- C) At the same conditions of compaction and density, can get higher strength from dry side compaction than from wet-side compaction.

These facts could be explained by the compaction theory, where the reduction in particle spacing increase the strength. Also there are evidence (Hilf, 1956) that clay compacted dry of optimum have negative pore water pressure which cause higher intergranular stresses and consequently higher strength. The double layers will not be fully developed because of insufficient moisture content and the soil will try to draw in the needed water. This will develop capillary menisci which transfer water tension into intergranular compression which increase strength. Another set of experiments done by (Ladd, 1957) proof that the dry-side compacted clays have a water deficiency where this deficiency came from the incomplete development of the double layer.

3.2.4.2 Strength of Saturated Samples

Huning (1957) ran triaxial tests on compacted samples and he found out that samples compacted dry of optimum and then saturated have more strength than those compacted wet of optimum and then saturated. Figure 3.6 shows that for a given

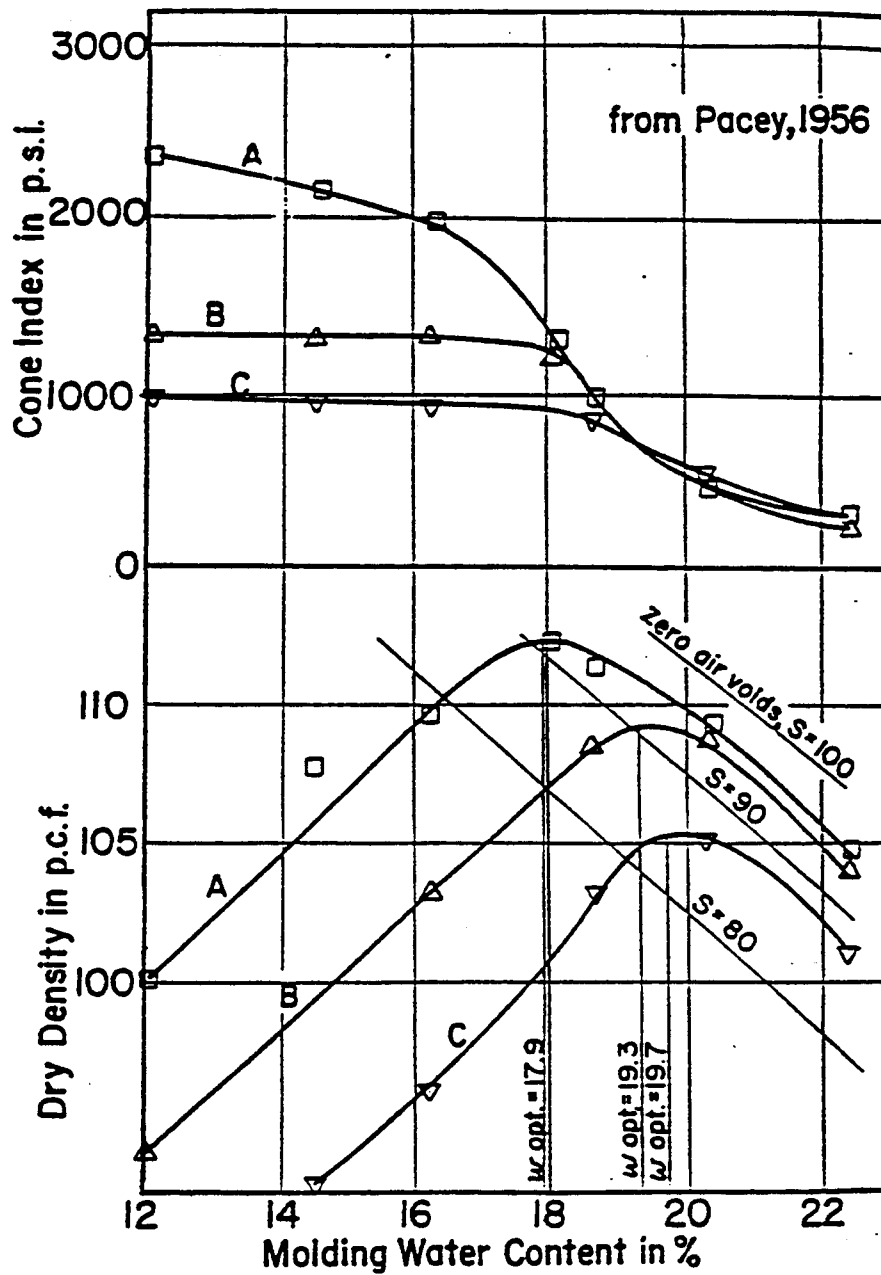


Figure (3.5) Cone Index and Dry Density versus Water Content.

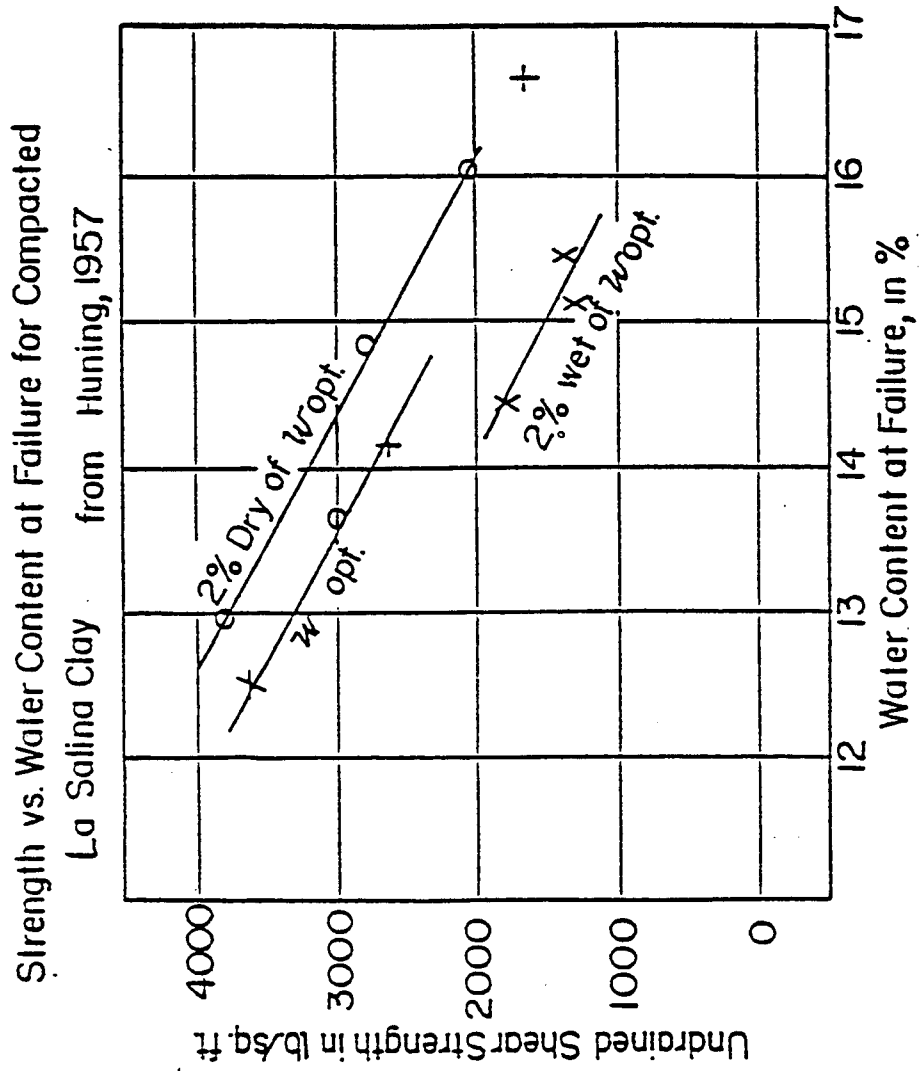


Figure (3.6) Shear Strength versus Water Content at Failure.

water content at failure the dry side compaction have higher strength than the wet side compaction. Notice that Huning's test procedures for saturation and consolidation subject the soil to severe stresses that destroyed the differences in soil structure that developed during compaction. That indicates the need for more tests to show the effect of compaction on shear strength.

3.2.5 Atterberg Limits

The liquid and plastic limits are proposed by A. Atterberg, a Swedish agricultural scientist. The definition of these limits (Bowles, 1986) are:

Liquid limit - moisture content below which the soil behaves as a plastic material. At this moisture content, the soil is on the verge of becoming a viscous fluid.

Plastic limit - moisture content below which the soil is non plastic.

Liquid and plastic limits are used for soil identification and classification and for strength correlations. The liquid and plastic limits were performed in the Colorado State University Geotechnical laboratory. The plasticity index is calculated from the difference between liquid limit and plastic limit. The study based on eleven natural soils (Smerdon and Beasley, 1961) found a correlation between critical tractive stress and plasticity index. Liou (1970), determined that, for Bentonite samples at about the liquid limit water content, there is an inverse correlation between the critical erosion shear and the plasticity index. But, Bentonite samples compacted at low water contents, there was no correlation and at different water contents, Bentonite gives different values of critical erosion shear. From that, Liou concluded that the plasticity index can not be used alone

to estimate clay erosion rate. Even when the plasticity index is constant, the rate of erosion is a function of other variables such as degree of compaction, moisture content, pore water chemistry, and others (Raudkivi, 1976).

CHAPTER 4

EXPERIMENTAL EQUIPMENT AND PROCEDURES

4.1 Introduction

The main objective of this experimental is to study the effects of water content, compaction, clay content, and type of minerals in the clay material on the resulting local abutment. A series of experiments were conducted using a rectangular vertical wall abutments placed in a laboratory test flumes. In the experiments, two different geometric scales were utilized. This chapter presents the equipment, materials, procedures, and the error analysis performed to the experimental work conducted for the study.

4.2 Equipment

4.2.1 Test Flumes

The cohesive abutment scour experiments were conducted in the Hydraulics laboratory at the Engineering Research Center of Colorado State University. In the experiments, two different recirculating flumes were used. The first test flume was 200 ft. long, 8 ft. wide, and 4 ft. deep. The slope of this flume can be adjusted to different settings through motorized gear arrangement. Water is pumped into the flume from a sump tank using three different pipes ranging from 18 inch to 30 inch diameter through three different pumps ranging from 125 to 250 hp which can be operated separately or

in combination with each other. The flow pumped into the flume is first introduced into a head box. This flow goes through series of flow straightness, a honey-comb mesh, and then through a gravel screen before it is introduced into the upstream end of the flume. A wooden floating screen is used to absorb the surface waves of the in coming water flow. A short concrete ramp placed following the gravel screen was used to reduce the turbulent eddies induced at the flume entrance and to accelerate the development of the fully turbulent boundary layer. Because of using a subcritical flow in all the experiments, the flow was subject to down stream control by an adjustable vertical gate placed at the down stream end of the flume to control the water depth and maintain uniformity of the flow. The test section about 60 feet long and was followed by a sediment trap at the end to store the sediment coming out of the scour hole. The discharge into the flume was measured by a calibrated orifice meter installed on each of the pipelines supplying water into the flume. The second test flume used in the experiments was 4 feet wide by 35 feet long and 2 feet deep. The 4-foot flume is used in the experiments with half the dimensions used in the 8-foot flume to guarantee geometrical similarity. Water is pumped into the flume from a sump tank using 16 inch diameter pipe and first introduced into a head box. This flow goes through a gravel screen followed by a wooden floating screen to absorb the surface waves of the in coming water flow. A short concrete ramp placed following the gravel screen was used to reduce the turbulent eddies induced at the flume entrance and to accelerate the development of the fully turbulent boundary layer. Because of using a subcritical flow in all the experiments, the flow was subject to down stream control by a series of vertical

plates placed at the down stream end of the flume to control the water depth and maintain uniformity of the flow. The discharge into the flume was measured by a calibrated orifice meter installed on the pipeline supplying water into the flume.

4.2.2 Abutments

In the experiments, two different model abutment sizes were used. The first model abutment was 1.44 feet long, 0.72 feet wide, and 4.0 feet tall. The second abutment model was chosen with dimensions half of the first abutment and was 0.72 feet long, 0.36 feet wide, and 2.0 feet tall. The abutments were manufactured out of plywood with plexiglass upstream panels. A measuring tape was installed on the plexiglass panel to measure the depth of scour with time during the experiments by the aid of an inclined mirror attached to a handle.

4.2.3 Currentmeter

Velocities in the experiments were measured by the use of a Marsh-Mc Birney Model 2000 magnetic flowmeter. The accuracy of this current meter is rated by Marsh Mc Birney as $\pm 2\%$ and its operating range is from -0.05 ft/sec. to +19.99 ft/sec in the range from 32 to 160 degree Fahrenheit. The accuracy of velocity measurement using the same velocity measuring arrangement was reported by Abdou (1993). The Figure (4.1) shows the results of Abdou's velocity measurements in the same 8-foot wide by 200 feet long flume.

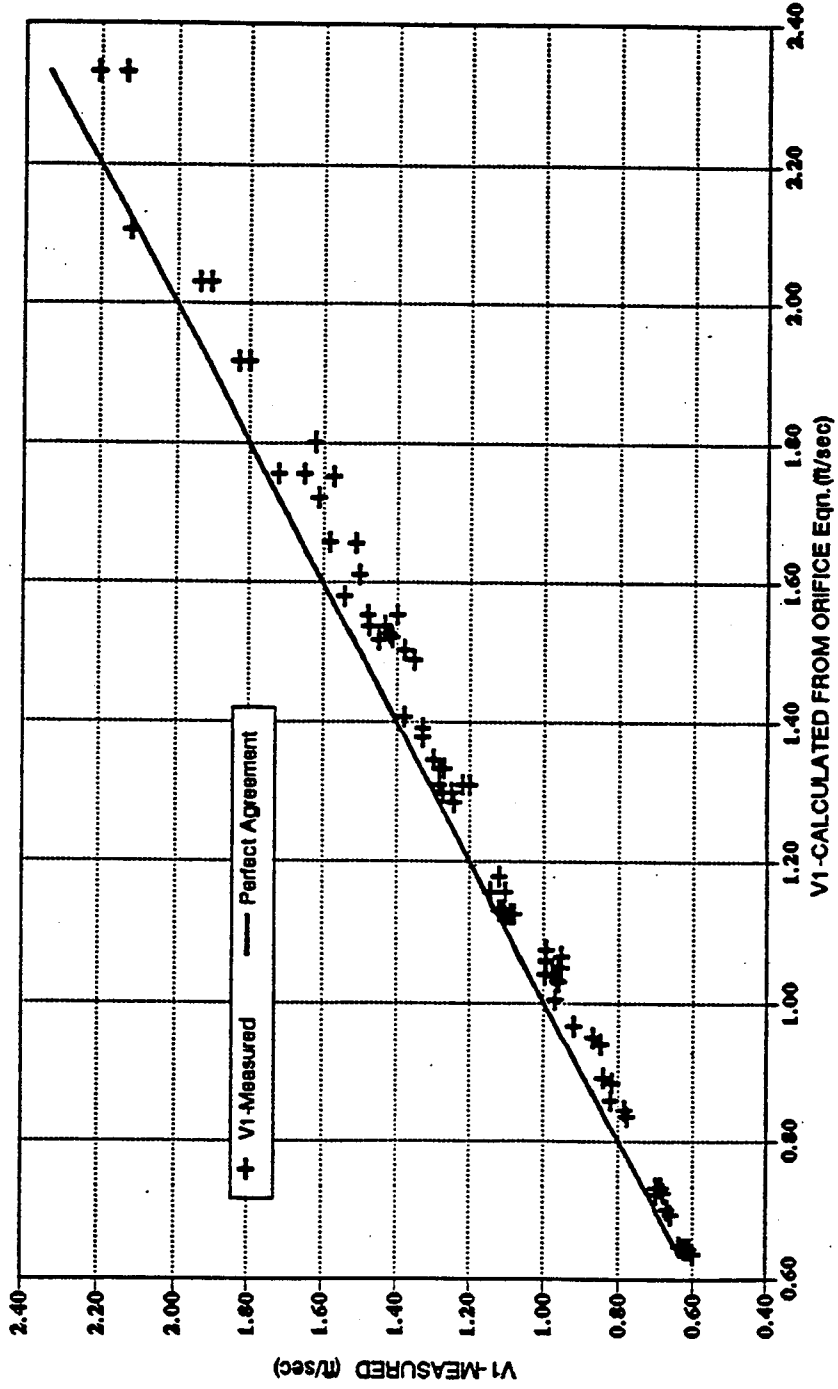


Figure (4.1) Measured and Calculated Velocities from Orifice Equation for the 8-foot Wide Flume (Abdou, 1993)

4.2.4 Torvane Gauge

Torvane gauge was used in measuring surface shear of the clay around the abutment. This instrument is a small cylinder equipped with several edges at the bottom and a dial gage at the top and is allowed to twist by hand. The sharp edges are pushed against the surface of the soil and then twisted until the soil beneath fails. The reading of the gage at this shear intensity is considered as the Torvane shear strength of the soil (kg/cm^2).

4.2.5 Point Gage

A point gage installed on a carriage running along the flume was used to measure the bed elevations, the scour hole geometry, and the water surface elevations. For velocity profile measurements, the point gage was also used to support the probe of the current meter. The resolution of the point gage used in the experiments was 0.001 feet.

4.3 Materials

4.3.1 Bed Material Proposed

The cohesive material used in the experiments were two different origin clays. The first of these clays was the Montmorillonite clay which was brought from Colorado State University's Nelson farm in Fort Collins. The second type of clay used in the experiments was the Kaolinite clay supplied by the Georgia company in Denver, Colorado. The clay samples used in the experiments were subjected to:

1. Different compactions

2. Different water contents
3. Different percentage of clay contents.

4.3.2 Compaction Tests

Compaction was computed from the same sample taken to calculate the water content. A cylinder open from both sides was used to take the sample from the surface of the compacted clay. After drying the sample, the weight of the dry clay divided by the volume of the cylinder will give the dry density of the clay. By dividing the dry density by the optimum density obtained from the proctor test, we will get the compaction of that clay sample. In 1933, R.R. Proctor presented the basis for the standard compaction test currently used. The objective of the test is to obtain the moisture content - specific weight relationship for a given compactive effort on a particular soil. The process of compacting begins with passing the soil through a No. 4 sieve, adding water, and compacting it into the mold in three layers with 25 blows per layer. The sample is then weighted. After repeating the process for different values of water content, a curve of dry unit weight versus. water content is drawn to define the location of maximum specific weight and the corresponding optimum moisture content. Figures 4.2 through 4.9 show the curves for Montmorillonite clay with 100%, 15%, 30%, and 40% clay contents and Kaolinite clay with 10%, 20%, 30%, and 50% clay contents.

4.3.3 Atterberg limits, Chemical, X-Ray Diffraction Tests

The liquid and plastic limits were proposed by A. Atterberg, a Swedish

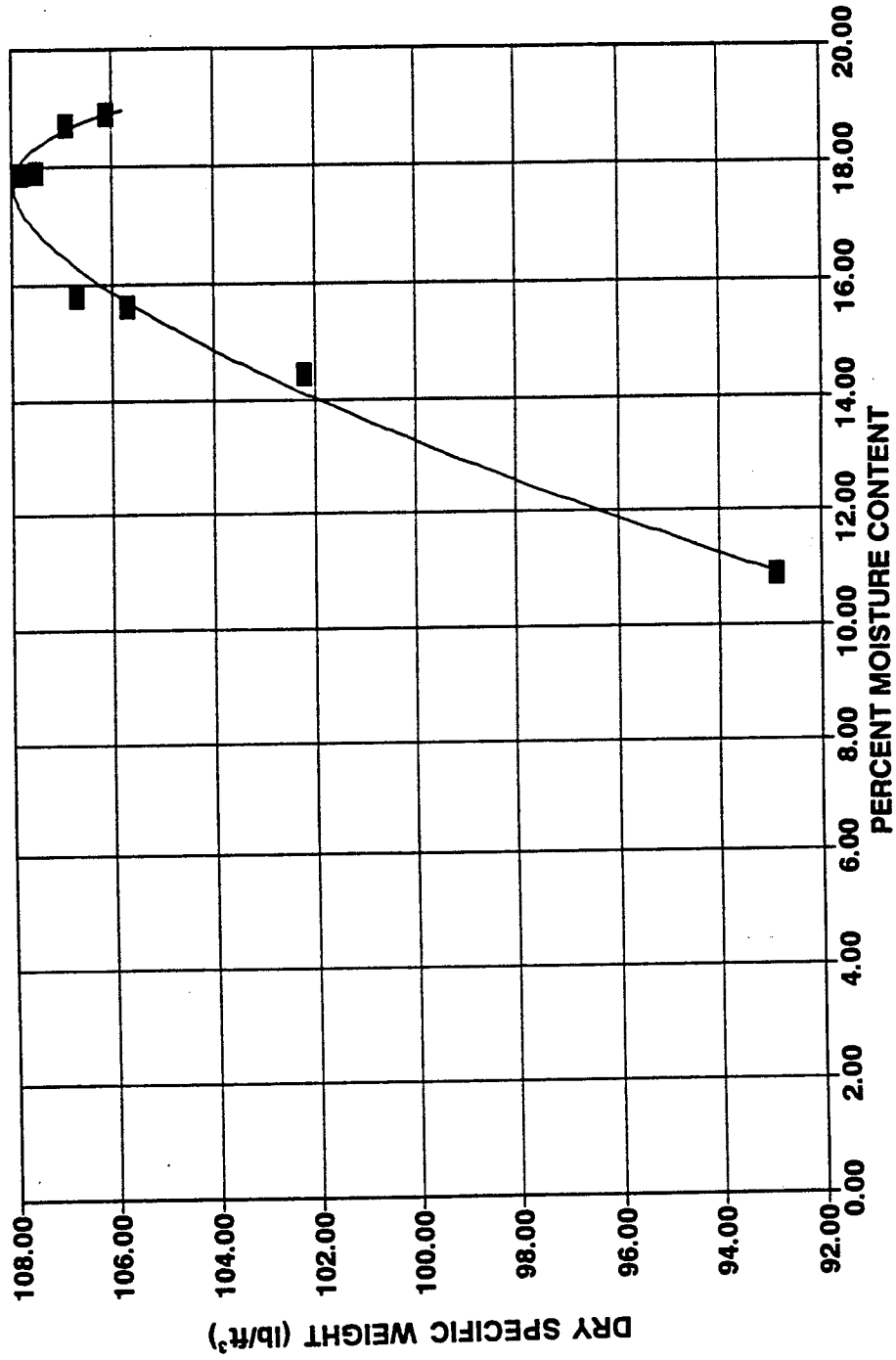


Figure (4.2) Moisture Content - Specific Weight Relationship from Compaction Test for 100 % Montmorillonite clay.

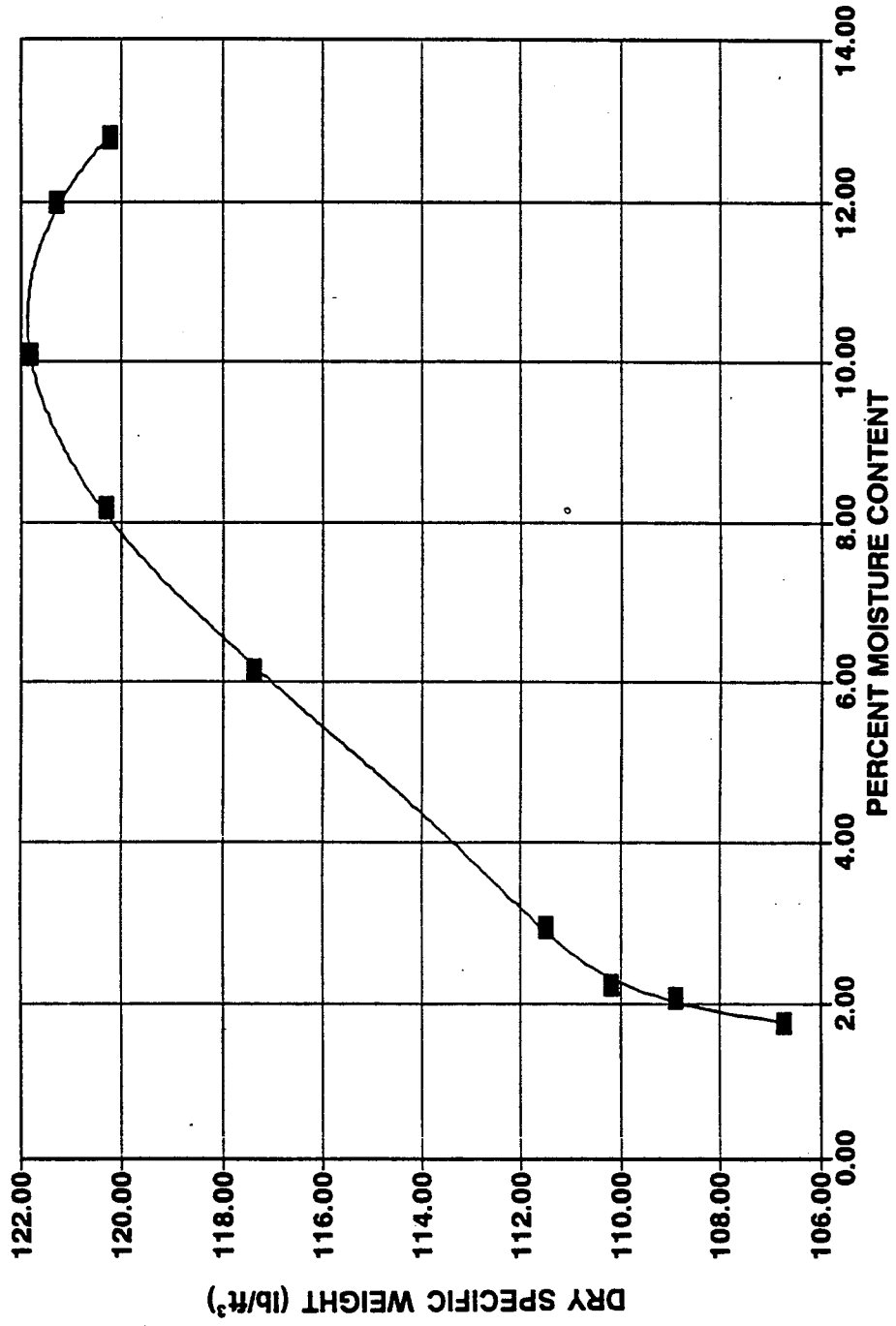


Figure (4.3) Moisture Content -Specific Weight Relationship from Compaction Test for 15 % Montmorillonite clay.

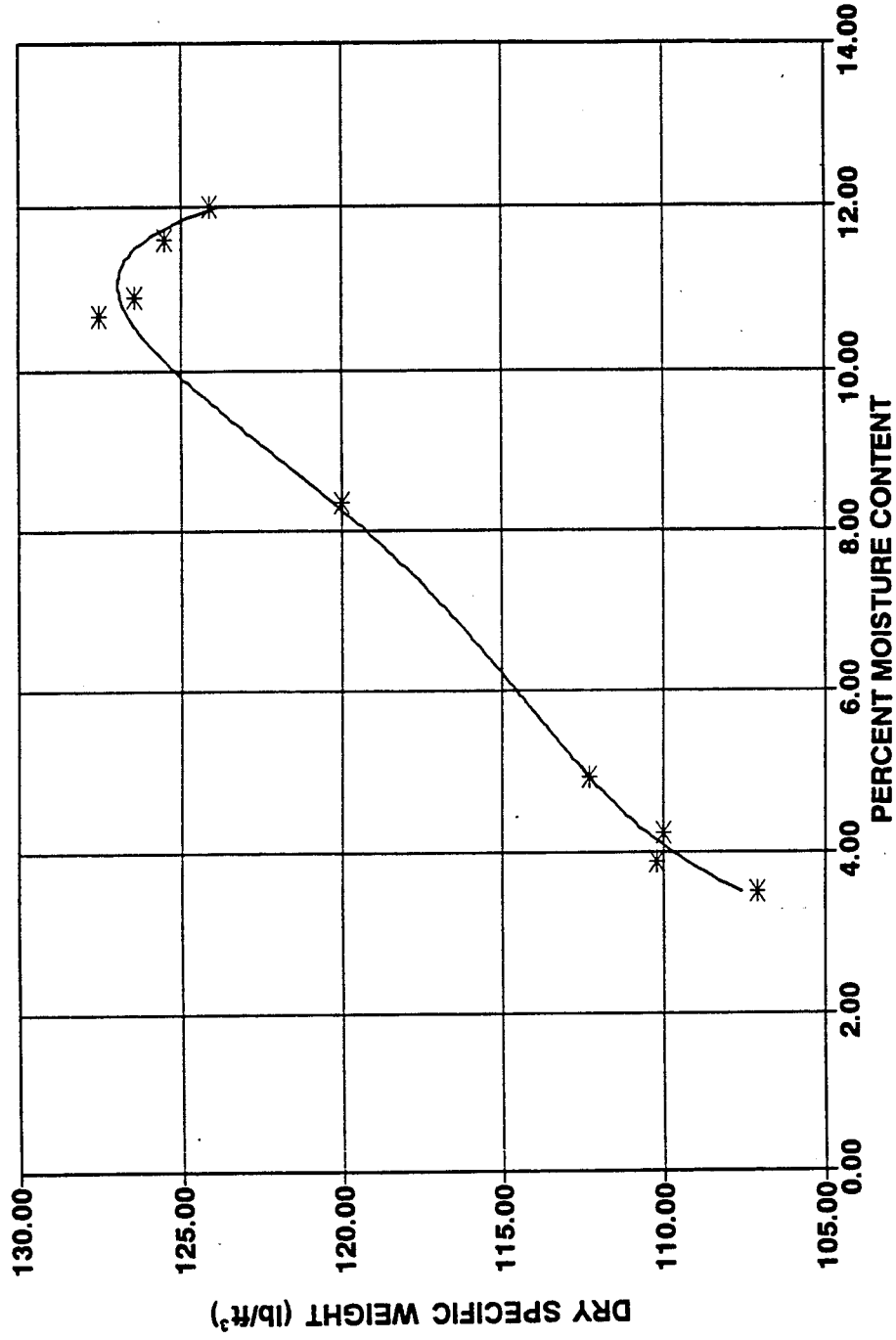


Figure (4.4) Moisture Content -Specific Weight Relationship from Compaction Test for 30 % Montmorillonite clay.

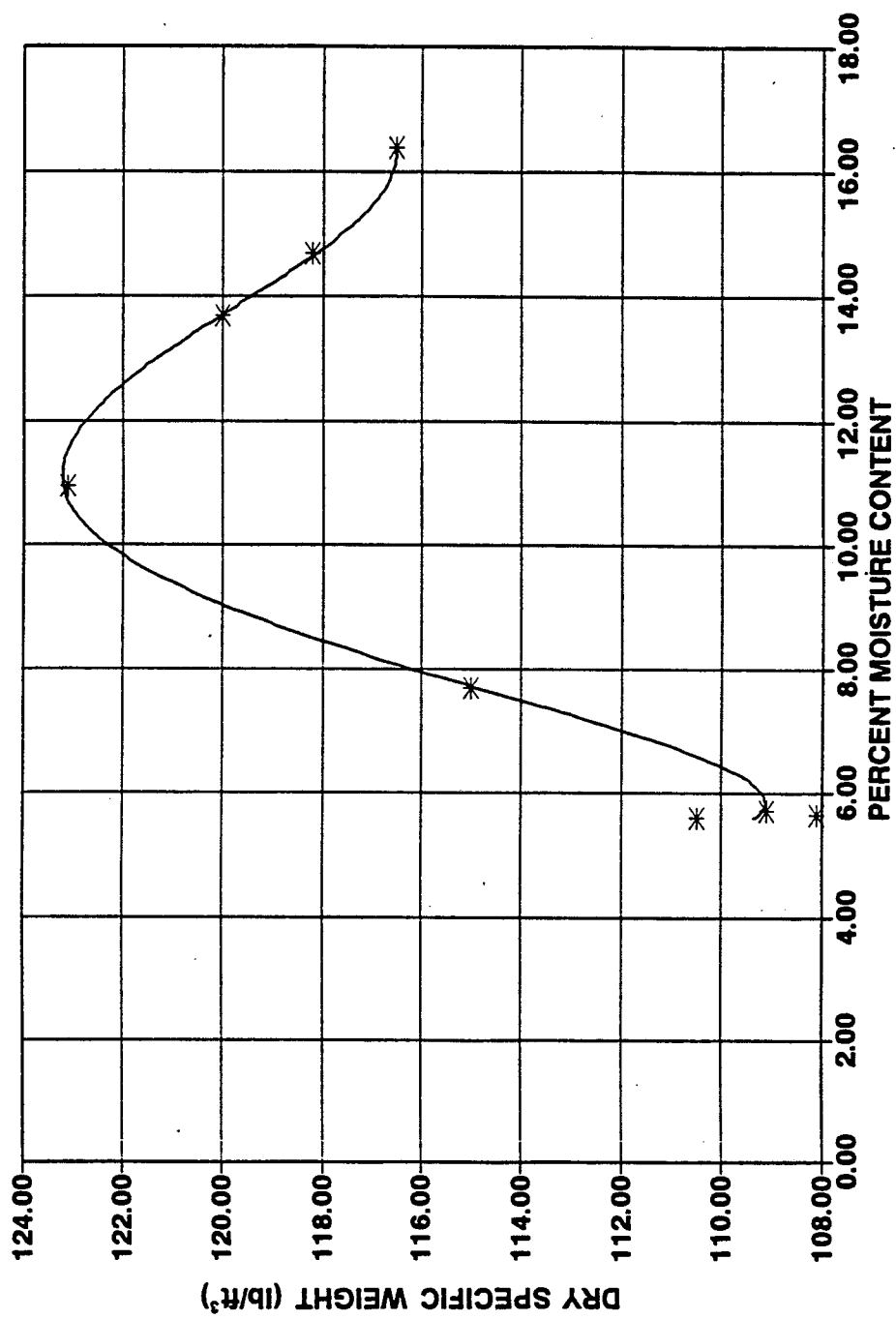


Figure (4.5) Moisture Content - Specific Weight Relationship from Compaction Test for 40 % Montmorillonite clay.

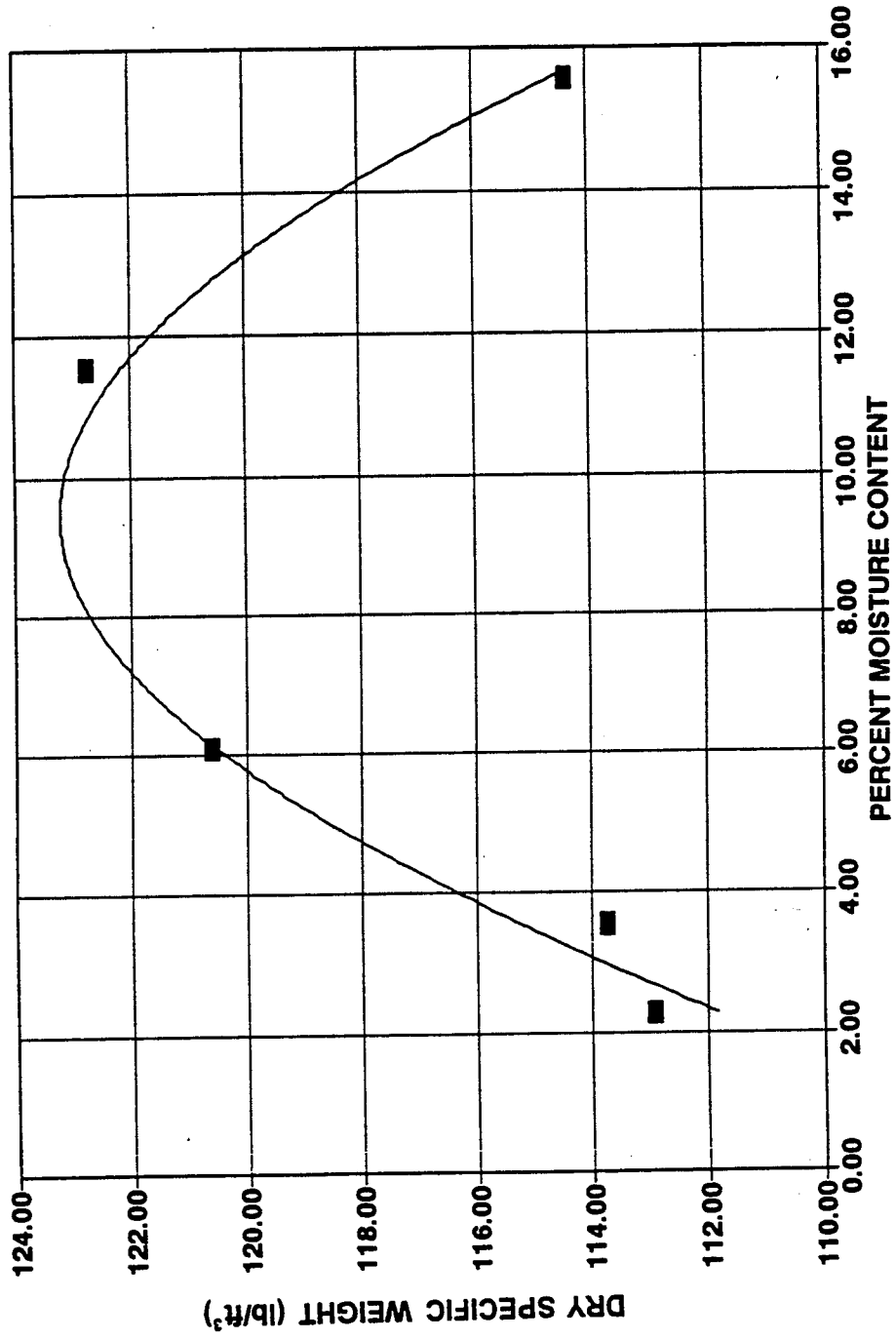


Figure (4.6) Moisture Content - Specific Weight Relationship from Compaction Tests for 10 % Kaolinite Clay

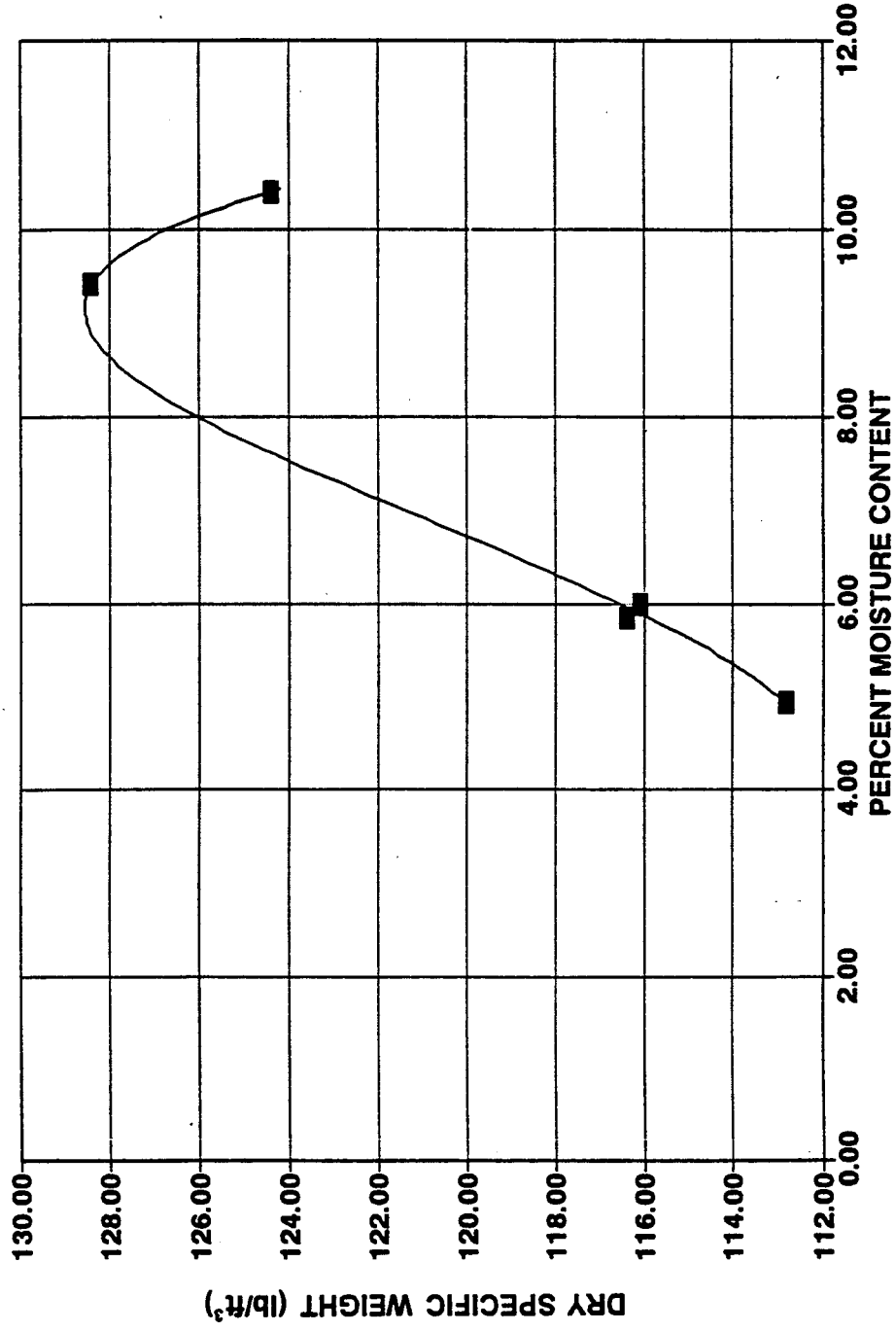


Figure (4.7) Moisture Content - Specific Weight Relationship from Compaction Tests for 20 % Kaolinite Clay

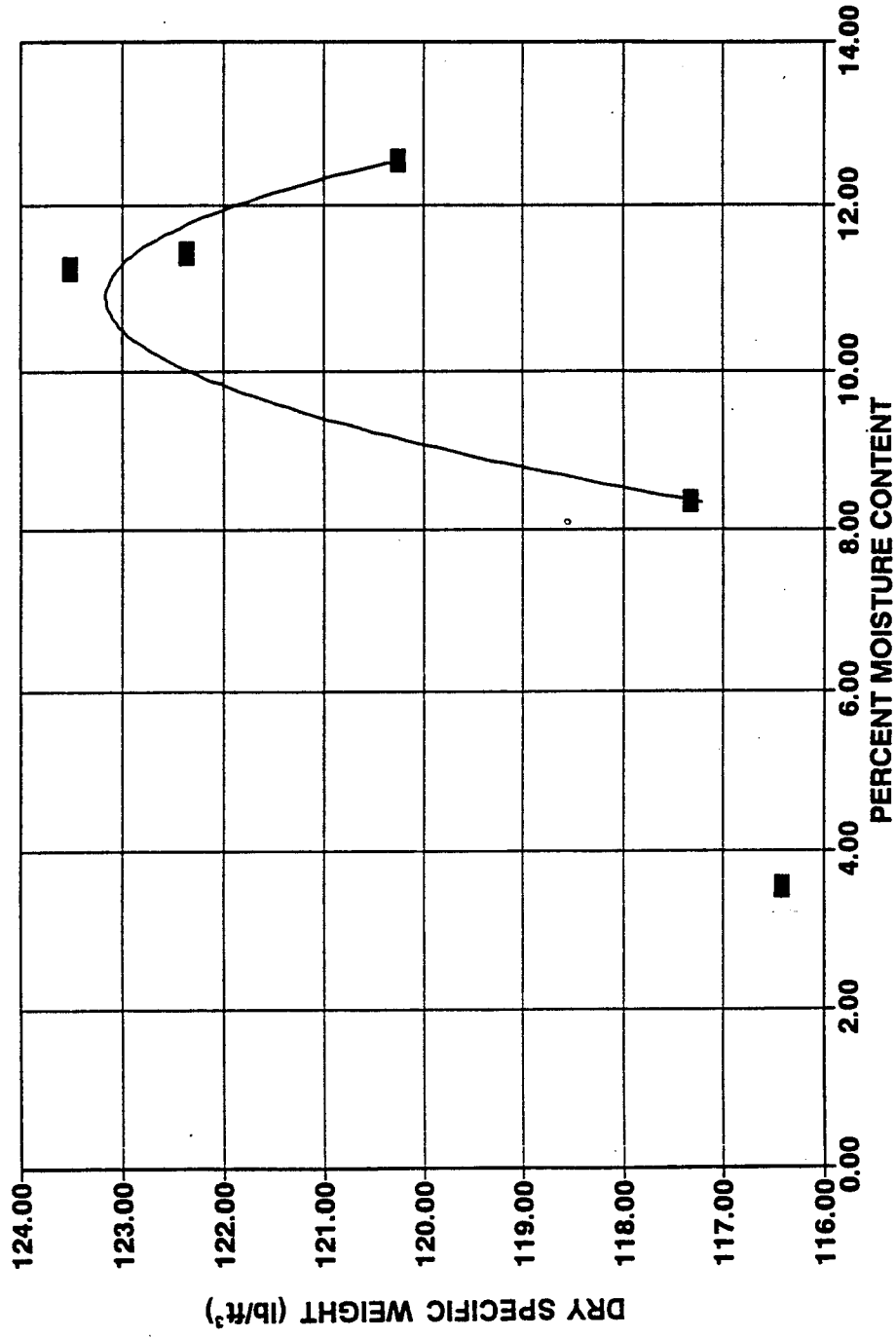


Figure (4.8) Moisture Content - Specific Weight Relationship from Compaction Tests for 30 % Kaolinite Clay

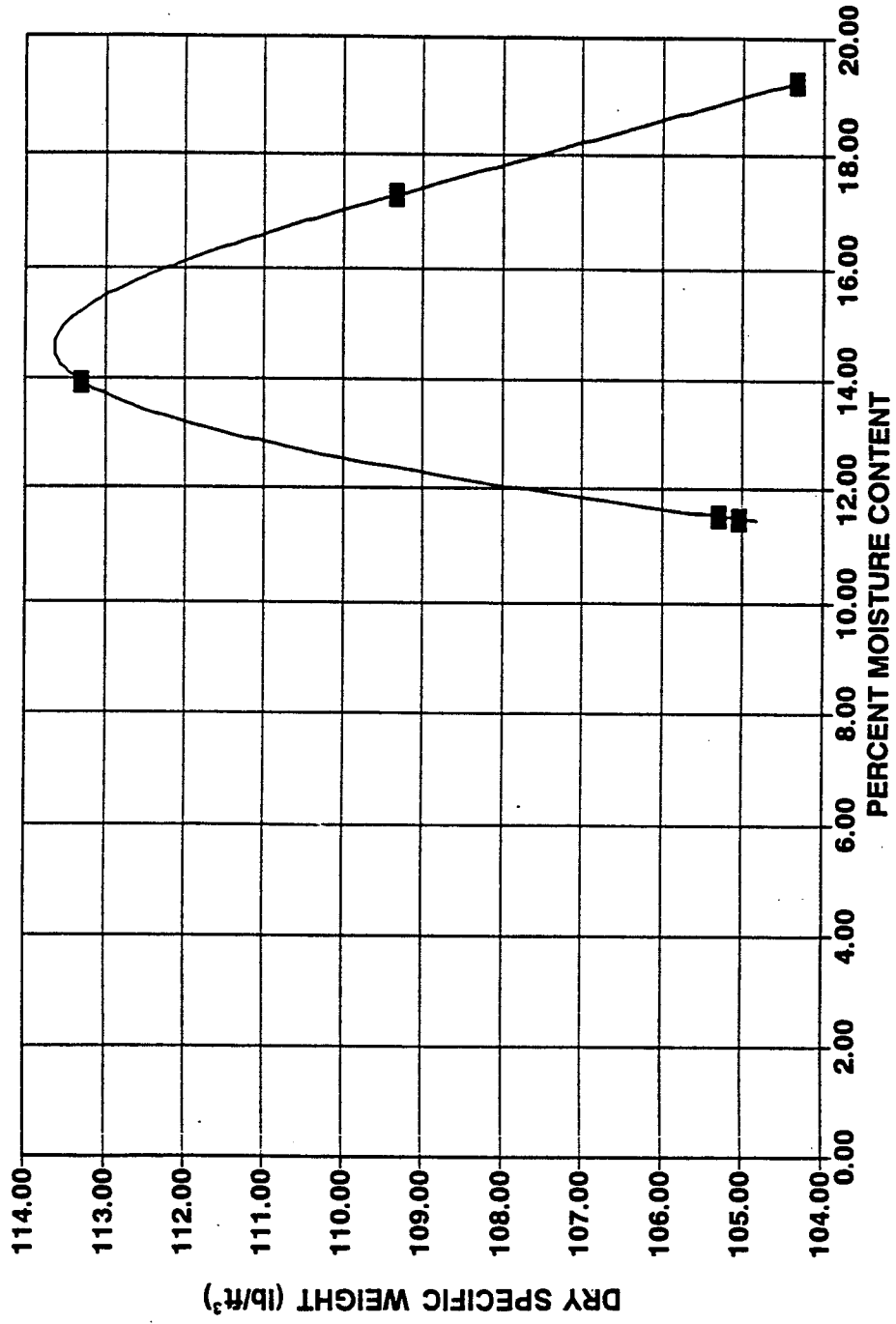


Figure (4.9) Moisture Content - Specific Weight Relationship from Compaction Tests for 50 % Kaolinite Clay

agricultural scientist. The definition of these limits are provided by (Bowles, 1986) as:

Liquid limit - moisture content below which the soil behaves as a plastic material. At this moisture content, the soil is on the verge of becoming a viscous fluid.

Plastic limit - moisture content below which the soil is non plastic.

Liquid and plastic limits are used for soil identification and classification and for strength correlations. The liquid and plastic limit measurements were performed at the Colorado State University Geotechnical laboratory. The results for Montmorillonite clay are as follows:

LIQUID LIMIT = 37.4

PLASTIC LIMIT = 17.8

PLASTICITY INDEX = 19.6

In order to have additional classification of the Montmorillonite clay, a sample was sent to Colorado State University Soil Testing Laboratory to determine the percentage of clay, silt, and sand in the soil and to chemically analyze the soil. The results are as follows:

Percentage of Sand = 40 %

Percentage of Silt = 30 %

Percentage of Clay = 30 %

Texture = Clay Loam Soil

Clay Mineral = Mostly Montmorillonite Clay

SAR (Sodium Adsorption Ratio) = 3.4

Na (Sodium) = 472 mg/kg

Ca (Calcium) = 489 mg/kg

Mg (Magnesium) = 258 mg/kg

Soil pH = 7.5

Kaolinite Clay used in the experiments was marketed under the commercial name of "Ajax P" and was supplied by Dry Branch Kaolin Company of Georgia. The physical and chemical properties of Kaolinite clay are:

Liquid Limit = 41

Plastic limit = 24

Plasticity Index = 17

Optimum Water Content = 24 %

Optimum Dry Density = 98 lb/ft³

Particle Size(<2 microns) = 92 %

Median Particle Size = .45 micron

325-Mesh Screen Residue(% max) = 0.03 %

pH (20 % solids) = 4.2

Moisture of natural clay = 3.0 %

Silicon Dioxide = 45.3 %

Aluminum Oxide = 38.4 %

Iron Oxide = 0.3 %

Titanium Dioxide = 1.4 %

Potassium Oxide = 0.04 %

Sodium Oxide = 0.3 %

Magnesium Oxide = 0.3 %

Calcium Oxide = 0.05 %

To identify the type of the clay minerals, X-ray diffraction test were performed at Colorado State University Soil Testing Laboratory. X-ray diffraction is the most widely used method for identification of fine-grained soil minerals and to study their crystal structure. A complete X-ray diffraction pattern consists of a series of reflections of different intensities. Each reflection must be assigned to some component of the sample. The test pattern may be compared directly with patterns for known materials (Mitchell, 1993) from the test results, the most common mineral in the clay is Montmorillonite.

4.3.4 Grain Size Analysis, Mechanical and Hydrometer Methods

Grain size analysis is used in the engineering classification of soils. Information obtained from grain-size analysis can be used to predict soil-water movement. The grain-size analysis is an attempt to determine the relative proportions of the different grain sizes that make up a given soil mass (Bowles, 1986). In this study, two methods were used: i) Mechanical grain size analysis for grain size larger than 0.075 mm (sieve No. 200); and ii) the Hydrometer method of grain size analysis for grain size smaller than 0.075 mm. For Montmorillonite clay, both tests were performed. The resulting classification was silty clay with low plasticity, $D_{50} = 0.012$ mm. These are graphically shown in Figure 4.10. The Mechanical grain size analysis was performed on medium sand which was used in sand-clay mixtures and the results are shown in Figure 4.11.

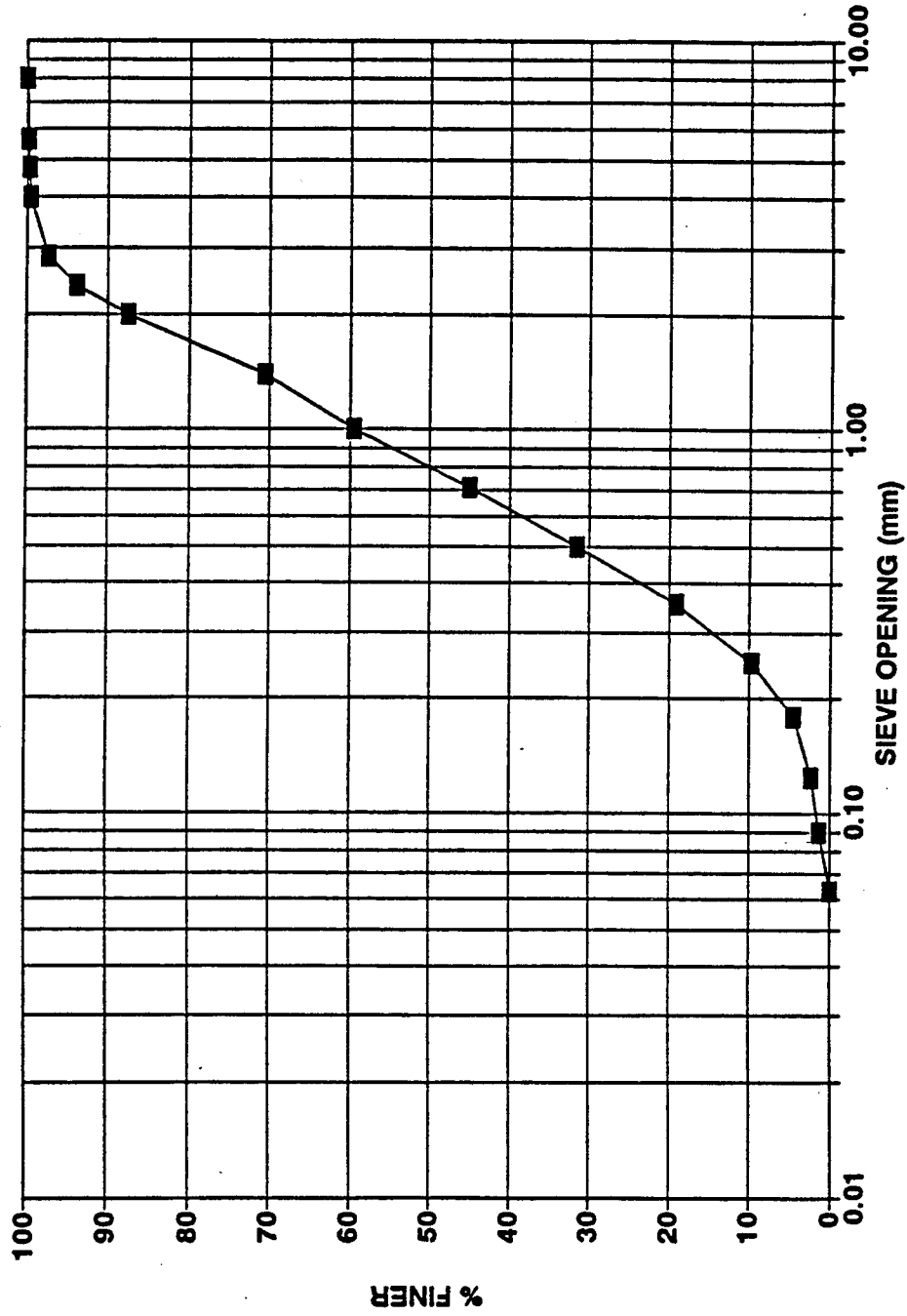


Figure (4.11) Grain Size Distribution for Medium Sand ($D_{50}=0.81$ mm, $\sigma_g=2.41$)

4.4 Procedures

In this section, the preparation of the soil is described. This is followed by the procedures of running the experiments. The last part is a detailed description of the individual measurements performed during each experiment.

4.4.1 Preparation of The Soil

The steps followed in preparing the soils used in the experiment are:

1. The locally obtained soil is sieved through #4 screen in order to obtain the uniform size soil and to achieve the homogeneous distribution of water content throughout the soil.
2. The soil is sampled and the exact water content is calculated by placing the sample in a drying oven for 24 hours and from the measuring the weight before and after drying, the exact water content is calculated.
3. Depending on the desired water content for the experiment, the required amount of soil for the abutment is weight and the corresponding dry weight is calculated. Next, from this dry weight, the amount of water by weight required to reach the desired water content is calculated. The difference between the amount of water present in the existing soil and the soil with the desired water content is added to the soil.
4. The soil is mixed with the added water until the water is distributed homogeneously and is left in a covered container for at least 24 hours to guarantee the even absorption and distribution throughout the soil.
5. The area around the abutment is prepared by removing the soil remaining from the

previous experiment. The area is dried and the water from previous experiment is completely drained.

6. The soil is mixed for a second time prior to placement around the abutment in several layers. Each layer is compacted by the standard compaction hammer to reach the desired compaction.
7. Prior to each experiment, the test flume slope is adjusted by leveling the surface of the bed. This is done by using a wood plank laid horizontally across the width of the flume and is attached to the movable instrument carriage through vertical connections and clamps. The carriage is moved along the length of the flume and the surface of the bed is set to the desired elevation.
8. After leveling the bed around the abutment and along the flume surface soil, samples are taken using 2-inch diameter hollow brass cylinder tubes. The tubes are pushed into the soil until the top surface of the cylinder is leveled with the bed. Samples are then removed and taken to the sediment laboratory and weighted. Following the oven drying, they are weighted again and the water content and the compaction of the soil are computed. The compaction is calculated by dividing the dry density of the sample by the optimum dry density obtained from the compaction test (Proctor test) that was done in the Soil Mechanics Laboratory at Colorado State University along with other soil tests.
9. The shear strength of the soil (Kg/Cm^2) is measured prior to each experiment by using the Torvane gauge by applying it to the surface of soil.
10. The soil surface in the vicinity of the abutment was covered to avoid any changes in the water content. The experiment was performed as soon as possible (usually within

16 hours) to assure that the measured initial conditions applied.

11. The procedures for experiments using a mixture of clay and sand is slightly modified. For these experiments, the percentage of sand to be added to the clay was determined by dry weight. The rest of the preparation procedure remains unchanged.

4.4.2 Running The Experiments

The procedures of performing each experiment are explained in details in the following steps:

1. Initial bed elevations are measured by the use of a point gage which is mounted on a movable carriage running along the flume. These measurements are used for calculating scour depth and to make sure that no bed movement took place during the experiments to satisfy the clear-water conditions. Also, the initial bed elevations are used in calculating the depth of water flow.
2. Prior to running the water in the flume, the intake sump is filled from the main sump. The pump is started and the water is introduced into the flume very slowly by opening the valve placed in the supply pipelines. The gate placed at the downstream end of the test flume is kept closed while filling the flume with water up to about 12 inch depth.
3. The valve controlling the flow discharge is gradually opened with the opening of the gate. The valve opening continued until the desired discharge is reached (which was determined from the orifice meter installed on the pipeline coming from the pump). Once the discharge is set, the gate is adjusted to obtain the desired flow depth. For the

0.72 feet wide abutment, the depth of flow was modified at 0.90 feet (+/- .10 feet). For the 0.36 feet wide abutment, the depth was set at 0.45 feet (+/- 0.10 feet).

4. After establishing the flow depth and discharge, the point gage mounted on the movable carriage was used to measure the water surface elevation along the flume. Throughout the duration of the experiment, the scour depth at each abutment was measured through a plexiglass panel placed in the abutment face. A simple periscope manufactured by the use of an inclined mirror and a measuring tape mounted on the abutment face was used in observing the development of scour with time throughout the duration of the experiment to establish the rate of scour.

5. The approach velocity is measured at two sections located 3 feet and 6 feet upstream of each abutment by a magnetic currentmeter mounted on a point gage. The vertical velocity profiles are measured at 0.35 feet, 0.72 feet, 2.0 feet, and 4.0 feet from the left wall of the flume across the channel. For each vertical velocity profile, 10 measurements are taken at each station at equal distances. For the 0.36 feet wide abutment (one-half of the previous abutment width), the location of stations across the channel as well as the vertical measurement points are scaled down in half to maintain a geometric similarity.

6. The duration of each experiment was kept 12 hours (or at least was 90 percent) to guarantee the development of maximum scour and stabilization of the scour hole.

7. At the end of each experiment, the valve placed in the supply pipelines is closed very slowly (up to 40 minutes) while simultaneously closing the downstream gate in order to avoid any disturbances. After closing the valve, the pump is turned off and the flume

is drained for at least 24 hours.

8. Using the point gage, the final bed elevations around the abutments are measured. These final bed elevation measurements are compared with the initial measurements to determine the shape of the scour hole and the maximum scour depth.
9. The volume of scour is measured by two methods. In the first method, the bed elevation measurements are used in calculating the volume of scour. In the second method, the volume of scour is measured by sealing off the scour hole and filling it with water of a known volume.
10. A sample from the scour hole is taken to the laboratory to calculate the final water content of the experiment by weighing the sample, oven dry it, and weight it again and the difference in weight will be used to calculate the percentage of final water content.
11. Finally, a number of photographs of the scour hole and the surrounding abutment area is taken for documentation purposes.

4.4.3 Individual Measurements

To achieve the goals of the experimental program, a series of measurements are taken during the experiment. These measurements are listed as:

Flow Property Measurements:

1. Flow discharge;
2. Flow depth;
3. Velocity;
4. Slope;

5. Flow temperature.

Scour Measurements:

6. Time rate of scour;

7. Initial and final bed topographies around abutments;

8. Volume of scour hole;

Soil Property Measurements:

9. Water content of clay

The details of each measurement is explained in the following paragraphs:

1. Flow Discharge (cfs)

The discharge is measured by using a mercury manometer to read the difference in pressure head upstream and downstream of a calibrated orifice meter installed on the discharge pipeline. By knowing the difference in head (ΔH) in inches, the discharge will be calculated in cubic feet per second by using the equation:

$$Q = 5.29 (\Delta H)^{1/2}$$

The flow discharge obtained from this equation was checked by integrated the measured vertical velocity distributions across the channel along the flume. The results of these measurements indicated a close agreement with a maximum of 5 percent discrepancy between the two values. Figure (4.1) demonstrate the comparison of measured and computed discharge values in the 8 feet flume setup used in the present study.

2. Flow Depth (ft)

A point gage is used to measure the bed surface and the water surface elevations.

The accuracy of the point gage measurements are within 0.01 feet. The flow depth is computed as the difference between the water surface and bed elevations averaged across the channel at 6 locations. These locations coincide with the locations used in calculating the average approach velocity.

3. Velocity (ft/sec)

The approach velocity for the 0.72 feet wide abutment is measured at 3 feet and 6 feet upstream from the face of the abutment. The vertical velocity profiles are measured in four lateral locations at each section, at 0.35 feet, 0.72 feet, 2.0 feet, and 4.0 feet across the channel. The vertical velocity measurements are made at 10 equal points throughout the depth of the flow as shown in Figure 4.12. The average approach velocity is then calculated by taking the average of all the vertically averaged velocity measurements at 0.35 feet, 0.72 feet, and 2.0 feet across the channel for the 3 feet and 6 feet sections (depth, width, and distance integrated average). The measurement at the center of the channel (at 4.0 feet across the channel) location is used for checking the discharge. For the 4.0 feet wide, velocity measurements are carried out at one half of the previous dimensions since the width of the abutment (0.36 feet wide) is also half the width of the abutment used in the 8.0 feet flume as shown in Figure (4.12).

4. Slope

The slope of the flume and of the water surface are measured along the flume using the point gage and the data obtained from leveling the entire length of the flume

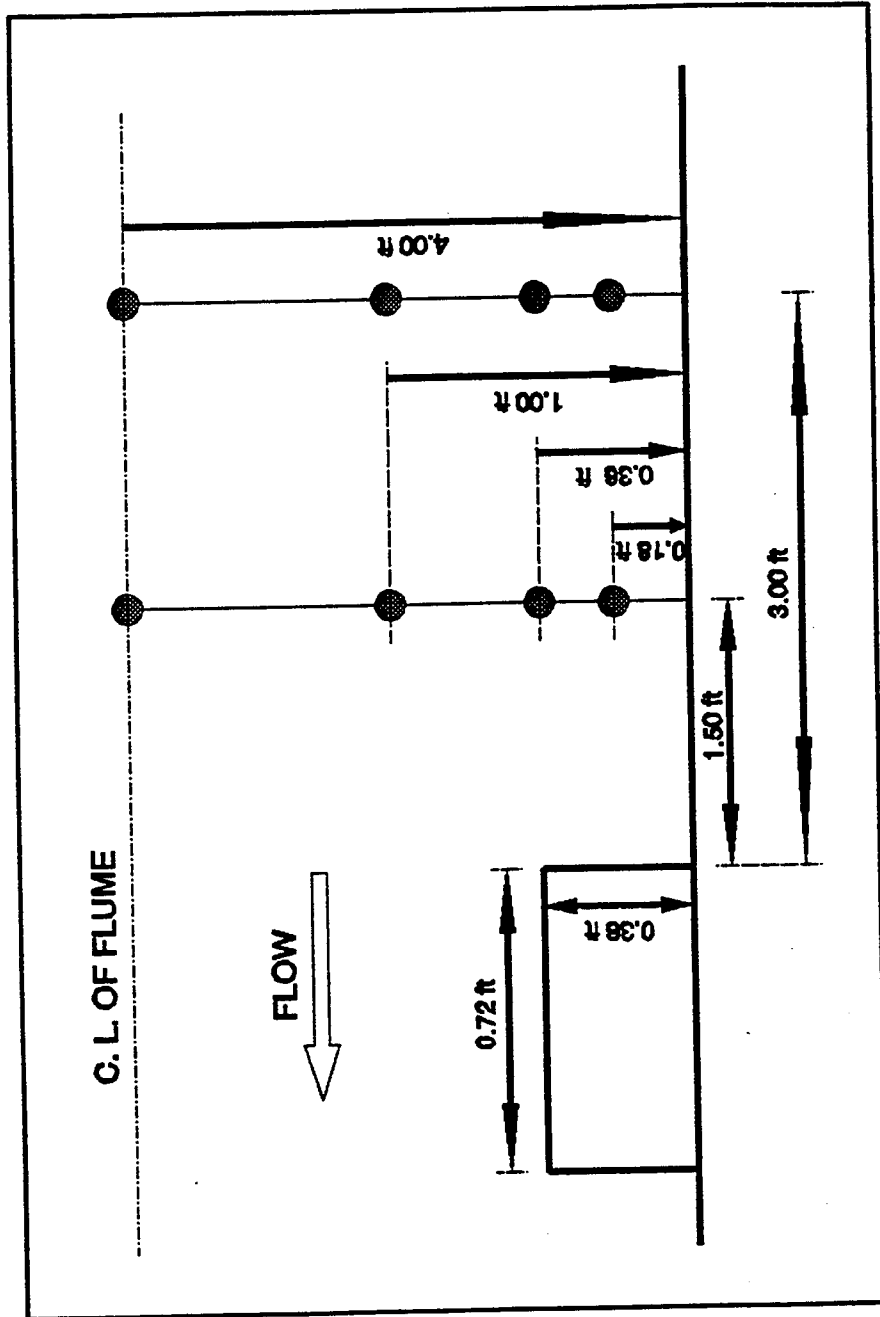


Figure (4.12) Locations of Measured Approach Velocity for the 0.36 foot Wide Abutment in the 8 feet Flume

by surveying equipment. The least-square method is used to fit the best line for each of the bed and of the water surface and to calculate the slope for each from the best fitted lines.

5. Flow Temperature

The water flow temperature is measured for each experiment using a glass mercury thermometer. The temperatures recorded in the experiments ranged from 54 to 68 degrees Fahrenheit.

6. Time Rate of Scour

The depth of scour is measured during the experiments at various time intervals to determine the rate of scour and to determine when the establishment of maximum scour depth and geometry. The scour depth through time is measured by the use of a measuring tape placed on the clear plexiglass and then by the aid of a simple periscope manufactured using an inclined mirror and a source of light.

7. Initial and Final Bed Topographies Around Abutments

Point gage is used to measure the initial bed elevation in the vicinity of each abutment. After scour experiments, the final bed topography measurements are conducted within 24 hours. The bed elevation measurements are made at the approach of each abutment and, more intensively, in the scour hole region. From these measurements, the maximum depth of scour (by calculating the difference between the

bed elevation in the channel side and the lowest point in the scour hole), the shape of the scour hole, and the slopes of the scour sides are determined. Also, validity of clear water scour conditions are checked.

8. Volume of Scour Hole

The volume of scour is measured by two methods. In the first method, the bed elevation measurements are used in calculating the volume of scour. In the second method, the volume of scour is measured by sealing off the scour hole and filling it with water of a known volume.

9. Water Content in Clay

After compacting and leveling the surface around the abutment, a 2-inch diameter brass cylinder open on both sides with a known volume of 87.36 cubic centimeters is pushed into the soil surface until level with the surface. The soil sample is then removed and weighted before and after oven drying. By computing the difference between the wet and dry weight of the sample, the water content can be determined by dividing the weight of water in the sample by the dry weight of the clay.

CHAPTER 5

ANALYSIS OF RESULTS

5.1 Introduction

This chapter discusses the effects of initial water content, compaction, and clay content on the local scour geometry around vertical wall abutment for the case of clear water scour. In the majority of experiments, except for the stream velocity, all other parameters were kept constant. These experiments were conducted in two geometrically similar settings of the constant parameters. The first setting uses an abutment length of 1.44 feet (in the direction of flow) and a width of 0.72 feet (perpendicular to flow) with a flow depth of 0.90 feet (+/- 0.10 feet). The second setting reduces the dimensions of the first setting by half in order to be geometrically similar. In each setting, the only variable which is allowed to change in the cohesive scour experiments is the flow velocity. This arrangement makes the Froude number a good dimensionless indicator of the flow condition. In reporting results, Froude number is used to analyze maximum scour depth for different initial clay conditions. The complete experimental records of this study are presented as a part of the data supplement for the project No. DTFH 61-91-C-00004 entitled " Effect of Sediment Gradation and Cohesion on Scour " for the U.S. Federal Highway Administration. All experiments were carried out under uniform (or near uniform) flow conditions and are classified as clear-water scour. The

experimental program was organized under three different sets: i) 8-foot flume Montmorillonite clay experiments; ii) 4-foot flume Montmorillonite clay experiments; iii) 8-foot flume Kaolinite clay experiments. The first and second set of experiments are conducted under geometrically similar settings. Also, the second set extends the range of Froude numbers. The third set utilizes the same geometric dimensions as the second set but introduces a different origin clay. The data from the experimental program are summarized in Tables 5.1 through 5.6. In tables 5.1 through 5.3, the parameters defining the flow and clay characteristics and the final scour measurements are reported. Parameters for these tables are: discharge (Q), percent clay content (CC), percent initial water content (IWC), dry density (DD), percent compaction (C), Torvane shear strength (TS), depth of flow (y), average approach velocity (U), scour depth (d_s), scour volume (V_s), temperature (T), duration of experiment (t).

5.2 Dimensional Analysis

Dimensional analysis utilized in this dissertation is based on a technique that has been used by researchers in many fields to group the variables and put it in a usable form using the Buckingham II- theorem. This technique is used to formulate a functional relationship between the maximum depth of abutment scour and the major affecting variables which can be expressed as:

$$d_s = f (d_s, y, a, L, U, WC, C, CC, CT, TS, T, t, g, \alpha, \phi, \rho, \nu) \quad (5.1)$$

where

$$d_s = \text{Depth of scour in cohesive sediment (ft)}$$

Table (5.1). Set No.1 Experiments Utilizing Montmorillonite Clay in the 8-foot Flume with 0.72 feet Abutment Width (39 Runs)

RUN ID	FLOW DISCHARGE Q (cfs)	% CLAY CONTENT CC (%)	% INITIAL W.C. (H.C.%)	DRY DENSITY DD (lb/ft ³)	% OF COMPAC. C (%)	TORVANE SHEAR TS (lb/ft ²)	FLOW DEPTH Y (ft)	APPROACH VELOCITY U (ft/s)	SCOUR DEPTH (ft)	SCOUR VOLUME V _{sc} (ft ³)	FLOW TEMP T (°F)	EXP DURAT t (hr)
8-12-MA	5.10	0	4.00	109.63	91.36	76.34	1.020	0.56	0.067	0.064	63	12
8-13-MA	6.50	0	4.00	109.63	91.36	76.34	1.025	0.73	0.190	0.145	63	12
8-14-MA	6.25	0	4.00	109.63	91.36	76.34	1.050	0.68	0.155	0.117	63	12
8-15-MA	7.00	0	4.00	109.63	91.36	76.34	1.014	0.77	0.196	0.148	63	12
8-16-MA	8.10	0	4.00	109.63	91.36	76.34	1.045	0.82	0.225	0.173	63	12
8-17-MA	9.08	0	4.00	109.63	91.36	76.34	1.058	0.94	0.362	0.321	63	12
8-18-MA	10.44	0	4.00	109.63	91.36	76.34	1.070	1.04	0.560	0.498	63	12
8-19-MA	8.56	0	4.00	109.63	91.36	76.34	1.074	0.83	0.286	0.120	63	12
8-20-MA	6.10	30	5.50	94.20	74.23	192.22	0.903	0.56	0.290	0.198	63	12
8-21-MA	5.20	30	5.50	94.20	74.23	192.22	0.926	0.53	0.088	0.072	63	10
8-22-MA	7.15	30	5.50	94.20	74.23	192.22	0.971	0.69	0.160	0.124	63	10
8-23-MA	8.20	30	5.50	94.20	74.23	192.22	0.949	0.75	0.200	0.152	63	10
8-24-MA	9.30	30	5.50	94.20	74.23	192.22	1.006	0.89	0.215	0.162	62	10
8-25-MA	11.00	30	5.50	94.20	74.23	192.22	0.979	1.12	0.465	0.388	62	10
8-26-MA	13.00	30	5.50	94.20	74.23	192.22	1.008	1.39	0.670	0.893	62	10
8-27-MA	11.00	100	29.73	92.48	85.79	204.39	0.805	1.47	0.000	0.000	56	12
8-27-MB	11.00	100	13.12	78.94	73.23	919.74	0.845	1.24	0.360	0.318	56	12
8-28-MA	18.30	100	27.48	92.48	85.79	306.58	0.813	2.31	0.000	0.000	54	13
8-28-MB	18.30	100	38.05	84.99	78.84	61.32	0.795	2.12	0.350	0.088	54	13

Table (5.1). (Continued)

RUN ID	FLOW DISCHARGE Q (cfs)	% CLAY CONTENT CC (%)	% INITIAL W.C. (%)	DRY DENSITY (pcf)	% OF COMPACT C (%)	TORVANE SHEAR τ_s (lb/ft ²)	FLOW DEPTH y (ft)	APPROACH VELOCITY U (ft/s)	SCOUR DEPTH (ft)	SCOUR VOLUME Y _{sc} (ft ³)	FLOW TEMP T (F)	EXP DURAT t (hr)
8-29-MA	28.00	100	27.48	68.02	63.10	306.58	0.802	2.85	0.000	0.000	54	10
8-29-MB	28.00	100	38.05	71.15	66.00	61.32	0.847	2.21	0.530	0.300	54	10
8-30-MA	13.00	100	16.70	79.25	73.52	981.06	0.827	1.80	0.817	0.547	55	12
8-30-MB	13.00	100	20.80	80.75	74.91	919.74	0.853	1.57	0.400	0.141	55	12
8-31-MA	13.00	100	17.72	62.40	57.88	367.90	0.843	1.48	1.160	1.907	54	10
8-31-MB	13.00	100	13.40	69.26	64.25	224.83	0.895	1.36	0.890	1.695	54	10
8-32-MA	9.00	40	8.70	98.59	80.01	245.26	0.827	1.15	0.460	0.371	56	10
8-32-MB	9.00	15	6.08	105.46	86.54	122.63	0.867	1.03	0.350	0.318	56	10
8-33-MA	11.00	40	6.36	84.30	68.41	245.26	0.830	1.43	0.910	0.989	55	12
8-33-MB	11.00	15	4.00	89.29	73.27	122.63	0.868	1.28	0.640	0.848	55	12
8-34-MA	15.00	40	2.42	88.55	71.86	204.39	0.763	2.12	1.460	3.355	56	11
8-34-MB	15.00	15	3.05	93.60	76.81	163.51	0.780	1.83	1.200	2.755	56	11
8-35-MA	15.00	100	17.11	81.43	75.54	1021.93	0.805	2.07	0.650	0.918	56	11
8-35-MB	15.00	100	16.36	78.56	72.88	715.35	0.800	1.95	1.170	1.589	56	11
8-36-MA	17.70	100	34.41	86.05	79.82	61.32	0.807	2.75	0.510	0.583	59	12
8-36-MB	17.70	100	44.57	77.31	71.72	20.44	0.755	2.62	0.780	0.918	59	12
8-37-MA	26.00	100	35.71	84.99	78.84	61.32	1.005	2.99	0.270	0.085	59	11
8-37-MB	26.00	100	45.26	82.87	76.87	20.44	0.958	3.12	0.890	1.554	59	11
8-38-MA	33.50	100	36.75	83.55	77.50	61.32	1.153	3.27	0.300	0.159	60	12
8-38-MB	33.50	100	44.44	77.13	71.55	20.44	1.050	3.41	1.110	3.390	60	12

Table (5.2). Set No.2 Experiments Utilizing Montmorillonite Clay In the 4 and 8 feet Flumes with 0.36 feet Abutment Width (49 Runs)

RUN ID	FLOW DISCHARGE Q (cfs)	% CLAY CONTENT CC (%)	% INITIAL W.C. (%)	DRY DENSITY DD (lb/ft ³)	% OF COMPAC. C (%)	TORVANE SHEAR TS (lb/ft ²)	FLOW DEPTH Y (ft)	APPROACH VELOCITY U (ft/s)	SCOUR DEPTH (ft)	SCOUR VOLUME V _{sc} (ft ³)	FLOW TEMP T (F)	EXP DURAT T (hr)
4-39	1.30	100	20.17	84.99	78.84	715.35	0.459	0.49	0.083	0.004	56	12
4-40	2.10	100	19.67	85.36	79.18	654.04	0.470	0.89	0.211	0.041	56	12
4-41	1.70	100	19.82	81.06	75.19	715.35	0.478	0.65	0.136	0.018	56	12
4-42	2.50	100	19.57	82.12	76.18	837.99	0.471	1.18	0.359	0.148	56	12
4-43	1.40	100	20.00	67.86	62.95	273.88	0.442	0.54	0.096	0.009	56	12
4-44	1.97	100	19.60	71.07	65.93	286.14	0.459	0.84	0.208	0.039	57	12
4-45	2.40	100	20.20	70.70	65.58	294.32	0.458	1.15	0.450	0.300	57	12
4-46	3.20	100	19.51	87.86	81.50	1379.61	0.422	1.65	0.552	0.335	57	12
4-47	1.75	100	12.26	75.69	70.21	776.67	0.429	0.78	0.266	0.120	57	12
4-48	1.30	100	12.26	72.85	67.58	756.23	0.424	0.63	0.162	0.044	57	12
4-49	1.95	100	11.06	71.07	65.93	572.28	0.432	1.02	0.475	0.343	57	12
4-50	2.35	100	10.81	71.14	65.99	490.53	0.443	1.22	0.634	0.618	57	12
4-51	1.60	15	6.23	91.79	75.32	114.46	0.425	0.73	0.103	0.015	57	12
4-52	2.50	15	6.23	91.79	75.32	114.46	0.429	1.24	0.425	0.406	57	12
4-53	1.90	15	6.23	91.79	75.32	114.46	0.426	1.00	0.234	0.067	57	12
4-54	1.25	15	6.23	91.79	75.32	114.46	0.413	0.55	0.100	0.004	57	12
4-55	3.10	15	6.23	91.79	75.32	114.46	0.426	1.66	0.685	0.901	57	12
4-56	1.35	40	11.24	92.16	74.79	572.28	0.434	0.65	0.099	0.004	56	12
4-57	1.70	40	11.24	92.16	74.79	572.28	0.423	0.74	0.180	0.030	56	12
4-58	2.00	40	11.24	92.16	74.79	572.28	0.444	1.01	0.314	0.113	57	12
4-59	2.30	40	11.24	92.16	74.79	572.28	0.428	1.17	0.425	0.194	56	12
4-60	2.90	40	11.24	92.16	74.79	572.28	0.423	1.61	0.448	0.251	55	12
4-61	2.85	100	35.57	85.49	79.30	98.11	0.424	1.58	0.266	0.021	56	12
4-62	3.60	100	30.43	88.11	81.73	102.19	0.430	2.02	0.118	0.067	56	12
4-63	4.25	100	29.03	88.55	82.14	114.46	0.438	2.24	0.110	0.078	56	12

Table (5.2). (Continued)

RUN ID	FLOW DISCHARGE Q (cfs)	% CLAY CONTENT GC (%)	% INITIAL W.C. (%)	DRY DENSITY DD (pcf)	% OF COMPACT C (%)	TORVANE SHEAR SS (psi)	FLOW DEPTH Z (ft)	APPROACH VELOCITY U (ft/s)	SCOUR DEPTH dsr (ft)	SCOUR VOLUME Vsc (ft ³)	FLOW TEMP T (F)	EXP DURAT t (hr)
4-64	3.75	100	35.27	86.05	79.82	69.49	0.441	2.09	0.279	0.124	56	12
4-65	4.30	100	34.82	88.23	81.85	89.93	0.436	2.25	0.352	0.138	58	12
4-66	1.85	100	43.29	82.49	76.52	32.70	0.424	0.94	0.242	0.049	58	12
4-67	2.30	100	40.34	84.99	78.84	24.53	0.428	1.26	0.304	0.078	58	12
4-68	2.90	100	44.53	82.49	76.52	28.61	0.419	1.58	0.391	0.191	57	12
4-69	1.70	100	45.75	84.24	78.14	28.61	0.431	0.82	0.145	0.011	56	12
4-70	3.70	100	45.75	84.24	78.14	28.61	0.462	2.03	0.564	0.205	57	12
8-80-MA	12.60	100	46.73	76.44	70.91	20.44	0.580	2.18	0.370	0.173	68	12
8-81-MA	8.50	0	4.00	109.63	91.36	76.34	0.510	1.65	0.830	0.742	65	12
8-81-MB	8.50	15	6.93	84.99	69.74	40.88	0.487	1.42	0.690	0.180	65	12
8-81-MC	8.50	30	11.35	91.23	71.89	163.51	0.507	1.26	0.430	0.034	65	12
8-81-MD	8.50	40	10.96	78.19	63.46	163.51	0.480	1.20	0.460	0.041	65	12
8-82-MA	6.10	0	4.00	109.63	91.36	76.34	0.500	1.18	0.520	0.600	66	12
8-82-MB	6.10	15	4.33	86.61	71.07	40.88	0.487	1.01	0.340	0.127	66	12
8-82-MC	6.10	30	10.08	90.36	71.20	163.51	0.517	0.91	0.240	0.039	66	12
8-82-MD	6.10	40	5.60	82.87	67.25	163.51	0.510	0.82	0.220	0.044	66	12
8-83-MA	4.70	0	4.00	109.63	91.36	76.34	0.470	0.92	0.370	0.230	67	12
8-83-MB	4.70	15	4.19	81.06	66.52	40.88	0.477	0.75	0.310	0.067	67	12
8-83-MC	4.70	30	8.46	82.31	64.86	163.51	0.487	0.67	0.220	0.030	67	12
8-83-MD	4.70	40	9.87	83.24	67.55	163.51	0.480	0.58	0.170	0.016	67	12
8-84-MA	10.60	0	4.00	109.63	91.36	76.34	0.510	2.23	0.900	2.260	68	12
8-84-MB	10.60	15	6.22	80.37	65.95	40.88	0.497	1.94	0.860	1.165	68	12
8-84-MC	10.60	30	11.27	74.44	58.66	163.51	0.497	1.75	0.500	0.600	68	12
8-84-MD	10.60	40	9.80	80.18	65.07	163.51	0.490	1.49	0.540	0.671	68	12

Table (5.3). Set No.3 Experiments Utilizing Kalonite Clay in the 8 feet Flume with 0.36 feet Abutment Width (33 Runs)

RUN I.D.	FLOW DISCHARGE Q (cfs)	% CLAY CONTENT CC (%)	% INITIAL W.C. (%)	DRY DENSITY DD (lb/ft ³)	% OF COMPACT C (%)	TORVANE SHEAR TS (lb/ft ²)	FLOW DEPTH Y (ft)	APPROACH VELOCITY U (ft/s)	SCOUR DEPTH d _{sc} (ft)	SCOUR VOLUME V _{sc} (ft ³)	FLOW TEMP. T (F)	EXP. DURAT. t (hr)
8-71-MA	5.55	30	14.83	103.58	84.10	633.60	0.580	1.01	0.050	0.016	67	12
8-71-MB	5.55	30	13.36	104.27	84.66	858.42	0.567	0.86	0.000	0.000	67	12
8-71-MC	5.55	30	13.27	105.02	85.27	878.86	0.552	0.78	0.180	0.046	67	12
8-72-MA	14.90	30	15.44	106.45	86.43	490.53	0.625	2.66	0.100	0.028	67	12
8-72-MB	14.90	30	14.66	109.64	89.02	858.42	0.600	2.69	0.120	0.034	67	12
8-72-MC	14.90	30	15.44	106.45	86.43	347.46	0.575	3.15	0.230	0.067	67	12
8-73-MA	10.10	30	20.07	108.58	88.16	163.51	0.523	2.09	0.070	0.023	66	12
8-73-MB	10.10	30	26.50	101.09	82.08	81.75	0.515	1.73	0.130	0.037	66	12
8-73-MC	10.10	30	29.70	94.97	77.11	40.88	0.542	1.50	0.120	0.035	66	12
8-74-MA	12.40	30	18.18	108.01	87.70	224.83	0.54	2.36	0.100	0.030	68	12
8-74-MB	12.40	30	23.39	102.34	83.10	102.19	0.507	2.25	0.150	0.042	68	12
8-74-MC	12.40	30	27.51	96.10	78.03	61.32	0.455	2.55	0.190	0.049	68	12
8-75-MA	8.40	30	21.79	105.71	85.83	102.19	0.52	1.68	0.000	0.000	68	12
8-75-MB	8.40	30	25.13	102.34	83.10	40.88	0.527	1.51	0.000	0.000	68	12
8-75-MC	8.40	30	29.72	95.53	77.57	20.44	0.557	1.44	0.000	0.000	68	12
8-76-MA	17.30	30	21.79	105.71	85.83	102.19	0.632	2.68	0.120	0.034	68	12

Table (5.3). (Continued)

RUN ID	FLOW DISCHARGE Q (cfs)	% CLAY CONTENT CO (%)	% INITIAL W.C. (M.C.%)	DRY DENSITY DD (lb/ft ³)	% OF COMPAG. C (%)	TORVANE SHEAR TS (lb/ft ²)	FLOW DEPTH Y (ft)	APPROACH VELOCITY U (ft/s)	SCOUR DEPTH (ft)	SCOUR VOLUME V _{sc} (ft ³)	FLOW TEMP. T (°F)	EXP. DURAT. (hr)
8-75-MB	17.30	30	25.13	102.34	83.10	40.88	0.580	2.65	0.220	0.064	68	12
8-75-MC	17.30	30	29.72	95.53	77.57	20.44	0.548	3.94	0.520	0.335	68	12
8-77-MA	6.03	10	15.54	105.71	85.79	61.32	0.500	0.99	0.480	0.283	67	12
8-77-MB	6.03	20	17.11	108.58	84.47	81.75	0.517	0.73	0.040	0.014	67	12
8-77-MC	6.03	50	16.61	96.78	85.17	940.18	0.567	0.64	0.310	0.124	67	12
8-77-MD	6.03	50	27.13	92.16	81.11	61.32	0.570	0.56	0.000	0.000	67	12
8-78-MA	8.30	10	13.54	105.52	85.64	61.32	0.510	1.68	0.750	0.494	67	12
8-78-MB	8.30	20	14.72	94.66	73.64	81.75	0.510	1.51	0.150	0.017	67	12
8-78-MC	8.30	50	15.67	83.24	73.26	940.18	0.550	1.44	0.630	0.230	67	12
8-78-MD	8.30	50	25.81	98.90	87.04	61.32	0.560	1.22	0.000	0.000	67	12
8-79-MA	10.20	10	16.17	114.82	93.18	61.32	0.530	1.91	0.840	0.742	68	12
8-79-MB	10.20	20	16.77	110.70	86.12	81.75	0.527	1.57	0.170	0.048	68	12
8-79-MC	10.20	50	15.67	83.24	73.26	940.18	0.572	1.39	0.580	0.424	68	12
8-79-MD	10.20	50	30.91	90.73	79.85	61.32	0.570	1.17	0.000	0.000	68	12
8-80-MB	12.60	20	16.77	110.70	86.12	81.75	0.557	1.99	0.500	0.388	68	12
8-80-MC	12.60	50	15.67	83.24	73.26	940.18	0.577	1.77	0.740	0.636	68	12
8-80-MD	12.60	50	30.91	90.73	79.85	61.32	0.550	1.55	0.000	0.000	68	12

Table (5.4). Set No.1 Experiments for Normalized Scour Depth (39 Runs)

RUN ID	ABUT. WIDTH a (ft)	FLOW DEPTH y (ft)	APPROACH VELOCITY U (ft/s)	SCOUR DEPTH dsc (ft)	FROUDE NUMBER U/sqrt(g.y)	dsc/ sqrt(a.y)
B-12-MA	0.72	1.020	0.56	0.067	0.098	0.078
B-13-MA	0.72	1.025	0.73	0.190	0.127	0.221
B-14-MA	0.72	1.050	0.68	0.155	0.116	0.178
B-15-MA	0.72	1.014	0.77	0.196	0.135	0.229
B-16-MA	0.72	1.045	0.82	0.225	0.141	0.259
B-17-MA	0.72	1.058	0.94	0.362	0.162	0.415
B-18-MA	0.72	1.070	1.04	0.560	0.178	0.638
B-19-MA	0.72	1.074	0.83	0.286	0.140	0.325
B-20-MA	0.72	0.903	0.56	0.290	0.104	0.360
B-21-MA	0.72	0.926	0.53	0.088	0.098	0.108
B-22-MA	0.72	0.971	0.69	0.160	0.124	0.191
B-23-MA	0.72	0.949	0.75	0.200	0.136	0.242
B-24-MA	0.72	1.006	0.89	0.215	0.157	0.253
B-25-MA	0.72	0.979	1.12	0.465	0.200	0.554
B-26-MA	0.72	1.008	1.39	0.670	0.244	0.786
B-27-MA	0.72	0.805	1.47	0.000	0.289	0.000
B-27-MB	0.72	0.845	1.24	0.360	0.238	0.462
B-28-MA	0.72	0.813	2.31	0.000	0.452	0.000
B-28-MB	0.72	0.795	2.12	0.350	0.419	0.463
B-29-MA	0.72	0.802	2.85	0.000	0.561	0.000
B-29-MB	0.72	0.847	2.21	0.530	0.423	0.679
B-30-MA	0.72	0.827	1.80	0.817	0.349	1.059
B-30-MB	0.72	0.853	1.57	0.400	0.300	0.510
B-31-MA	0.72	0.843	1.48	1.160	0.284	1.489
B-31-MB	0.72	0.895	1.36	0.890	0.253	1.109
B-32-MA	0.72	0.827	1.15	0.460	0.223	0.596
B-32-MB	0.72	0.867	1.03	0.350	0.195	0.443
B-33-MA	0.72	0.830	1.43	0.910	0.277	1.177
B-33-MB	0.72	0.868	1.28	0.640	0.242	0.810
B-34-MA	0.72	0.763	2.12	1.460	0.428	1.970
B-34-MB	0.72	0.780	1.83	1.200	0.365	1.601
B-35-MA	0.72	0.805	2.07	0.650	0.407	0.854
B-35-MB	0.72	0.800	1.95	1.170	0.384	1.542
B-36-MA	0.72	0.807	2.75	0.510	0.540	0.669
B-36-MB	0.72	0.755	2.62	0.780	0.532	1.058
B-37-MA	0.72	1.005	2.99	0.270	0.526	0.317
B-37-MB	0.72	0.958	3.12	0.890	0.562	1.072
B-38-MA	0.72	1.153	3.27	0.300	0.537	0.329
B-38-MB	0.72	1.050	3.41	1.110	0.587	1.277

Table (5.5). Set No.2 Experiments for Normalized Scour Depth (49 Runs)

RUN I.D.	ABUT. WIDTH x (ft)	FLOW DEPTH y (ft)	APPROACH VELOCITY U (ft/s)	SCOUR DEPTH d _{so} (ft)	FROUDE NUMBER U/sqrt(g.y)	d _{sc} /sqrt(a.y)
4-39	0.36	0.459	0.49	0.083	0.126	0.204
4-40	0.36	0.470	0.89	0.211	0.229	0.513
4-41	0.36	0.478	0.65	0.136	0.167	0.328
4-42	0.36	0.471	1.18	0.359	0.304	0.872
4-43	0.36	0.442	0.54	0.096	0.142	0.241
4-44	0.36	0.459	0.84	0.208	0.219	0.512
4-45	0.36	0.458	1.15	0.450	0.300	1.108
4-46	0.36	0.422	1.65	0.552	0.448	1.416
4-47	0.36	0.429	0.78	0.266	0.210	0.677
4-48	0.36	0.424	0.63	0.162	0.170	0.415
4-49	0.36	0.432	1.02	0.475	0.274	1.204
4-50	0.36	0.443	1.22	0.634	0.324	1.588
4-51	0.36	0.425	0.73	0.103	0.196	0.263
4-52	0.36	0.429	1.24	0.425	0.334	1.081
4-53	0.36	0.426	1.00	0.234	0.271	0.598
4-54	0.36	0.413	0.55	0.100	0.151	0.259
4-55	0.36	0.426	1.66	0.685	0.448	1.749
4-56	0.36	0.434	0.65	0.099	0.173	0.250
4-57	0.36	0.423	0.74	0.180	0.201	0.461
4-58	0.36	0.444	1.01	0.314	0.268	0.785
4-59	0.36	0.428	1.17	0.425	0.314	1.083
4-60	0.36	0.423	1.61	0.448	0.436	1.148
4-61	0.36	0.424	1.58	0.266	0.429	0.681
4-62	0.36	0.430	2.02	0.118	0.542	0.300
4-63	0.36	0.438	2.24	0.110	0.598	0.277
4-64	0.36	0.441	2.09	0.279	0.554	0.700
4-65	0.36	0.436	2.25	0.352	0.599	0.888
4-66	0.36	0.424	0.94	0.242	0.255	0.619
4-67	0.36	0.428	1.26	0.304	0.340	0.774
4-68	0.36	0.419	1.58	0.391	0.431	1.007
4-69	0.36	0.431	0.82	0.145	0.219	0.368
4-70	0.36	0.462	2.03	0.564	0.527	1.383
5-80-MA	0.36	0.580	2.18	0.370	0.505	0.810
5-81-MA	0.36	0.510	1.65	0.830	0.407	1.937
5-81-MB	0.36	0.487	1.42	0.690	0.359	1.648
5-81-MC	0.36	0.507	1.26	0.430	0.312	1.006
5-81-MD	0.36	0.480	1.20	0.460	0.305	1.107
5-82-MA	0.36	0.500	1.18	0.520	0.294	1.226
5-82-MB	0.36	0.487	1.01	0.340	0.255	0.812
5-82-MC	0.36	0.517	0.91	0.240	0.223	0.556
5-82-MD	0.36	0.510	0.82	0.220	0.202	0.513
5-83-MA	0.36	0.470	0.92	0.370	0.237	0.900
5-83-MB	0.36	0.477	0.75	0.310	0.191	0.748
5-83-MC	0.36	0.487	0.67	0.220	0.169	0.525
5-83-MD	0.36	0.480	0.58	0.170	0.148	0.409
5-84-MA	0.36	0.510	2.23	0.900	0.551	2.100
5-84-MB	0.36	0.497	1.94	0.860	0.485	2.033
5-84-MC	0.36	0.497	1.75	0.500	0.438	1.182
5-84-MD	0.36	0.490	1.49	0.540	0.375	1.286

Table (5.6). Set No.3 Experiments for Normalized Scour Depth (33 Runs)

RUN I.D.	ABUT. WIDTH a (ft)	FLOW DEPTH y (ft)	APPROAC VELOCITY U (ft/s)	SCOUR DEPTH dsp (ft)	FROUDE NUMBER U/sqrt(g.y)	dsc/ sqrt(a.y)
8-71-MA	0.36	0.580	1.01	0.050	0.234	0.109
8-71-MB	0.36	0.567	0.86	0.000	0.201	0.000
8-71-MC	0.36	0.552	0.78	0.180	0.185	0.404
8-72-MA	0.36	0.625	2.66	0.100	0.593	0.211
8-72-MB	0.36	0.600	2.69	0.120	0.612	0.258
8-72-MC	0.36	0.575	3.15	0.230	0.732	0.506
8-73-MA	0.36	0.523	2.09	0.070	0.509	0.161
8-73-MB	0.36	0.515	1.73	0.130	0.425	0.302
8-73-MC	0.36	0.542	1.50	0.120	0.359	0.272
8-74-MA	0.36	0.54	2.36	0.100	0.566	0.227
8-74-MB	0.36	0.507	2.25	0.150	0.557	0.351
8-74-MC	0.36	0.455	2.55	0.190	0.666	0.469
8-75-MA	0.36	0.52	1.68	0.000	0.411	0.000
8-75-MB	0.36	0.527	1.51	0.000	0.367	0.000
8-75-MC	0.36	0.557	1.44	0.000	0.340	0.000
8-76-MA	0.36	0.632	2.68	0.120	0.594	0.252
8-76-MB	0.36	0.580	2.65	0.220	0.613	0.481
8-76-MC	0.36	0.548	3.94	0.520	0.938	1.171
8-77-MA	0.36	0.500	0.99	0.480	0.247	1.131
8-77-MB	0.36	0.517	0.73	0.040	0.179	0.093
8-77-MC	0.36	0.567	0.64	0.310	0.150	0.686
8-77-MD	0.36	0.570	0.56	0.000	0.131	0.000
8-78-MA	0.36	0.510	1.68	0.750	0.415	1.750
8-78-MB	0.36	0.510	1.51	0.150	0.373	0.350
8-78-MC	0.36	0.550	1.44	0.630	0.342	1.416
8-78-MD	0.36	0.560	1.22	0.000	0.287	0.000
8-79-MA	0.36	0.530	1.91	0.840	0.463	1.923
8-79-MB	0.36	0.527	1.57	0.170	0.381	0.390
8-79-MC	0.36	0.572	1.39	0.580	0.324	1.278
8-79-MD	0.36	0.570	1.17	0.000	0.273	0.000
8-80-MB	0.36	0.557	1.99	0.500	0.470	1.117
8-80-MC	0.36	0.577	1.77	0.740	0.411	1.624
8-80-MD	0.36	0.550	1.55	0.000	0.368	0.000

d_w = Depth of scour in non-cohesive sediments for conditions
corresponding to d_w (ft)

y = Flow depth (ft)

a = Width of abutment (ft)

L = Length of abutment (ft)

U = Mean approach velocity (ft/s)

WC = Initial water content of clay (%)

CC = Sample clay content (%)

C = Sample compaction related to the optimum compaction (%)

CT = Clay type

TS = Torvane shear stress (lb/ft²)

T = Temperature (°F)

t = Duration of the experiment

g = Gravitational acceleration (ft/s²)

α = Angle of attack

ϕ = Shape factor

ρ = Water density (lb/ft³)

ν = Kinematic viscosity (ft²/s)

The Π - theorem is used to perform the dimensional analysis with the repeated variables d_w , U , and ρ which have the three principal dimensions of M, L, and T (Mass, Length, and Time respectively). The analysis is as follows:

Using $\pi_1 = d_w^{k_1} U^{m_1} \rho^{n_1} d_w$

therefore $M^0 L^0 T^0 = (L)^{k_1} (LT^{-1})^{m_1} (ML^{-3})^{n_1} (L)$

By equating the exponents in both sides, get:

for M: $0 = n_1$, get $n_1 = 0$

for T: $0 = -m_1$, get $m_1 = 0$

for L: $0 = k_1 + m_1 - 3n_1 + 1$, get $k_1 = -1$

therefore:

$$\pi_1 = d_w d_w^{-1}$$

or

$$\pi_1 = d_w / d_w \quad (5.1 a)$$

similarly

$$\pi_2 = L / d_w \quad (5.2 b)$$

and

$$\pi_3 = y / d_w \quad (5.1 c)$$

and

$$\pi_4 = a / d_w \quad (5.1 d)$$

Using $\pi_5 = d_w^{k_5} U^{m_5} \rho^{n_5} t$

therefore $M^0 L^0 T^0 = (L)^{k_5} (LT^{-1})^{m_5} (ML^{-3})^{n_5} (T)$

By equating the exponents in both sides, get:

for M: $0 = n_5,$ get $n_5 = 0$

for T: $0 = -m_5 + 1,$ get $m_5 = 1$

for L: $0 = k_5 + m_5 - 3n_5,$ get $k_5 = -1$

therefore:

$$\pi_5 = U t d_m^{-1}$$

or

$$\pi_5 = U t / d_m \quad (5.1 e)$$

Using $\pi_6 = d_m^{n_6} U^{m_6} \rho^{k_6} T$

therefore $M^0 L^0 T^0 = (L)^{n_6} (LT^{-1})^{m_6} (ML^{-3})^{k_6} (ML^{-1}T^{-2})$

By equating the exponents in both sides, get:

for M: $0 = n_6 + 1,$ get $n_6 = -1$

for T: $0 = -m_6 - 2,$ get $m_6 = -2$

for L: $0 = k_6 + m_6 - 3n_6 - 1,$ get $k_6 = 0$

therefore:

$$\pi_6 = T U^2 \rho^{-1}$$

or

$$\pi_6 = T / U^2 \rho \quad (5.1 f)$$

Using $\pi_7 = d_m^{n_7} U^{m_7} \rho^{k_7} v$

therefore $M^0 L^0 T^0 = (L)^{n_7} (LT^{-1})^{m_7} (ML^{-3})^{k_7} (L^2T^{-1})$

By equating the exponents in both sides, get:

for M: $0 = n_7$, get $n_7 = 0$

for T: $0 = -m_7 - 1$, get $m_7 = -1$

for L: $0 = k_7 + m_7 - 3n_7 + 2$, get $k_7 = -1$

therefore:

$$\pi_7 = v d_w^{-1} U^{-1}$$

or

$$\pi_7 = v / d_w U \quad (5.1 g)$$

Using $\pi_8 = d_w^{k_8} U^{m_8} \rho^{n_8} g$

therefore $M^0 L^0 T^0 = (L)^{k_8} (LT^{-1})^{m_8} (ML^{-3})^{n_8} (L T^{-2})$

By equating the exponents in both sides, get:

for M: $0 = n_8$, get $n_8 = 0$

for T: $0 = -m_8 - 2$, get $m_8 = -2$

for L: $0 = k_8 + m_8 - 3n_8 + 1$, get $k_8 = 1$

therefore:

$$\pi_8 = d_w g U^{-2}$$

or

$$\pi_8 = d_w g / U^2 \quad (5.1 h)$$

Also the following is the non-dimensional π -terms:

$$\pi_9 = \phi \quad (5.1 i)$$

$$\pi_{10} = \alpha \quad (5.1 j)$$

$$\pi_{11} = WC \quad (5.1 k)$$

$$\pi_{12} = CC \quad (5.1 \text{ l})$$

$$\pi_{13} = C \quad (5.1 \text{ m})$$

$$\pi_{14} = CT \quad (5.1 \text{ n})$$

$$\pi_{15} = T \quad (5.1 \text{ o})$$

collecting all the π terms, the final form of the equation becomes:

$$\frac{d_{sc}}{d_{ss}} = f\left(\frac{y}{d_{ss}}, \frac{L}{d_{ss}}, \frac{a}{d_{ss}}, WC, CC, C, CT, \frac{U_t}{d_{ss}}, \frac{v}{Ud_{ss}}, \frac{TS}{\rho U^2}, \frac{d_{ss}g}{U^2}, \alpha, \phi, T\right) \quad (5.2)$$

$$\frac{d_{sc}}{d_{ss}} = f\left(\frac{d_{ss}}{a} \cdot \frac{y}{d_{ss}}, \frac{L}{d_{ss}} \cdot \frac{d_{ss}}{a}, WC, CC, C, CT, \frac{U_t}{d_{ss}} \cdot \frac{d_{ss}}{y}, \frac{v}{Ud_{ss}} \cdot \frac{d_{ss}}{y}, \frac{TS}{\rho U^2}, \frac{d_{ss}g}{U^2} \cdot \frac{y}{d_{ss}}, \alpha, \phi, T\right) \quad (5.3)$$

$$\frac{d_{sc}}{d_{ss}} = f\left(\frac{y}{a}, \frac{L}{a}, WC, CC, C, CT, \frac{U_t}{y}, R_s, \frac{TS}{U^2 \rho}, F_r, \alpha, \phi, T\right) \quad (5.4)$$

Further analysis and simplifications of this equation will be performed in section 5.6 of abutment scour prediction equations for cohesive materials.

5.3 Geometry of the Scour Hole

The scour hole at the upstream nose of the vertical wall abutment takes the shape of partial inverted cones. The deepest point of the scour hole is located at the upstream nose of the abutment. As shown in Figure 5.1 for Run No. 30-A, heading from

upstream to downstream, the slope of the scour hole is relatively high until reaching the upstream face of the abutment. This slope is reduced in the downstream direction and flattens out near the downstream end of the abutment. Figures 5.2 a and b show the 3-dimensional and actual photograph of the same abutment scour for the same run. The slope angle and width-depth ratio of the scour hole are functions of initial water content, compaction, and clay content. These relationships will be developed in the later sections.

5.4 Montmorillonite Clay Experiments

Due to the complexity of abutment scour in cohesive material, up to this pioneering study, there have been no published systematic investigation of the effect of cohesion on local abutment scour. All previous experimental studies were conducted on cohesionless material. In this study three clay properties were used to investigate their effect on maximum depth of abutment scour. These properties are: initial water content, compaction, and clay content. In the present experimental program, two types of clays were used: Montmorillonite clay, and Kaolinite clay. This section presents the effect of the three clay properties on maximum depth of scour for Montmorillonite clay.

5.4.1 Effect of Initial Water Content on the Clay Mixture

This section will include the investigations of the scour depth as a function of Froude number for various initial water contents. The effects of the initial water content on time rate of scour, cross-sectional profile, side slope, and longitudinal slope of the scour hole. The results are expressed in functional relationships whenever possible.

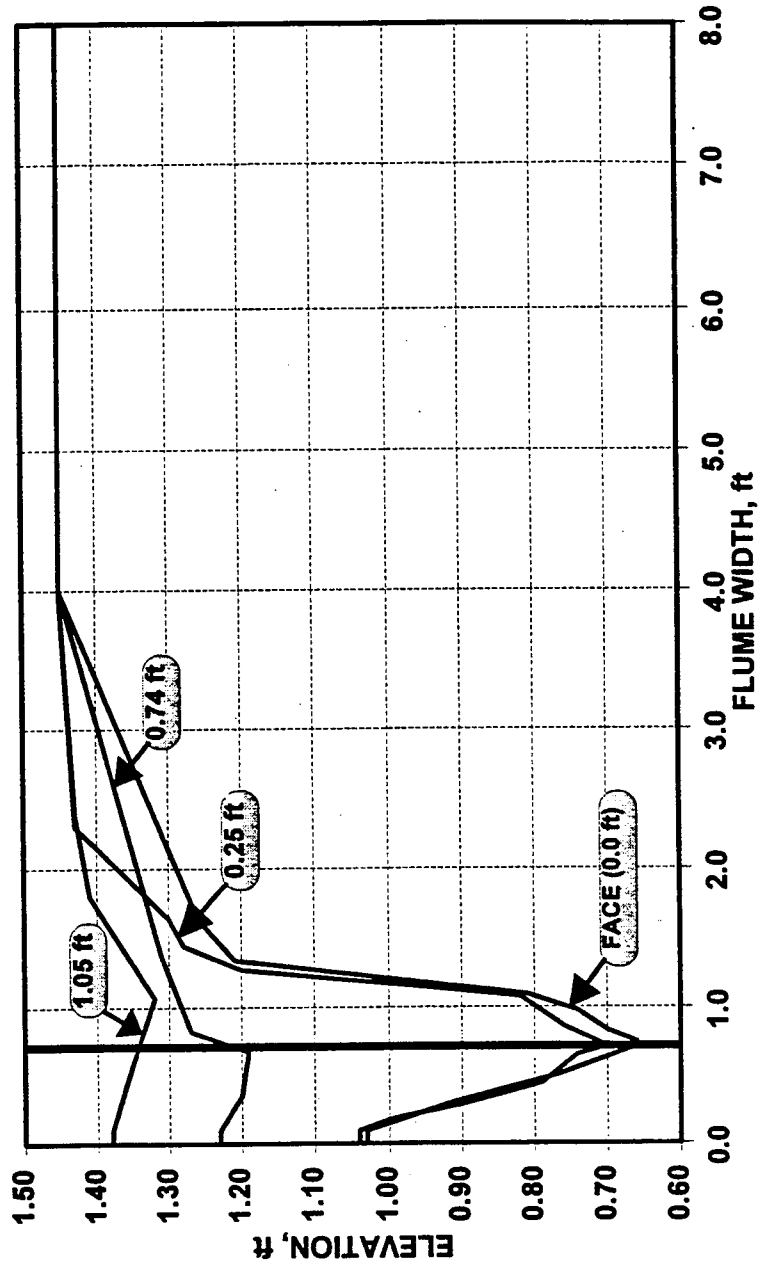


Figure (5.1) Cross-Section along the Abutment Scour Hole in the Upstream Direction for Run No.30-A.

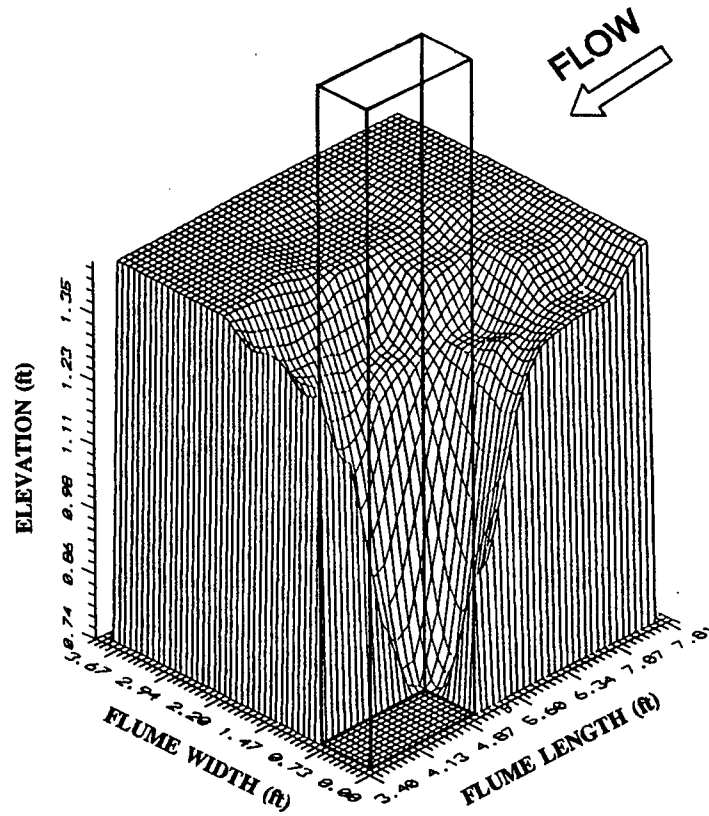


Figure (5.2 a) Three Dimensional View of Abutment Scour Hole Geometry for Run No. 30-A.

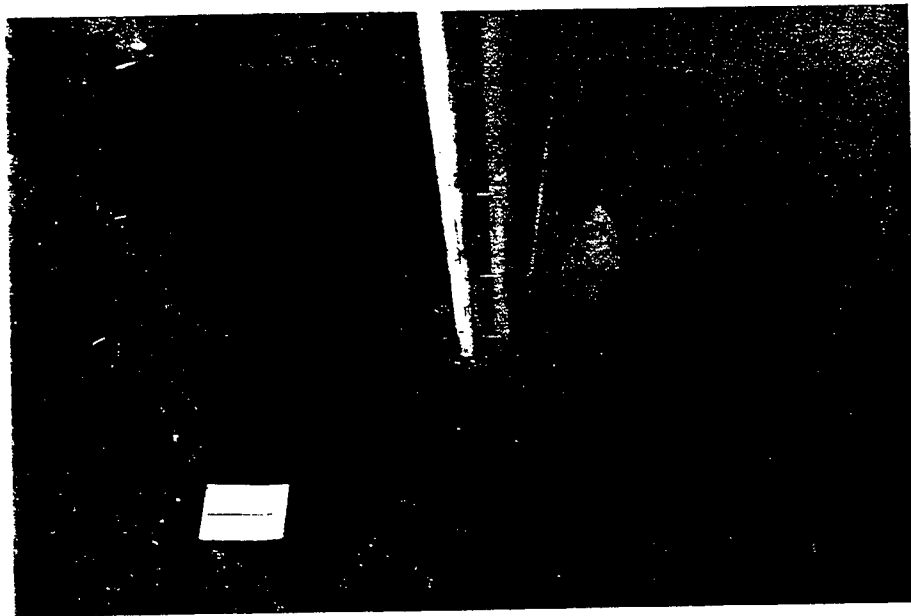


Figure (5.2 b) Photograph of Abutment Scour Hole Geometry for Run No. 30-A.

5.4.1.1 Variation of Scour Depth with Approach Flow Conditions

The effect of initial water content in Montmorillonite clay was investigated by maintaining the same range of mixture compaction and clay content and by changing only the initial water content of the soil. The five initial water contents used in the experiments were 12 %, 20 %, 28 %, 35 %, and 45 %. Figure 5.3 relates the scour depth which is normalized by the square root of abutment width and flow depth to the intensity of flow conditions expressed through the Froude number. As shown in Figure 5.3, for a given Froude number, the scour depth decreases as the initial water content is increased from 12 % to 20 % and it keeps on decreasing until the initial water content is increased to 28 %. By increasing the initial water content beyond 28 %, the depth of scour begins to increase again. As shown in the Figure 5.3, for a given Froude number, increasing the initial water content from 28 % to 35 %, causes the depth of scour to increase. While keeping the Froude number the same, by increasing the initial water content further from 35 % to 45 %, the depth of scour is increased as shown in Figure 5.3. The scour depth in clay can be related to the corresponding scour depth in sand for the same value of Froude number. This relation makes it possible to use any applicable equation for predicting abutment scour depth for sand and then predicting the abutment scour depth for the clay-bed by applying the effect of clay content, water content, and compaction. Figure 5.4 gives the abutment scour for the 0.81 mm sand which was used for normalizing the corresponding clay scour under the same flow conditions. To isolate the effect of initial water content, first a relationship between percentage of initial water content and depth of scour normalized by square root of abutment width and flow depth

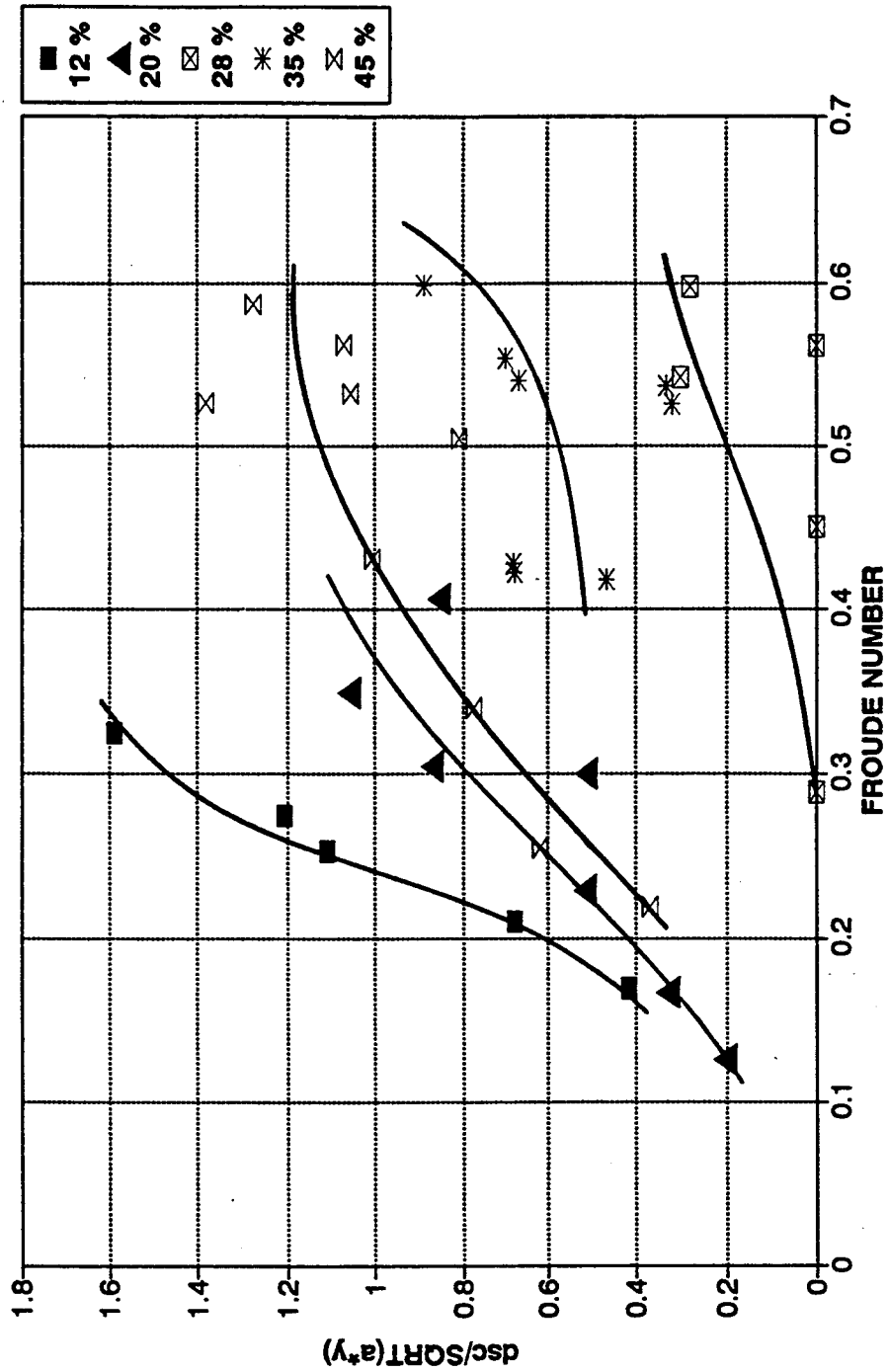


Figure (5.3) Variation of Dimensionless Abutment Scour Depth with Froude Number for Montmorillonite Clay.

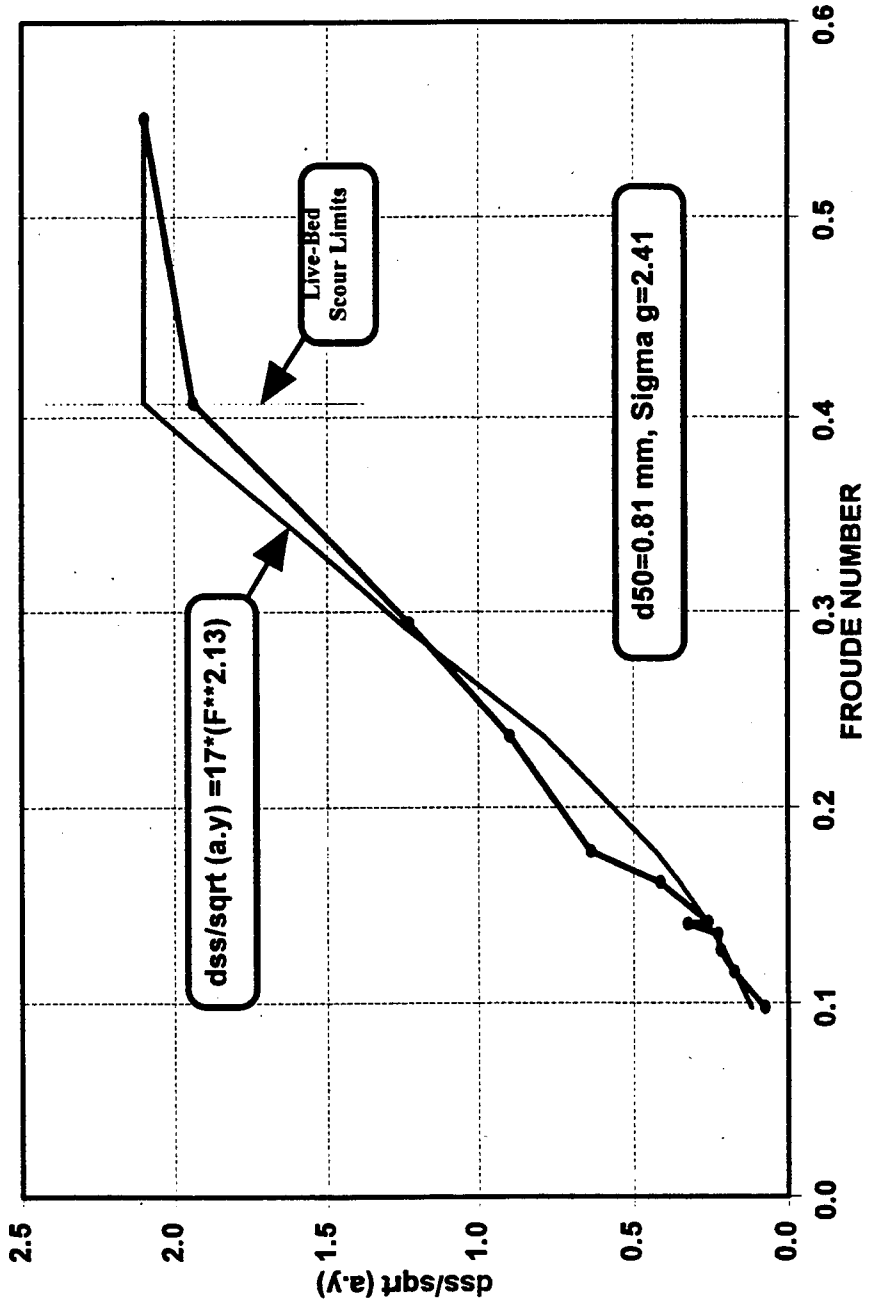


Figure (5.4) Variation of Dimensionless Abutment Scour Depth with Froude Number for the Medium Sand Bed ($D_{50} = 0.81 \text{ mm}$).

is drawn for different Froude numbers as shown in Figure 5.5. These contour lines of equal Froude numbers were first drawn using the computer program of "Surfer", but the resulting contour lines were irregular because of the computational methods used inside the program which makes the resulting fitting physically inappropriate and was replaced by manual drawing method. Secondly, the depth of clay scour is normalized by the corresponding depth of sand scour for the same Froude number using the relationship given in Figure 5.4. Finally the average scattered experimental values of clay scour to sand scour ratios for various initial water contents are calculated. Figure 5.6 presents this relationship along with its upper and lower bounding limits.

5.4.1.2 Cross-Sectional Profile of the Scour Holes

To study the effect of initial water content of Montmorillonite clay on the geometry of the resulting scour hole, a comparison of different cross sectional profiles passing through the upstream face of the abutments is conducted. The locations of cross-sectional and longitudinal profiles are illustrated in Figure 5.7. The comparison of cross-sectional profiles is illustrated in Figures 5.8 through 5.12 for initial water content values of 12 %, 20 %, 28 %, 35 %, and 45 % for different Froude numbers representing different flow conditions. The scour dimensions defined by the depth, width, and side slope corresponding to maximum scour conditions are presented in Table 5.7. From Figures 5.8 through 5.12 and Table 5.7, it can be concluded that the depth of scour first decreases as the initial water content is increased from 12 % up to 28 % and then increases again as the initial water content is increased further from 28 % to 45 %.

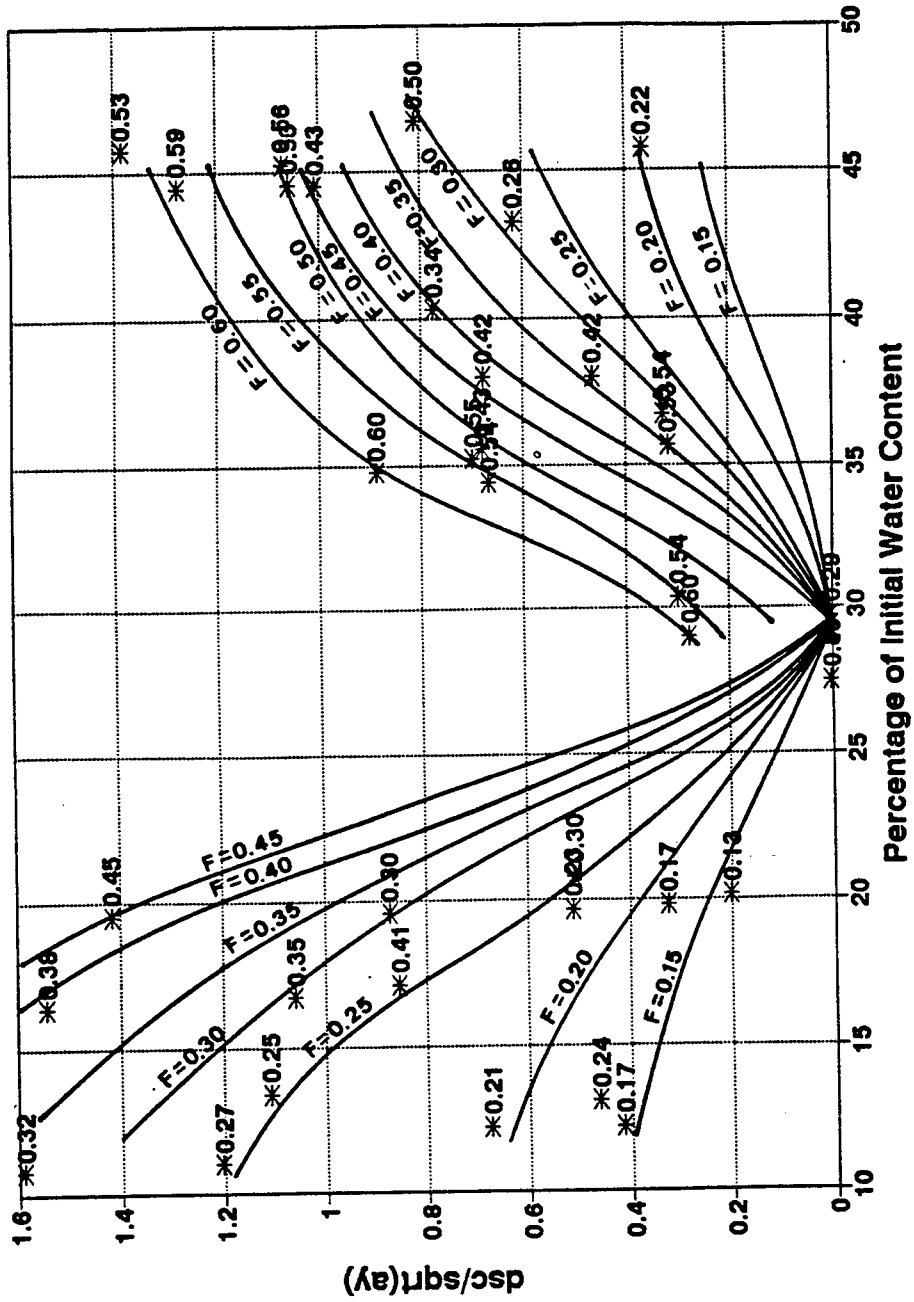


Figure (5.5) Effect of Initial Water Content on Dimensionless Abutment Scour Depth for Montmorillonite Clay.

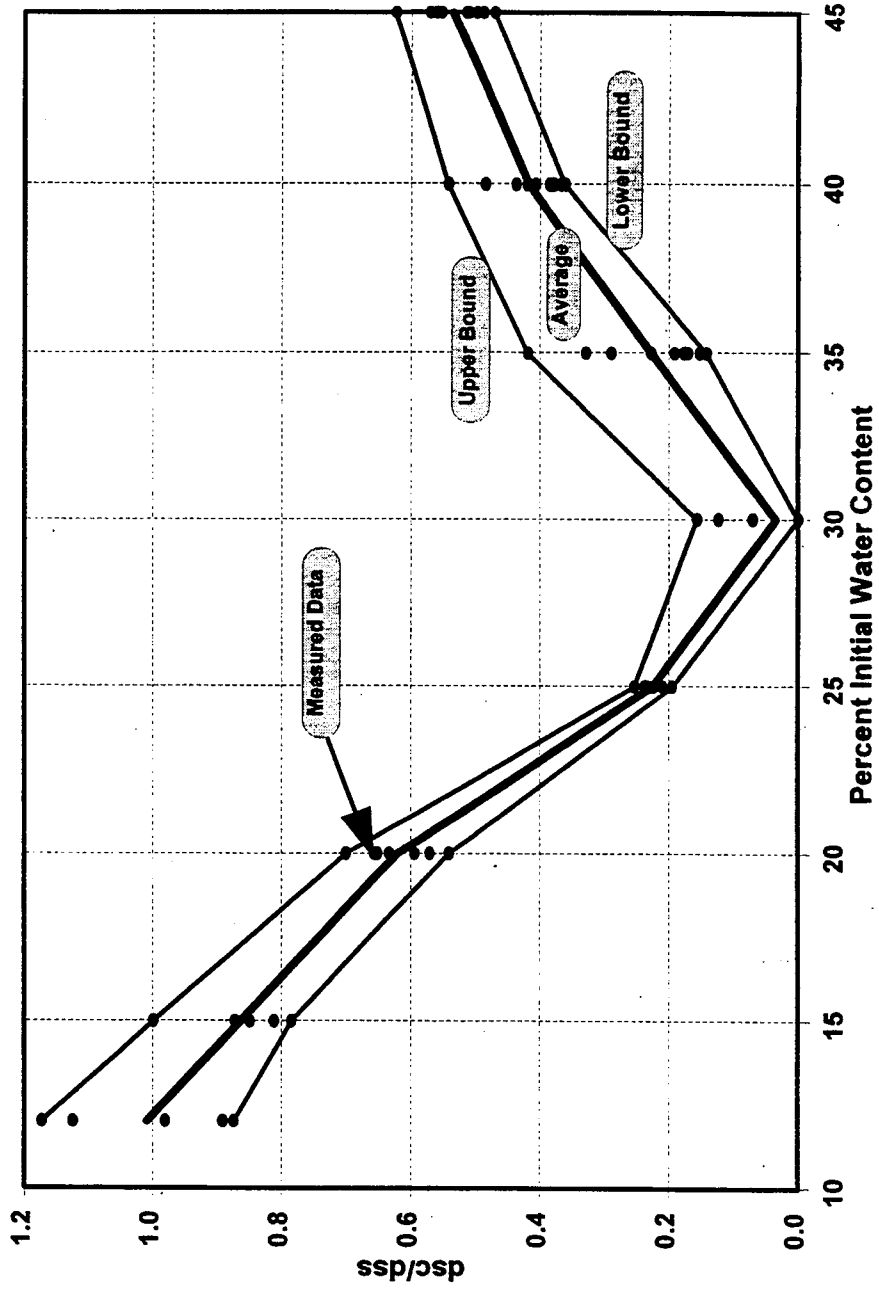


Figure (5.6) Variation of Normalized Scour Depth with Initial Water Content for Montmorillonite Clay.

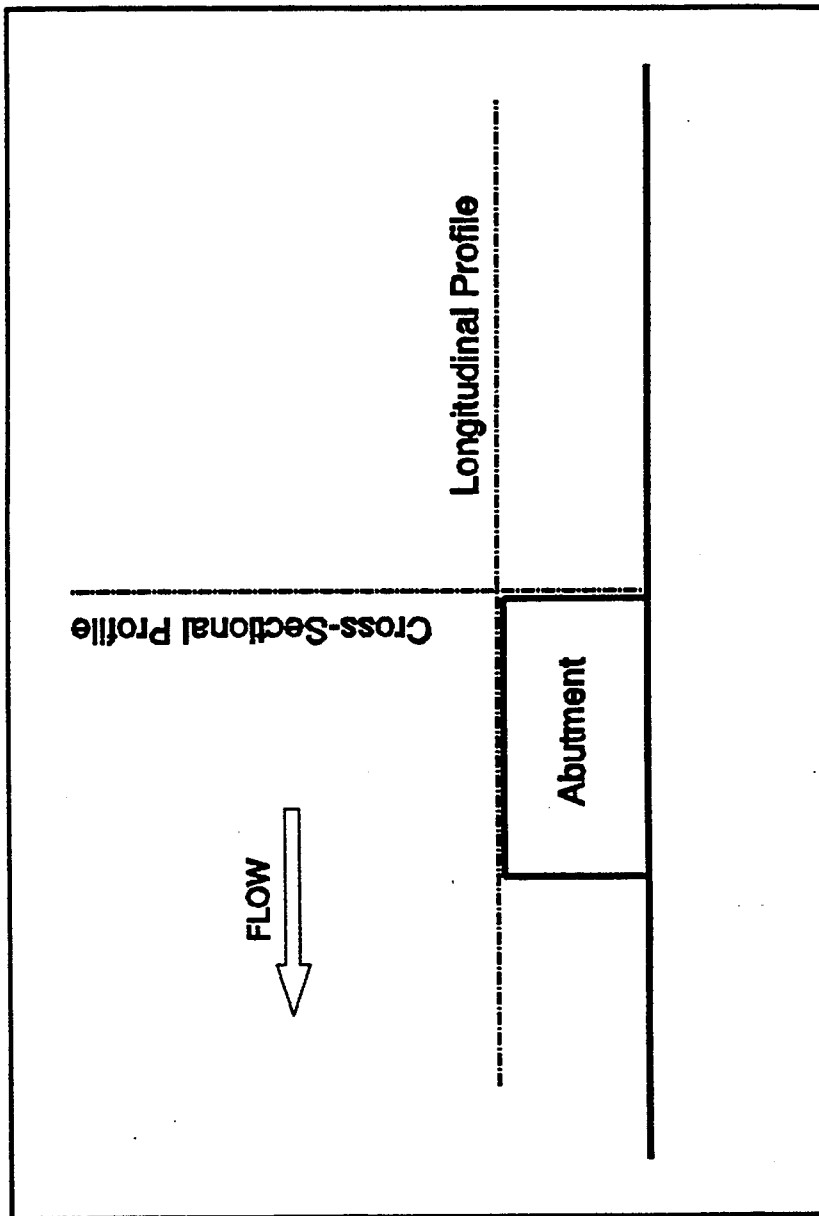


Figure (5.7) The Locations of Cross-Sectional and Longitudinal Profiles of the Abutment Scour Hole.

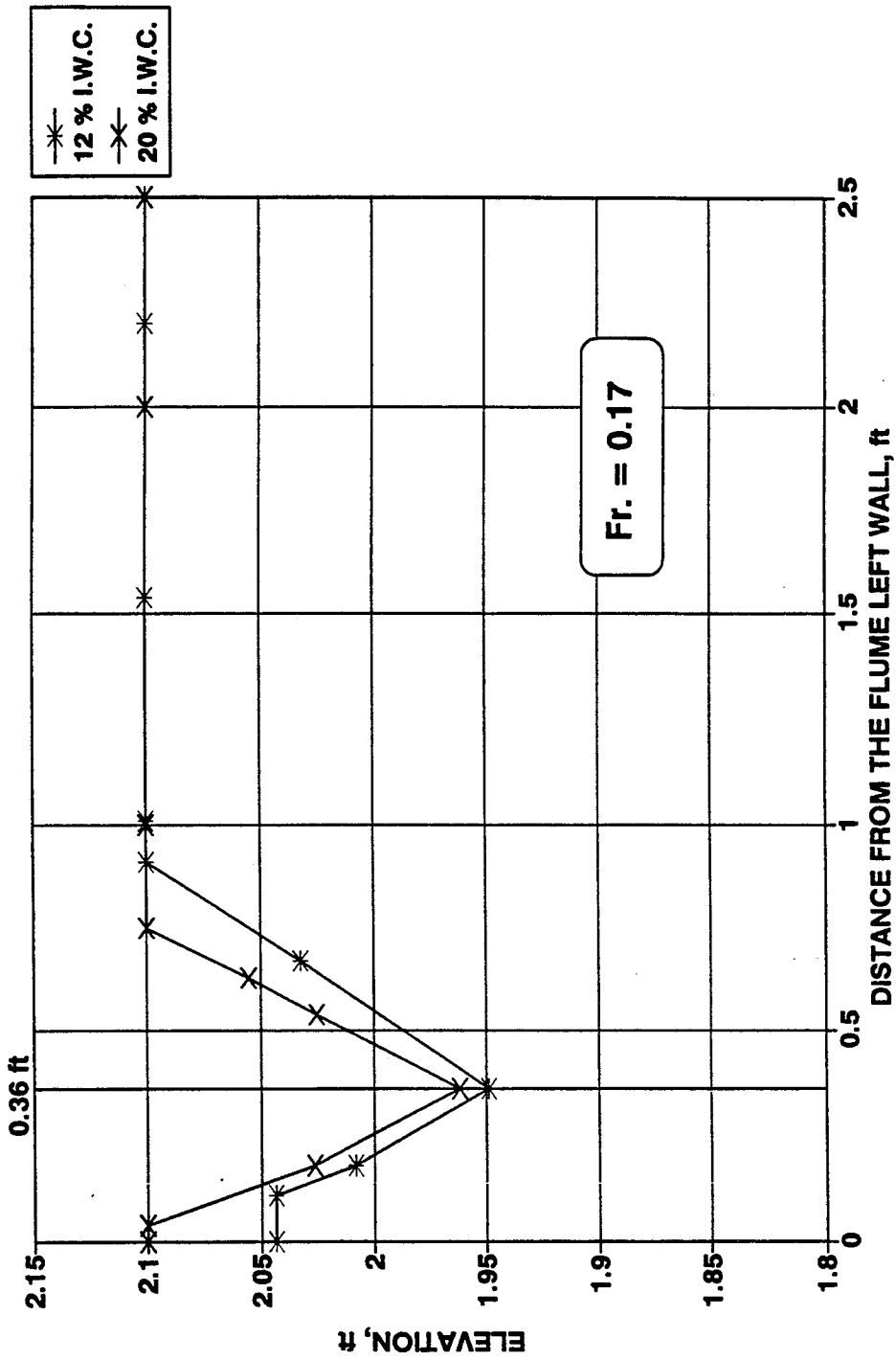


Figure (5.8) Effect of Initial Water Content on the Scour Hole Geometry at the Upstream Abutment Face.

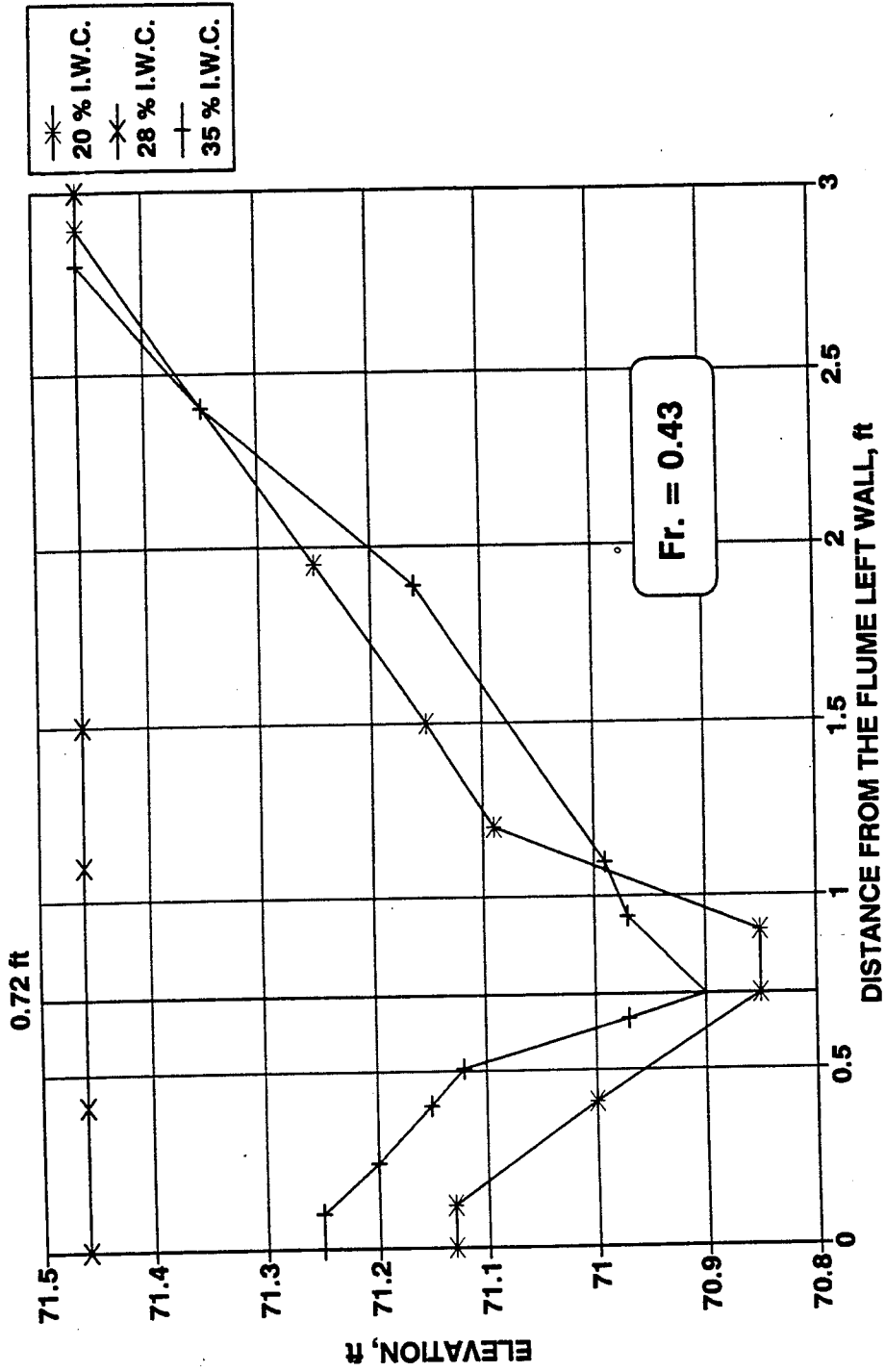


Figure (5.9) Effect of Initial Water Content on the Scour Hole Geometry at the Upstream Abutment Face.

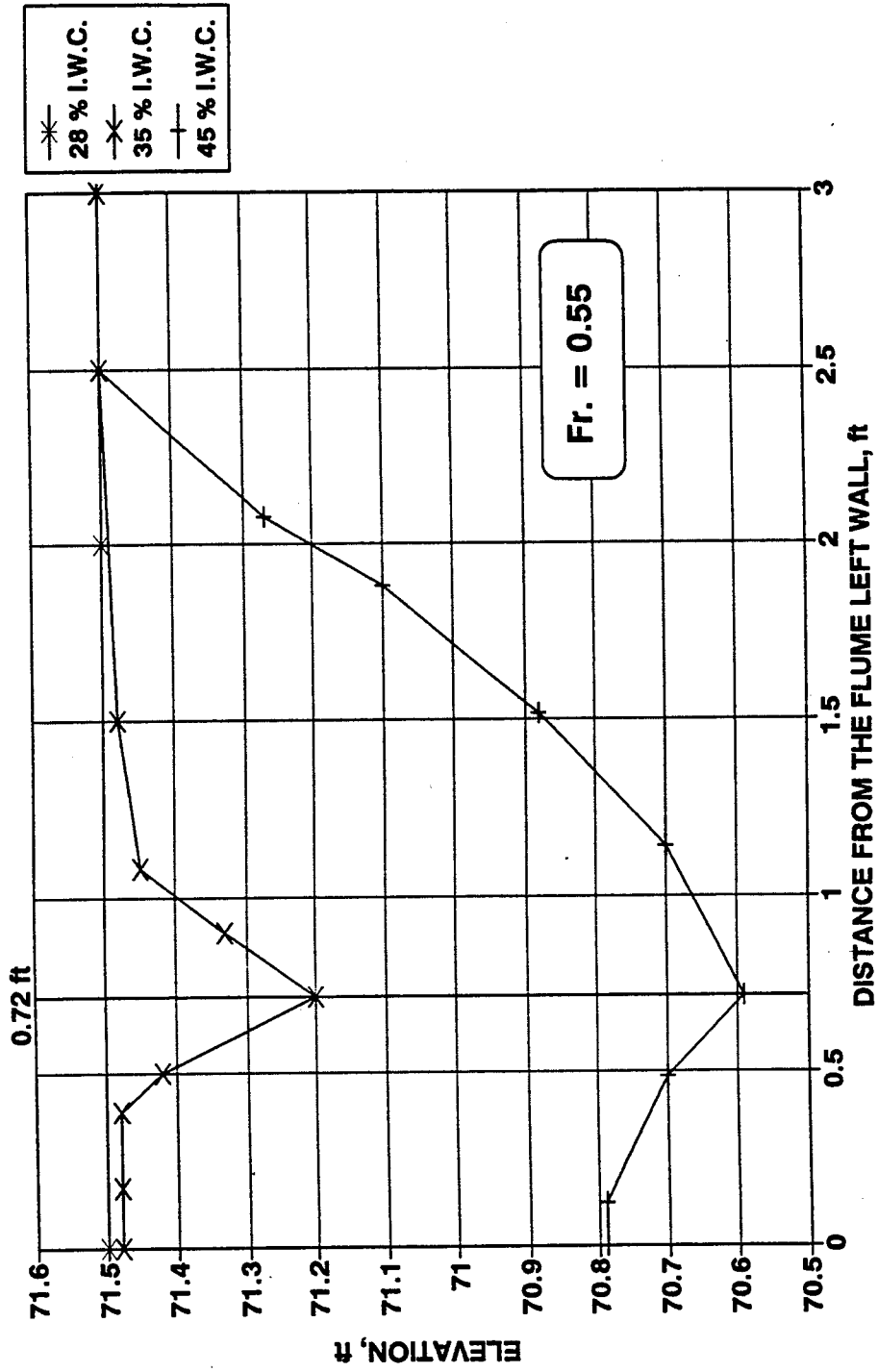


Figure (5.10) Effect of Initial Water Content on the Scour Hole Geometry at the Upstream Abutment Face.

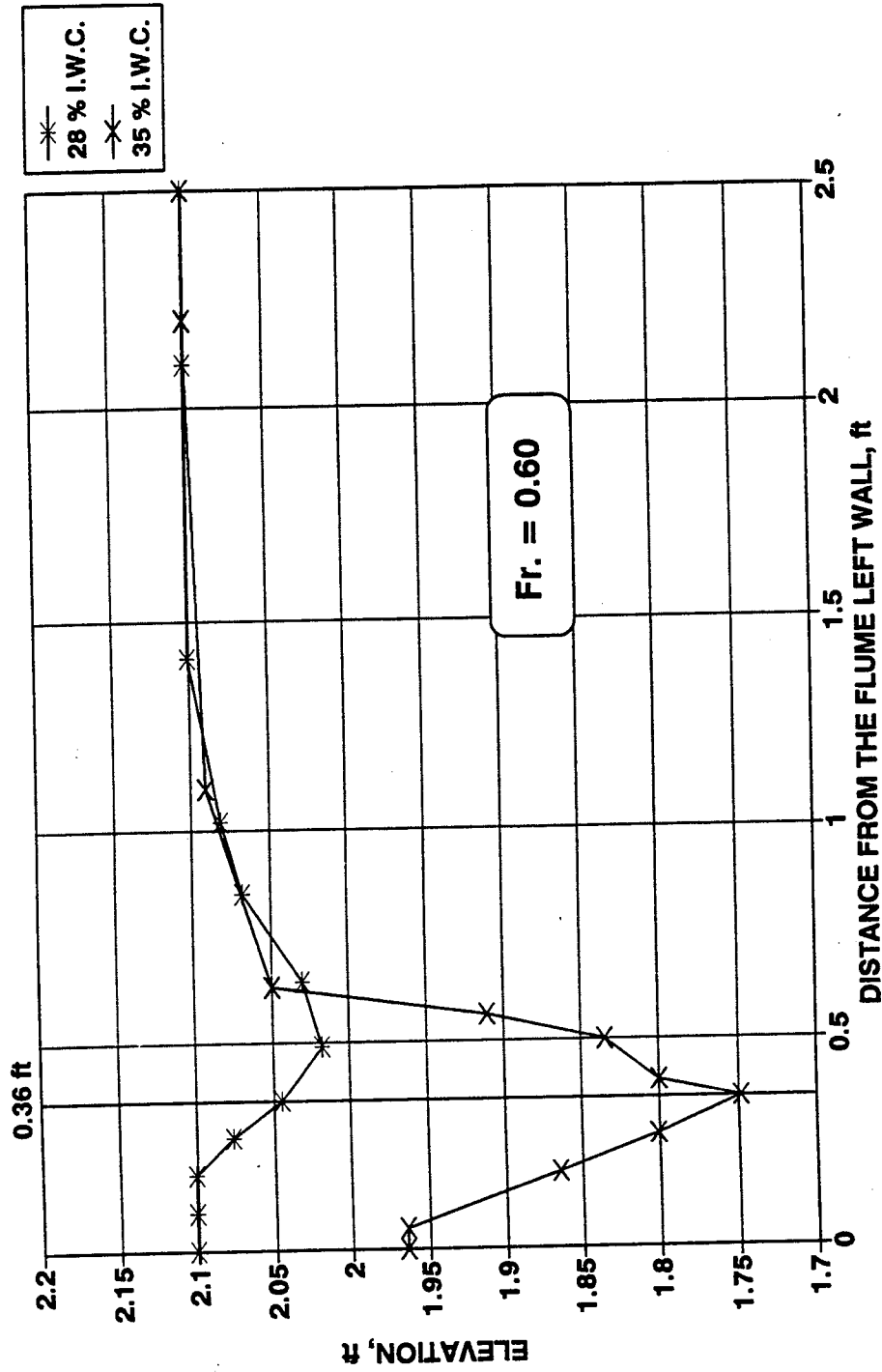


Figure (5.11) Effect of Initial Water Content on the Scour Hole Geometry at the Upstream Abutment Face.

Figures 5.12 a, b, c, and d show actual photographs of abutment scour hole geometry for runs number 4-49, 4-44, 4-64, and 4-70 with initial water contents of 11 %, 20 %, 35 %, and 46 %.

Table 5.7 Effect of Initial Water Content on Scour Geometry for Montmorillonite Clay

Run No.	Initial Water Content (%)	Depth (ft)	Normalized Depth	Width (ft)	Side Slope (degrees)
4-48	12	0.162	1.066	0.55	16.41
4-41	20	0.136	0.875	0.39	19.22
8-35-A	20	0.650	0.407	2.00	18.00
4-63	28	0.110	0.132	1.05	5.98
8-29-A	28	0.0	0.0	0.0	0.0
8-28-A	28	0.0	0.0	0.0	0.0
4-65	35	0.352	0.423	0.27	52.51
8-38-A	35	0.300	0.157	0.36	39.81
8-29-B	35	0.530	0.323	2.08	14.3
8-37-B	45	0.890	0.510	1.78	26.57

5.4.1.3 Longitudinal Slope of the Scour Holes

For each soil mixture, the scour hole will have a certain slope along the longitudinal direction of the flow adjacent to the abutment wall (Figure 5.7). In order to calculate this slope for each soil mixture, channel cross sections were plotted for different Froude numbers. The slope was then calculated as an average slope value for that soil mixture for the entire range of flow conditions. Figures 5.13 through 5.17



Figure (5.12 a) View of Abutment Scour Hole Geometry for 11 % IWC (Run 4-49).



Figure (5.12 b) View of Abutment Scour Hole Geometry for 20 % IWC (Run 4-44).

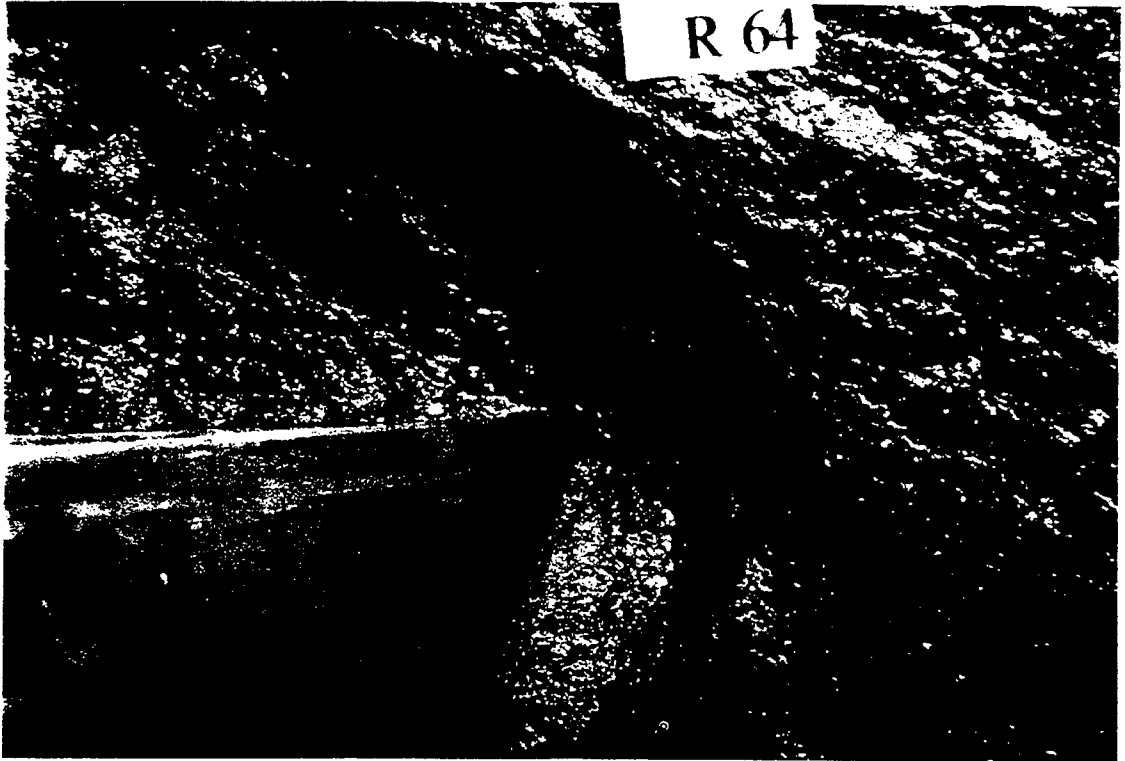


Figure (5.12 c) View of Abutment Scour Hole Geometry for 35 % IWC (Run 4-64).



Figure (5.12 d) View of the Abutment Scour Hole Geometry for 45 % IWC (Run 4-70).

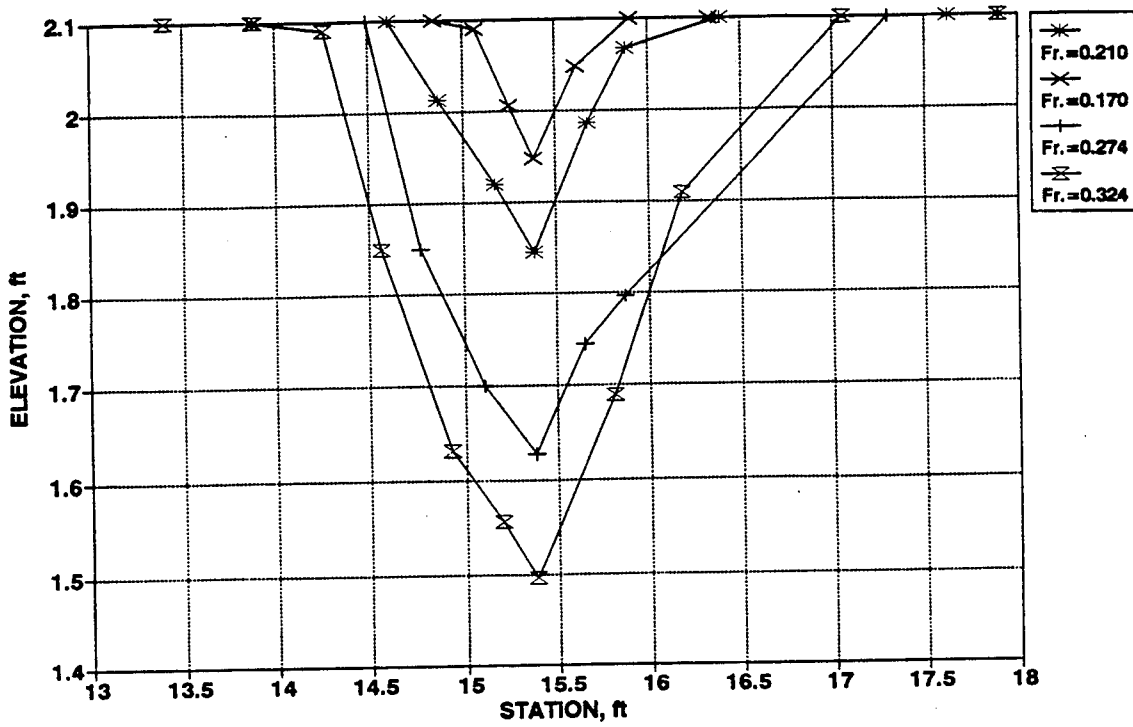


Figure (5.13) Longitudinal Profile of the Scour Hole for 12 % Initial Water Content.

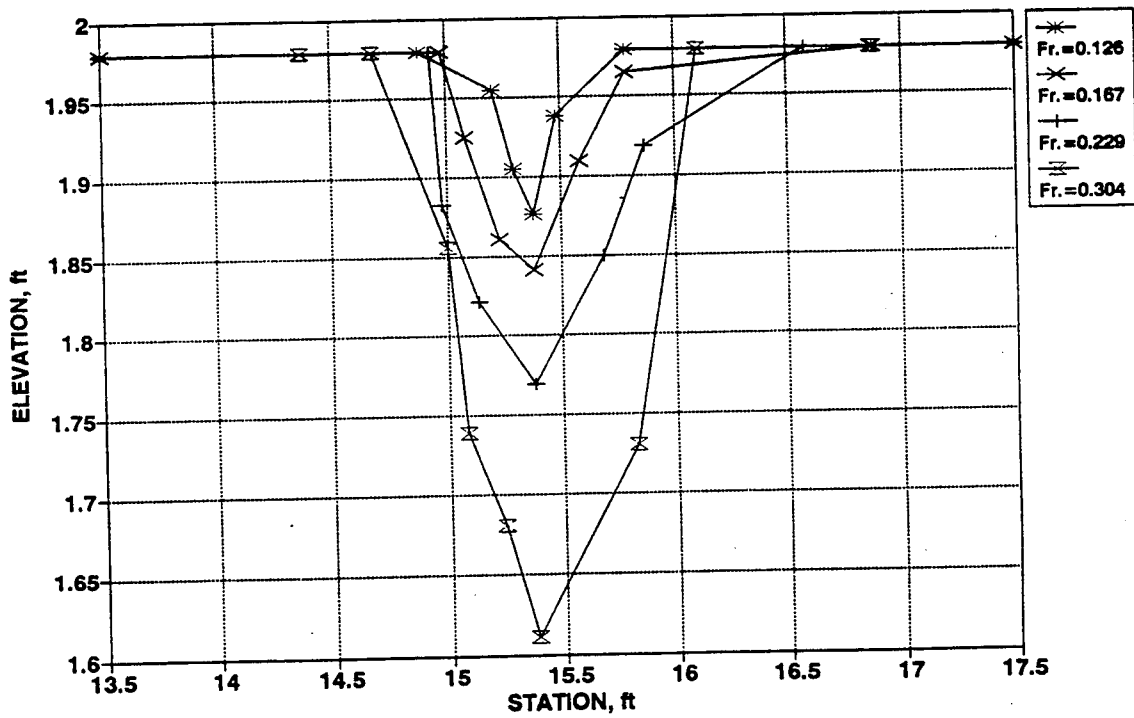


Figure (5.14) Longitudinal Profile of the Scour Hole for 20 % Initial Water Content.

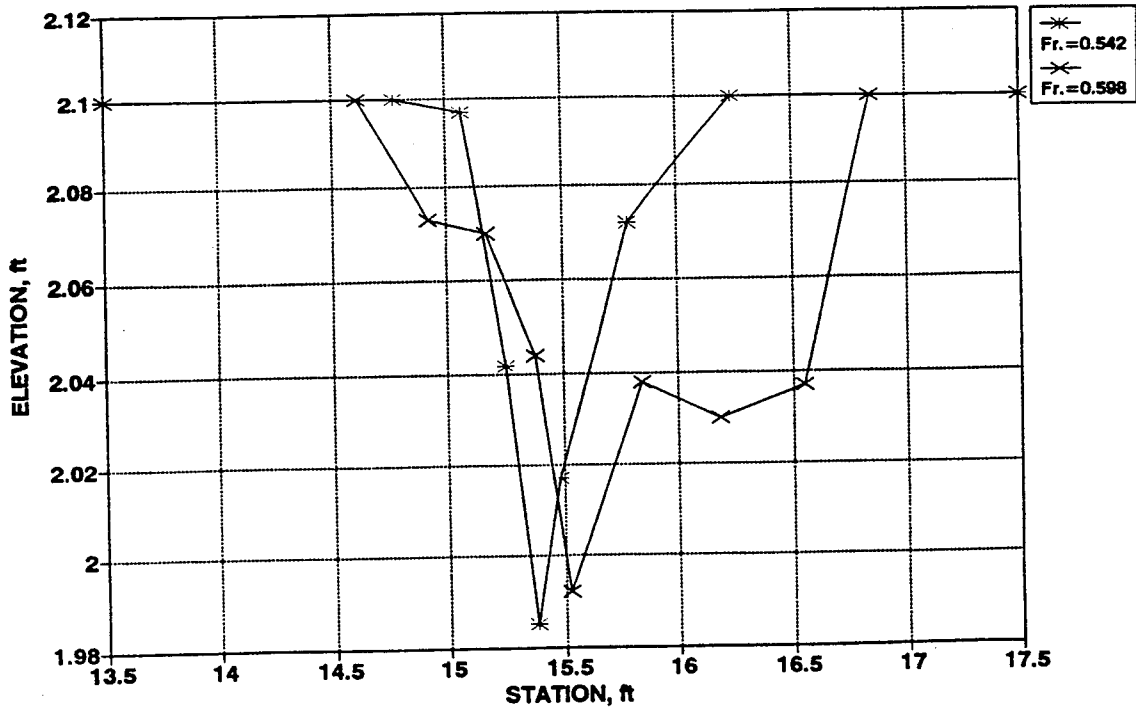


Figure (5.15) Longitudinal Profile of the Scour Hole for 28 % Initial Water Content.

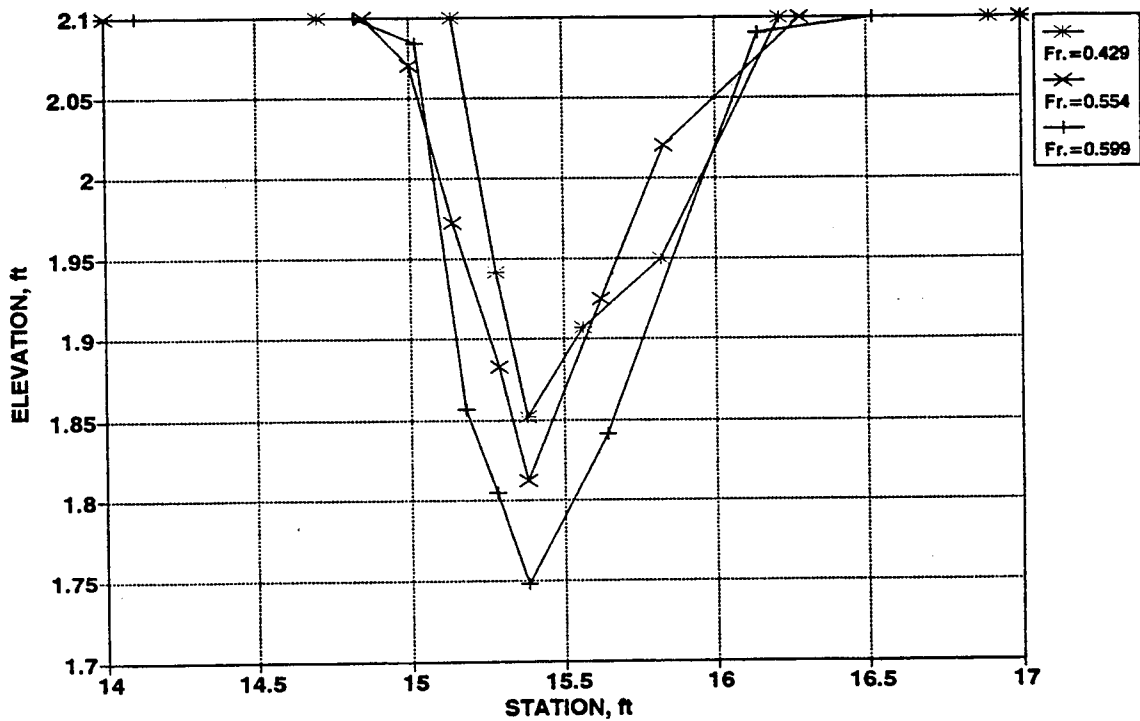


Figure (5.16) Longitudinal Profile of the Scour Hole for 35 % Initial Water Content.

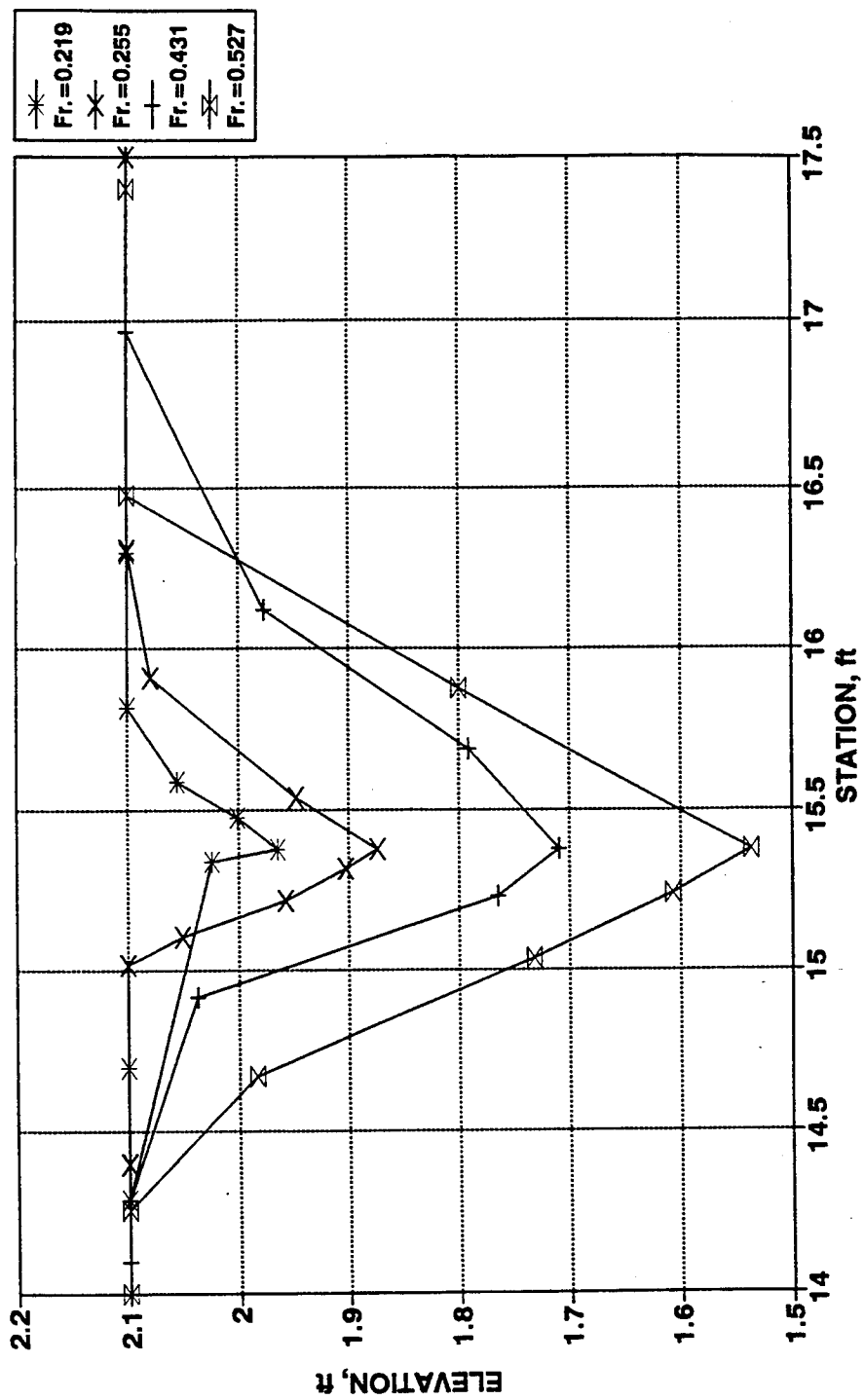


Figure (5.17) Longitudinal Profile of the Scour Hole for 45 % Initial Water Content.

presents cross section plots for the Montmorillonite clay with initial water contents of 12 %, 20 %, 28 %, 35 %, and 45 %. The summary of the longitudinal slope variation with initial water content is presented in Figure 5.18. In Figure 5.18 a distinction was made between the slope upstream from the abutment nose and in the downstream direction. From this figure it can be shown that, in the downstream direction the slope decreases from 22° to 14° as the initial water content is increased from 12 % to 28 %. The slope increases again from 14° to 26° as the initial water content is increased further from 28 % to 45 %. In the upstream direction on the sloping surface in front of the abutment, the slope follows the same trend but with steeper angles varying from 26° to 40°.

5.4.1.4 Effect of Initial Water Content on Time Rate of Scour

The time rate of scouring during the runs was recorded using a simple periscope manufactured using an inclined mirror. This periscope was moved up and down inside the abutment and depths were observed through a plexiglass panel by using a measuring tape mounted on the abutment wall. The scour depth development with time was recorded. The development of scour with time is a function of the rate of shear stress applied to the abutment base by the flow, and to the resistance of the bed material to erosion represented by the initial water content. At the initial phase of scour development, the strength of the horse shoe vortex is high, resulting in higher erosion rates. As the scour hole gets deeper, the horseshoe vortex gets weaker and consequently, the rate of applied shear stress and the rate of scour decreases until the equilibrium condition is reached. Starting from the basic functional relationship given by:

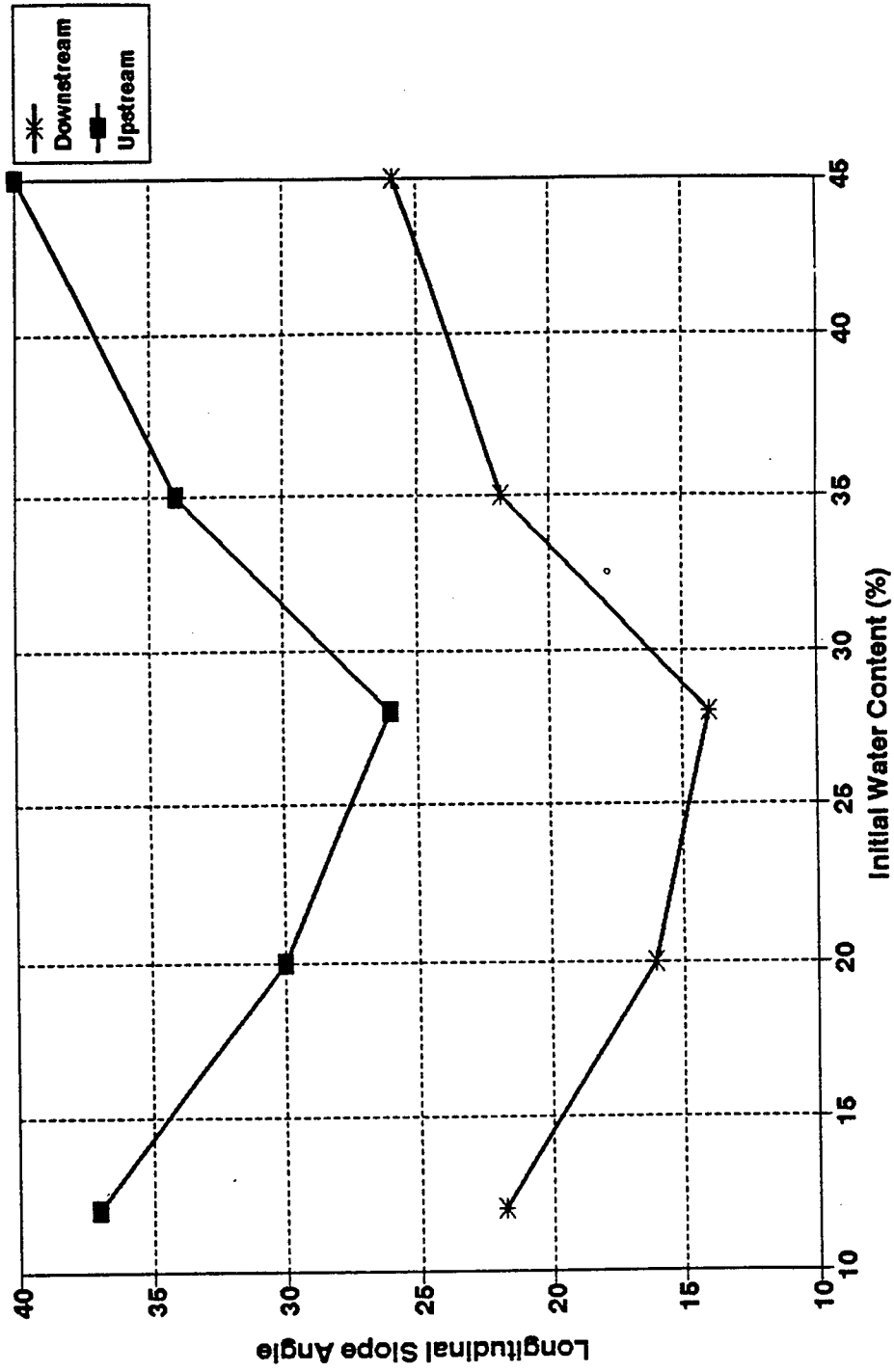


Figure (5.18) Variation of Longitudinal Slope Angles with Different Initial Water Content.

$$d_{sc}(t) = d_{scm} (1 - e^{-Kt}) \quad (5.5)$$

Where

d_{scm} = Maximum depth of abutment scour

$d_{sc}(t)$ = Abutment scour at time (t)

t = time of measurement (Minutes)

K = Coefficient which is a function of soil properties which affect resistance to scour such as initial water content, compaction, clay content, mineralogy, etc.

In this equation, the value of K controls how fast the scour reaches its maximum depth value. A statistical analysis was used to determine the best-fitting K value to the measured scour rate data. For the statistical analysis, both linear and nonlinear methods were investigated. For the initial times, the nonlinear form described the time rate of erosion more accurately. Various forms of time rate of erosion equations were investigated. Equation 5.5 was found to best fit the present data statistically. In this relationship, at (t=0) the value of scour is zero. As t increases, the value of $d_{sc}(t)$ approaches to that of d_{scm} . Also, as the value of K increases, the time required for the maximum depth of scour to reach equilibrium is reduced. The value of maximum depth of scour is dependent upon the flow conditions. Normalizing the depth of scour by maximum depth of scour, the rate of scour is made independent of the approach flow conditions. Therefore the value of K represent the erodibility of bed material. The duration of the runs were around 12 hours. Figures 5.19 through 5.21 show the development of scour depth with time for initial water contents of 12 %, 20 %, 35 %, and 45 % for different values of approach Froude numbers for Montmorillonite clay. As given in Figure 5.19, the value of K for the 12% initial water content (IWC) case is

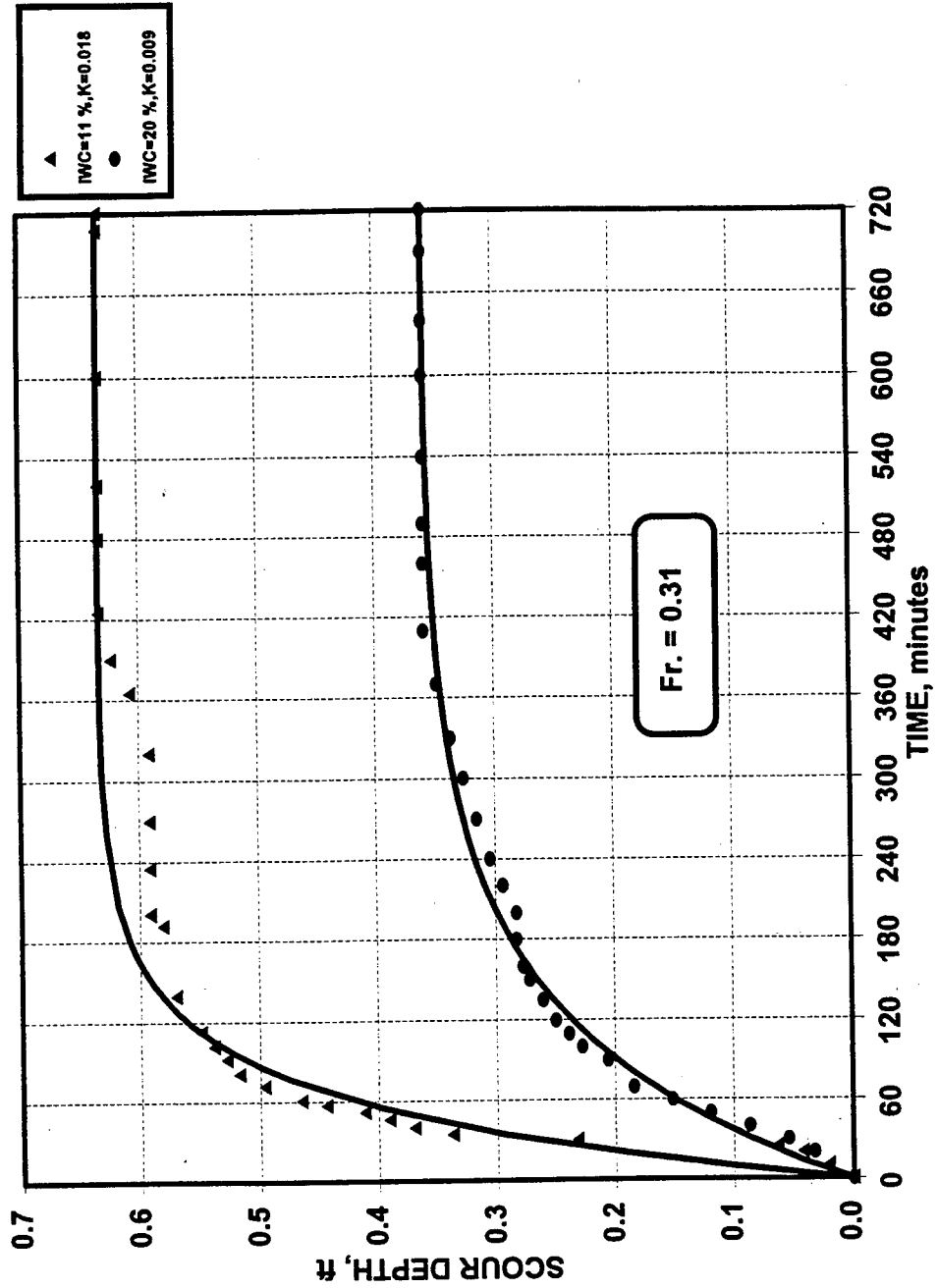


Figure (5.19) Time Rate of Scour for Initial Water Content of 11 % and 20 % (Runs 4-50 and 4-42).

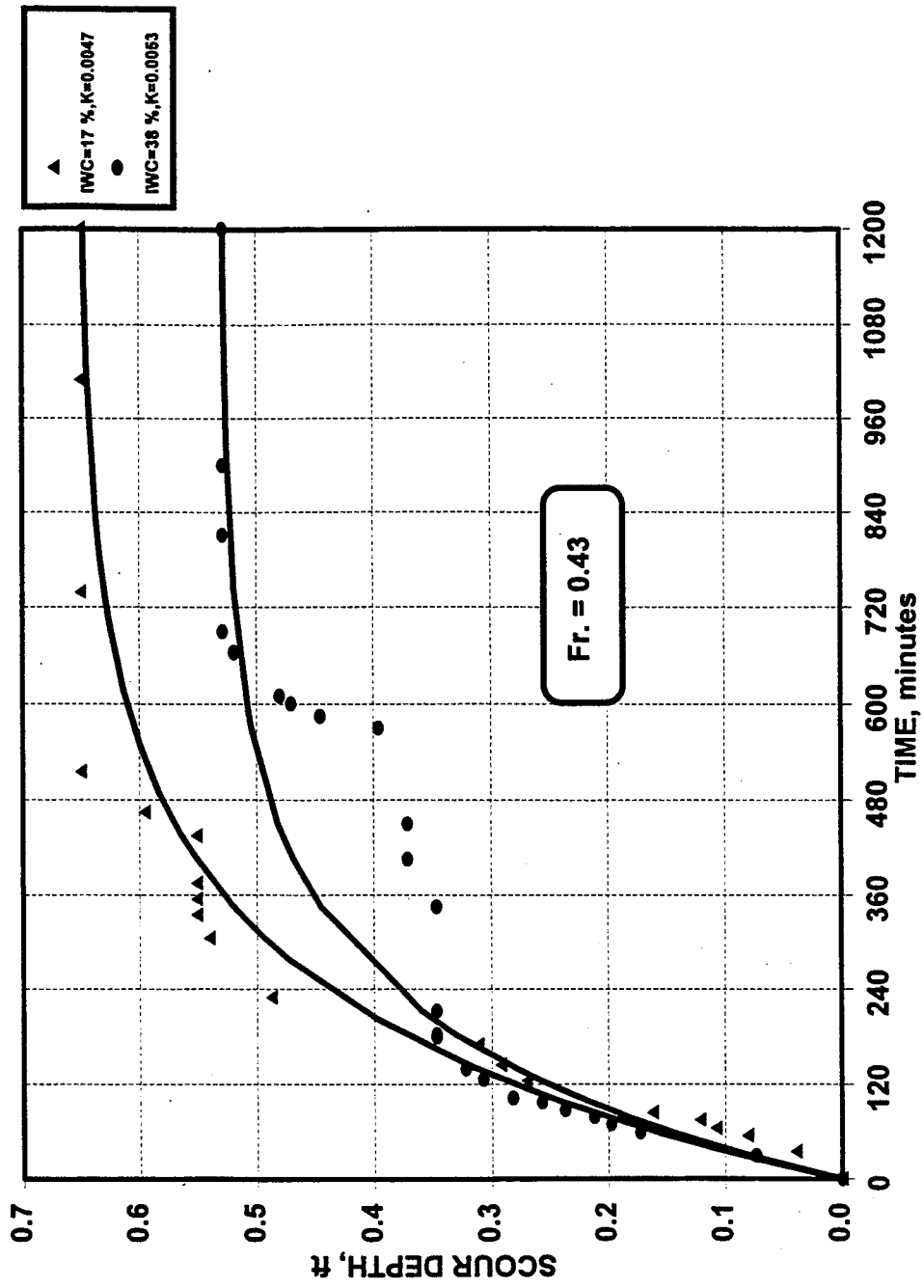


Figure (5.20) Time Rate of Scour for Initial Water Content of 17 % and 38 % (Runs 8-35-A and 8-29-B).

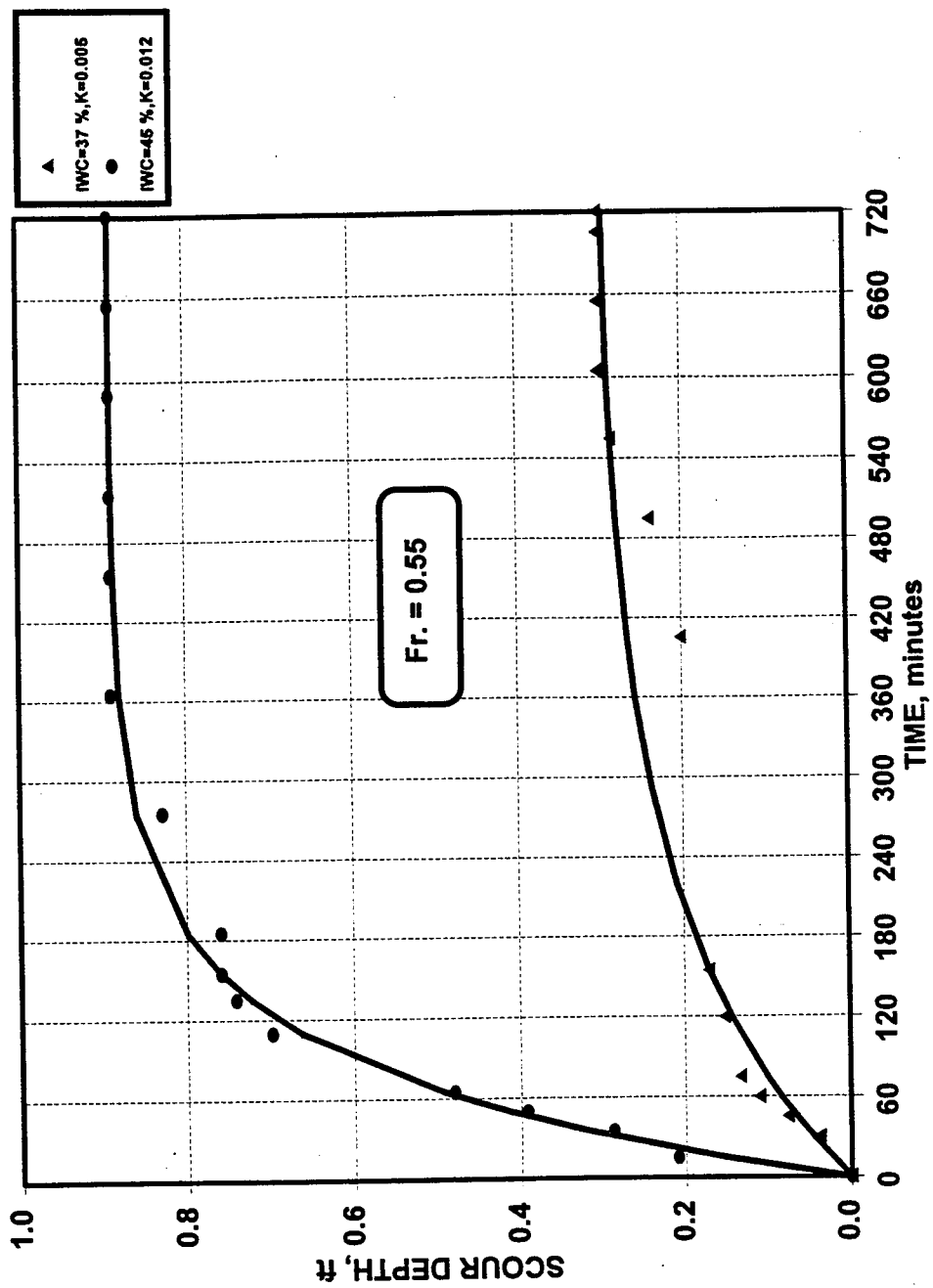


Figure (5.21) Time Rate of Scour for Initial Water Content of 37 % and 45 % (Runs 8-38-A and 8-37-B).

slightly higher than the K value for 20 % IWC case for the same flow condition which indicates that the rate of erosion for the 12 % IWC should reach equilibrium condition slightly faster than the 20 % IWC case. In Figure 5.20, the K value for the 20 % IWC is almost the same as the K value for the 35 % IWC and in Figure 5.21 the K value for 35 % IWC is lower than the K value for 45 % IWC case. This indicates that the time needed to reach equilibrium condition (time to equilibrium) for the bed material is increasing with the increase of initial water content from 12 % IWC to 28 % IWC. For 28 % IWC, time to equilibrium is maximum (no scour case). Increasing the initial water content further from 28 % IWC up to 45 % IWC, decreases the time to equilibrium. Also, as shown in Figure 5.22, for Montmorillonite clay with the same initial water content (about 15 % IWC) and the same compaction (about 78 %) and with different Froude number values (0.238 and 0.384), the K value is almost the same. This indicates that the time rate of scour is dependent on soil properties alone. Table 5.8 includes all the values of K for different initial water contents used in the figures. Since the value of K is dependent on erodibility of cohesive material, for other types of soils, similar analysis should be conducted and tables similar to Table 5.8 have to be developed.

Table 5.8 Effect of Initial Water Content on Time Rate of Scour for Montmorillonite Clay

Run No.	Compaction (%)	Initial Water Content (%)	K Value
4-50	66	11	0.018
4-42	76	20	0.009
8-38-A	78	37	0.005
8-37-B	77	45	0.012
8-35-A	76	17	0.005
8-29-B	66	38	0.005
8-27-B	73	13	0.011
8-35-B	73	16	0.010

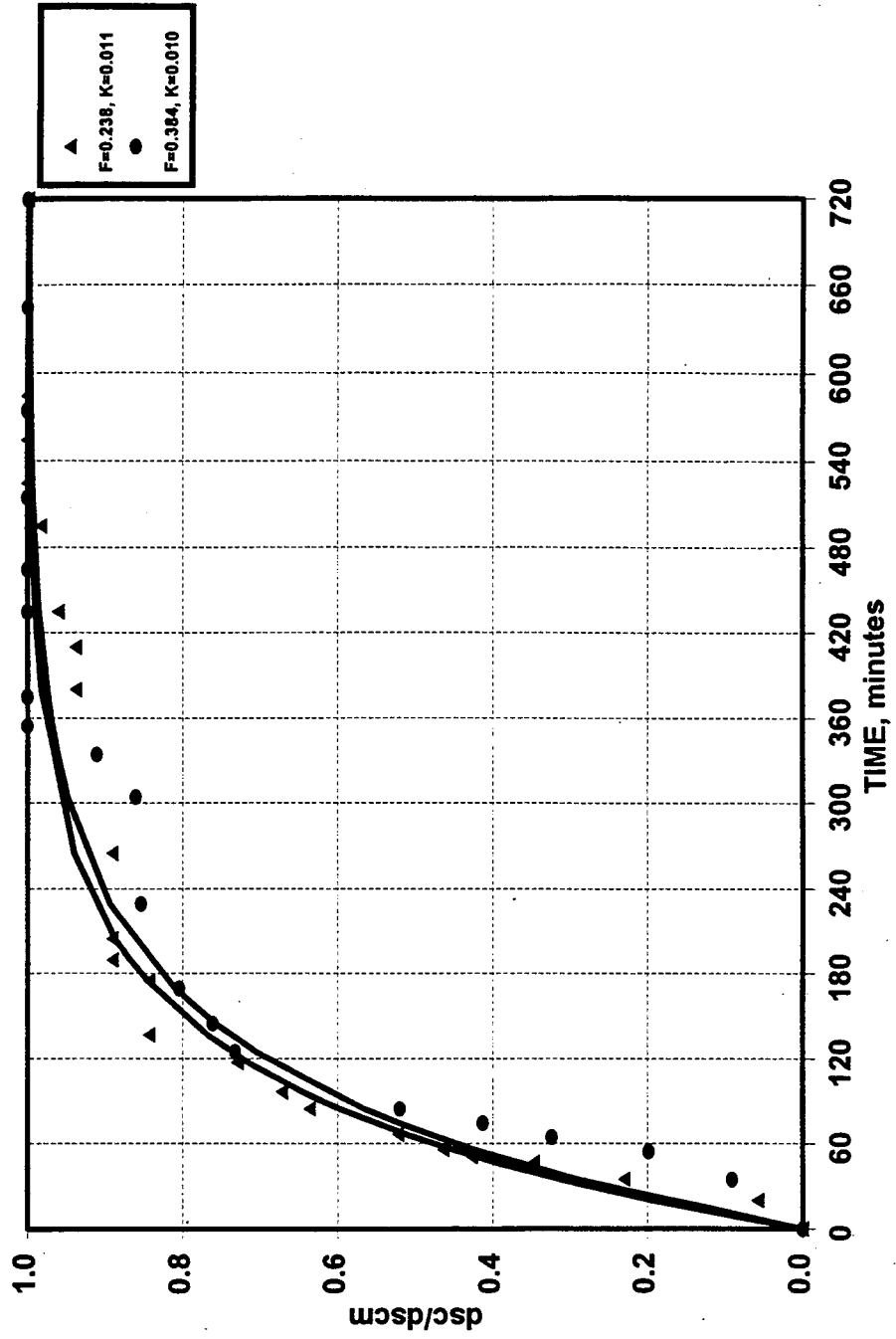


Figure (5.22) Time Rate of Normalized Scour for Different Flow Conditions (Runs 8-27-B and 8-35-B).

5.4.2 Effect of Clay Compaction on the Clay Mixture

This section will include the investigation of: the scour depth is expressed as a function of Froude number for various clay compactions, the effect of compaction on the cross-sectional profile of the scour hole. Also, the side slope of the scour hole, the longitudinal slope of the scour hole, and time rate of scour. The results are expressed in functional relationships whenever possible.

5.4.2.1 Variation of Scour Depth with Approach Flow Conditions

The effect of compaction in Montmorillonite was investigated by maintaining the same range of mixture initial water content and by changing only percentage of clay compaction under varying flow conditions. The initial water content used for the experiments of compaction effect was 20 % with two ranges of compaction--around 63 % for low compaction, and around 77 % for high compaction--. Figure 5.23 shows the relationship between Froude number and the scour depth normalized by the square root of abutment width and flow depth. For the same flow conditions (for a given Froude number), the depth of maximum scour decreases as the percentage of clay compaction increases from low to high compaction. Also, for the same low compaction as the initial water content is increased from 12 % to 20 % IWC, the depth of scour increases. Figure 5.24 presents the relationship between normalized scour depth and compaction in a family of curves for different Froude numbers for a 12 % initial water content. Figure 5.25 shows the same for a 20% initial water content. For the Montmorillonite clay, up to 20 % initial water content, it was possible to apply compaction. For 28 %

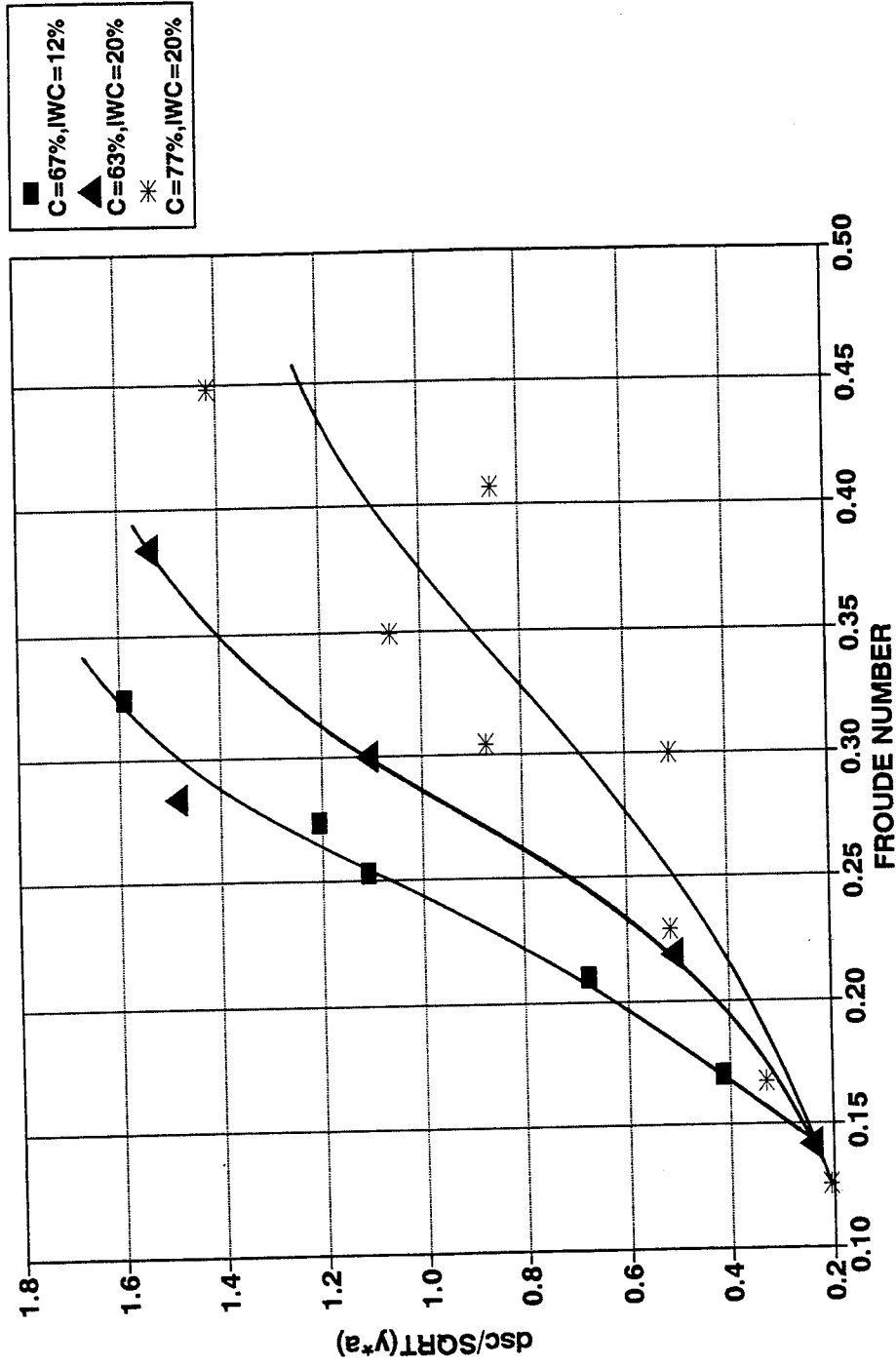


Figure (5.23) Variation of Dimensionless Abutment Scour Depth with Froude Number for Montmorillonite Clay.

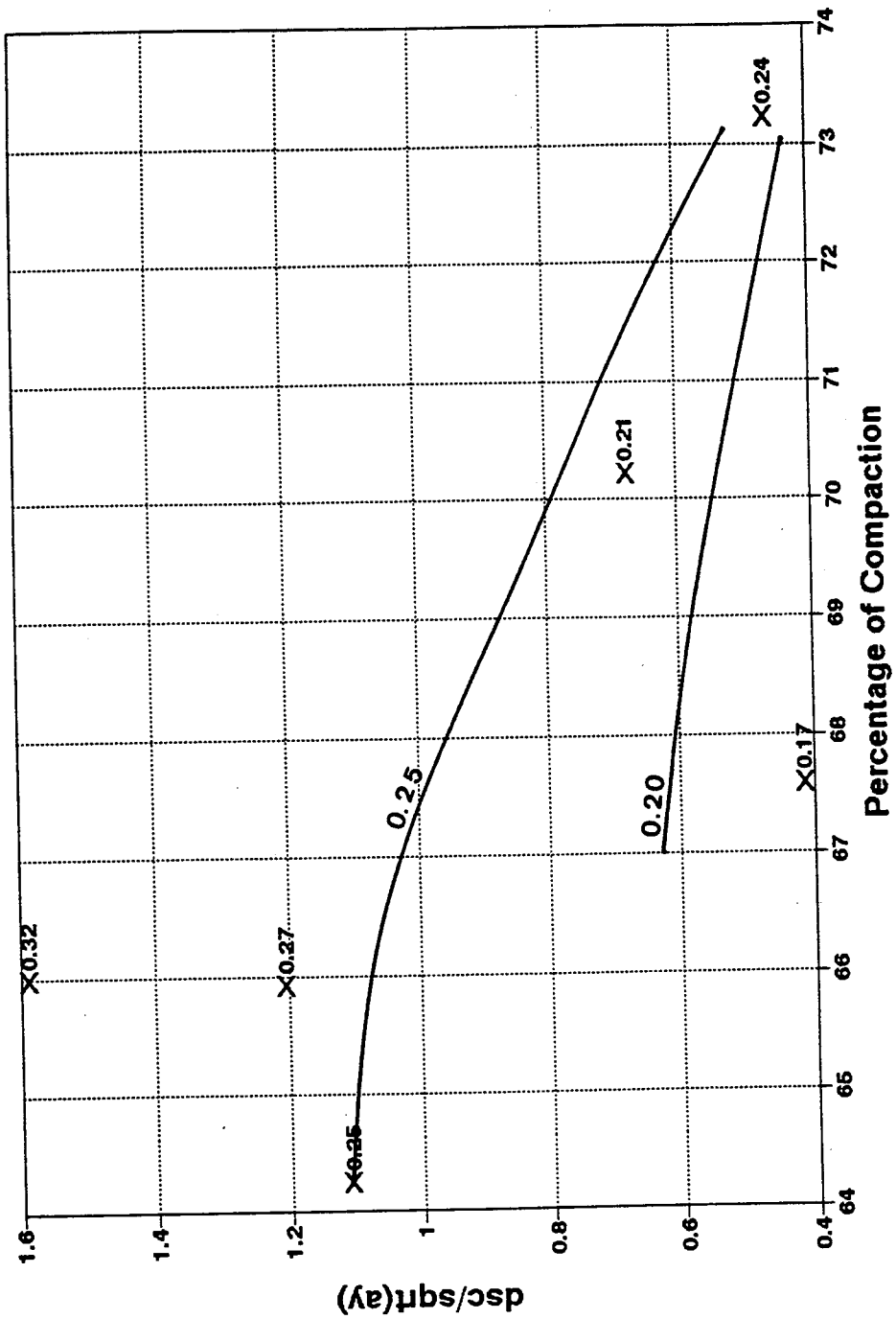


Figure (5.24) Effect of Compaction on Dimensionless Abutment Scour Depth for Montmorillonite Clay with 12 % IWC.

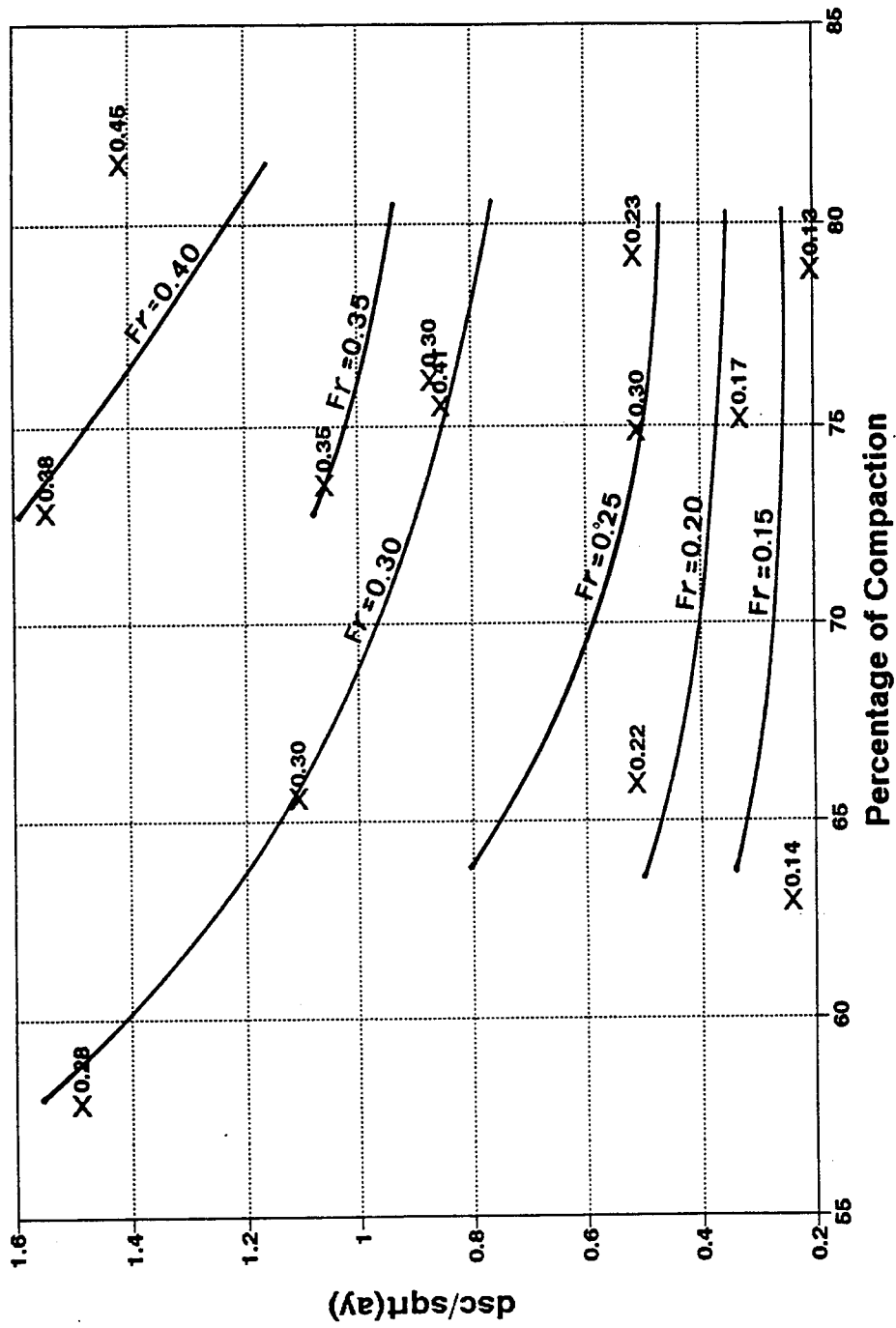


Figure (5.25) Effect of Compaction on Dimensionless Abutment Scour Depth for Montmorillonite Clay with 20 % IWC.

and higher initial water content it is not possible to perform any compaction because of exceeding the saturation conditions. Average normalized scour depth for both 12 % and 20 % initial water content is shown in Figure 5.26 for different degrees of compaction. In this figure the scour depth for clay was normalized with the corresponding depth of abutment scour for sand using Figure 5.4.

5.4.2.2 Cross-Sectional Profile of the Scour Holes

To study the effect of compaction on the geometry the resulting scour hole for Montmorillonite clay, a comparison of different cross-sectional profiles passing through the upstream face of the abutments was conducted using two different compaction ratios with two different Froude numbers. The comparison of the cross-section profiles are presented in Figures 5.27 and 5.28. Figures 5.29 a, and b show actual photographs of abutment scour hole geometry for runs number 4-40, and 4-45 with percent compaction of 79 %, and 66 %. The scour dimensions defined by the depth, width, and side slope corresponding to maximum scour conditions are presented in Table 5.9. Figure 5.27 shows the cross-sectional profiles for compactions of 73 % and 64 % at initial water content of 12 % and Figure 5.28 illustrates the cross-sectional profiles for compactions of 75 % and 58 % at initial water content of 20 %. From Figures 5.27 and 5.28 and Table 5.9, it can be concluded that the depth of scour decreases as the percentage of compaction is increased. Also, the side slope is flatter for the initial water content of 12 % than for the initial water content of 20 %.

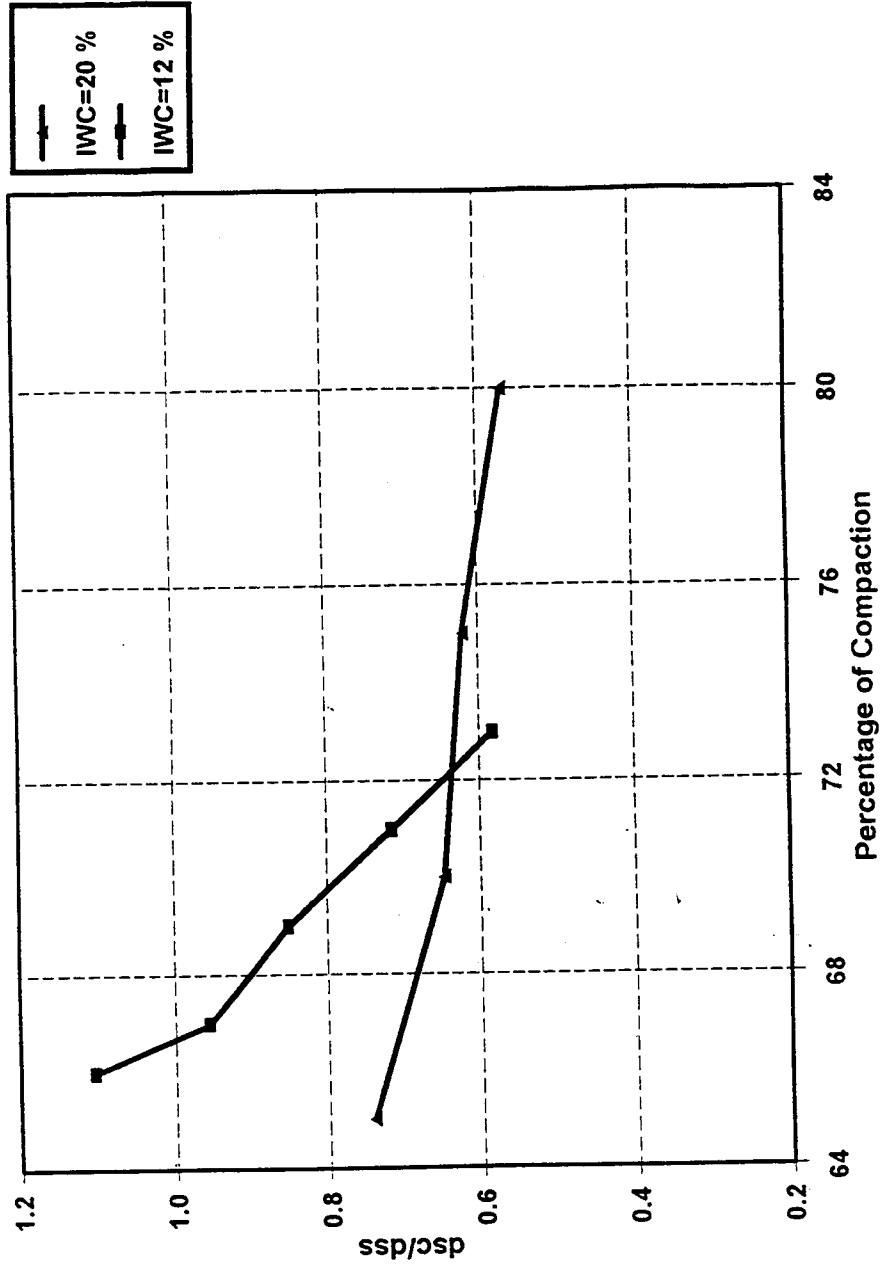


Figure (5.26) Variation of Normalized Scour Depth with Compaction for Montmorillonite Clay with 12 %, and 20 % IWC.

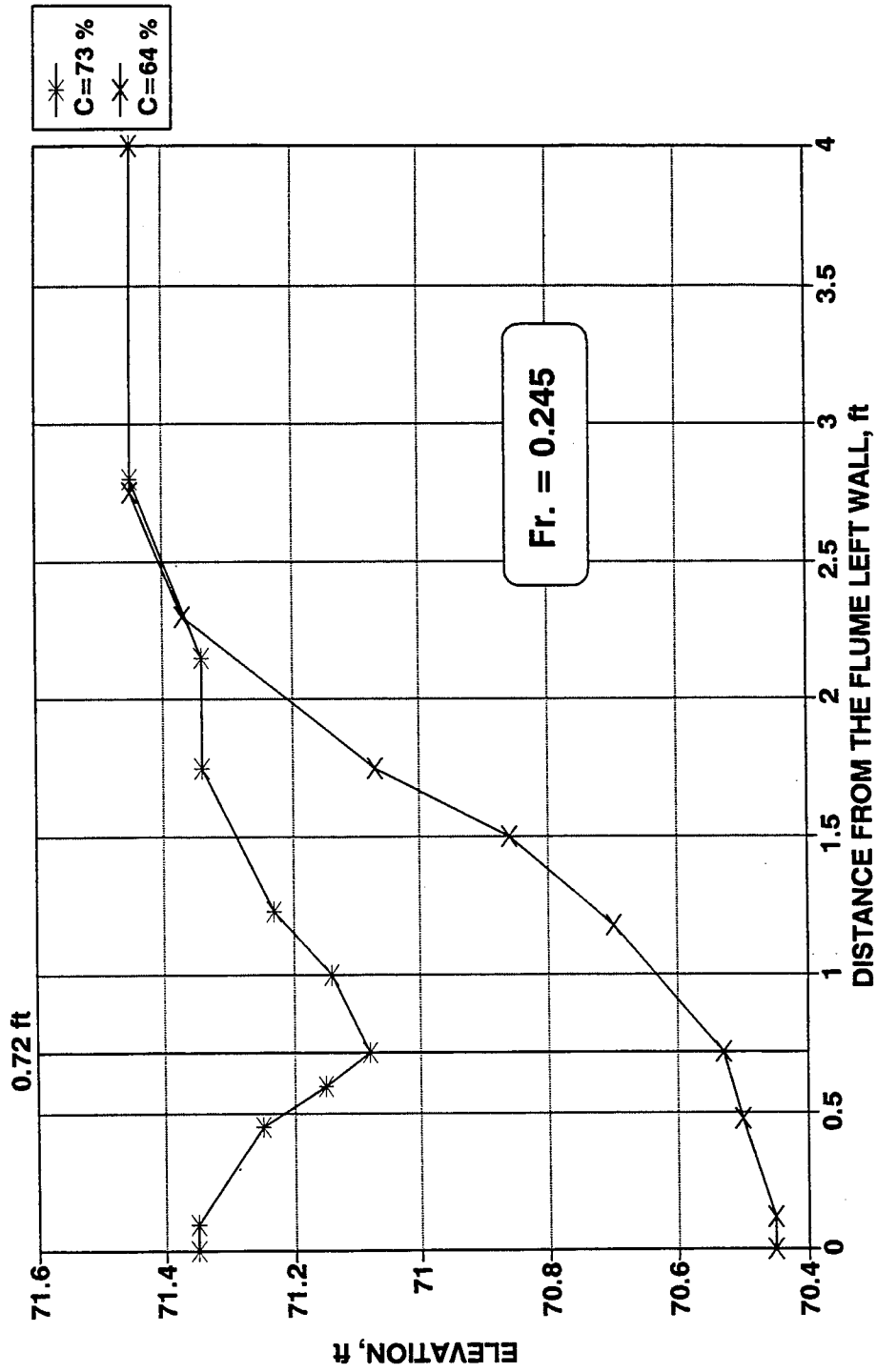


Figure (5.27) Effect of Compaction on the Scour Hole Geometry at the Upstream Abutment Face (IWC = 12 %).

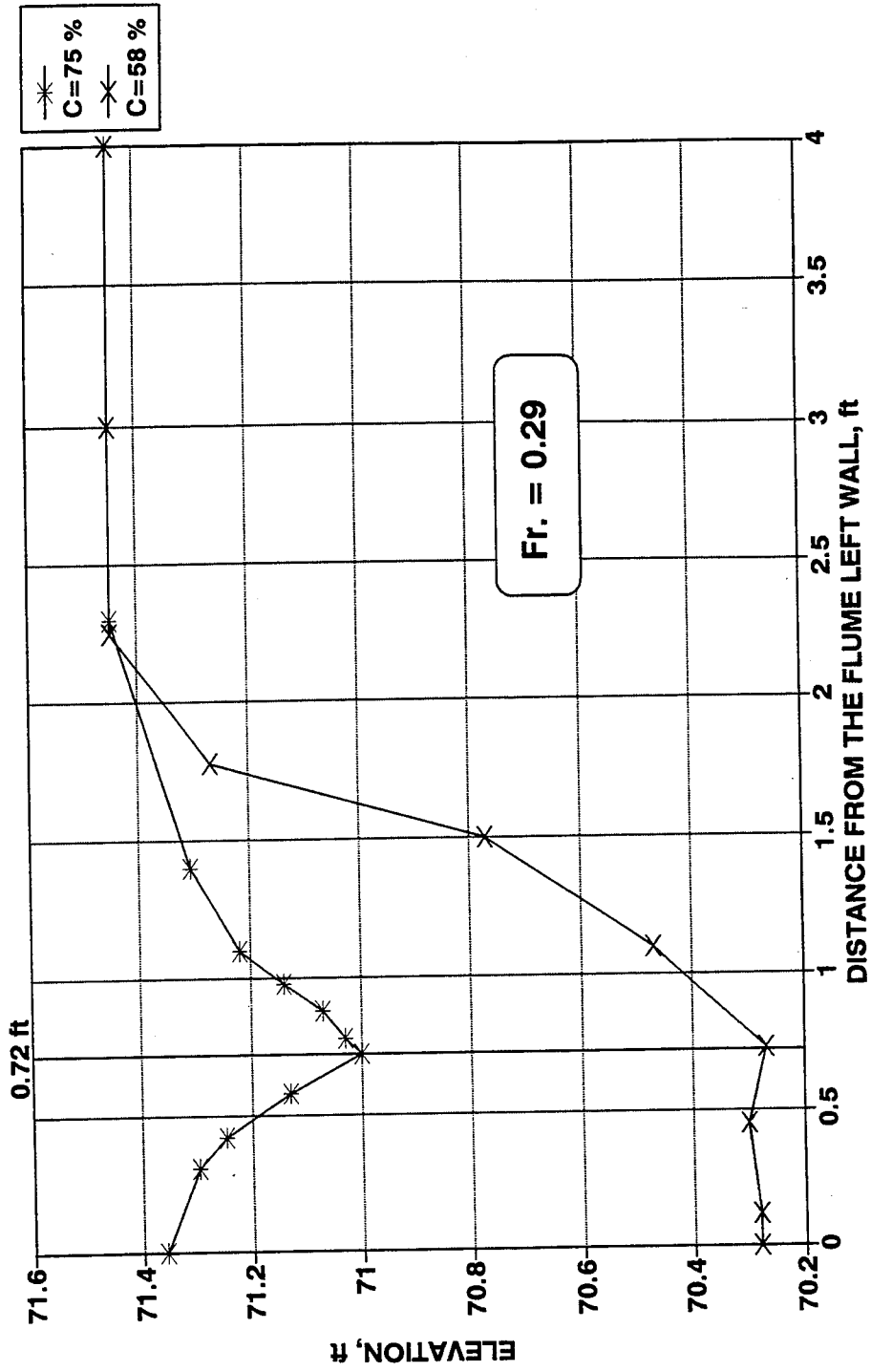


Figure (5.28) Effect of Compaction on the Scour Hole Geometry at the Upstream Abutment Face (IWC=20 %).

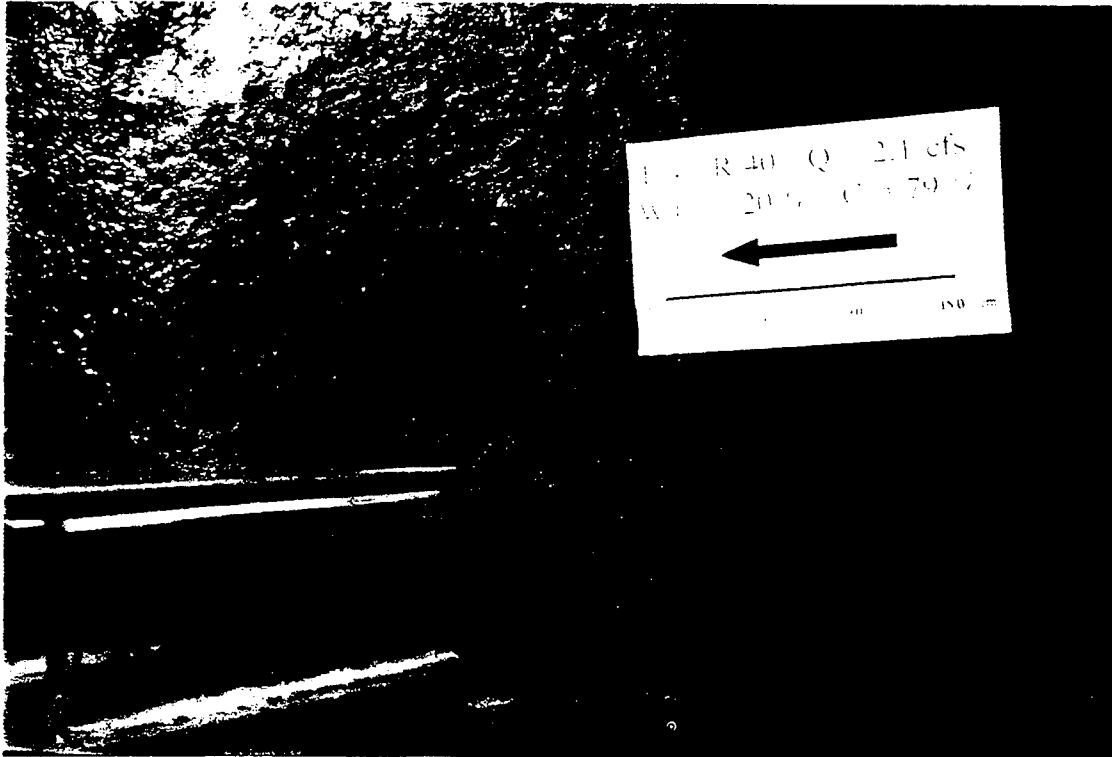


Figure (5.29 a) View of Abutment Scour Hole Geometry for 79 % C (Run 4-40).

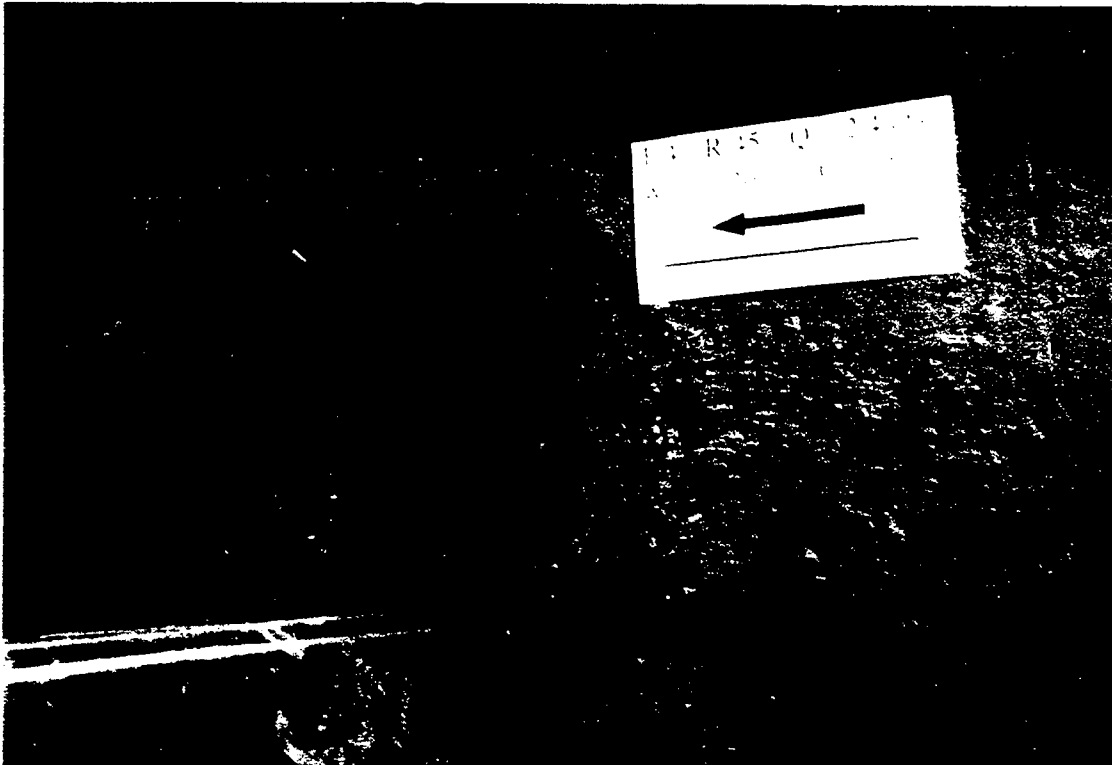


Figure (5.29 b) View of Abutment Scour Hole Geometry for 66 % C (Run 4-45).

Table 5.9 Effect of Compaction on the Scour Geometry for Montmorillonite Clay

Run No.	Compaction	Depth (ft)	Normalized Depth	Width (ft)	Side Slope (degrees)
8-30-B	75	0.400	0.391	1.58	14.21
8-27-B	73	0.360	0.579	2.08	9.82
8-31-B	64	0.890	1.214	2.03	23.67
8-31-A	58	1.160	1.279	1.53	37.17

5.4.2.3 Longitudinal Slope of the Scour Holes

For each soil mixture, the scour hole will have a certain slope along the longitudinal direction of the flow adjacent to the abutment wall (Figure 5.7). In order to calculate this slope for each soil compaction, channel cross sections were plotted for different Froude numbers. The slope was then calculated as an average slope value for that soil compaction for the entire range of flow conditions. Figures 5.14 and 5.30 presents cross section plots for the Montmorillonite clay with high compaction and low compaction respectively. In these figures the same initial water content of 20 % was used for different values of Froude number. The summary of the longitudinal slope variation with compaction is given in Figure 5.31. From these figures, it can be shown that in the downstream direction the slope decreases from 22° to 16° as the compaction is increased from 63 % to 77 %. In the upstream direction on the sloping surface in front of the abutment, the slope decreases from 42° to 30° as the percentage of compaction is increased from 63 % to 77 % which is steeper than the downstream slopes. Notice that this relation follows the same trend between maximum depth of scour and percentage of compaction where as the percentage of compaction increase, the depth of scour decrease.

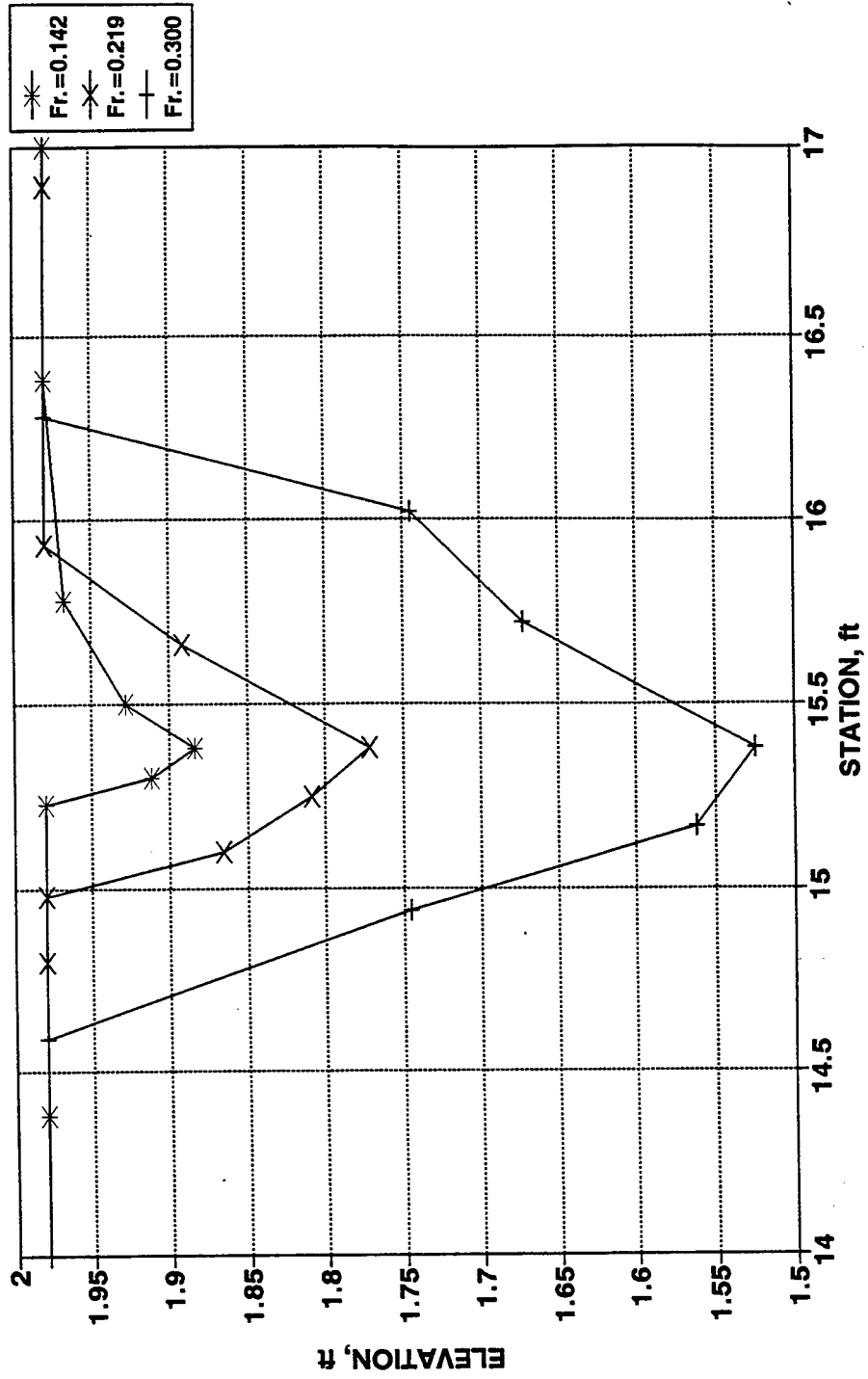


Figure (5.30) Longitudinal Profile of the Scour Hole for Low Compaction (IWC=20 %).

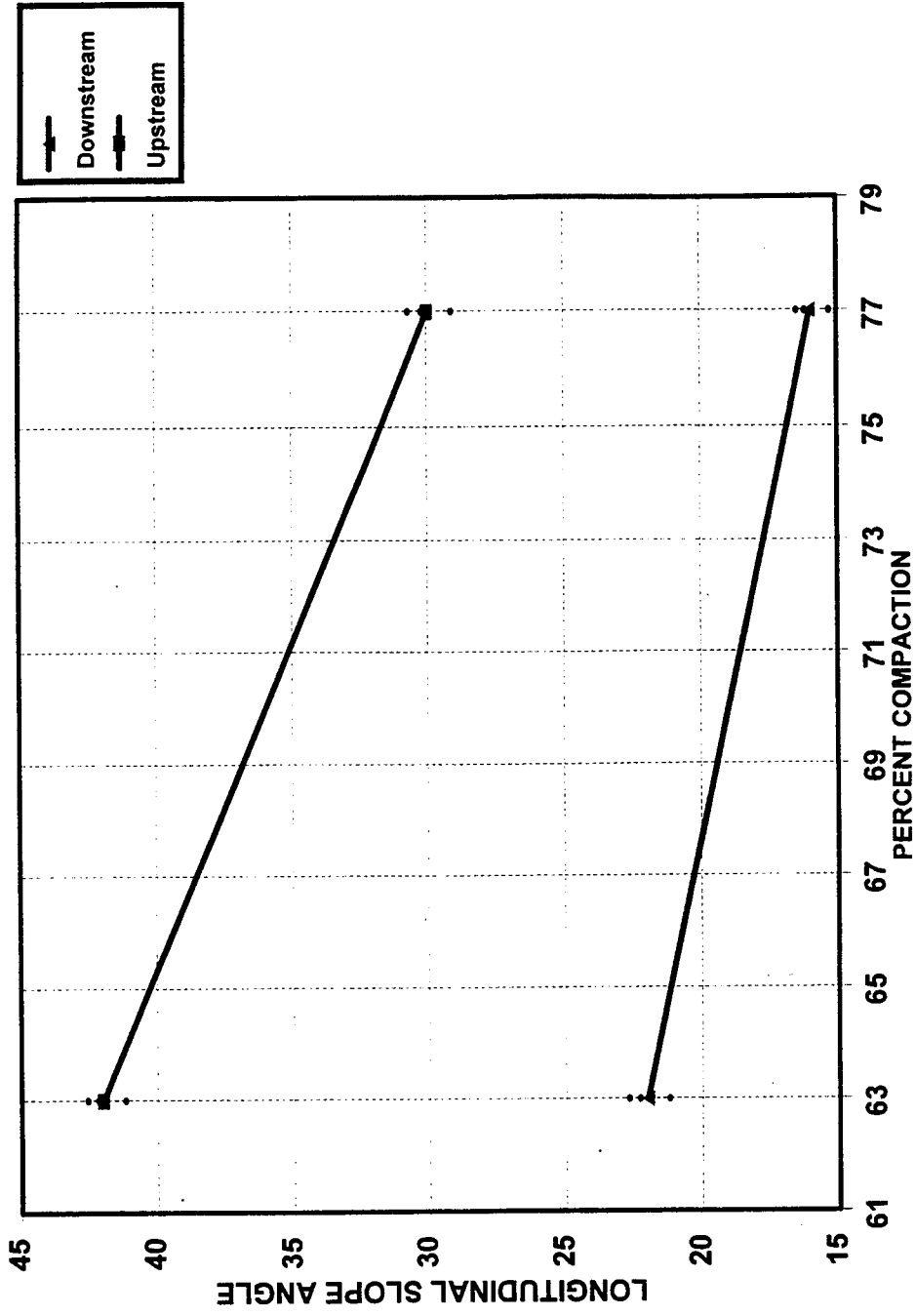


Figure (5.31) Variation of Longitudinal Slope Angles with Compactions of 63 %, and 77 %.

5.4.2.4 Effect of Clay Compaction on Time Rate of Scour

Figures 5.32 and 5.33 present the development of scour depth with time in Montmorillonite clay for low and high compaction for two different cases of initial water contents of 13 % and 20 %. As seen in Figure 5.32, for 13 % initial water content, the K value in the time rate of scour equation 5.5 decreases as the percentage of compaction is increased from 64 % to 73 % for the same flow conditions indicating that the rate of erosion for the low compaction clays reach equilibrium condition faster than the clays with high compaction. For the case of about 20 % initial water content, as given in Figure 5.33, the K value decreases as the percentage of compaction is increased from 58 % to 75 % for the same flow conditions which indicates that, again, the rate of erosion for low compaction reach equilibrium condition faster than the clay with high compaction. Table 5.10 includes all the values of K for different clay compaction conditions shown in the figures.

Table 5.10 Effect of Compaction on Time Rate of Scour for Montmorillonite Clay

Run No.	Compaction (%)	Initial Water Content (%)	K Value
8-27-B	73	13	0.011
8-30-B	75	21	0.005
8-31-A	58	18	0.013
8-31-B	64	13	0.021

5.4.3 Effect of Clay Content on Clay Mixture

This section will include the investigation of: the scour depth as a function of the approach flow conditions for various clay contents, the effect of clay content on the

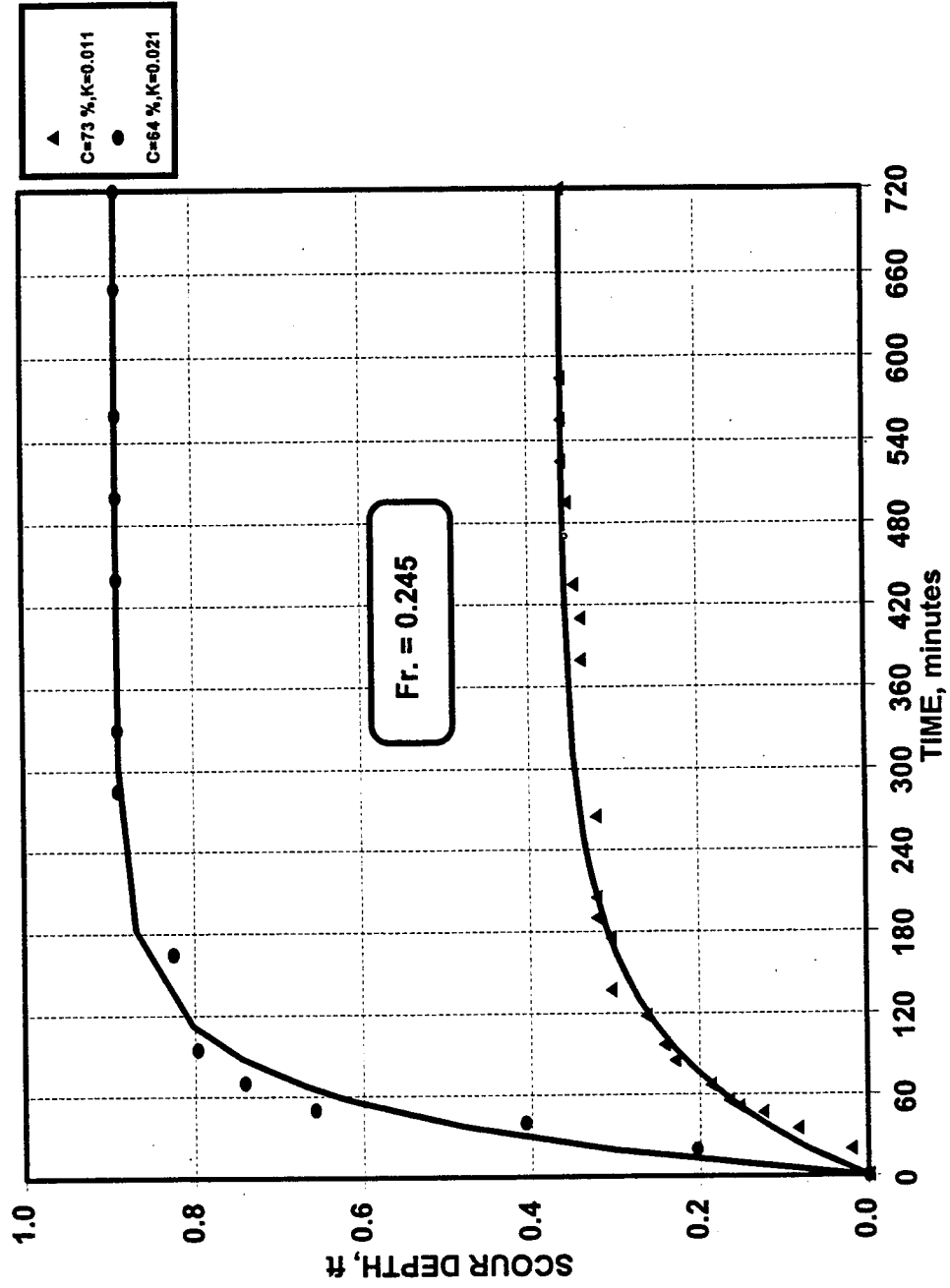


Figure (5.32) Time Rate of Scour for Compaction Ratios of 73 % and 64 % with 13 % IWC (Runs 8-27-B and 8-31-B).

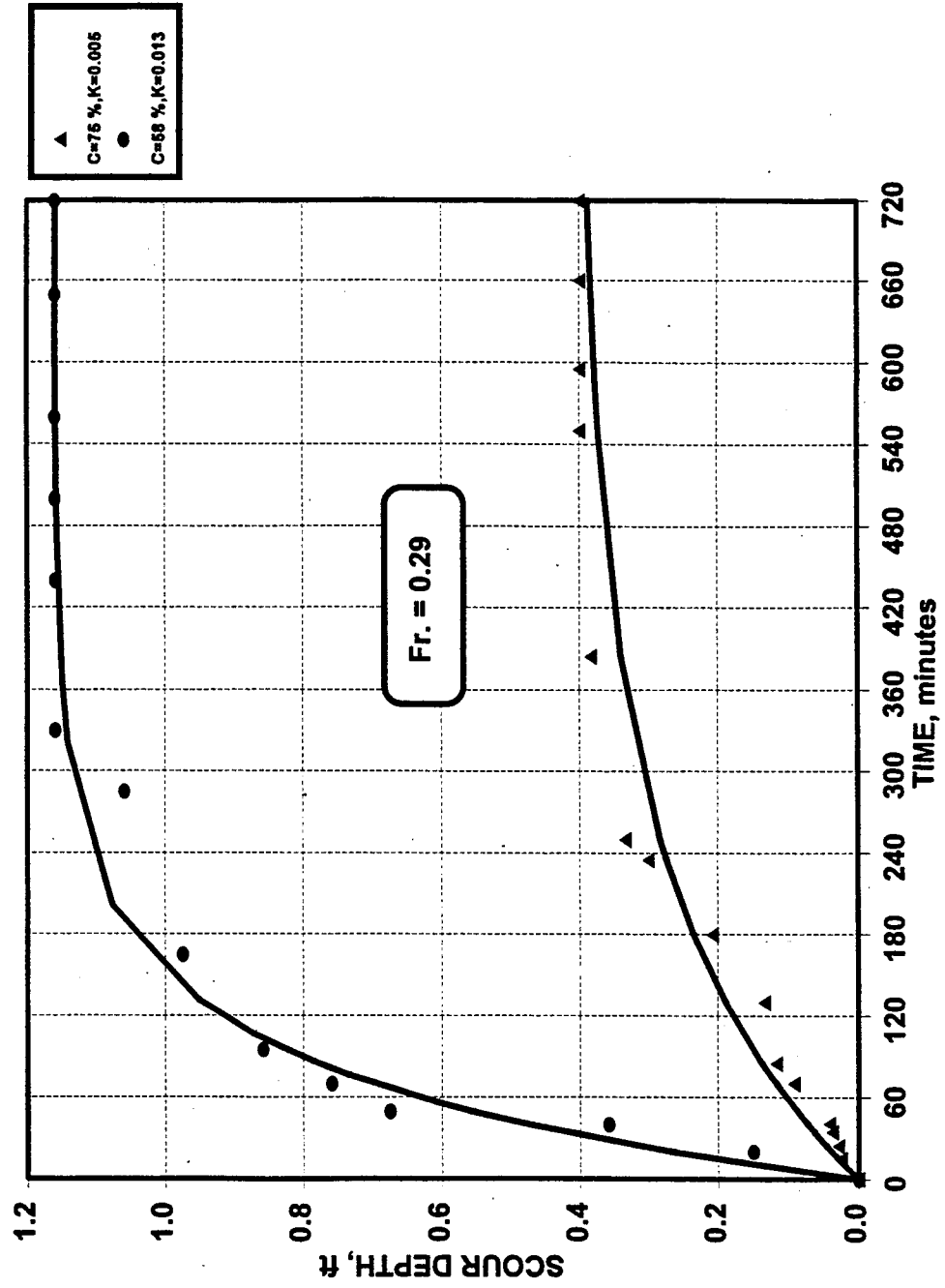


Figure (5.33) Time Rate of Scour for Compaction Ratios of 75 % and 58 % with 20 % IWC (Runs 8-30-B and 8-31-A).

cross-sectional profile of the scour hole. Also, the side slope of the scour hole, the longitudinal slope of the scour hole, and time rate of scour. The results are expressed in functional relationships whenever possible.

5.4.3.1 Variation of Scour Depth with Approach Flow Conditions

The effect of the percentage of clay content in the mixture of Montmorillonite clay and sand was investigated by varying the percentage of clay in the mixture. The clay content varied in the mixture from 0 % clay (medium sand) to 15 %, 30 %, and 40 %. Figure 5.34 relates the dimensionless scour depth -- depth of scour normalized by the square root of abutment width and flow depth -- to the intensity of flow conditions expressed by the Froude number. As shown in Figure 5.34, for a given Froude number, the scour depth decreases as the percentage of clay content in the mixture is increased from 0 % to 15 %. Increasing the percentage of clay further from 15 % to 30 %, the depth of scour keeps on decreasing. By increasing the percentage of clay content beyond 30 % to 40 %, the depth of scour showed little or no increase. This phenomena was more obvious for the high Froude number experiments than the low Froude number experiments. From this, it is concluded that up to 30 % clay content, there are no (or little) cohesion effect on the depth of scour. Beyond 30 % clay content, the Initial Water Content and compaction stat to show their effect. To separate the clay content effect, the values of dimensionless scour depth in Figure 5.34 for various clay contents are normalized by the corresponding dimensionless scour depth in sand (d_s/d_m) for the same flow conditions as shown in Figure 5.35. Finally, the average scattered experimental

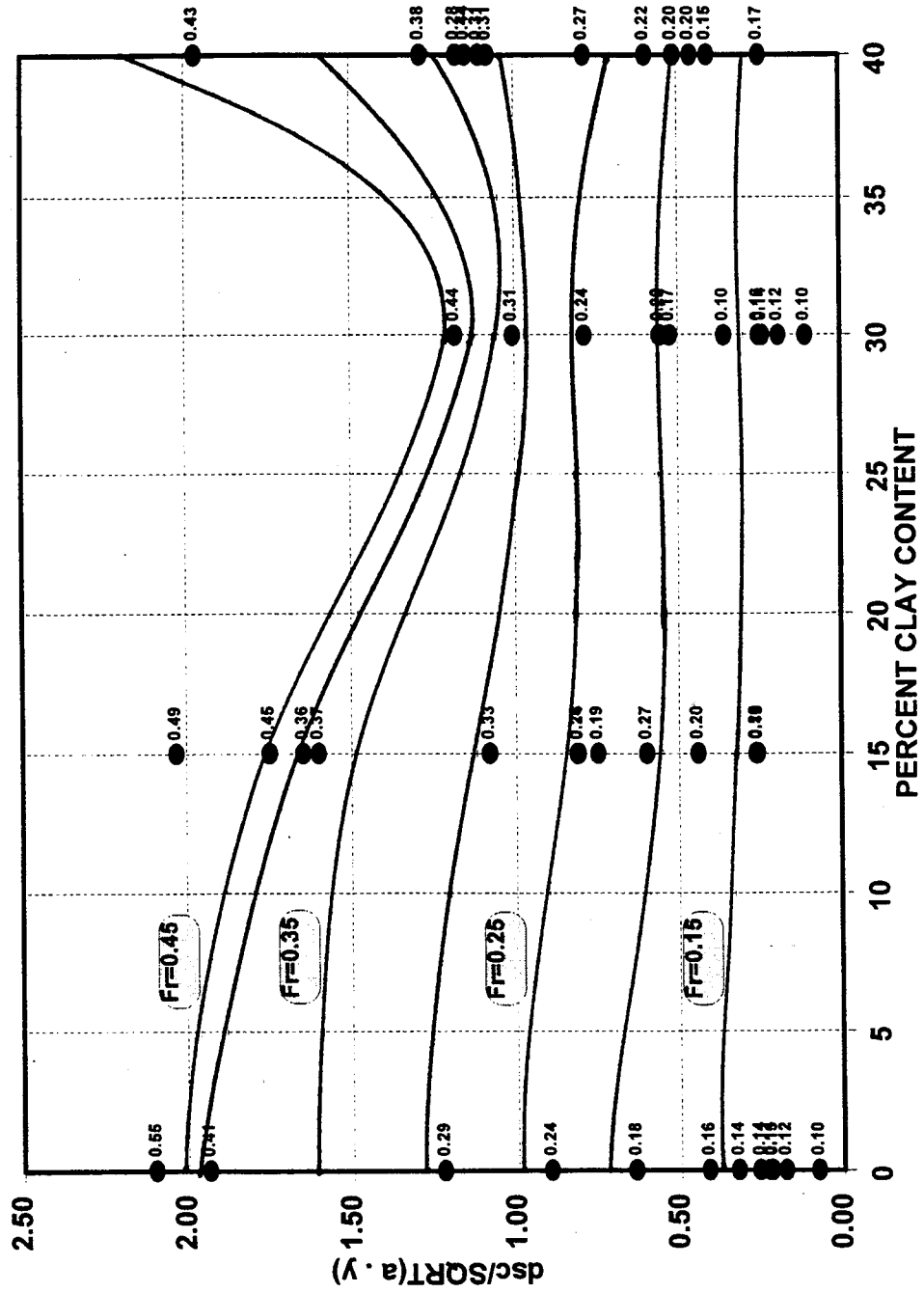


Figure (5.34) Effect of Clay Content on Dimensionless Abutment Scour Depth for Montmorillonite Clay.

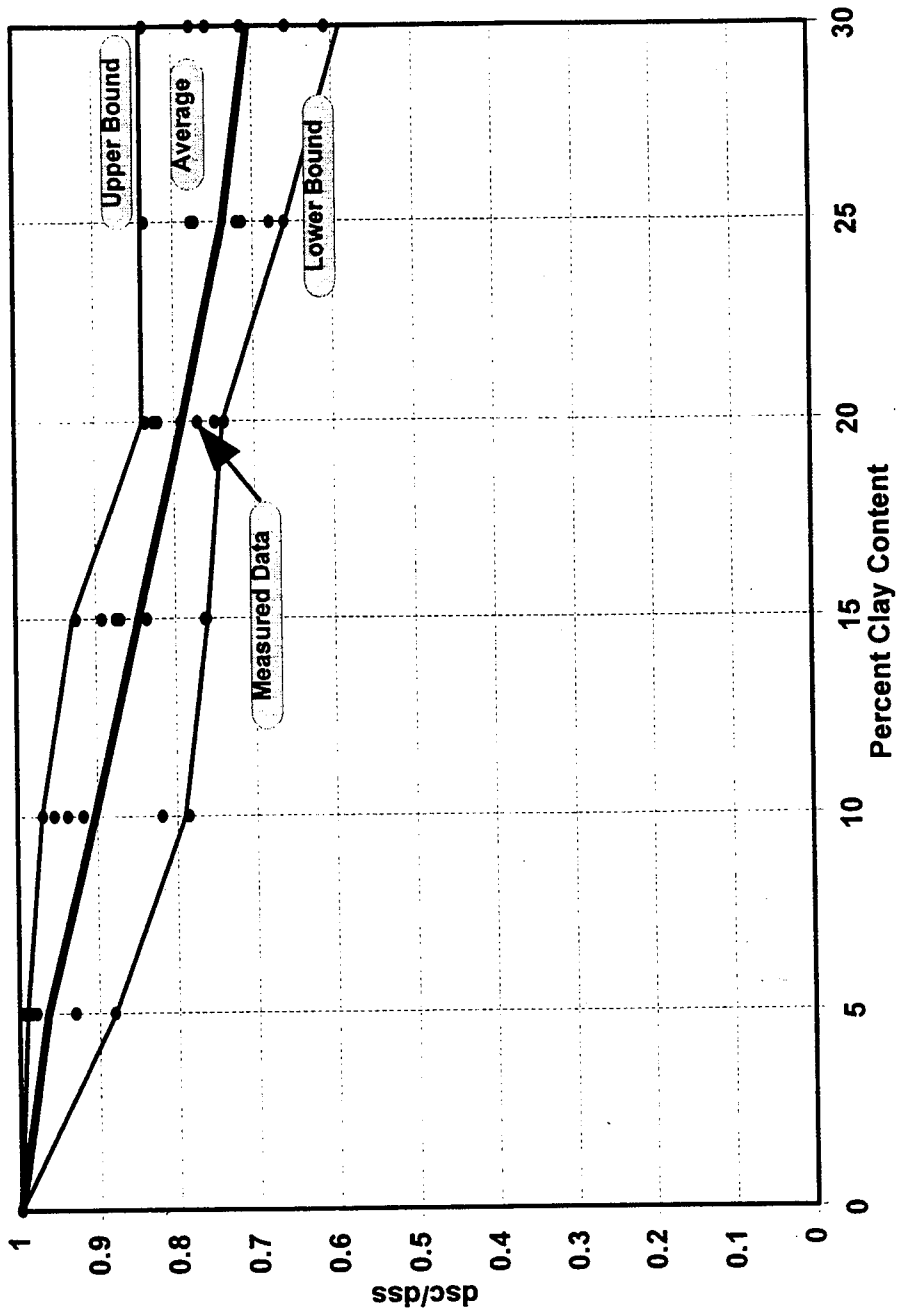


Figure (5.35) Variation of Normalized Scour Depth with Clay Content for Montmorillonite Clay.

values of clay scour to sand scour ratios for various clay contents are calculated up to 30 % clay content. Figure 5.35 presents also this relationship along with its upper and lower bounding limits. Figure 5.35 is used in deriving the equation which relates the clay content to the resulting depth of scour.

5.4.3.2 Cross-Sectional Profile of the Scour Holes

To study the effect of Montmorillonite clay content on the geometry of the resulting scour hole, a comparison of different cross sectional profiles passing through the upstream face of the abutment is conducted. The comparison of the cross-sectional profiles are illustrated in Figures 5.36 through 5.39 for clay contents of 0 %, 15 %, 30 % and 40 % for different Froude numbers representing different flow conditions. The scour dimensions defined by the depth, width, and side slope corresponding to maximum scour conditions are summarized in Table 5.11. From Figures 5.36 through 5.39 and Table 5.11, it can be seen that the depth of scour decreases as the percentage of clay content increases in the mixture from 0 % to 30 %. By increasing the clay content to 40 %, the depth of scour stays almost the same for 30 % and 40 %. This is due to the effect of cohesion variables such as initial water content and compaction which will begin to show their effects after increasing clay content to beyond 30 %.

5.4.3.3 Longitudinal Slope of the Scour Holes

For each soil mixture, the scour hole will have a certain slope along the longitudinal direction of the flow adjacent to the abutment wall (Figure 5.7). In order

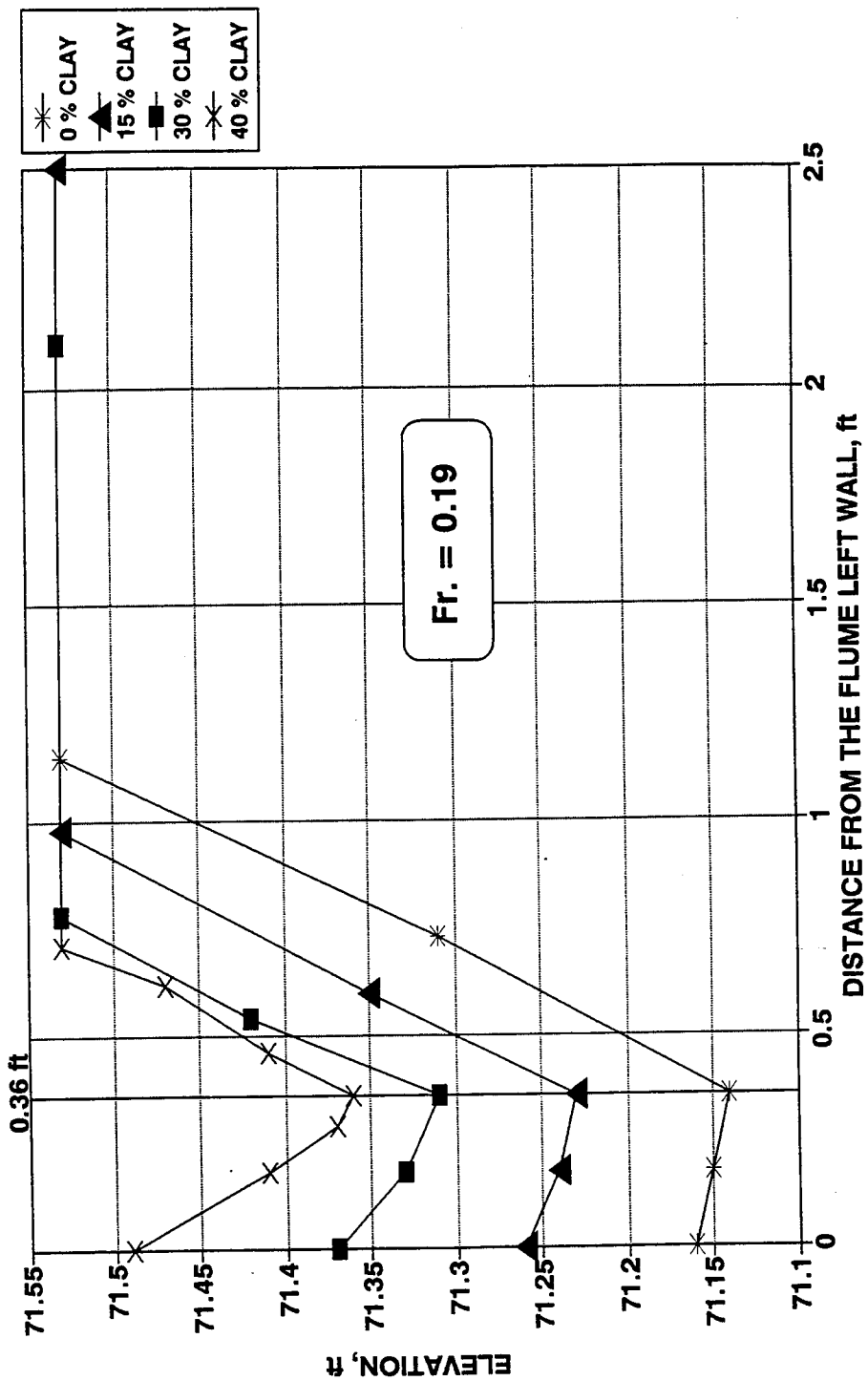


Figure (5.36) Effect of Clay Content on the Scour Hole Geometry at the Upstream Abutment Face (Fr=0.19).

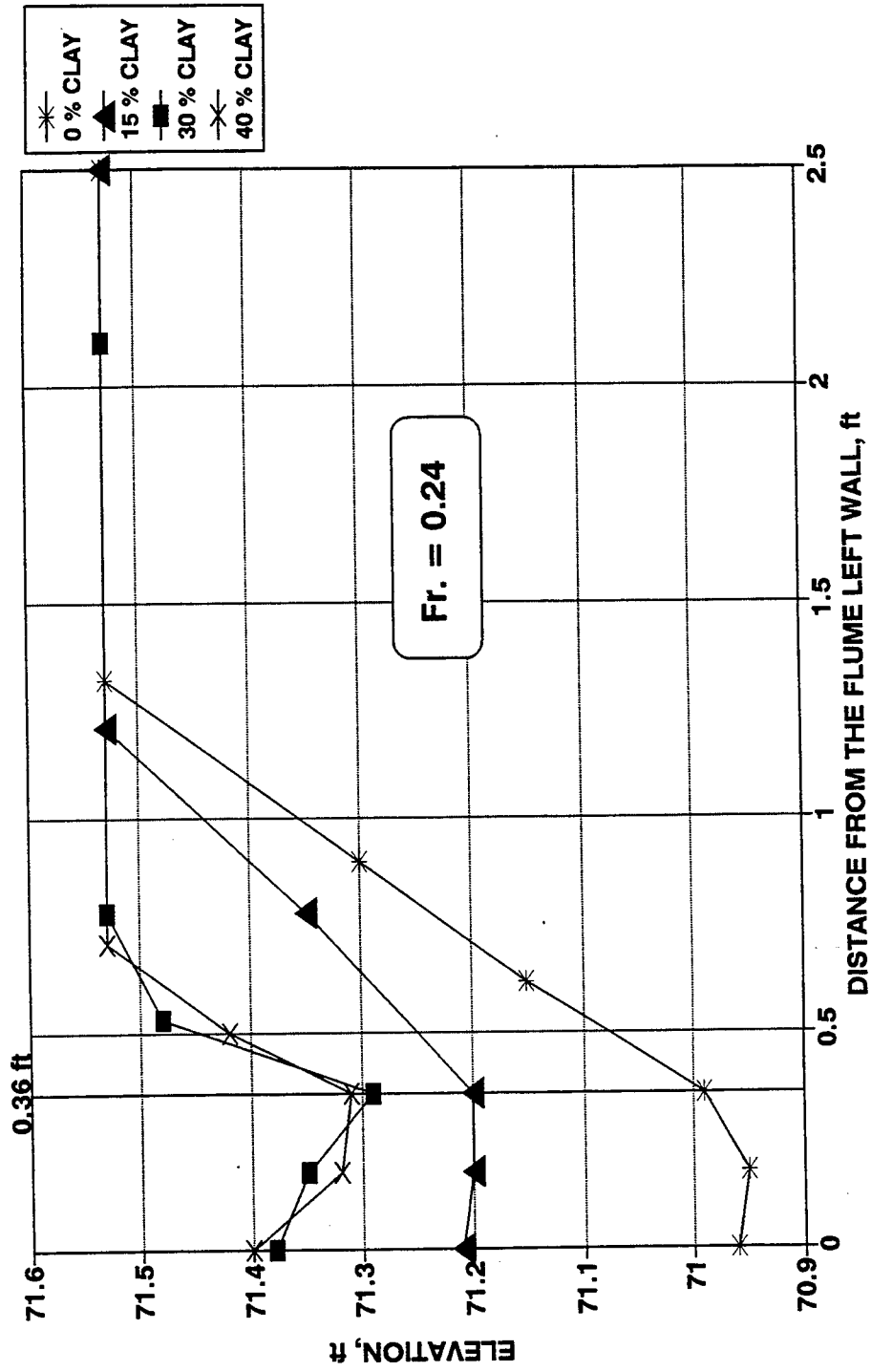


Figure (5.37) Effect of Clay Content on the Scour Hole Geometry at the Upstream Abutment Face ($Fr=0.24$).

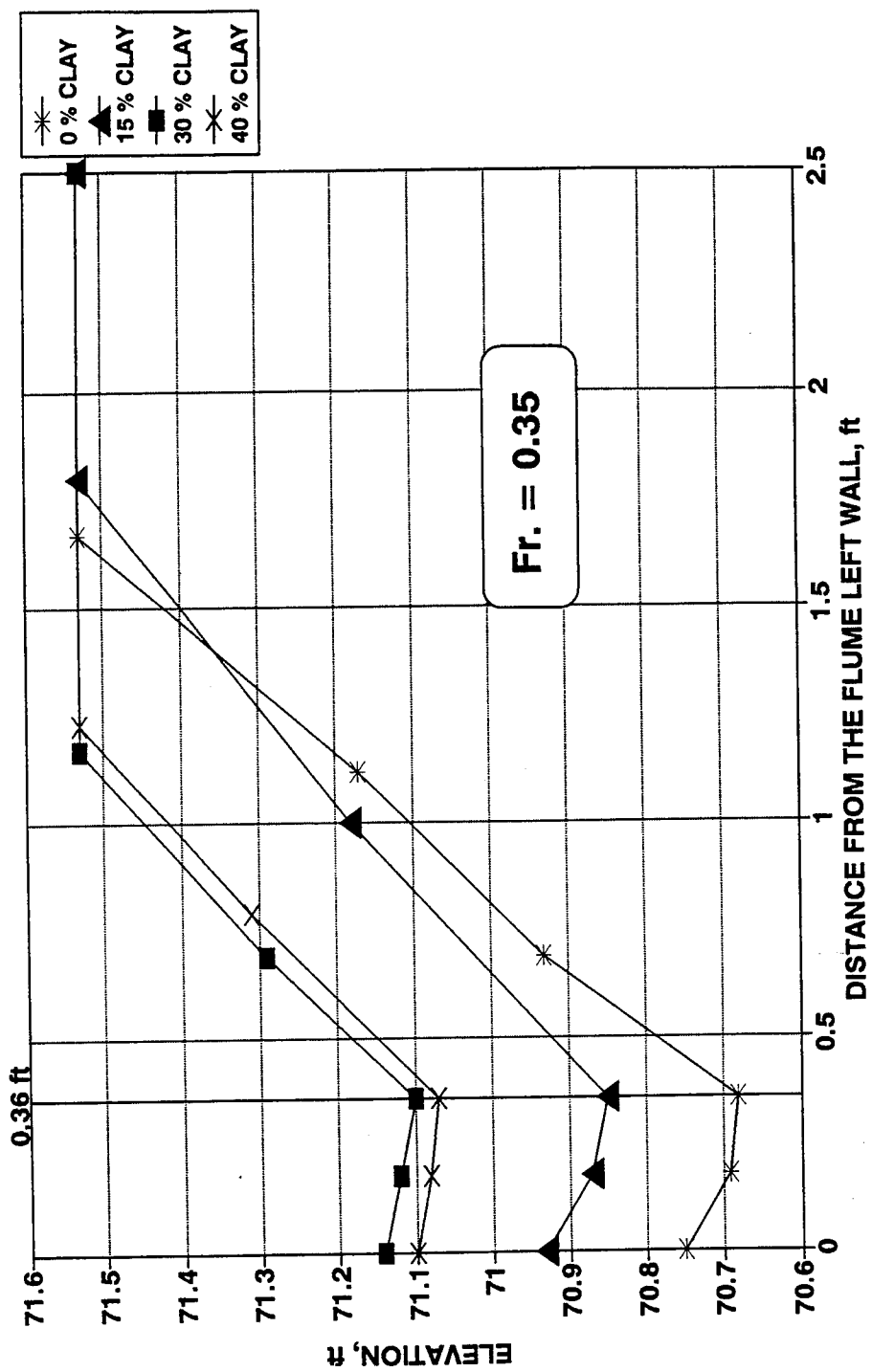


Figure (5.38) Effect of Clay Content on the Scour Hole Geometry at the Upstream Abutment Face (Fr=0.35).

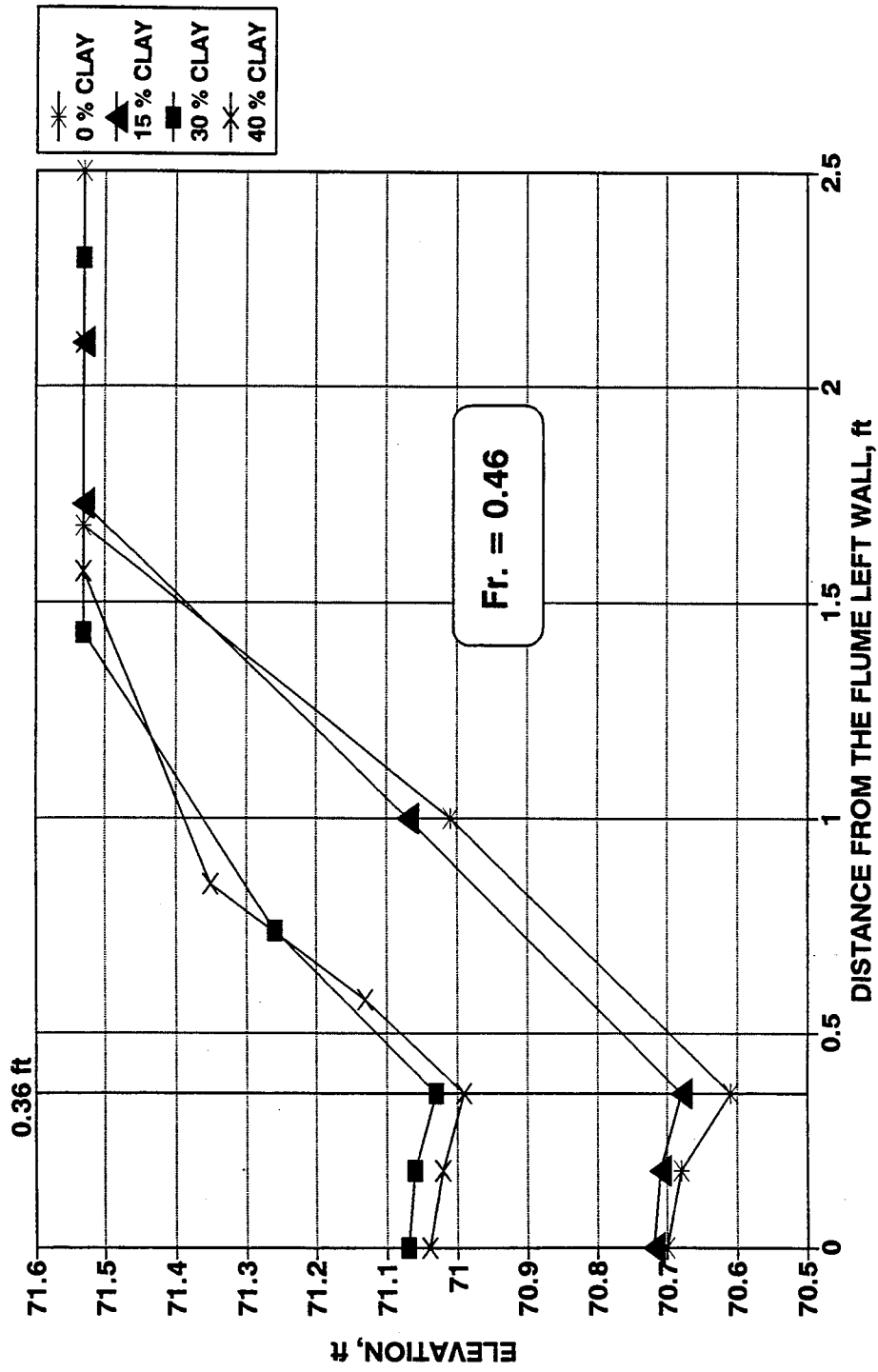


Figure (5.39) Effect of Clay Content on the Scour Hole Geometry at the Upstream Abutment Face (Fr = 0.46).

Table 5.11 Effect of Clay Content on Scour Geometry for Montmorillonite Clay

Run No.	Clay Content (%)	Depth (ft)	Normalized Depth	Width (ft)	Side Slope (degrees)
81-A	0	0.83	1.000	1.31	32.36
82-A	0	0.52	1.000	0.96	28.44
83-A	0	0.37	1.000	0.79	25.10
84-A	0	0.90	1.000	1.32	34.29
81-B	15	0.69	0.883	1.44	25.60
82-B	15	0.34	0.805	0.85	21.80
83-B	15	0.31	1.209	0.62	26.57
84-B	15	0.86	1.005	1.37	32.12
81-C	30	0.43	0.743	0.81	27.96
82-C	30	0.24	0.684	0.42	29.74
83-C	30	0.22	1.083	0.42	27.65
84-C	30	0.50	0.600	1.07	25.05
81-D	40	0.46	0.843	0.87	27.87
82-D	40	0.22	0.749	0.35	32.15
83-D	40	0.17	1.145	0.35	25.91
84-D	40	0.54	0.740	1.21	24.05

to compute the longitudinal slope for each mixture clay content, channel cross sections were plotted for different Froude numbers. The slope was then calculated as an average slope value for that soil mixture for the entire range of flow conditions. Figures 5.40 through 5.43 present cross section plots for the Montmorillonite clay contents of 0 %, 15 %, 30 %, and 40 % with a range of flow conditions for each clay. The summary of the scour hole longitudinal slope variation with clay content is presented in Figure 5.44. From this figure it can be shown that as the percentage of clay increases from 0 % to 15

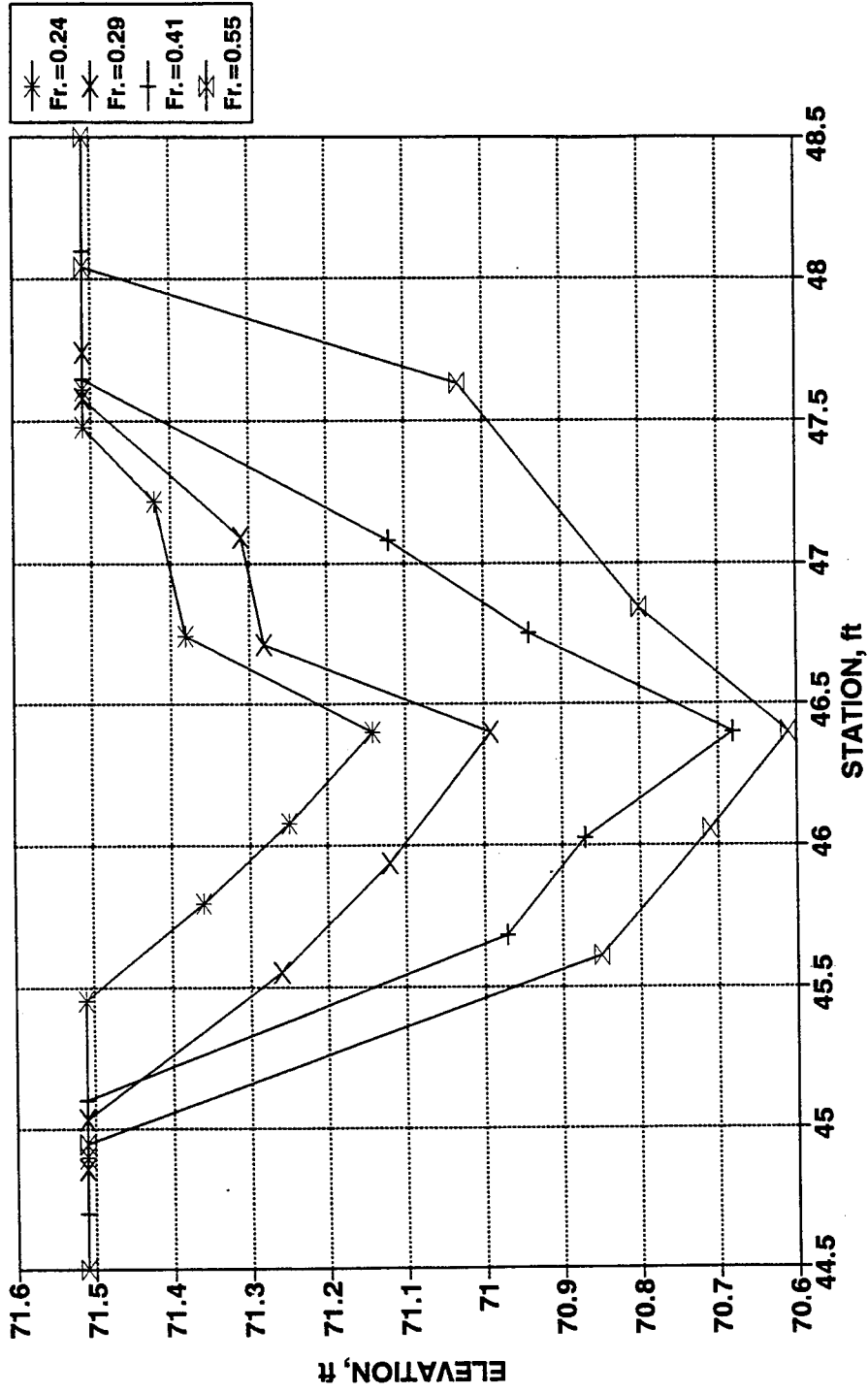


Figure (5.40) Longitudinal Profile of the Scour Hole for Medium Sand ($D_{50} = 0.81$ mm).

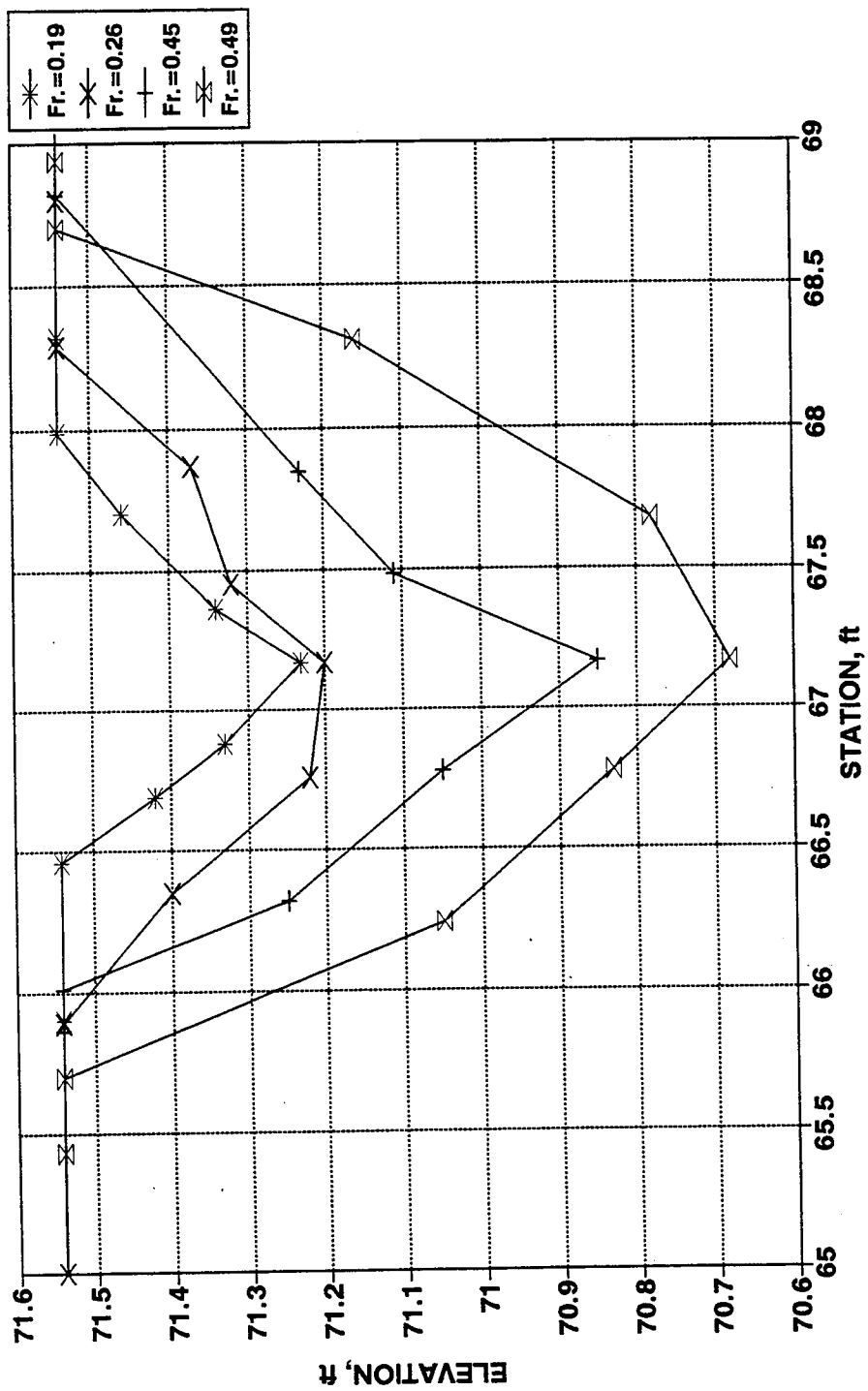


Figure (5.41) Longitudinal Profile of the Scour Hole for 15 % Clay Content.

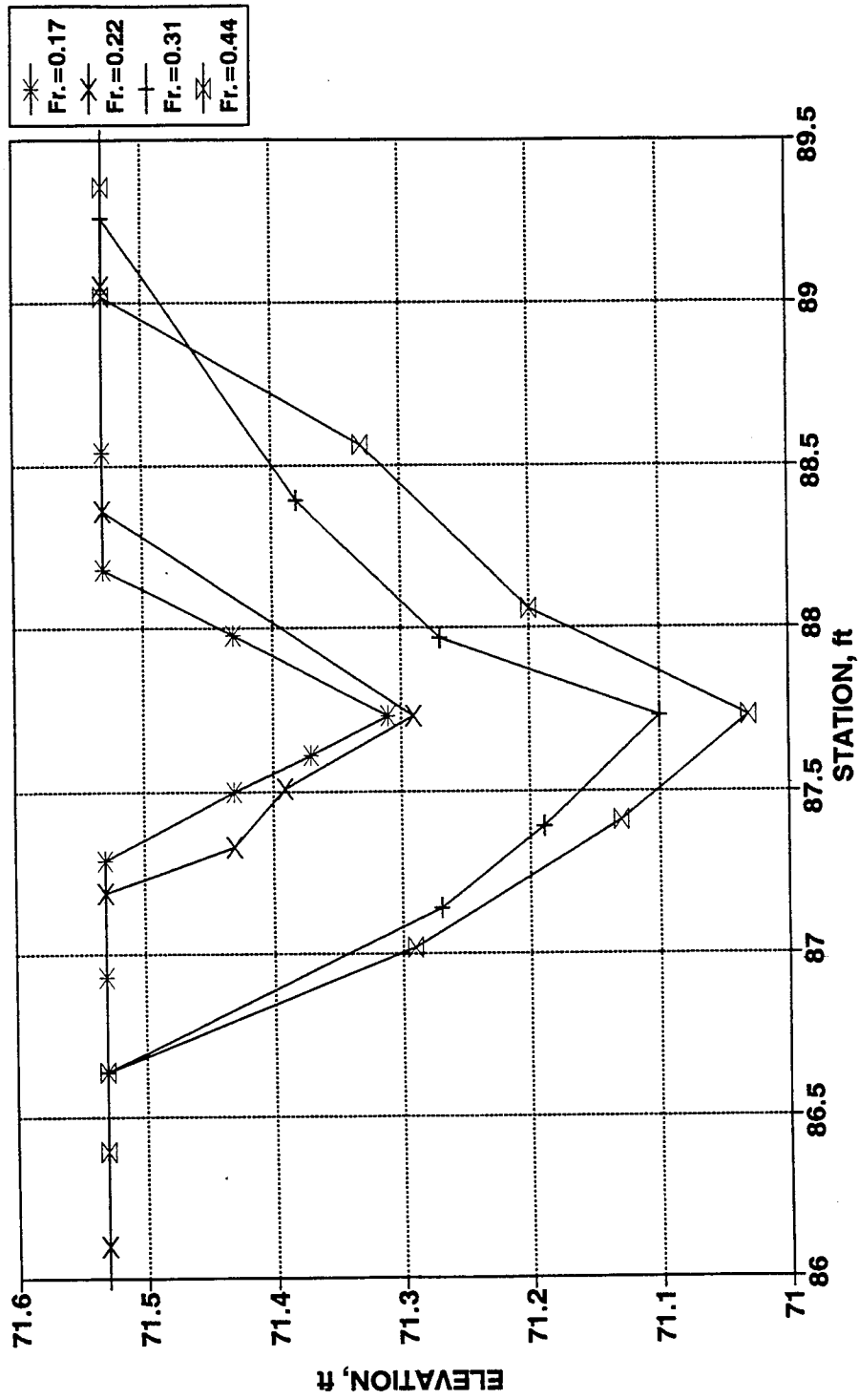


Figure (5.42) Longitudinal Profile of the Scour Hole for 30 % Clay Content.

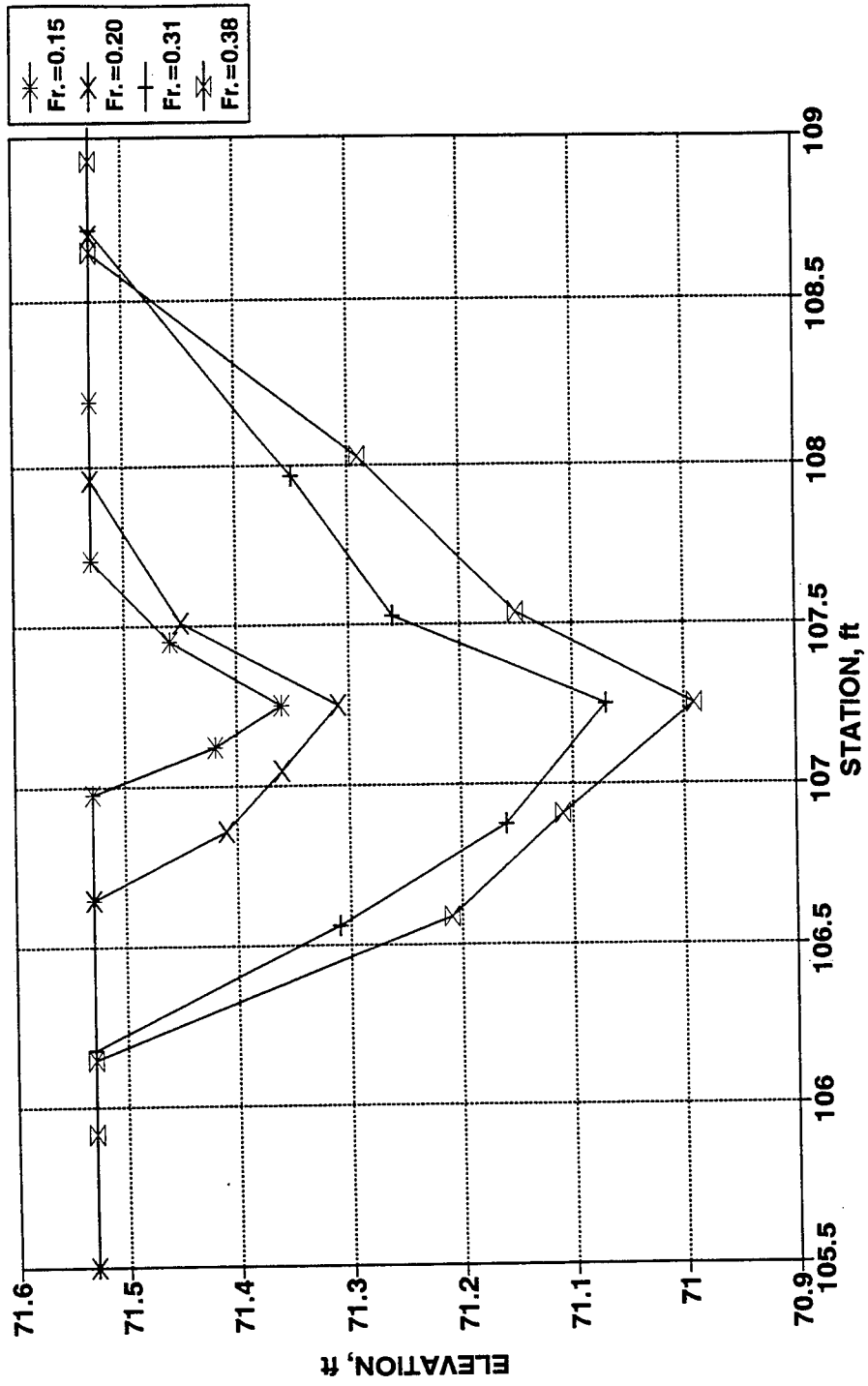


Figure (5.43) Longitudinal Profile of the Scour Hole for 40 % Clay Content.

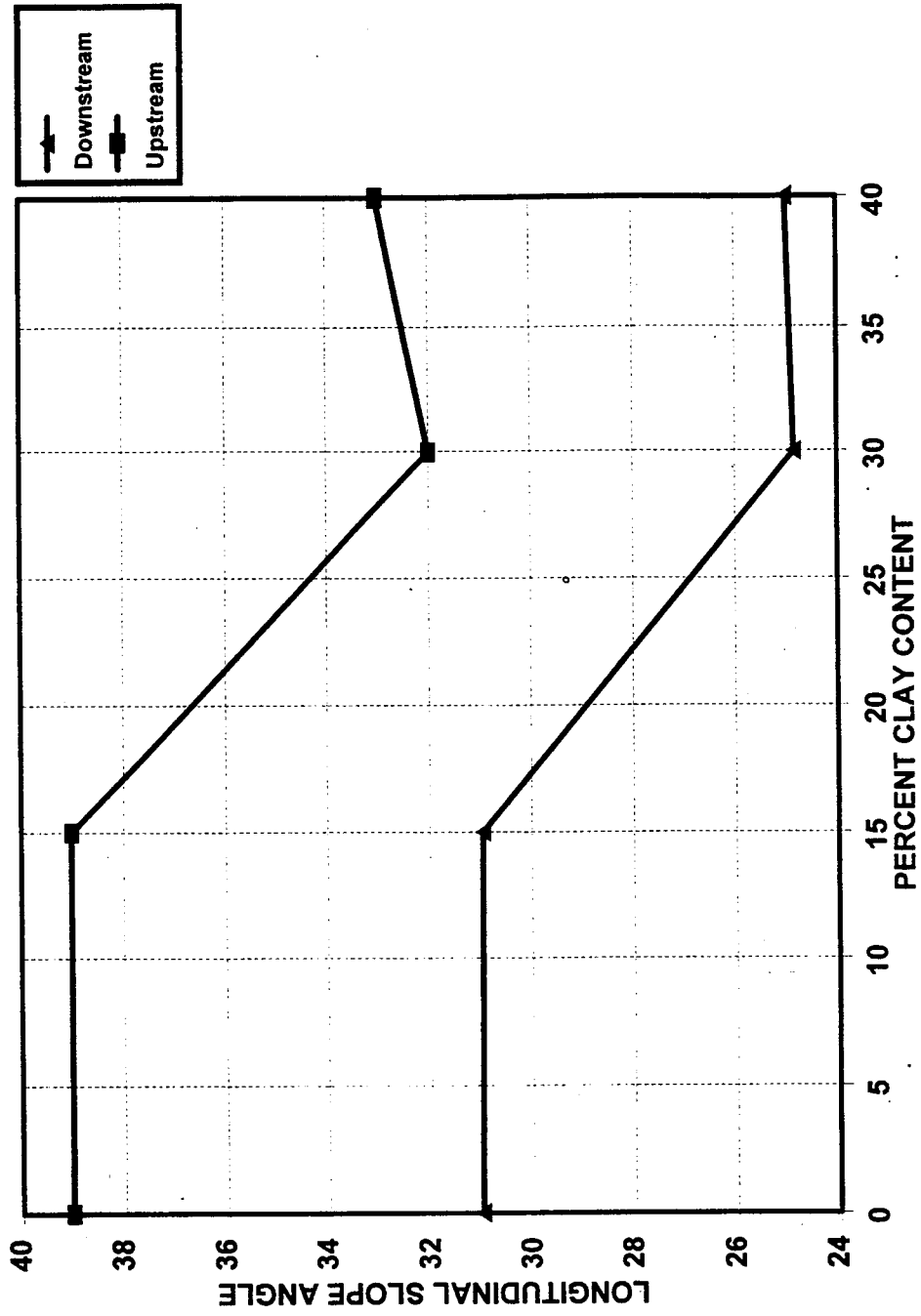


Figure (5.44) Variation of Longitudinal Slope Angles with Different Clay Contents.

%, the downstream slope shows no change and stays the same at 31°. By increasing clay content from 15 % to 30 %, the slope is decreased from 31° to 25°. By increasing the clay content from 30 % to 40 %, the slope stays almost the same at 25°. Beyond 30 % clay content, the cohesion variables such as initial water and compaction start to show their effect. In the upstream direction, the slope shows no change and stays at 39° as the clay content is increased from 0 % to 15 % and then decreases to 32° as the clay content is increased from 15 % to 30 %. By increasing the clay content from 30 % to 40 %, the slope stays almost the same at 33°. It is observed from these slopes that the upstream slopes are steeper than the downstream slopes.

5.4.3.4 Effect of Clay Content on Time Rate of Scour

Figures 5.45 through 5.47 shows the development of scour with time for four clay contents of 0 %, 15 %, 30 % and 40 % for different values of Froude numbers. As shown in these figures, as a general trend, as the value of clay content is increased from 0 % to 40 %, the value of the parameter K used in the time rate of scour equation 5.5 increases. This indicates that as the percentage of clay content in the mixture increases, the time needed for the scour hole to reach equilibrium condition decreases. For 40 % clay content, the K values are almost the same regardless of the flow conditions (Froude number). This indicates that the time rate of erosion is a constant for 40 % clay content. Table 5.12 includes all the values of K for different percentage of clay contents conditions shown in the figures.

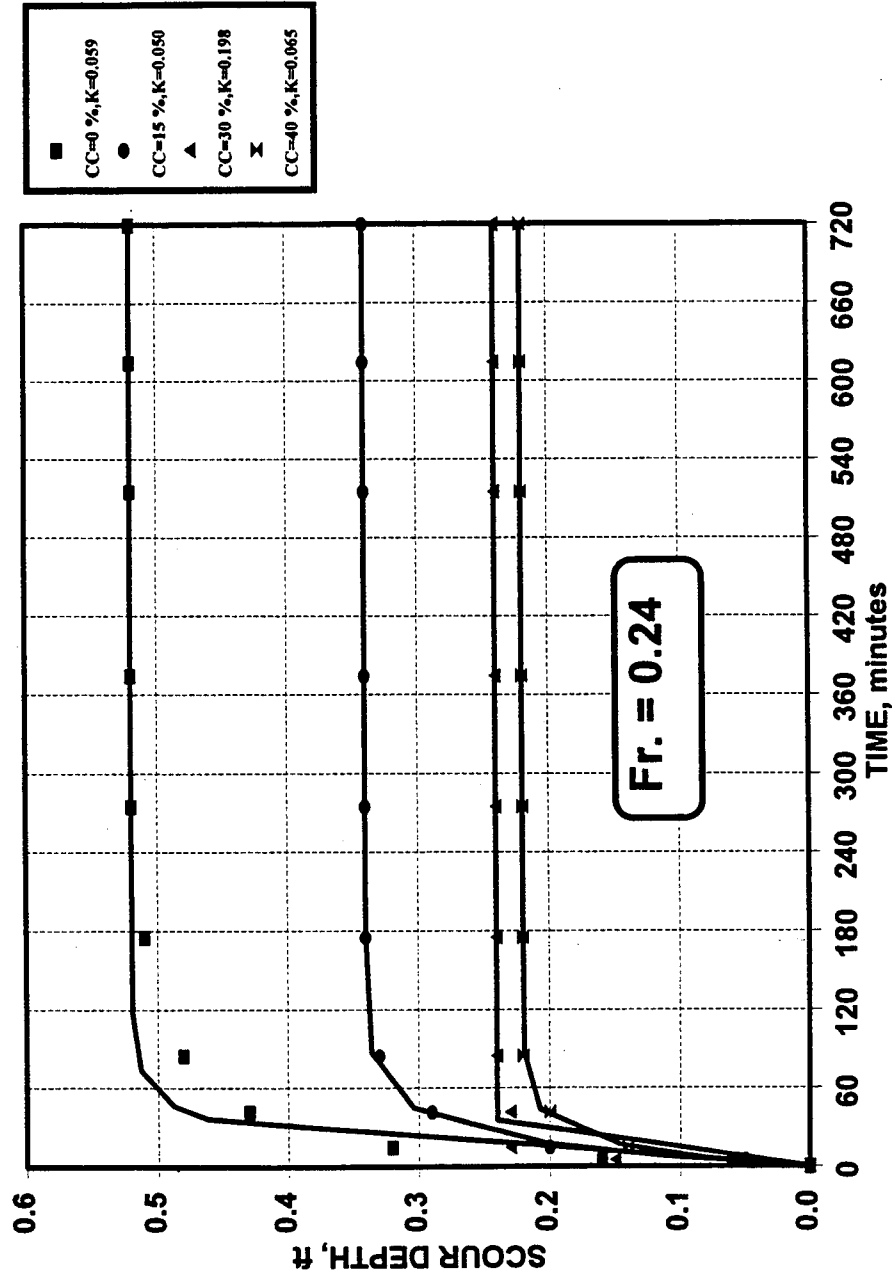


Figure (5.45) Variation of Time Rate of Scour with Clay Content (Fr = 0.24, Runs 8-82-A ,B ,C , and D).

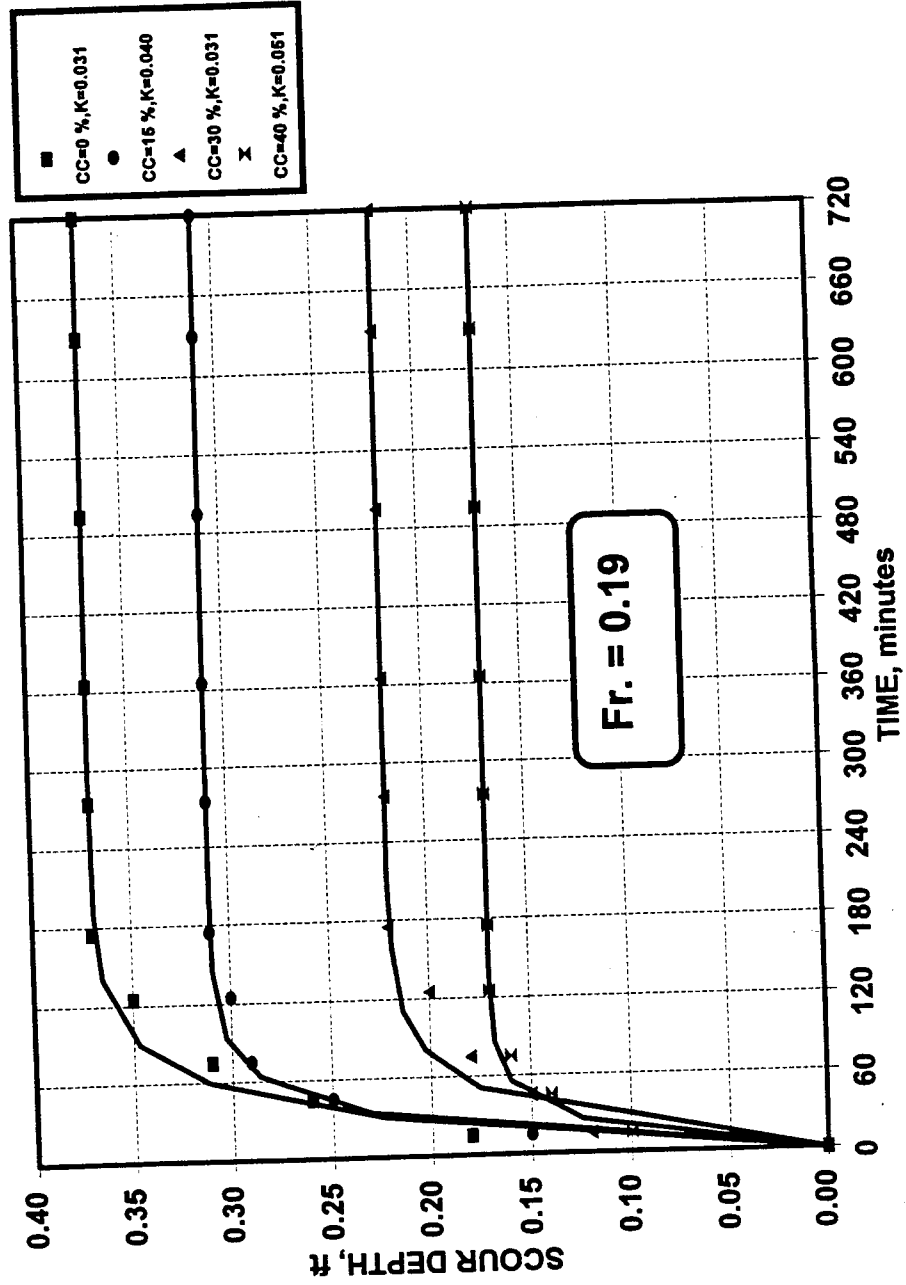


Figure (5.46) Variation of Time Rate of Scour with Clay Content (Fr=0.19, Runs 8-83-A, B, C, and D).

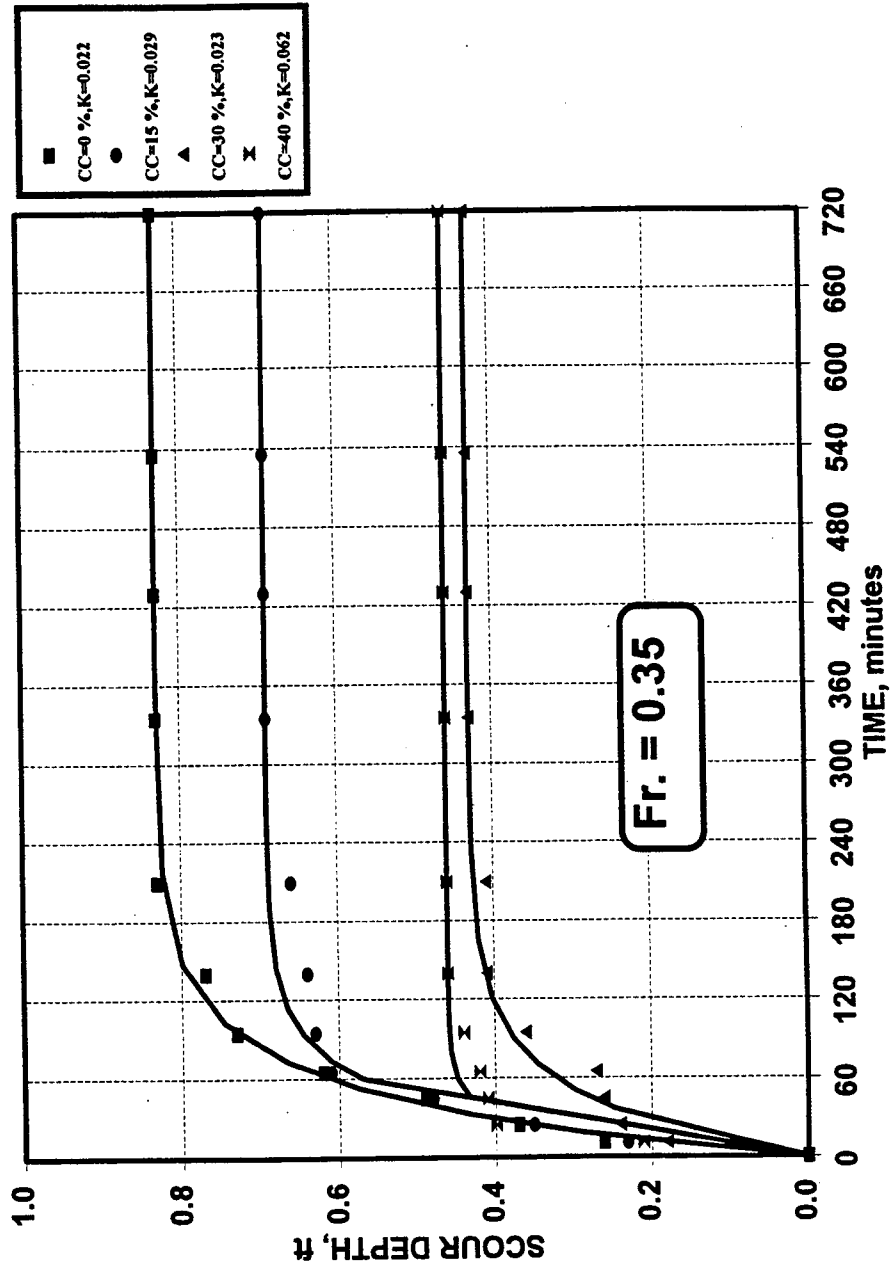


Figure (5.47) Variation of Time Rate of Scour with Clay Content (Fr=0.35, Runs 8-81-A ,B , C , and D).

Table 5.12 Effect of Clay Content on Time Rate of Scour for Montmorillonite Clay

Run No.	Clay Content (%)	K Value	Clay Content versus K Value
8-81-A	0	0.022	
8-81-B	15	0.029	
8-81-C	30	0.023	
8-81-D	40	0.062	
8-82-A	0	0.059	
8-82-B	15	0.050	
8-82-C	30	0.020	
8-82-D	40	0.065	
8-83-A	0	0.031	
8-83-B	15	0.040	
8-83-C	30	0.031	
8-83-D	40	0.051	

5.4.4 Comparison between Compaction and Torvane Shear Strength

The Torvane shear gauge was used around the abutment to measure the shear strength of the soil. The relationship between the Torvane shear strength and percentage of compaction for Montmorillonite is presented in Figure 5.48 for the range of different initial water contents used in the experiments. From this figure It can be shown that three groups are formed with three different curves. The first curve is for initial water contents of 12 % and 20 % where the Torvane shear increases as the compaction increases which is the case for unsaturated clay. The second curve is for the initial water contents of 28 % and 35 % where the Torvane shear increases as the compaction increases but changes very little. Finally, the third curve is for 45 % initial water content where there is no change in Torvane shear value and it is very small due to high

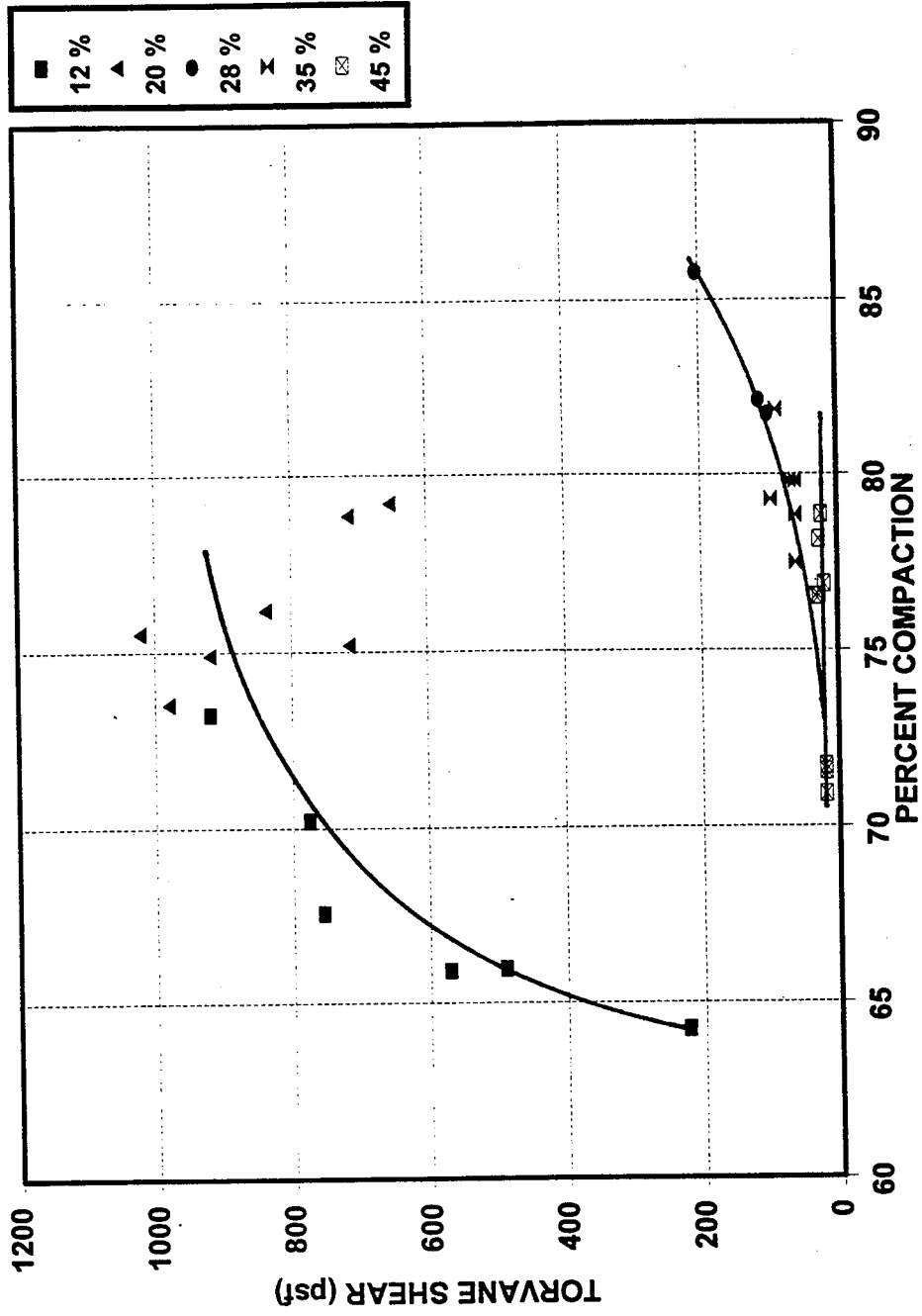


Figure (5.48) Relationship between Compaction and Torvane Shear for Montmorillonite Clay.

percentage of initial water content. The initial water contents from 28 % to 45 % are in the range of saturated clay and the measured values are too small to be used as an indicator of maximum depth of scour. For unsaturated clay (12 % to 20 %) it is noticed that the Torvane shear increases as the compaction increases. For this range of initial water content, the Torvane shear strength can be used to express the resulting maximum scour depth.

$$TS = -26588 + (730 \cdot C) - (4.85 \cdot C^2) \quad (5.6)$$

where

TS = Torvane shear strength

C = Percent compaction

5.5 Kaolinite Clay Experiments

Two clay properties were used to investigate maximum depth of abutment scour for Kaolinite clay. These properties are: initial water content and clay content. This section presents in detail the resulting effects of the two clay properties on maximum depth of scour for Kaolinite clay.

5.5.1 Effect of Initial Water Content on the Clay Mixture.

The effect of initial water content in this section covers a mixture contains 30 % Kaolinite clay and 70 % medium sand. This section will include the investigations of: the scour depth as a function of flow condition (Froude number) for various initial water contents, the effects of the initial water content on the cross-sectional profile of the scour

hole, the side slope of the scour hole, the longitudinal slope, and time rate of scour. The results are expressed in functional relationships whenever possible.

5.5.1.1 Variation of Scour Depth with Approach Flow Conditions

The effect of initial water content in Kaolinite clay was investigated by maintaining the same range of mixture compaction and clay content and by changing only the initial water content of the soil. The four initial water contents used in the experiments were 15 %, 20 %, 25 %, and 30 %. The experiments were divided into two groups: one including 15 % and 20 %, and the other one including 25 % and 30 % IWC. Figure 5.49 shows the variation of dimensionless scour -- the scour depth normalized by square root of abutment width and flow depth -- with Froude number. From Figure 5.49 it can be seen that the data points for initial water contents of 15 % and 20 % follow one pattern while points for 25 % and 30 % IWC follow another pattern. For the same Froude number, as the initial water content increases from the 15-20 % range to the 25-30 % range, the depth of maximum scour increases. At high Froude numbers the measured scour depth for both ranges converge to the same value regardless of the initial water content. The procedure for normalizing initial water content in Montmorillonite clay with sand was also performed on the initial water content for Kaolinite as shown in Figures 5.50 and 5.51. Figure 5.50 shows the measured values of dimensionless clay scour depth for different Froude numbers. Figure 5.51 is produced by normalizing the clay scour with the corresponding sand scour and then taking the average of all the Froude number curves at different percentage of initial water contents. Figure 5.51 also shows the lower and upper limits of the measured values. This figure

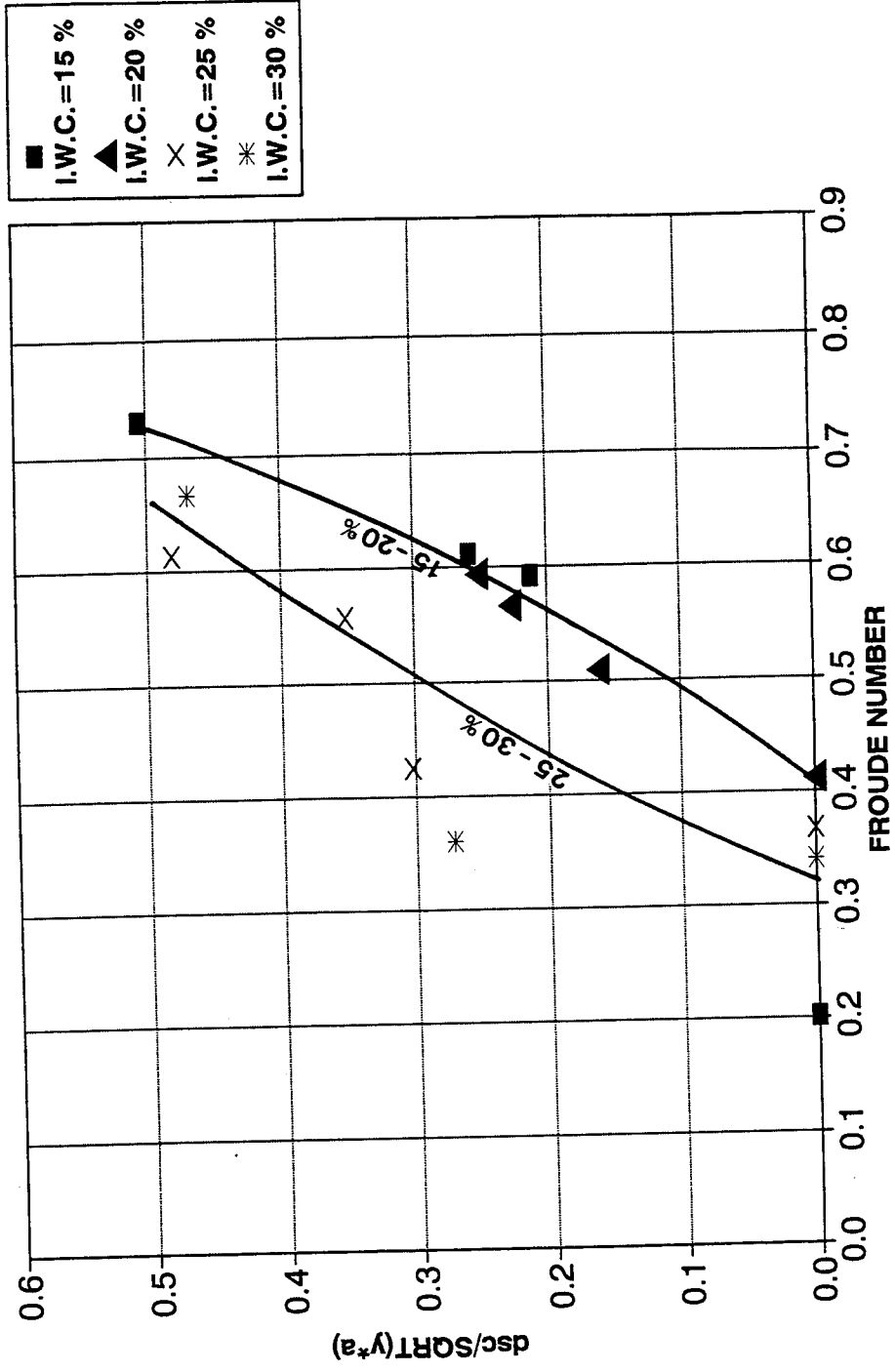


Figure (5.49) Variation of Dimensionless Abutment Scour Depth with Froude Number for Kaolinite Clay.

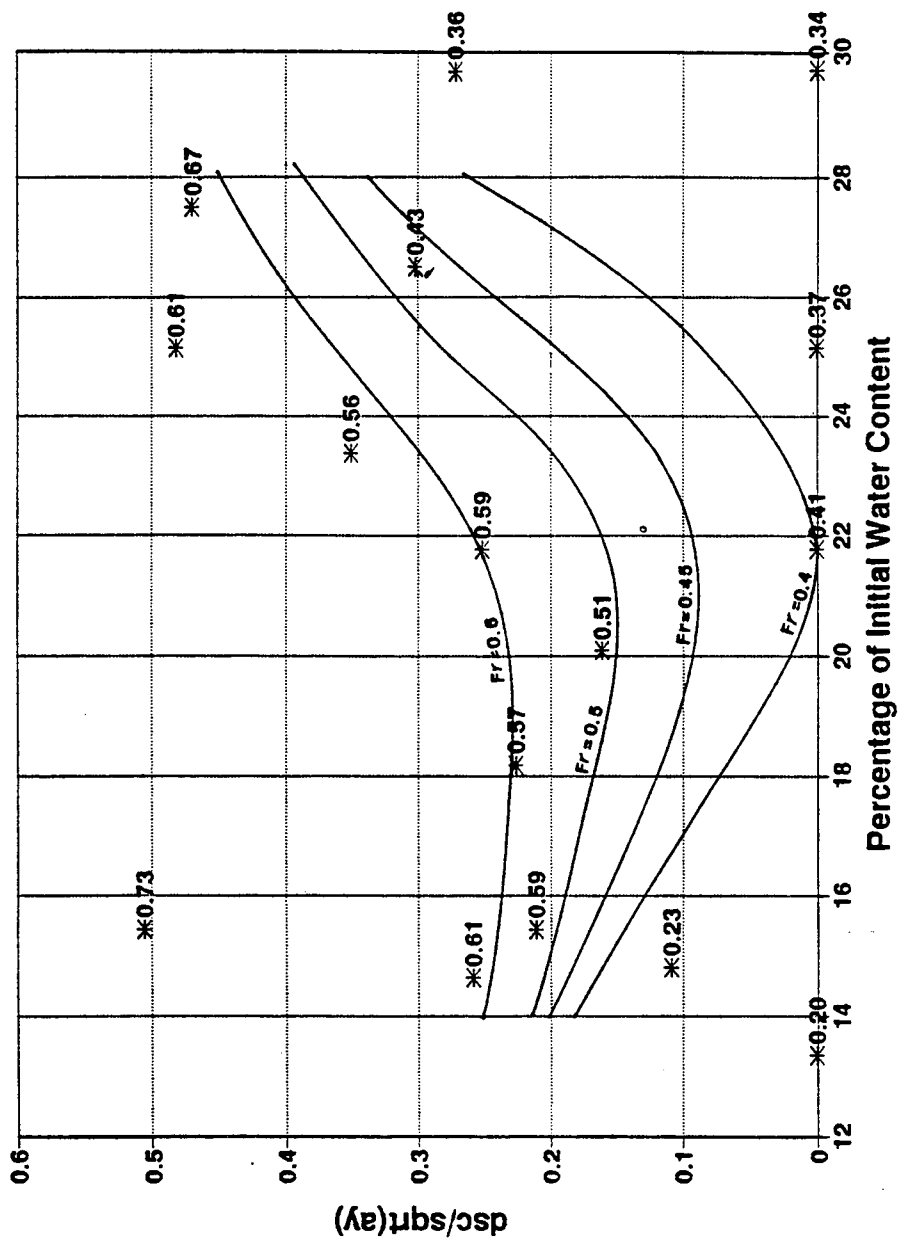


Figure (5.50) Variation of Dimensionless Abutment Scour Depth with Initial Water Content for Different Froude Numbers.

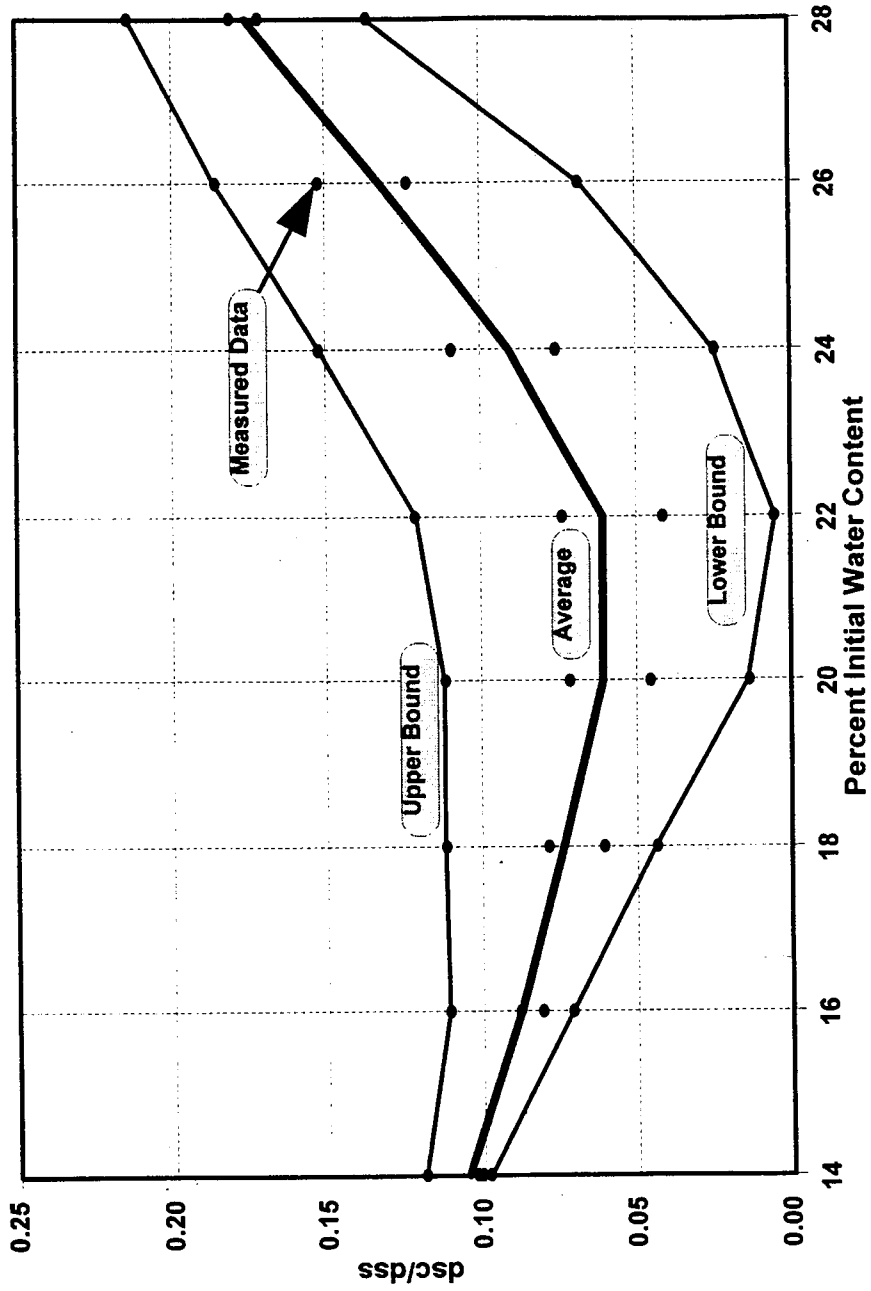


Figure (5.51) Variation of Normalized Scour Depth with Initial Water Content for Kaolinite Clay.

is used in deriving the prediction equation for the effect of initial water content on Kaolinite clay.

5.5.1.2 Cross-Sectional Profile of the Scour Holes

To study the effect of initial water content of Kaolinite clay on the geometry of the resulting scour hole, a comparison of different cross sectional profiles passing through the upstream face of the abutments is conducted. The locations of cross-sectional and longitudinal profiles are illustrated in Figure 5.7. The comparison of cross-sectional profiles is illustrated in Figures 5.52 through 5.54 for initial water content values of 15 %, 20 %, 25 %, and 30 % for different Froude numbers representing different flow conditions. The scour dimensions defined by the depth, width, and side slope corresponding to maximum scour conditions are presented in Table 5.13. From Figures 5.52 through 5.54 and Table 5.13, it can be concluded that the depth of scour increases as the initial water content is increased from 15 % to 30 % for the same flow conditions.

Table 5.13 Effect of Initial Water Content on Scour Geometry for Kaolinite Clay

Run No.	Initial Water Content (%)	Depth (ft)	Normalized Depth	Width (ft)	Side Slope (degrees)
72-A	15	0.10	0.100	0.74	7.70
74-A	20	0.10	0.108	0.02	78.69
76-A	20	0.12	0.120	0.16	36.87
75-B	25	0.0	0.000	0.0	0.0
76-B	25	0.22	0.229	0.14	57.53
74-B	25	0.15	0.167	0.21	35.544
73-C	30	0.12	0.141	0.34	19.44

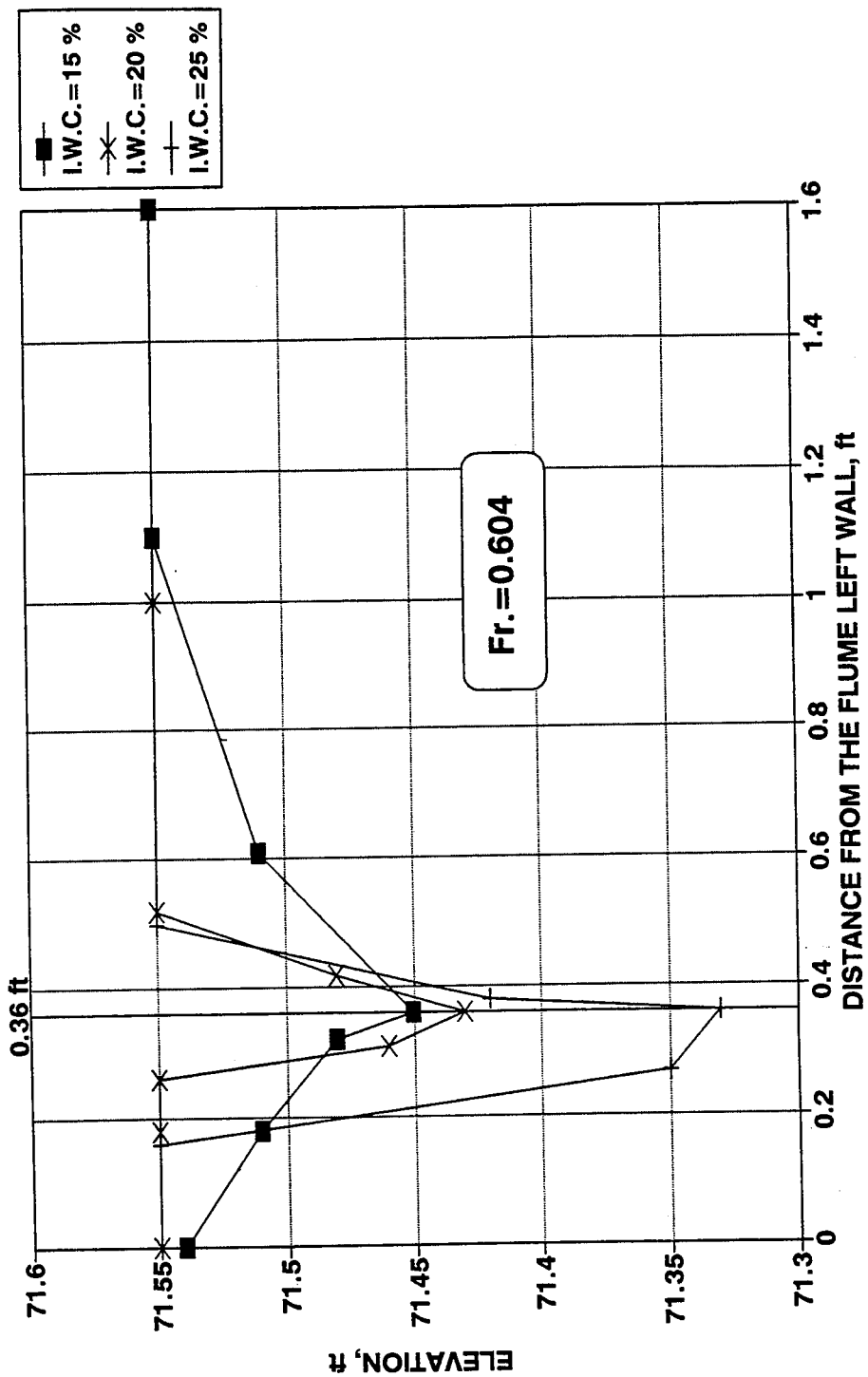


Figure (5.52) Effect of Initial Water Content on the Scour Hole Geometry at the Upstream Abutment Face ($Fr = 0.604$).

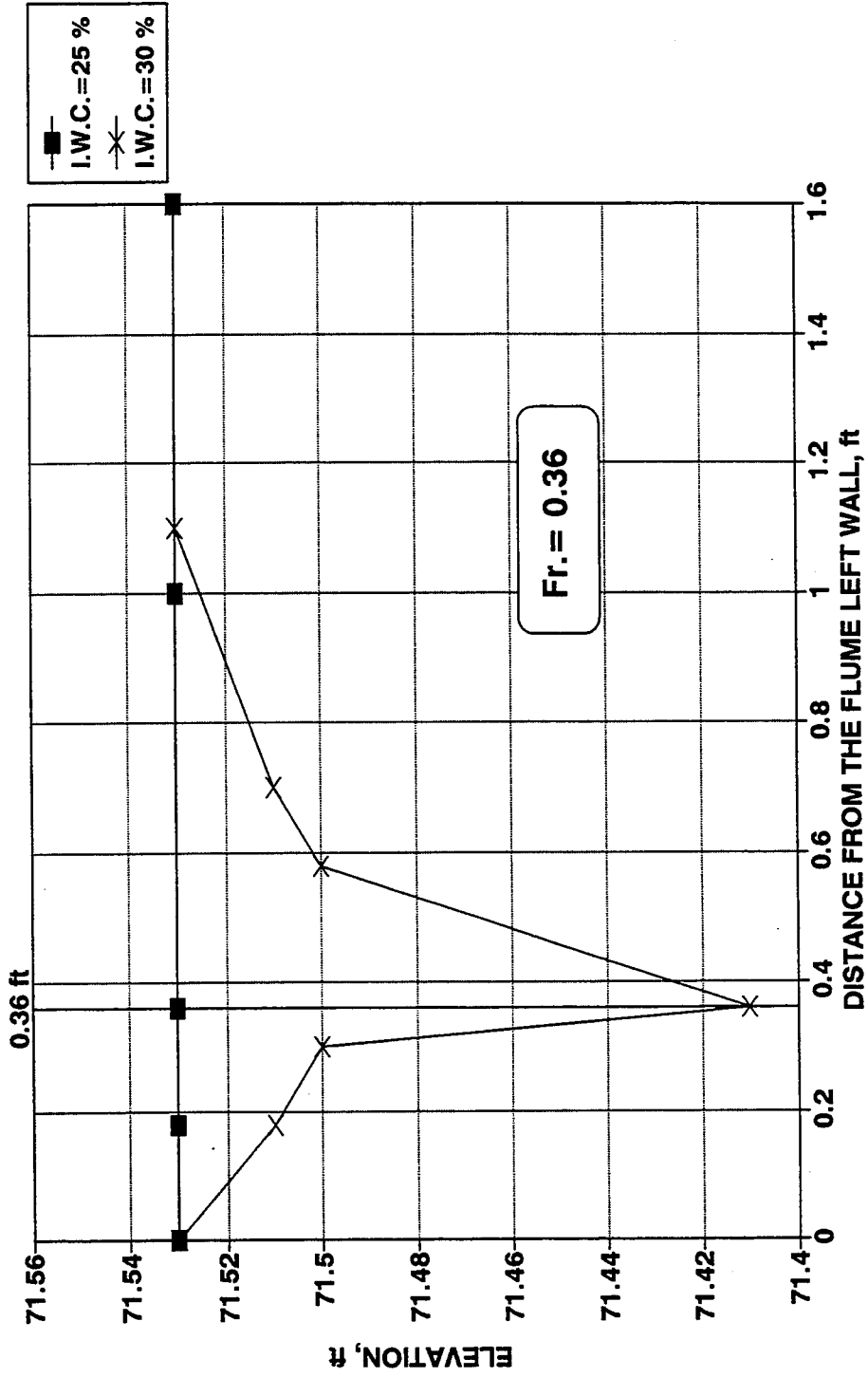


Figure (5.53) Effect of Initial Water Content on the Scour Hole Geometry at the Upstream Abutment Face ($Fr=0.36$).

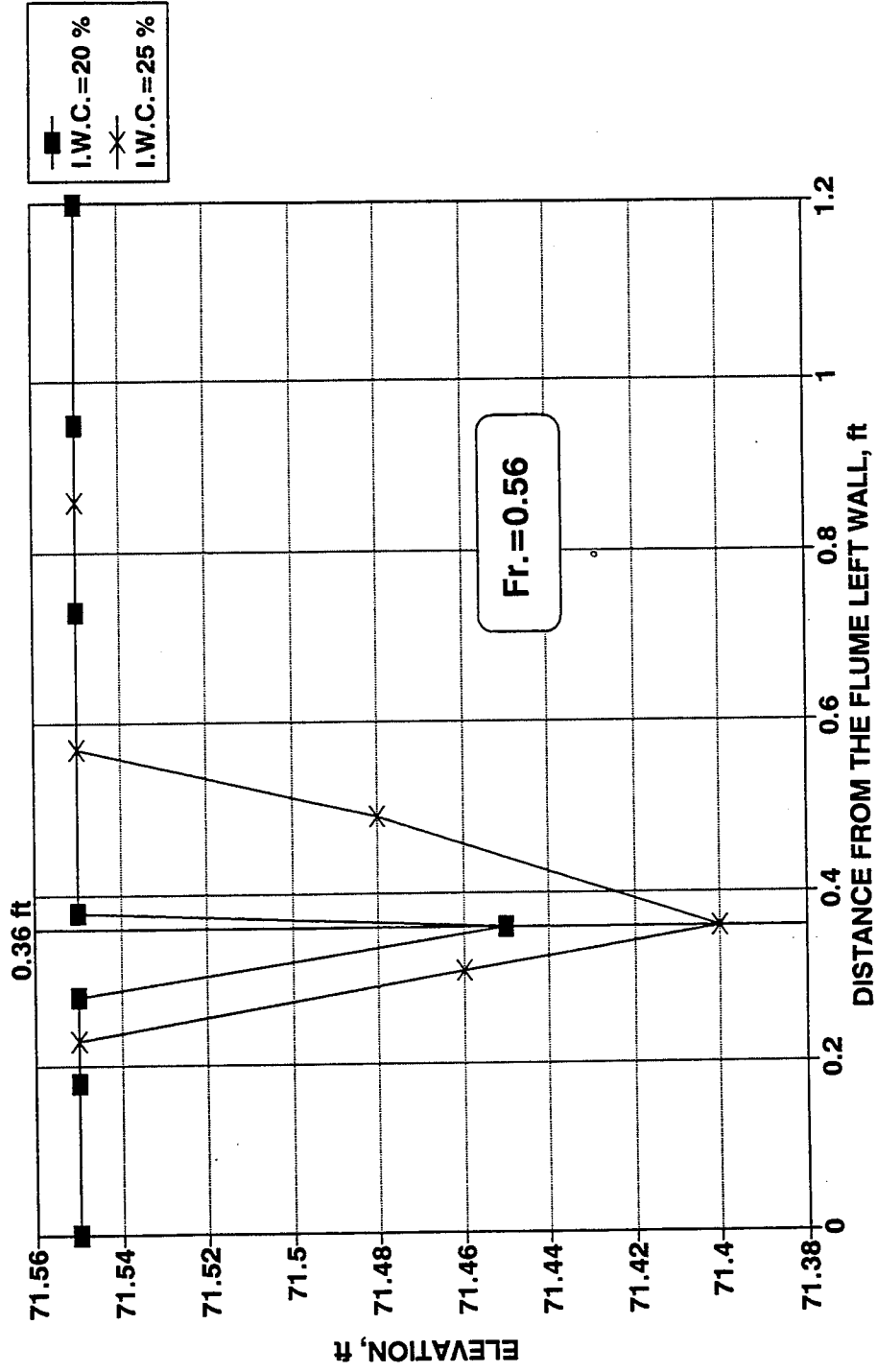


Figure (5.54) Effect of Initial Water Content on the Scour Hole Geometry at the Upstream Abutment Face ($Fr=0.56$).

5.5.1.3 Longitudinal Slope of the Scour Holes

For each soil mixture, the scour hole assumes a certain slope along the flow direction. For Kaolinite clay, a mixture of 30 % clay and 70 % medium sand was used to apply different initial water contents. The Kaolinite clay in this mixture was obtained commercially as a pure Kaolinite clay. Figures 5.55 through 5.58 present cross section plots for the Kaolinite clay with initial water contents of 15 %, 20 %, 25 %, and 30 % for different flow conditions. The summary of the longitudinal slope variation with initial water content is presented shown in Figure 5.59. From Figure 5.59, it can be shown that, in the downstream direction the slope increases from 21° to 34° as the initial water content is increased from 15 % to 20 %. The slope shows little or no change as the initial water content increases from 20 % to 30 %. In the upstream direction, the scour hole slopes are steeper. The slope increases from 43° to 48° as the percentage of initial water content is increased from 15 % to 20 % and then remains the same as the initial water content is further increased from 20 % to 30 %.

5.5.1.4 Effect of Initial Water Content on Time Rate of Scour

In this section, the effect of initial water content on the resulting time rate of scour for Kaolinite clay is analyzed using initial water contents ranging from 15 % to 25 %. Figure 5.60 shows the development of scour depth with time for initial water contents of 15 %, 22 %, and 25 % and Figure 5.61 for initial water contents of 18 % and 23 %. From Figures 5.60 and 5.61, the value of K increases as the initial water content increases from 15 % to 20 %, . The K value shows little change as the initial

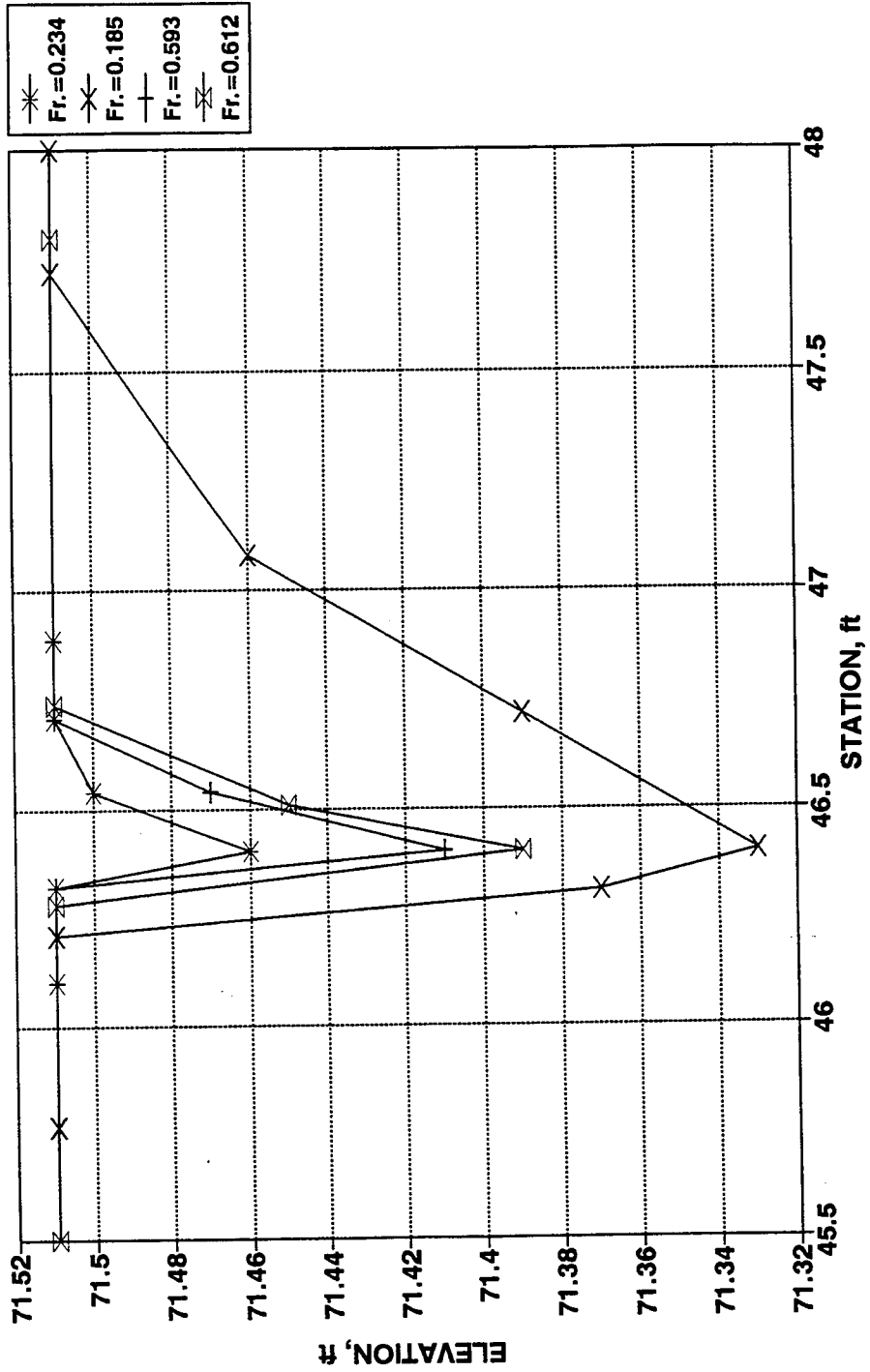


Figure (5.55) Longitudinal Profile of the Scour Hole for 15 % Initial Water Content.

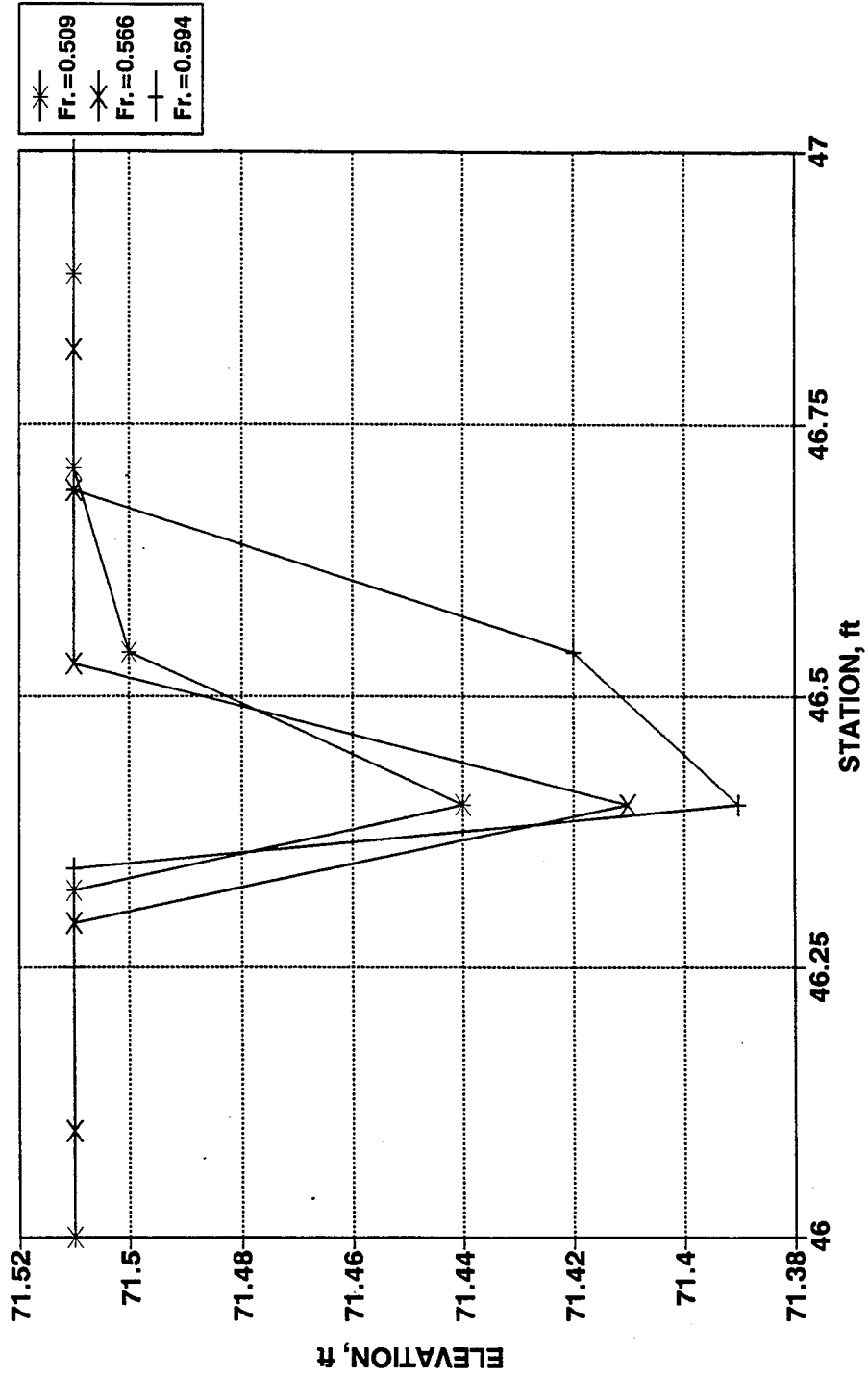


Figure (5.56) Longitudinal Profile of the Scour Hole for 20 % Initial Water Content.

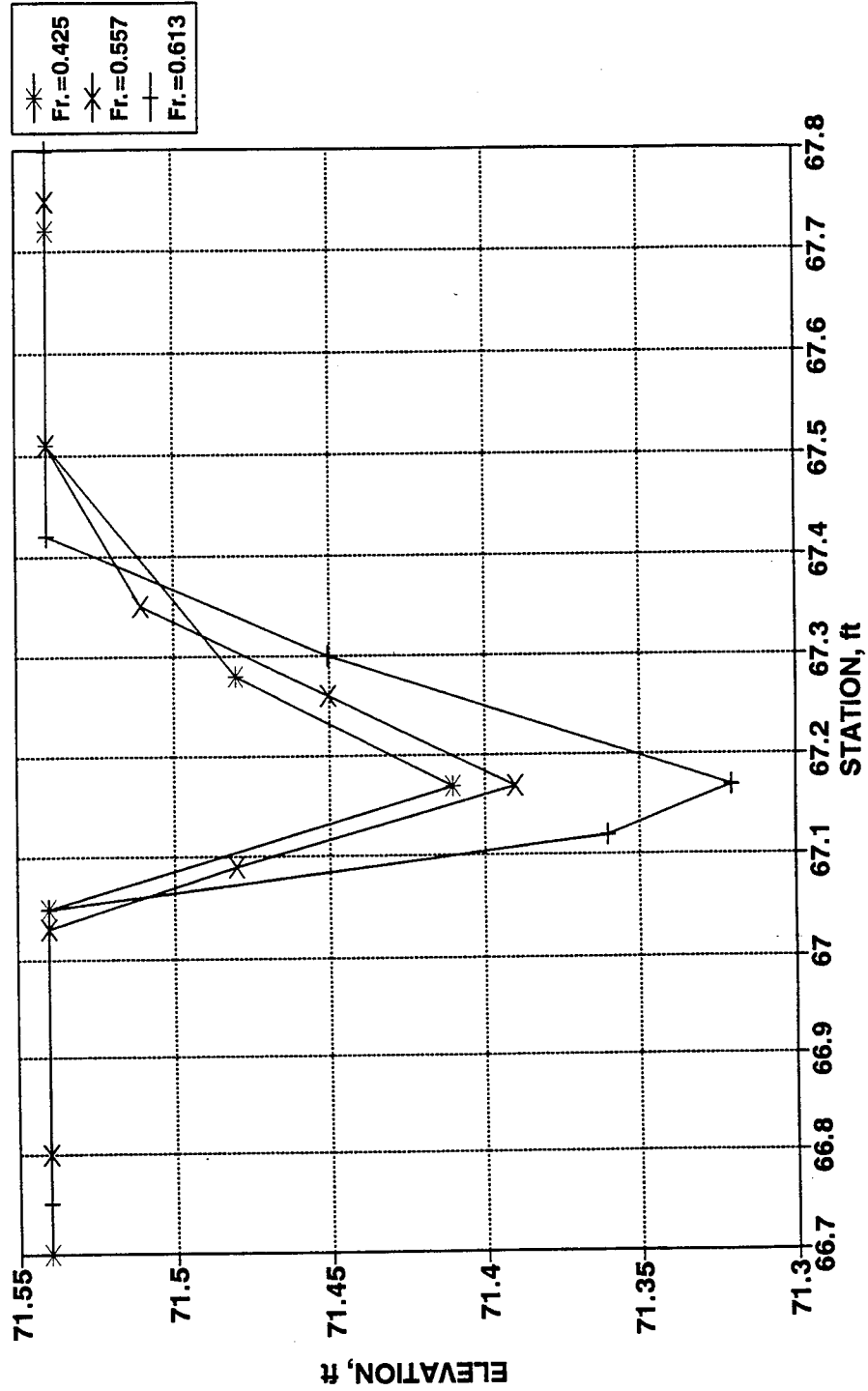


Figure (5.57) Longitudinal Profile of the Scour Hole for 25 % Initial Water Content.

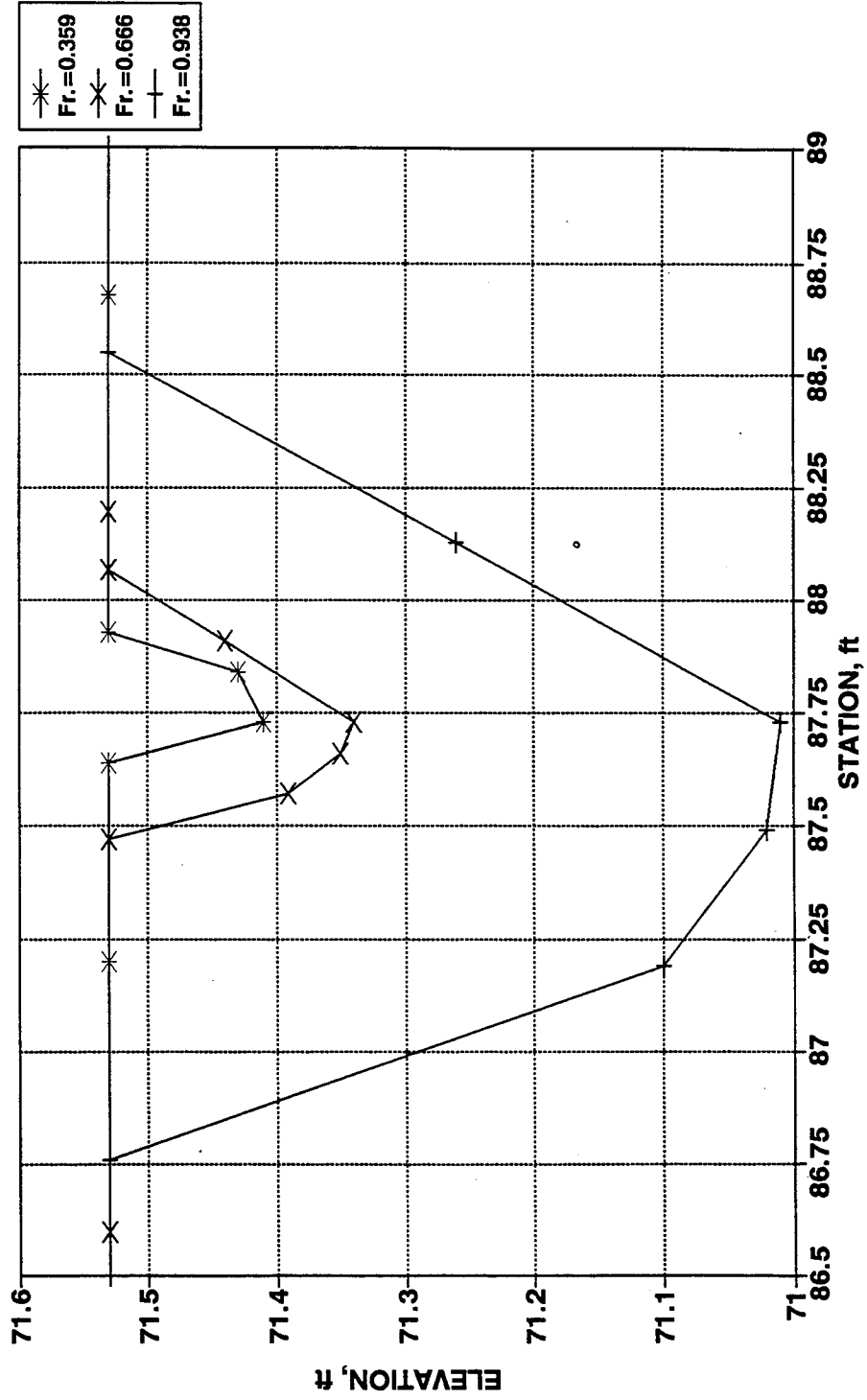


Figure (5.58) Longitudinal Profile of the Scour Hole for 30 % Initial Water Content.

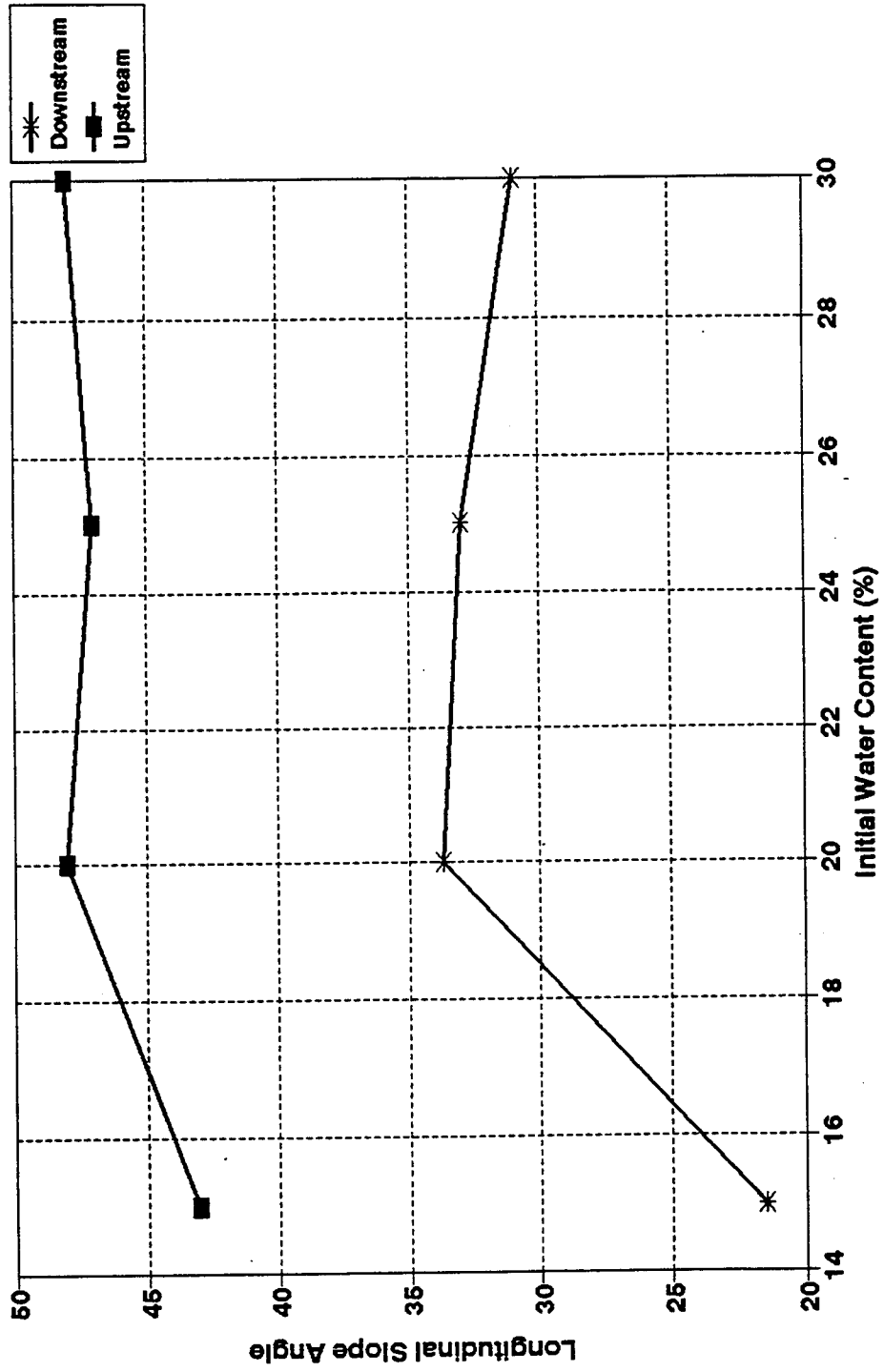


Figure (5.59) Variation of Longitudinal Slope Angles with Different Initial Water Content.

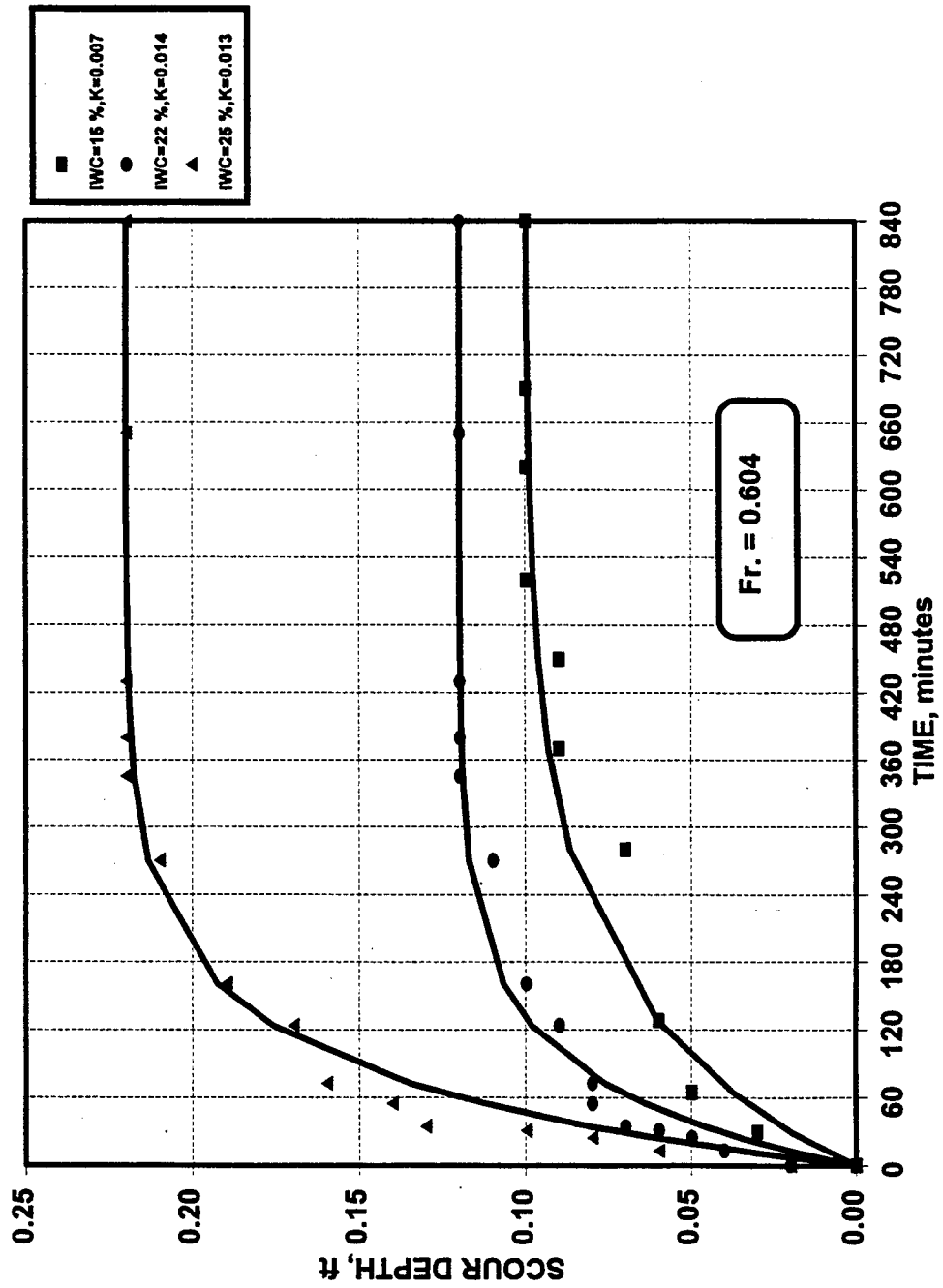


Figure (5.60) Time Rate of Scour for Initial Water Content of 15 %, 22, and 25 % (Runs 8-72-A and 8-76-A, B):

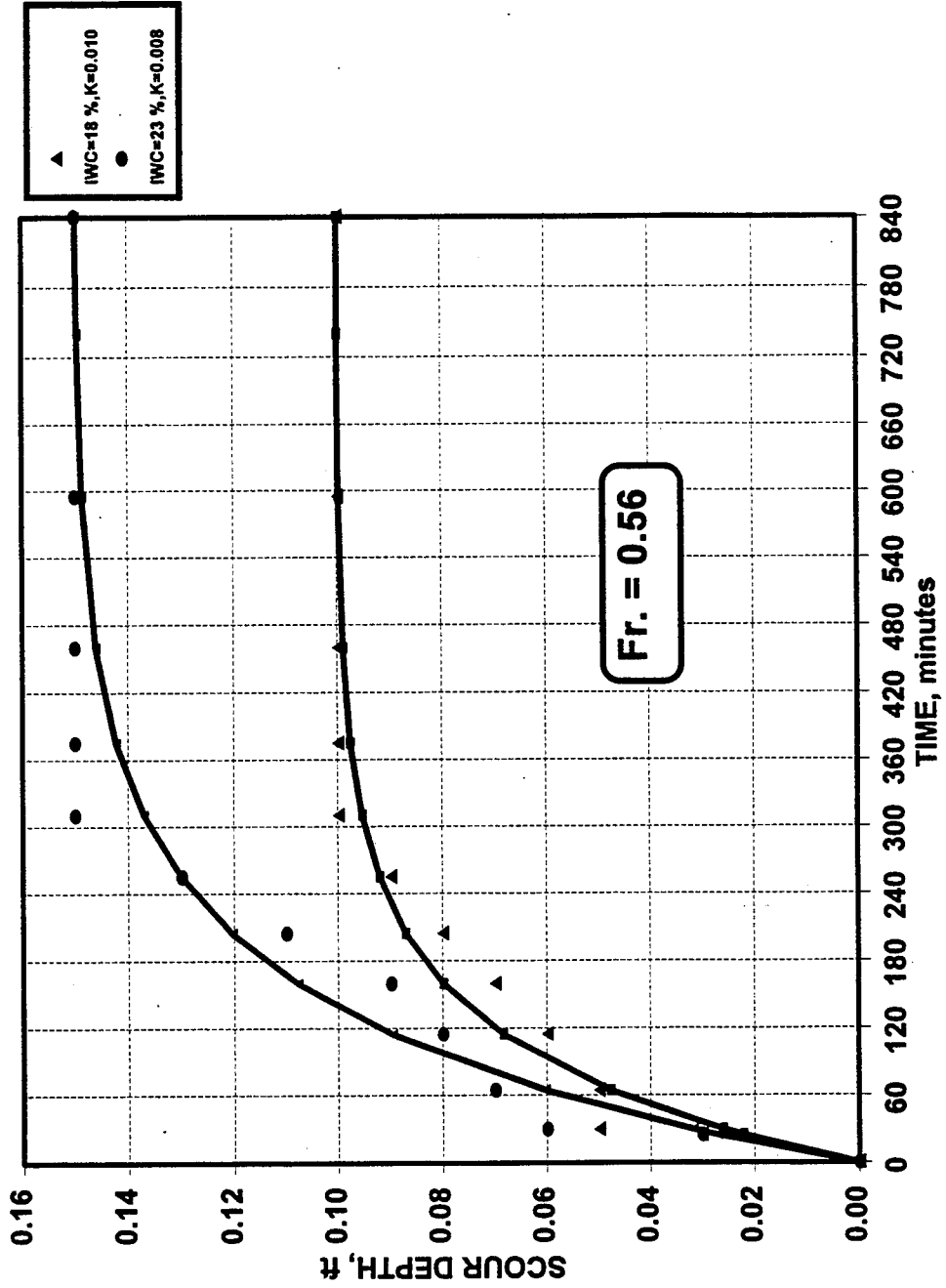


Figure (5.61) Time Rate of Scour for Initial Water Content of 18 % and 23 % (Runs 8-74-A, B).

water content is increased from about 20 % to about 25 %. By comparing the normalized time rate of scour for the Kaolinite clay with 15 % initial water content but with different values of Froude numbers as shown in Figure 5.62, it can be shown that they have almost the same value of K. This indicates that by increasing the Froude number for the same soil, the time rate of scour remains constant. Table 5.14 includes all the values of K for different conditions of initial water content used in the figures.

Table 5.14 Effect of Initial Water Content on Time Rate of Scour for Kaolinite Clay

Run No.	Compaction (%)	Initial Water Content (%)	K Value
8-72-A	86	15	0.007
8-76-A	86	22	0.014
8-76-B	83	25	0.013
8-74-A	88	18	0.010
8-74-B	83	23	0.008
8-71-A	00	00	0.006

5.5.2 Effect of Clay Content on Clay Mixture

This section will include the investigation of: the scour depth as a function of the approach flow conditions for various clay contents, the effect of clay content on the cross-sectional profile of the scour hole. Also, the side slope of the scour hole, the longitudinal slope of the scour hole, and time rate of scour. The results are expressed in functional relationships whenever possible.

5.5.2.1 Variation of Scour Depth with Approach Flow Conditions

The effect of the percentage of clay content in the mixture of Kaolinite clay and sand was investigated by varying the percentage of clay in the mixture. The clay content

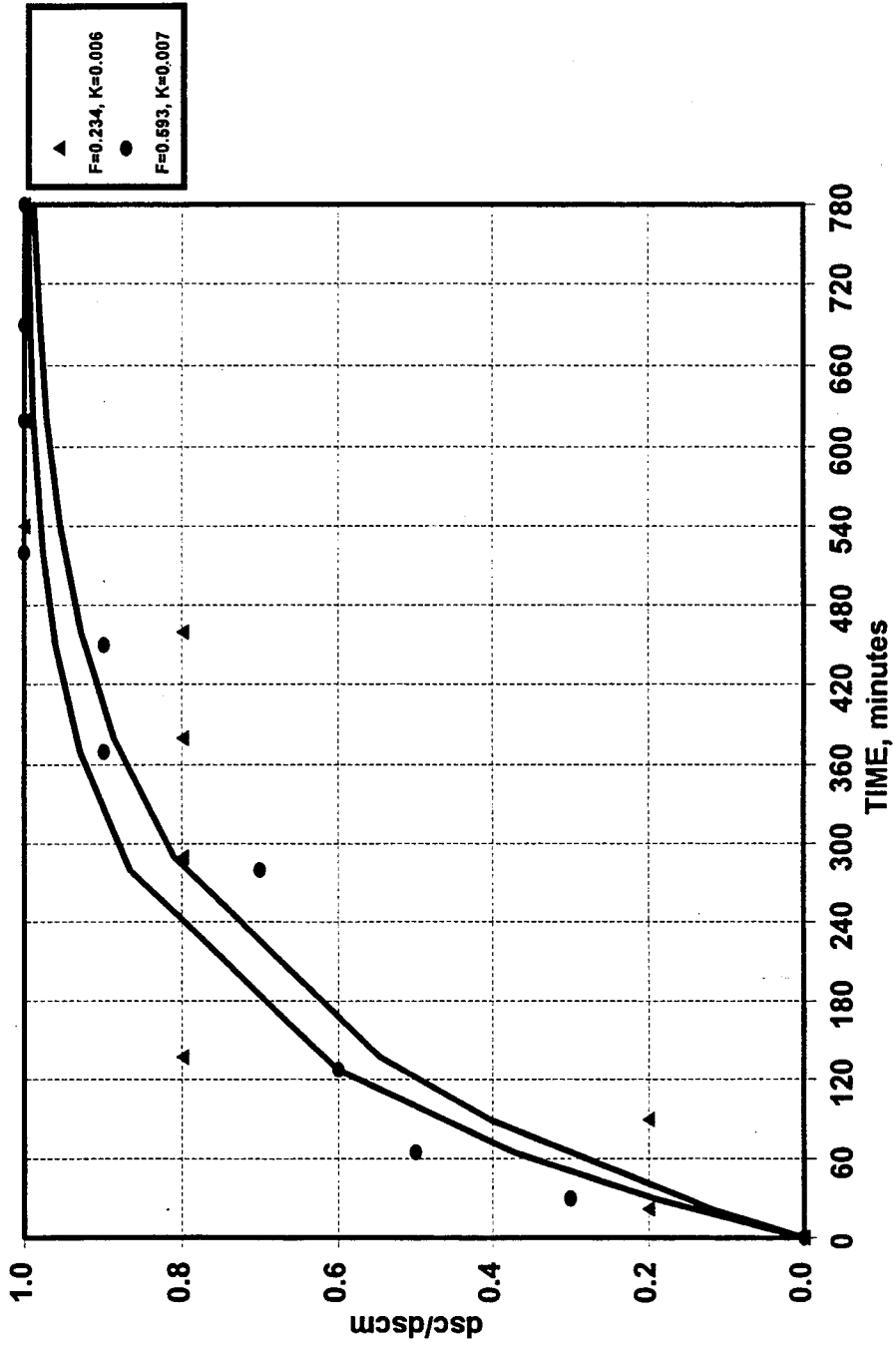


Figure (5.62) Time Rate of Normalized Scour for Different Flow Conditions (Runs 8-71-A and 8-72-A).

varied in the mixture from 0 % clay (medium sand) to 10 %, 20 %, 30 % and 50 %. Figure 5.63 relates the dimensionless scour depth -- depth of scour normalized by the square root of abutment width and flow depth -- to the intensity of flow conditions expressed by the Froude number. As shown in Figure 5.63, for a given Froude number, the scour depth decreases as the percentage of clay content in the mixture is increased from 0 % to 10 %. Increasing the percentage of clay further from 20 % to 30 %, the depth of scour keeps on decreasing. By increasing the percentage of clay content beyond 30 % to 50 %, the depth of scour start to increase again. From this, it is concluded that up to 30 % clay content, there are no (or little) cohesion effect on the depth of scour. Beyond 30 % clay content, the Initial Water Content and compaction start to show their effect. To separate the clay content effect, the values of dimensionless scour depth in Figure 5.63 for various clay contents are normalized by the corresponding dimensionless scour depth in sand (d_s/d_w) for the same flow conditions as shown in Figure 5.7. Finally, the average scattered experimental values of clay scour to sand scour ratios for various clay contents are calculated up to 30 % clay content. Figure 5.64 presents also this relationship along with its upper and lower bounding limits. Figure 5.64 is used in deriving the equation which relates the clay content to the resulting depth of scour.

5.5.2.2 Cross-Sectional Profile of the Scour Holes

To study the effect of Kaolinite clay content on the geometry of the resulting scour hole, a comparison of different cross sectional profiles passing through the upstream face of the abutment is conducted. The comparison of the cross-sectional profiles are illustrated in Figures 5.65 through 5.67 for clay contents of 0 %, 10 %, 20

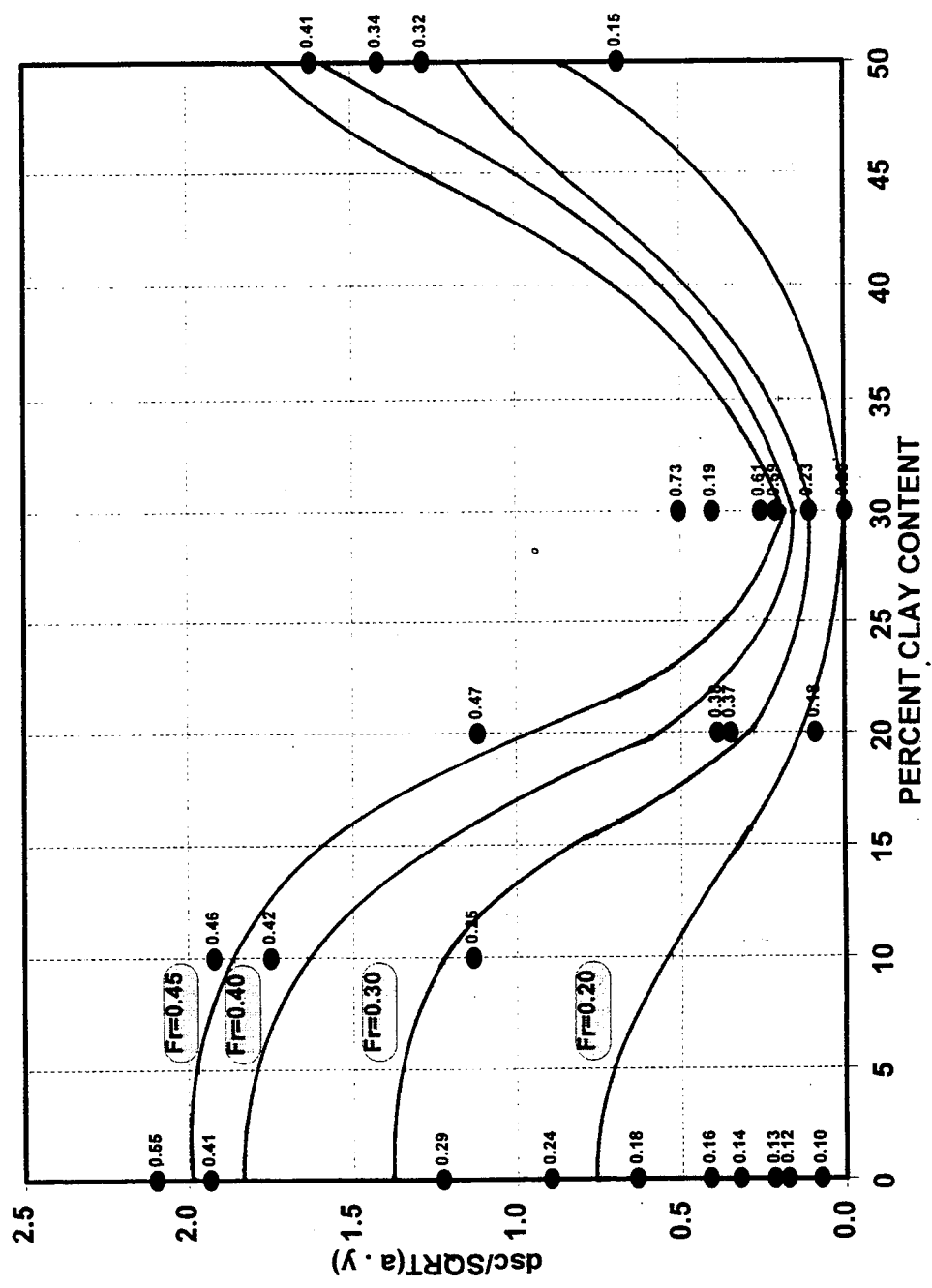


Figure (5.63) Effect of Clay Content on Dimensionless Abutment Scour Depth for Kaolinite Clay.

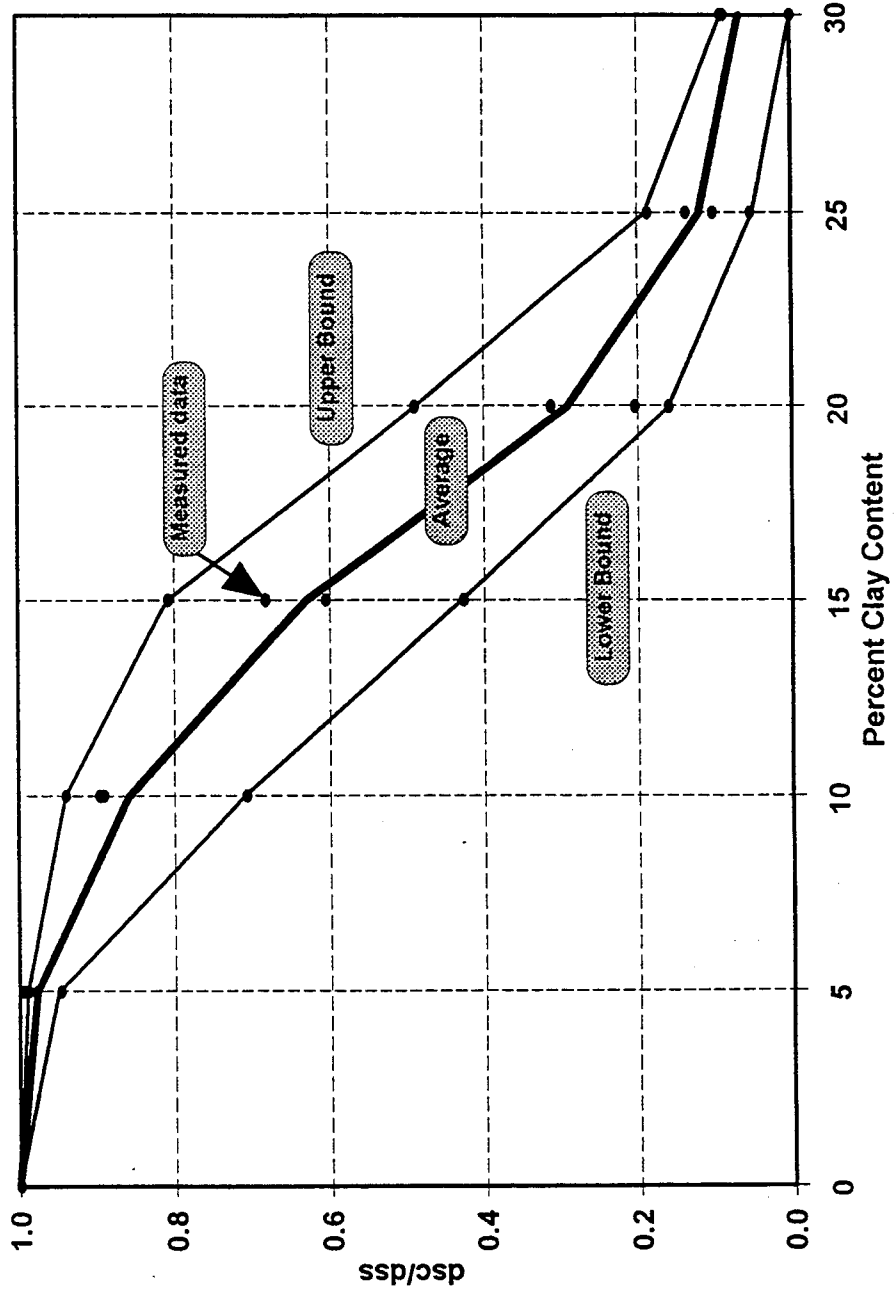


Figure (5.64) Variation of Normalized Scour Depth with Clay Content for Kaolinite Clay.

%, 30 % and 50 % for different Froude numbers representing different flow conditions. Figure 5.68 a, b, c, and d show actual photographs of abutment scour hole geometry for runs number 8-78-A, 8-78-B, 8-74-A, and 8-78-C with percent clay content of 10 %, 20 %, 30 %, and 50 %. Scour dimensions defined by the depth, width, and side slope are summarized in Table 5.15. From Figures 5.65 through 5.67 and Table 5.15, the depth of scour decreases as the percentage of clay content increases in the mixture from 0 % to 30 %. By increasing the clay content to 50 %, the depth of scour increases again. This is due to the effect of cohesion variables such as initial water content and compaction which will begin to show their effects after increasing clay content to beyond 30 %.

Table 5.15 Effect of Clay Content on Scour Geometry for Kaolinite Clay

Run No.	Clay Content (%)	Depth (ft)	Normalized Depth	Width (ft)	Side Slope (degrees)
81-A	0	0.83	1.000	1.31	32.36
84-A	0	0.90	1.000	1.32	34.29
78-A	10	0.75	0.834	1.26	30.76
79-A	10	0.84	0.916	1.31	32.67
79-B	20	0.17	0.186	0.13	52.59
80-B	20	0.50	0.532	0.68	36.33
77-B	20	0.04	0.213	0.05	38.66
72-A	30	0.10	0.100	0.74	7.70
71-B	30	0.0	0.000	0.0	0.0
80-C	50	0.74	0.773	1.21	31.45
77-C	50	0.31	2.301	1.07	16.16

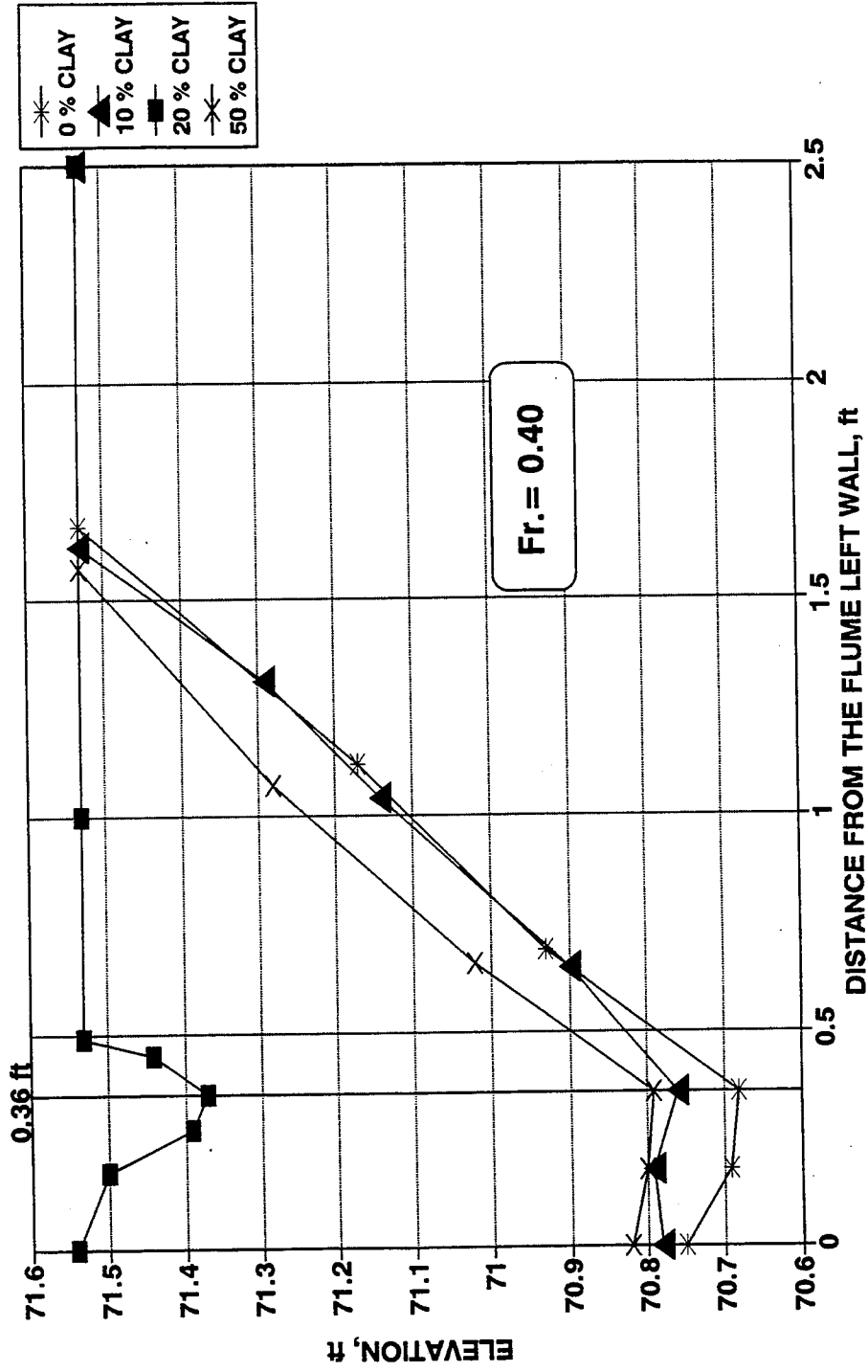


Figure (5.65) Effect of Clay Content on the Scour Hole Geometry at the Upstream Abutment Face (Fr=0.40).

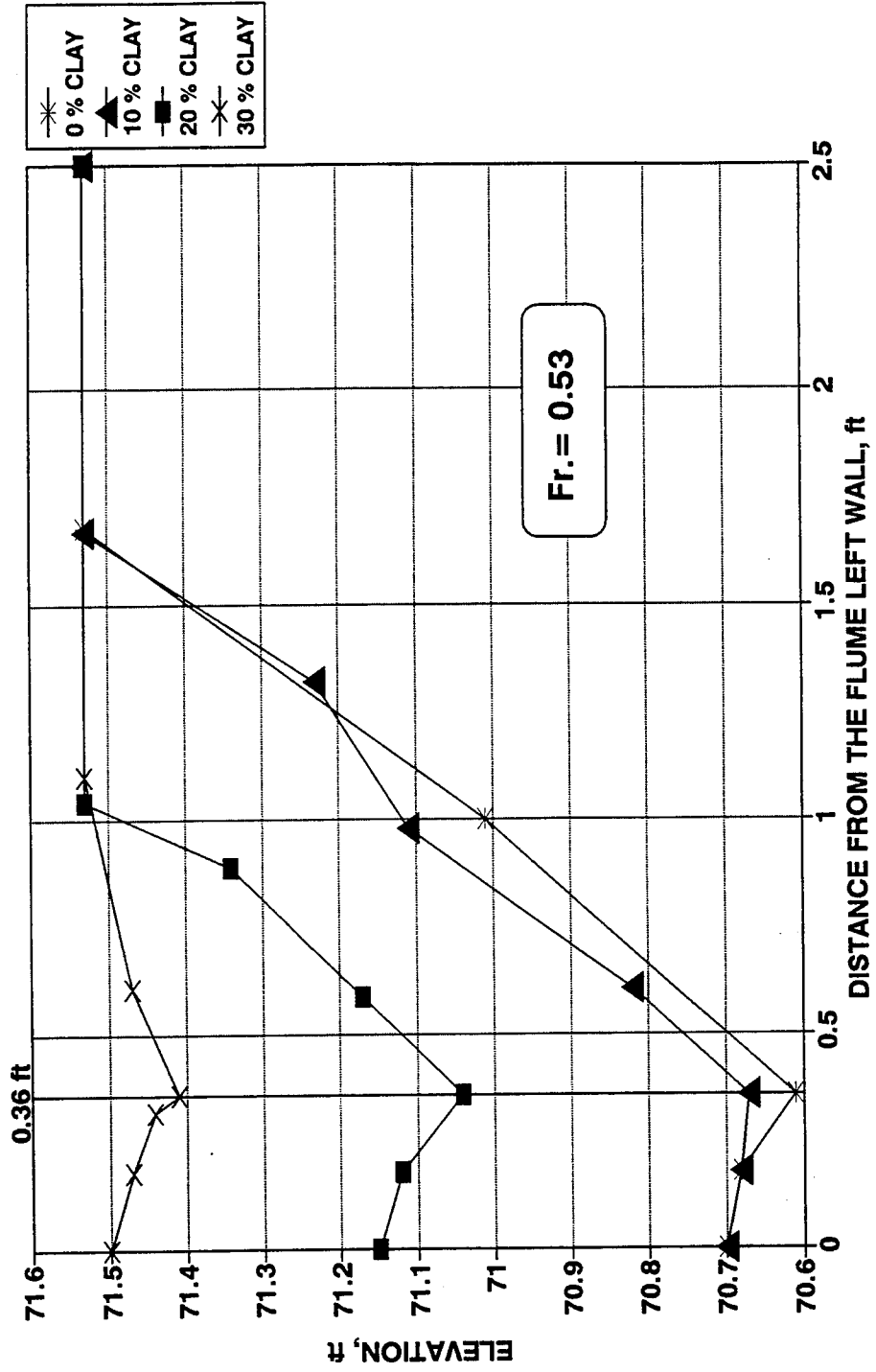


Figure (5.66) Effect of Clay Content on the Scour Hole Geometry at the Upstream Abutment Face (Fr=0.53).

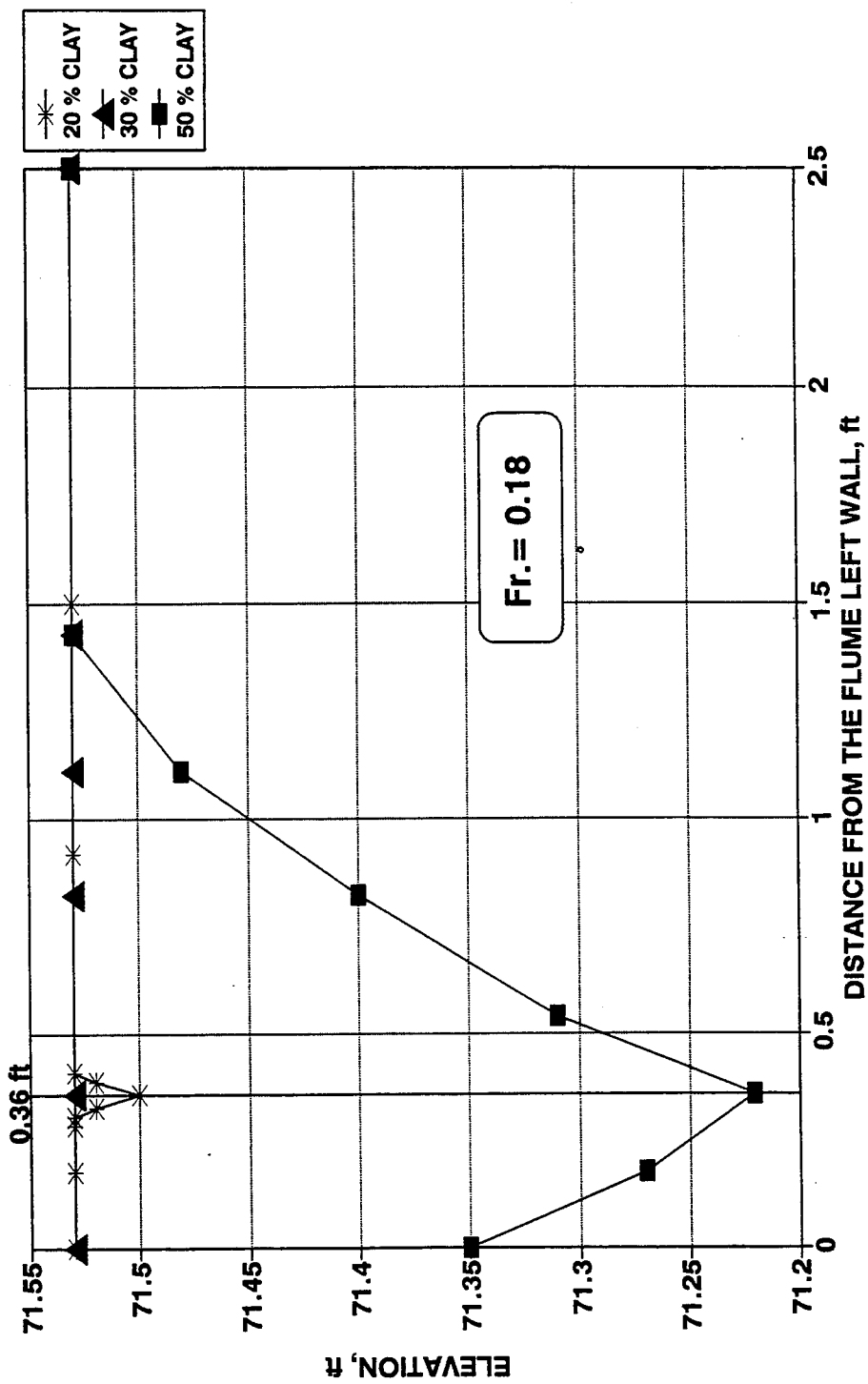


Figure (5.67) Effect of Clay Content on the Scour Hole Geometry at the Upstream Abutment Face ($Fr=0.18$).



Figure (5.68 a) View of Abutment Scour Hole Geometry for 10 % CC (Run 8-78-A).

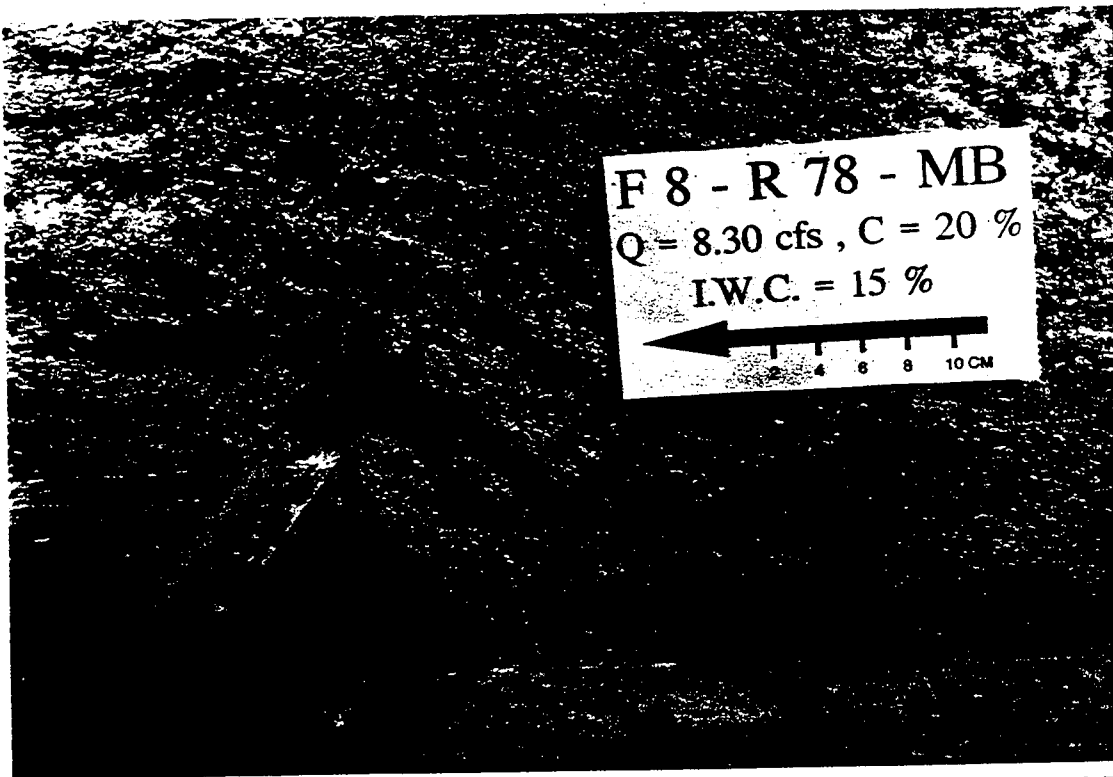


Figure (5.68 b) View of Abutment Scour Hole Geometry for 20 % CC (Run 8-78-B).



Figure (5.68 c) View of Abutment Scour Hole Geometry for 30 % CC (Run 8-74-A).



Figure (5.68 d) View of Abutment Scour Hole Geometry for 50 % CC (Run 8-78-C).

5.5.2.3 Longitudinal Slope of the Scour Holes

For each soil mixture, the scour hole will have a certain slope along the longitudinal direction of the flow adjacent to the abutment wall (Figure 5.7). In order to compute the longitudinal slope for each mixture clay content, channel cross sections were plotted for different Froude numbers. The slope was then calculated as an average slope value for that soil mixture for the entire range of flow conditions. Figures 5.40, 5.69, 5.70, 5.55, and 5.71 present cross section plots for the Kaolinite clay contents of 0 %, 10 %, 20 %, 30 %, and 50 % with a range of flow conditions for each clay. The summary of the scour hole longitudinal slope variation with clay content is presented in Figure 5.72. From this figure it can be shown that as the percentage of clay increases from 0 % to 30 %, the downstream slope is decreased from 31° to 21°. By increasing clay content from 30 % to 50 %, the slope increases again from 21° to 34°. Beyond 30 % clay content, the cohesion variables such as initial water and compaction start to show their effect. In the upstream direction, the slope increases from 39° to 42° as the clay content is increased from 0 % to 30 % and then increases to 48° as the clay content is increased from 30 % to 50 %. It is observed from these slopes that the upstream slopes are steeper than the downstream slopes.

5.5.2.4 Effect of Clay Content on Time Rate of Scour

Figures 5.73 and 5.74 shows the development of scour with time for five clay contents of 0 %, 10 %, 20 %, 30 %, and 50 % for different values of Froude numbers. As shown in these figures, as a general trend, as the value of clay content is increased

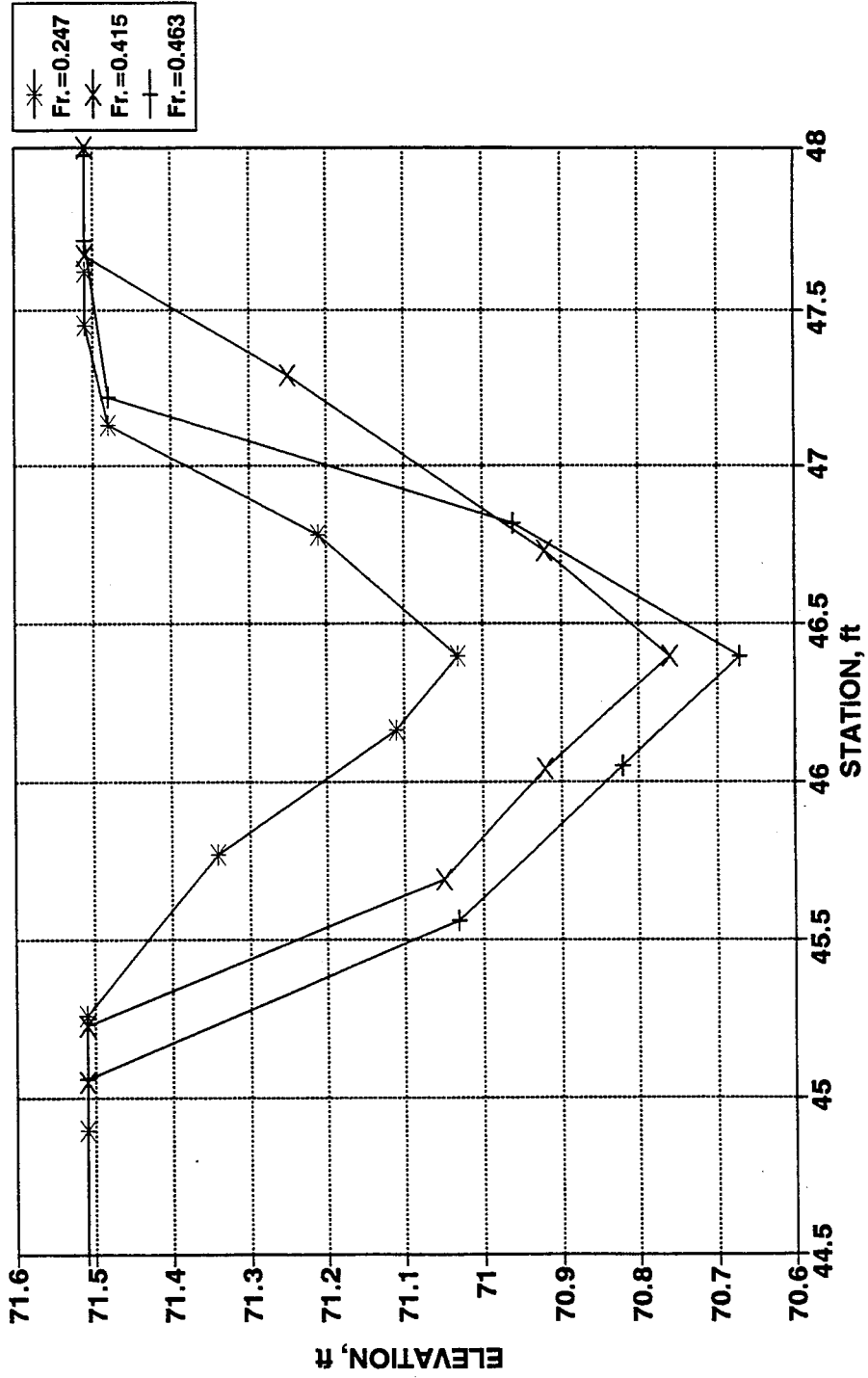


Figure (5.69) Longitudinal Profile of the Scour Hole for 10 % Clay Content.

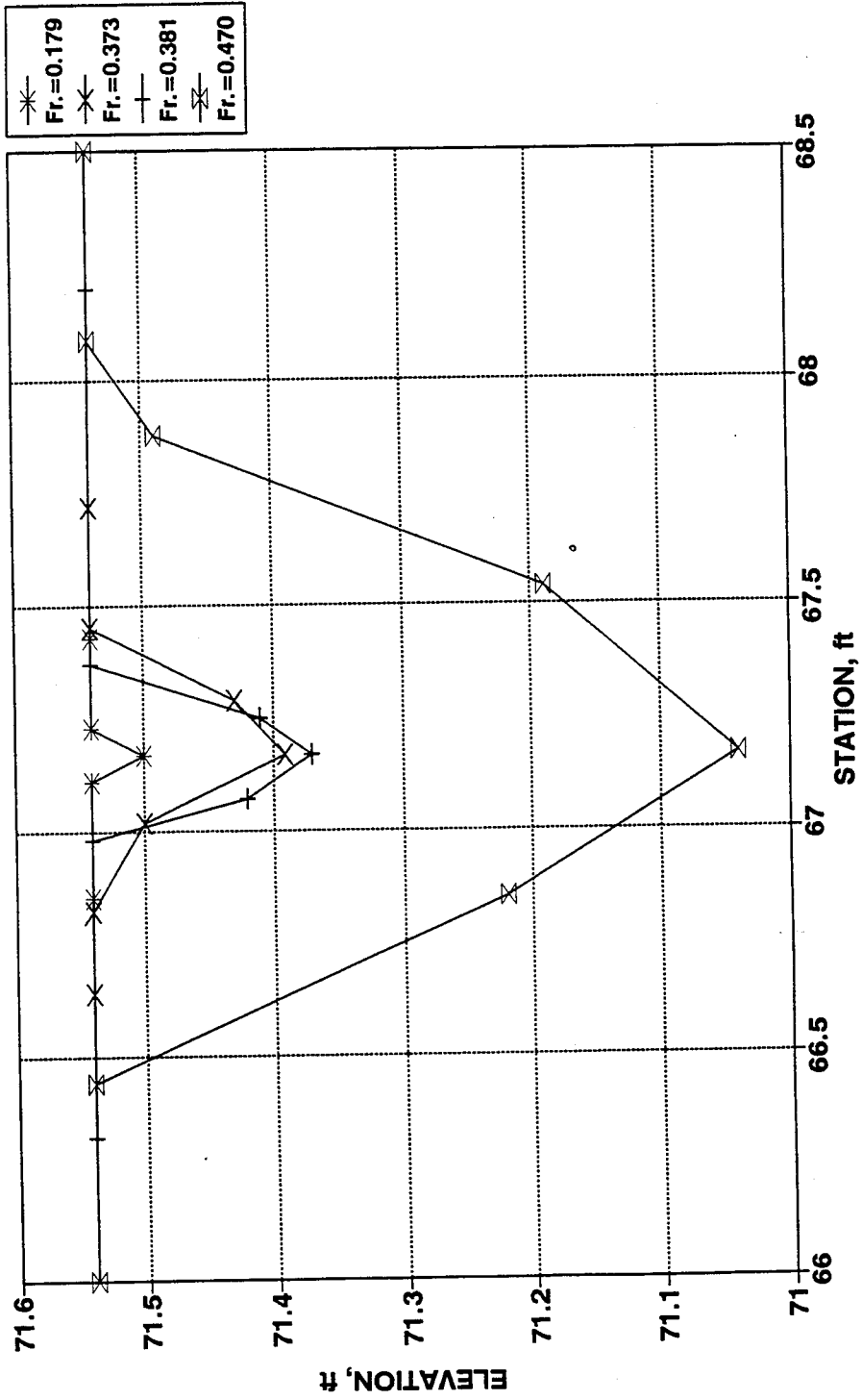


Figure (5.70) Longitudinal Profile of the Scour Hole for 20 % Clay Content.

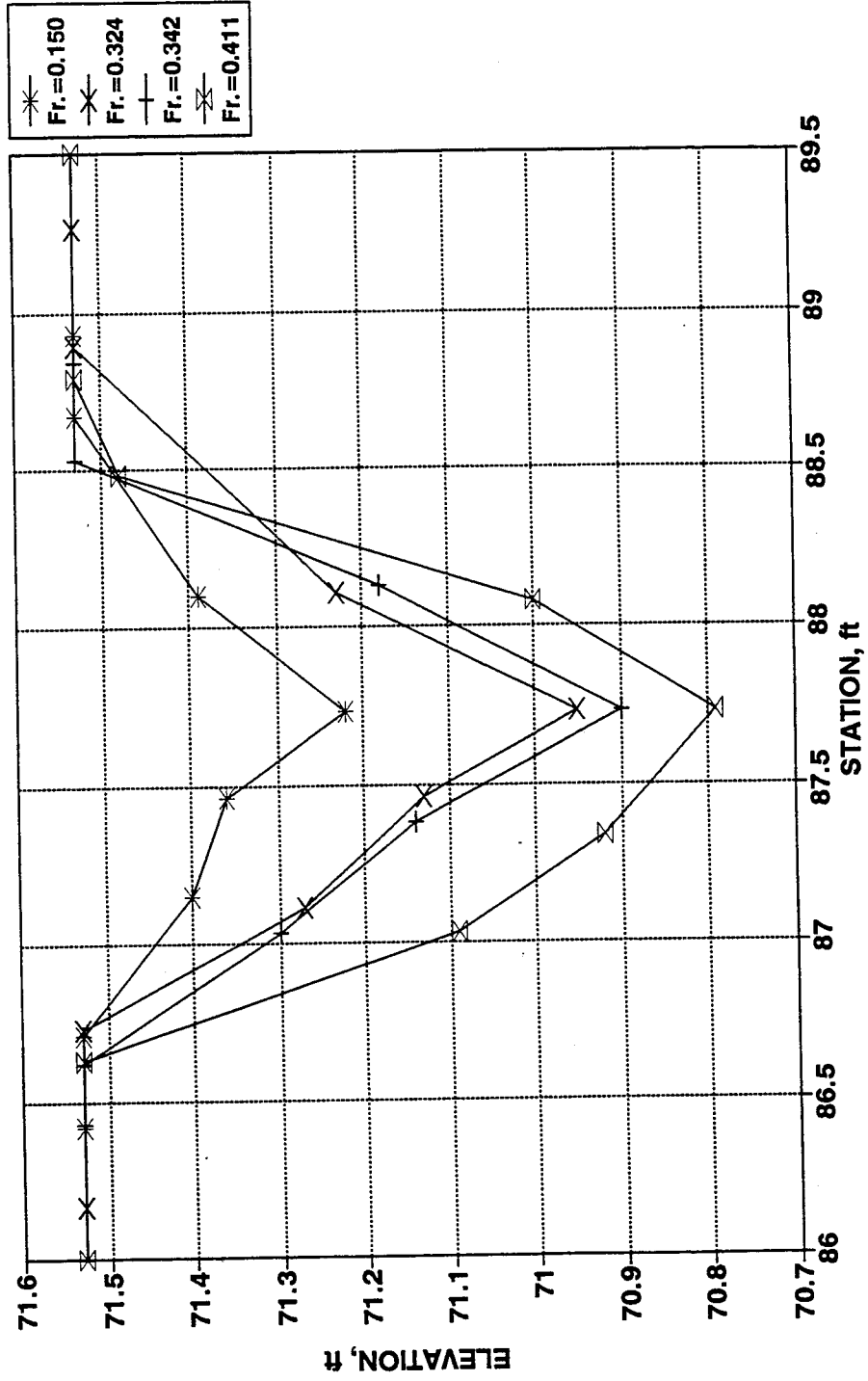


Figure (5.71) Longitudinal Profile of the Scour Hole for 50 % Clay Content.

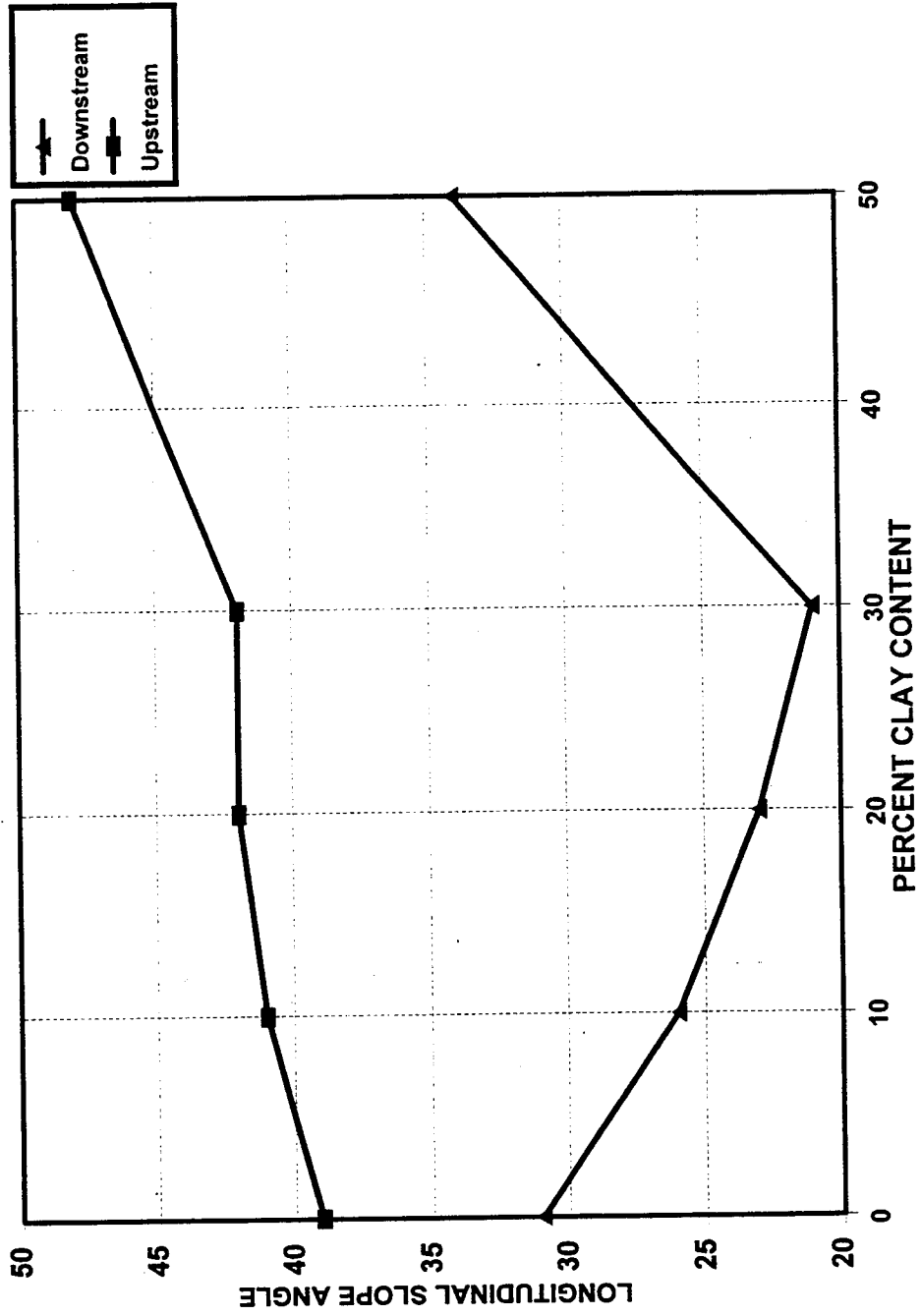


Figure (5.72) Variation of Longitudinal Slope Angles with Different Clay Contents.

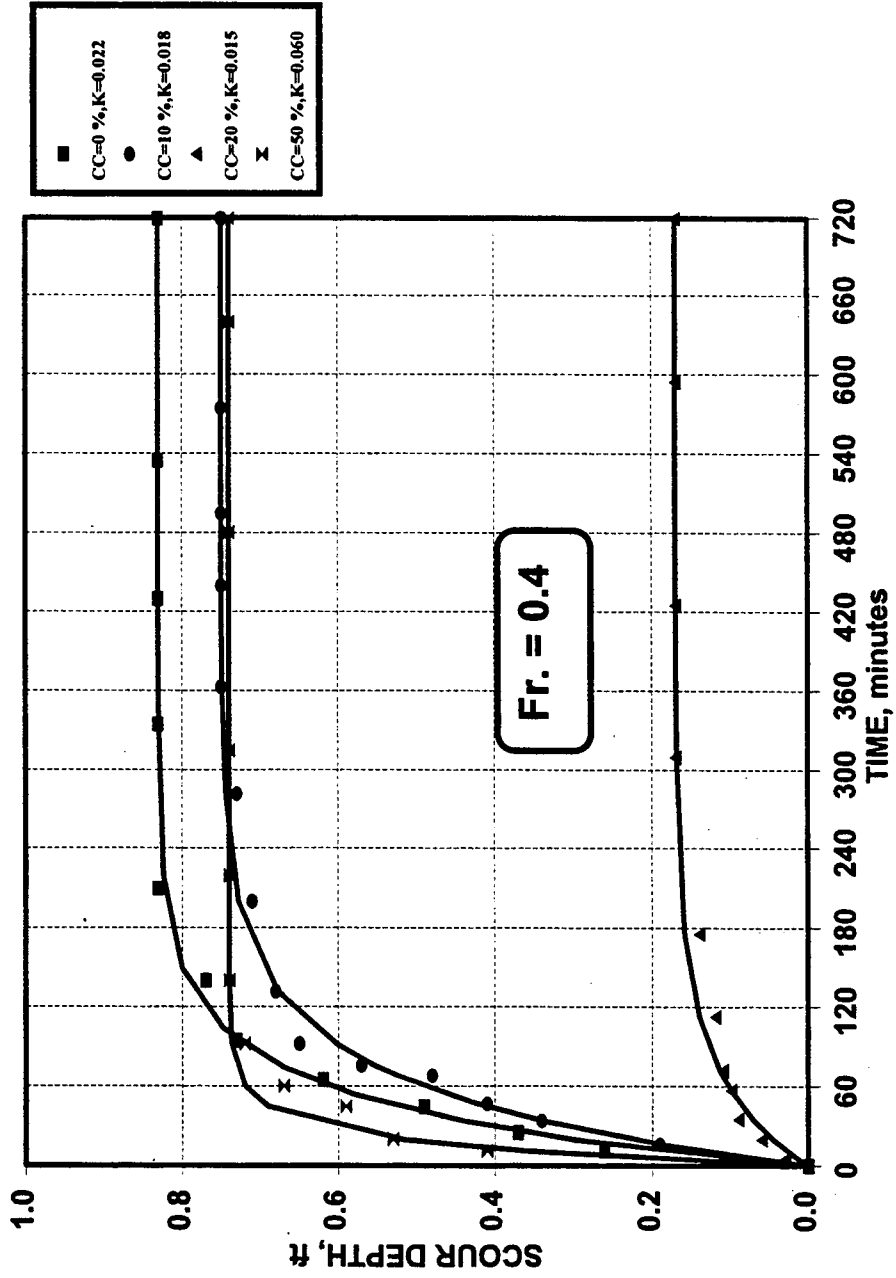


Figure (5.73) Variation of Time Rate of Scour with Clay Content (Fr=0.40, Runs 8-81-A , 8-78-A, 8-79-B, and 8-80-C).

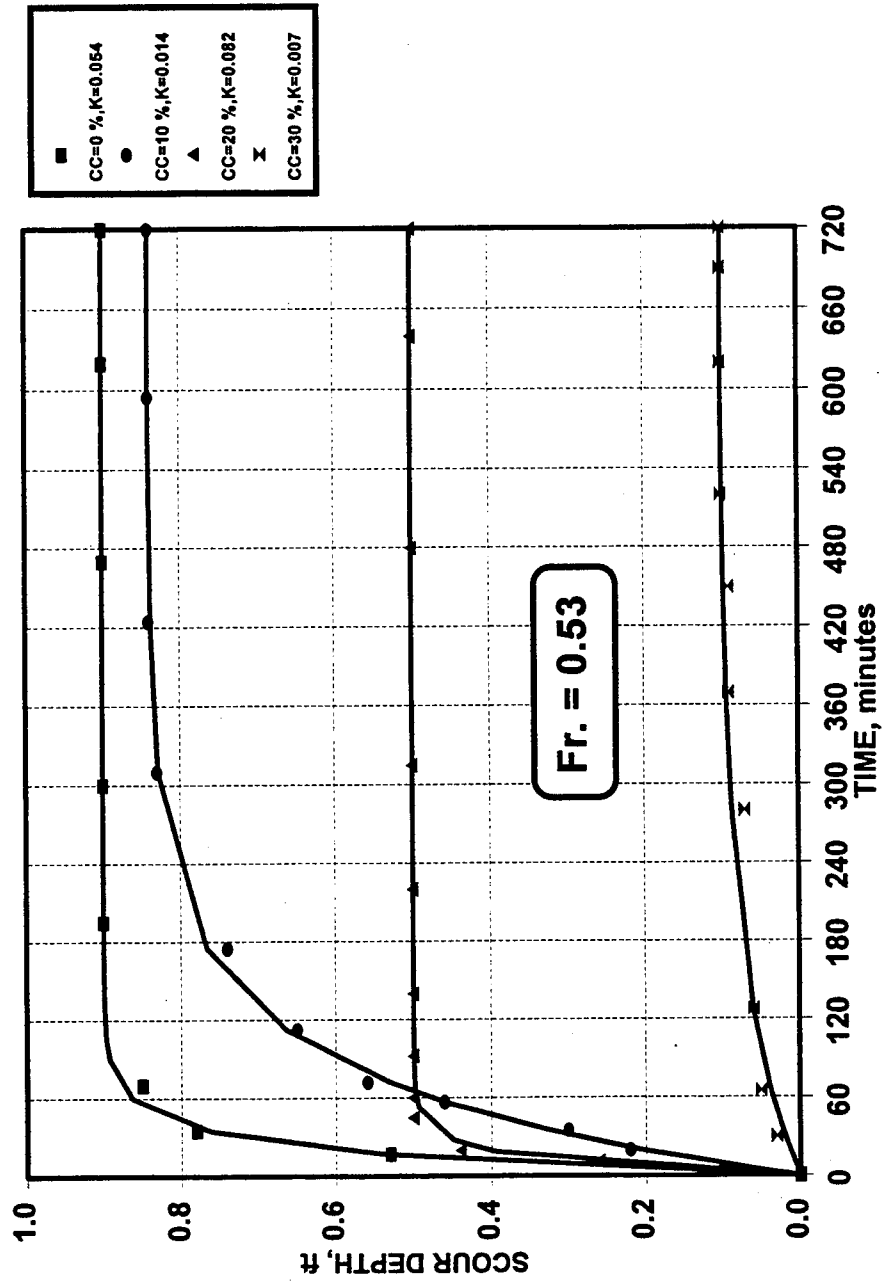


Figure (5.74) Variation of Time Rate of Scour with Clay Content (Fr=0.53, Runs 8-84-A, 8-79-A, 8-80-B, and 8-72-A).

from 0 % to 30 %, the value of the parameter K used in the time rate of scour equation 5.5 decreases. This indicates that as the percentage of clay content in the mixture increases, the time needed for the scour hole to reach equilibrium condition increases. By increasing the percentage of clay content in the mixture to 50 %, the time needed for the scour hole to reach equilibrium condition decreases. Table 5.16 includes all the values of K for different percentage of clay contents conditions shown in the figures.

Table 5.16 Effect of Clay Content on Time Rate of Scour for Kaolonite Clay

Run No.	Clay Content (%)	K Value	Clay Content versus K Value
8-72-A	30	0.007	
8-81-A	0	0.022	
8-78-A	10	0.018	
8-79-A	10	0.014	
8-79-B	20	0.015	
8-80-C	50	0.060	
8-84-A	0	0.054	

Comparison of Tables 5.12 and 5.16 indicates that K is dependent on the mineralogy of clayey-sand mixtures as well as the cohesive soil content. K value and the rate of scour hole development in Kaolinite mixtures are half as much as that in Montmorillonite mixtures.

5.5.3 Comparison between Compaction and Torvane Shear Strength

The Torvane shear gauge was used around the abutment to measure the shear strength of the soil. The relationship between the Torvane shear strength and percentage of compaction for Kaolinite clay is presented in Figure 5.75 for the range of different initial water contents used in the experiments. Figure 5.75 shows that as the compaction increases the Torvane shear strength very gradually increases up to a certain value of compaction. Beyond this limiting value, while the compaction stays almost constant the Torvane shear strength value keeps on increasing. In other words, for the some value

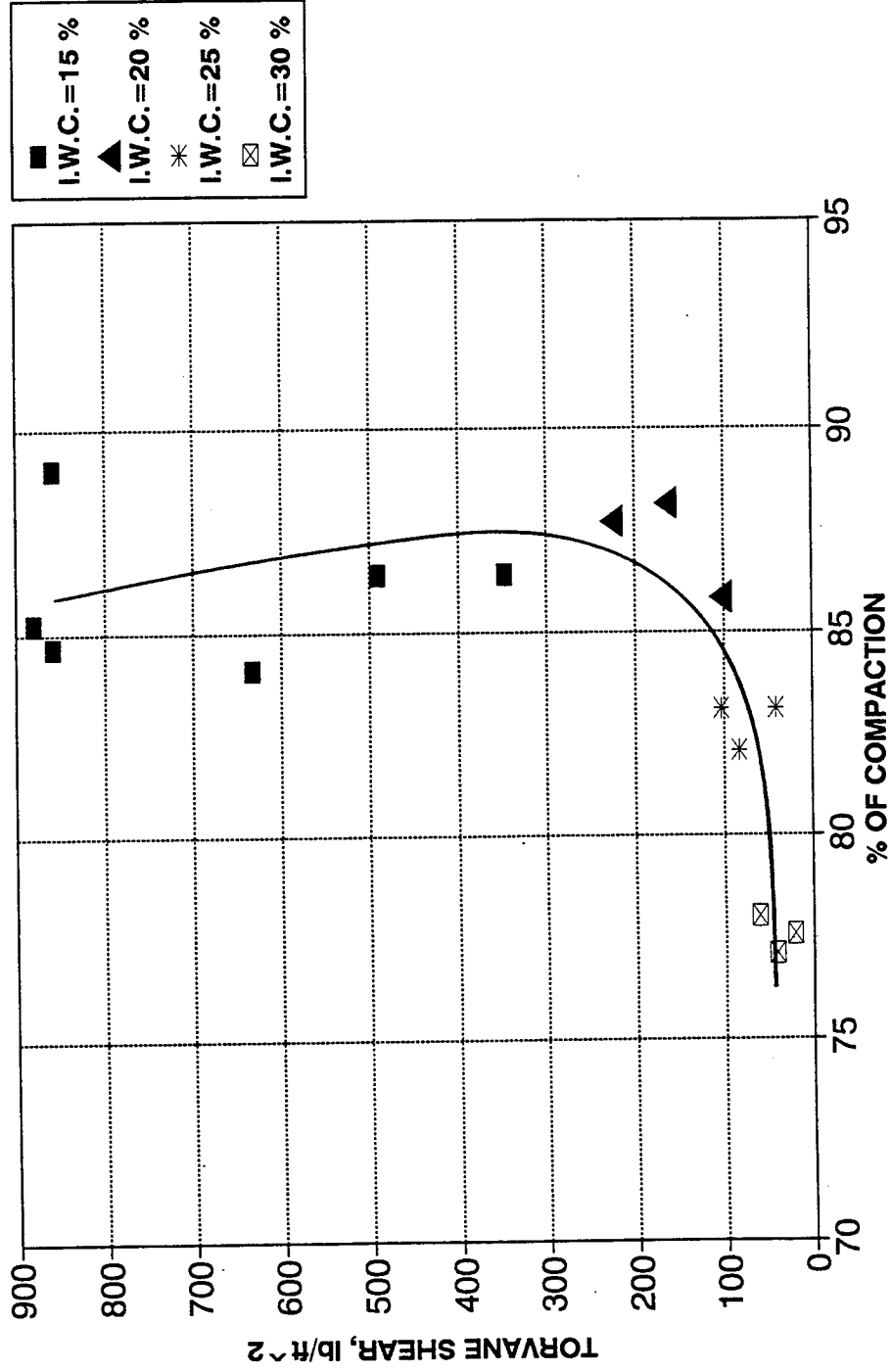


Figure (5.75) Relationship between Compaction and Torvane Shear for Kaolinite Clay.

of compaction, there are more than one value of corresponding Torvane shear strength which makes it impossible to use the Torvane shear strength as one of the variables in predicting maximum depth of abutment scour.

5.6 Abutment Scour Prediction Equations for Cohesive Materials

A regression analysis was performed using non-linear multiple regression analysis of the SAS program which is based on non-linear least squares method. The expression for abutment scour in cohesive materials was developed earlier in section 5.2 from the dimensional analysis (Equation 5.4) and is given as:

$$\frac{d_{sc}}{d_{sc}} = f\left(\frac{y}{a}, \frac{L}{a}, WC, CC, C, CT, \frac{Ut}{y}, R_s, \frac{TS}{U^2 \rho}, F_r, \alpha, \phi, T\right) + e \quad (5.4)$$

In this section, using this expression, along with statistical analysis of measured data, abutment scour equations for cohesive material will be developed. In Equation 5.4, since the relationship between the depth of flow and the width of the abutment remained relatively constant, (y/a) will be constant. Also, since the relationship between the length and the width of the abutment is kept constant, (L/a) will be constant. The values of α and ϕ are kept constant throughout the experiments. The time rate of scour in Equation 5.4 is represented by (Ut/y) . Since long time duration is used in the experiments, the scour depth reaches its maximum value and is stabilized, the time has no effect which makes the (Ut/y) term has on effect on the regression analysis. For free surface open channel flow, R_s is in the fully turbulent zone and its effect will be negligible in the equation. From the analysis of Torvane shear strength measurements, it was noticed that

for the same value of Torvane shear strength, there was more than one value of scour depth with different initial water content which makes (TS) an unreliable indicator of scour. The Froude number will be used to predict the depth of scour for sand. The cohesive variables will be then used to adjust sand scour depth to accommodate the cohesive material scour depth. Since the Froude number will be included in the sand scour predictor, there is no need to include this term in the equation. The final equation becomes:

$$\frac{d_{sc}}{d_{ss}} = f(WC, CC, C, CT) \quad (5.7)$$

In which d_{sc} is the depth of abutment scour occurring in sand for corresponding flow conditions. This equation hypothesizes that maximum depth of scour depends on initial water content, percentage of clay content, percentage of compaction, and type of clay. In the following sections, various equations will be developed for different conditions.

5.6.1 Montmorillonite Clay Equation

For Montmorillonite clay, three equations will be developed. The first two equations will cover the natural clay with 100 % Montmorillonite clay with different initial water contents and compactions. The third equation will cover Montmorillonite clay mixed with different percentages of sand. This equation will cover the range from medium sand with 0 % clay to 30 % clay with intermediate values of initial water content.

1. Initial Water Content and Compaction Equations

The regression analysis is performed on 100% Na-montmorillonite clay with different initial water contents and compactions. The variables which are included in the equation are only the initial water content and the compaction since the type of clay was kept the same and the percentage of clay content was not changed. The actual data which is used in the regression is divided into two groups. The first equation will cover the unsaturated soil group with up to 20 % initial water content. The second equation will cover the saturated soil group ranging from 28 % to 45 %.

For unsaturated soil, the regression analysis utilizing the non-linear least squares analysis method resulted in the prediction equation for the relationship between normalized depth of scour, initial water content, and compaction as follows:

$$\frac{d_{sc}}{d_{ss}} = [X_1 + (X_2 \cdot WC)] + [X_3 + (X_4 \cdot C) + (X_5 \cdot C^2) + (X_6 \cdot C^3)] \quad (5.8)$$

where:

$$X_1 = 2.186;$$

$$X_2 = -5.342;$$

$$X_3 = 15.407;$$

$$X_4 = -52.202;$$

$$X_5 = 60.873;$$

$$X_6 = -23.512;$$

The corresponding non-linear least squares summary statistics is as follows:

SOURCE	DF	SS	MS=SS/DF	R ²
REGRESSION	5	14.198	2.840	89.1
RESIDUAL	14	0.099	0.007	
UNCORRECTED TOTAL	19	14.297		
CORRECTED TOTAL	18	0.913		

where:

DF = Degree of Freedom;

SS = Sum of Squares;

MS = Mean Square;

R² = The equivalent non-Linear coefficient of determination;

= Residual/Corrected Total;

For saturated soil, the regression analysis resulted in the following prediction equation relating the normalized scour depth to initial water content and compaction:

$$\frac{d_{sc}}{d_{sc}} = [X_1 + (X_2 \cdot WC) + (X_3 \cdot WC^2) + (X_4 \cdot WC^3)] * [X_5 + (X_6 \cdot C)] \quad (5.9)$$

where:

$$X_1 = 4.76;$$

$$X_2 = -45.1;$$

$$X_3 = 136.1;$$

$$X_4 = -126.0;$$

$$X_5 = -0.339;$$

$$X_6 = 1.744;$$

The corresponding non-linear least squares summary statistics is as follows:

SOURCE	DF	SS	MS=SS/DF	R ²
REGRESSION	6	3.187	0.531	79.4
RESIDUAL	16	0.193	0.012	
UNCORRECTED TOTAL	22	3.380		
CORRECTED TOTAL	21	0.918		

The comparison of measured and computed values from these equations are shown in Figure 5.76 which shows that the fitting equations are in very good agreement with measured data. The graphical interpretation of these equations is given in Figure 5.77 where it is shown that in the unsaturated range, the percentage of compaction has a very big influence on the resulting normalized scour depth. For the saturated clays, since for each percentage of initial water content there is almost one corresponding percentage of compaction, the range of compaction for each initial water content is very limited. Figure 5.77 shows that for saturated clays, the reduction of scour is very significant at 28-30 percent IWC.

2. Clay Content Equation

The regression analysis is performed on Montmorillonite clay with different percentages of clay content varying from medium sand with 0 % clay up to 30 % clay. In this low clay content range, the percentage of sand in the soil mixture is high and makes the soil unable to retain water (no more than about 10 %). The soil also does not respond to the compactive efforts. Therefore, in the prediction equation the initial water

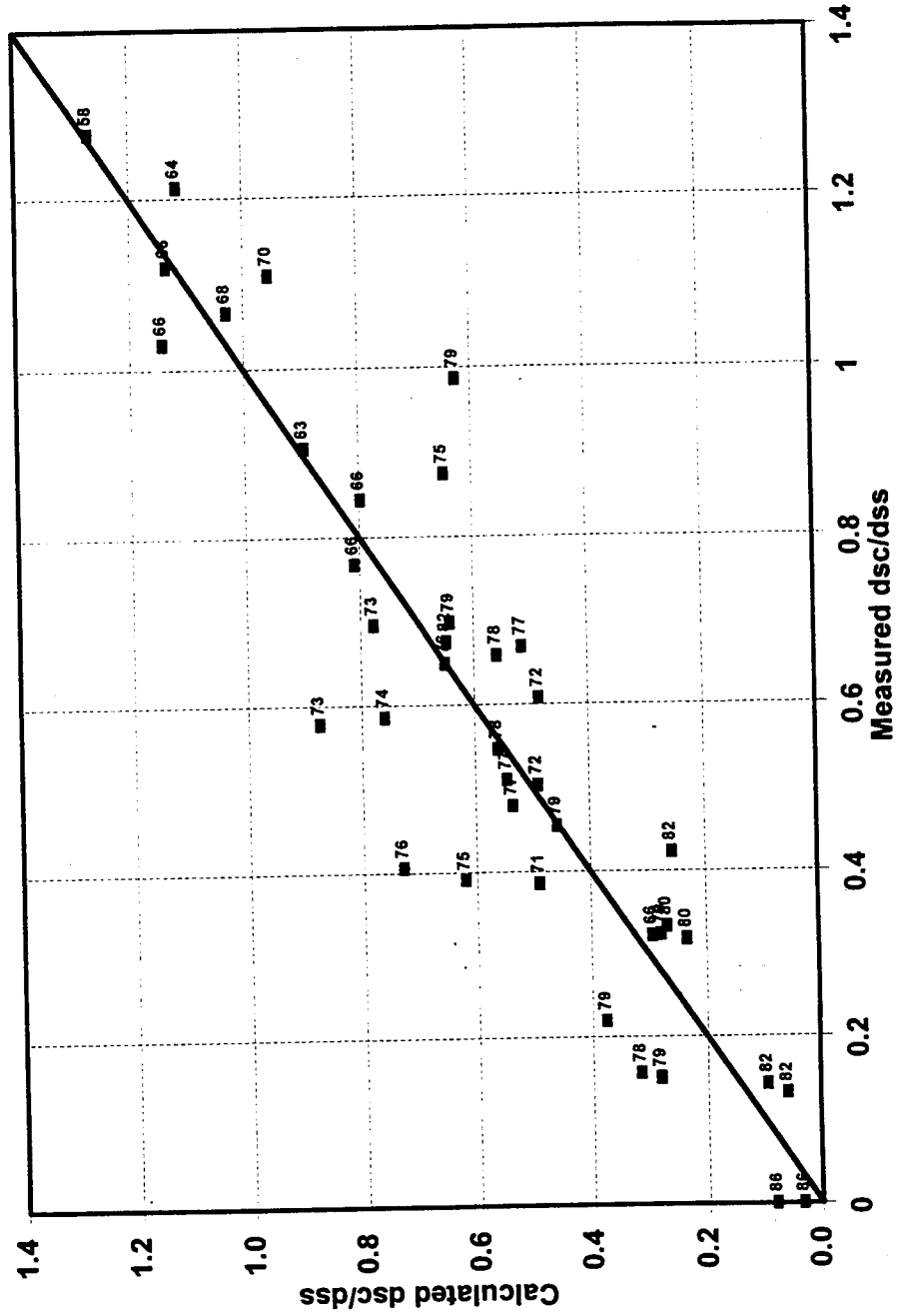


Figure (5.76) Comparison between Measured and Predicted Normalized Scour Depth

using Equations 5.8 and 5.9 for Montmorillonite Clays.

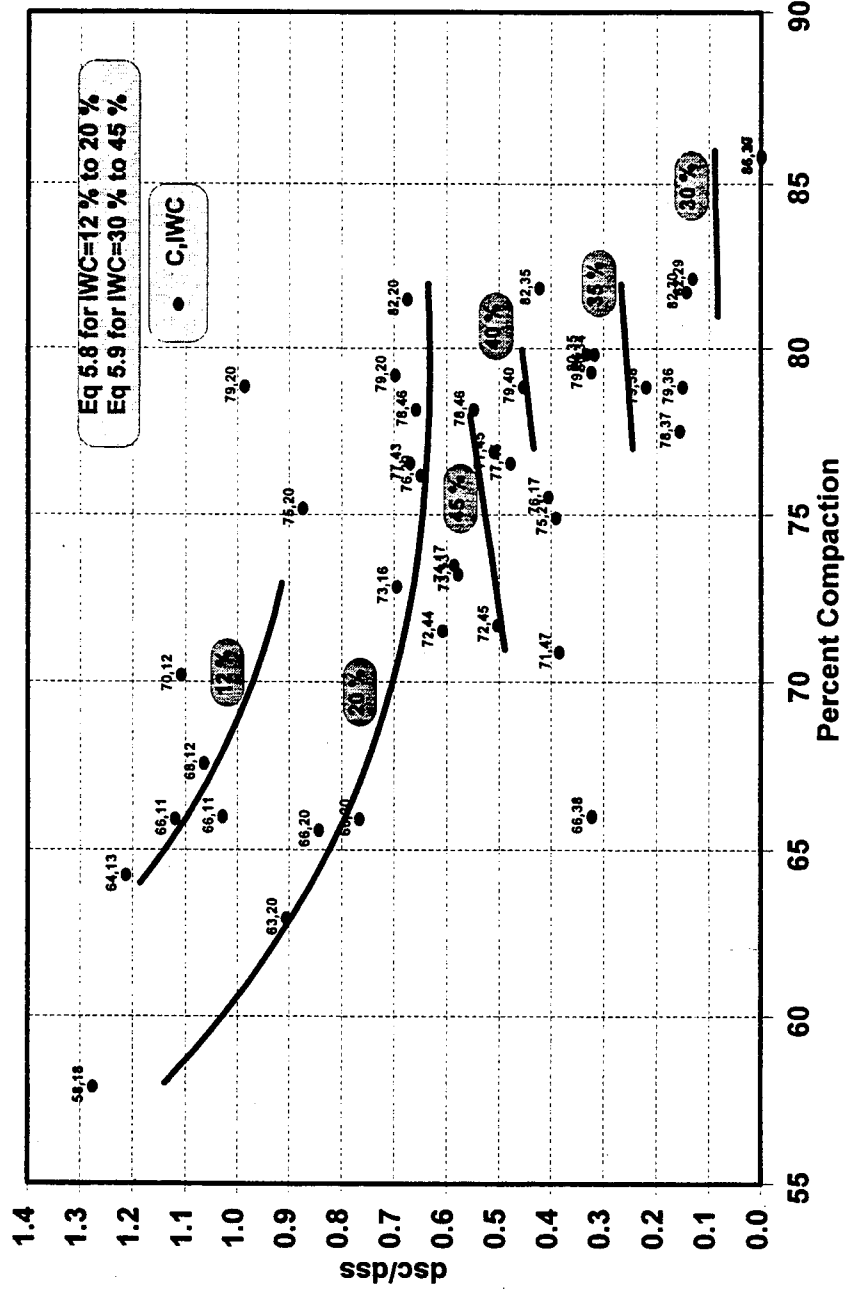


Figure (5.77) Comparison of Prediction Equations for Normalized Scour Depth for Montmorillonite Clay with Actual Data.

content and compaction will not be considered; only the percentage of clay content will be included. Figure 5.35 is used to obtain the normalized depth of scour for different values of Froude number. These interpolated values is used in the final regression analysis and these values are shown in Table 5.17.

Table 5.17 Interpolated Values of Normalized Depth of Scour for different Percentages of Montmorillonite Clay Content

Froude Number	Sand	5 % Clay	10 % Clay	15 % Clay	20 % Clay	25 % Clay	30 % Clay
0.45	1.00	0.99	0.95	0.89	0.79	0.68	0.61
0.40	1.00	0.94	0.94	0.87	0.77	0.66	0.59
0.35	1.00	0.97	0.97	0.93	0.83	0.72	0.66
0.30	1.00	0.94	0.94	0.88	0.82	0.77	0.76
0.25	1.00	0.92	0.92	0.84	0.84	0.84	0.84
0.20	1.00	0.82	0.82	0.76	0.75	0.78	0.78
0.15	1.00	0.79	0.79	0.76	0.74	0.71	0.71

From Table 5.17, the regression analysis between the normalized depth of scour and the percentage of clay content gives:

$$\frac{d_x}{d_s} = X_1 + (X_2 \cdot CC) + (X_3 \cdot CC^2) + (X_4 \cdot CC^3) \quad (5.10)$$

where:

$$X_1 = 1.0;$$

$$X_2 = -0.608;$$

$$X_3 = -4.286;$$

$$X_4 = 10.159;$$

The non-linear least squares using the interpolated normalized scour depth resulted in the following summary statistics:

SOURCE	DF	SS	MS=SS/DF	R ²
REGRESSION	4	35.926	8.981	77.7
RESIDUAL	45	0.150	0.003	
UNCORRECTED TOTAL	49	36.076		
CORRECTED TOTAL	48	0.673		

As seen from this table, there is a strong correlation between clay content and the normalized scour depth.

5.6.2 Kaolinite Clay Equations

1. Initial Water Content and Compaction

The regression analysis is performed on 30 % Kaolinite Clay with different initial water content and compactions. In the experiments for Kaolinite clay, the compaction values ranged from 77 % to 89 % and the initial water content ranged from 13 % to 30 %. The effects of initial water content and compaction on the maximum depth of scour were isolated to determine the correlation of each one alone. Figure 5.78 shows the effect of compaction on maximum depth of scour. In this Figure, there are three vertical lines representing three ranges of compaction. From these vertical lines it is clear that for the same degree of compaction, there are a range of values of maximum depth of scour. From that it is concluded that for a mixture with 30 % clay content, the maximum depth of scour is not effected by the degree of compaction. Figure 5.79 shows

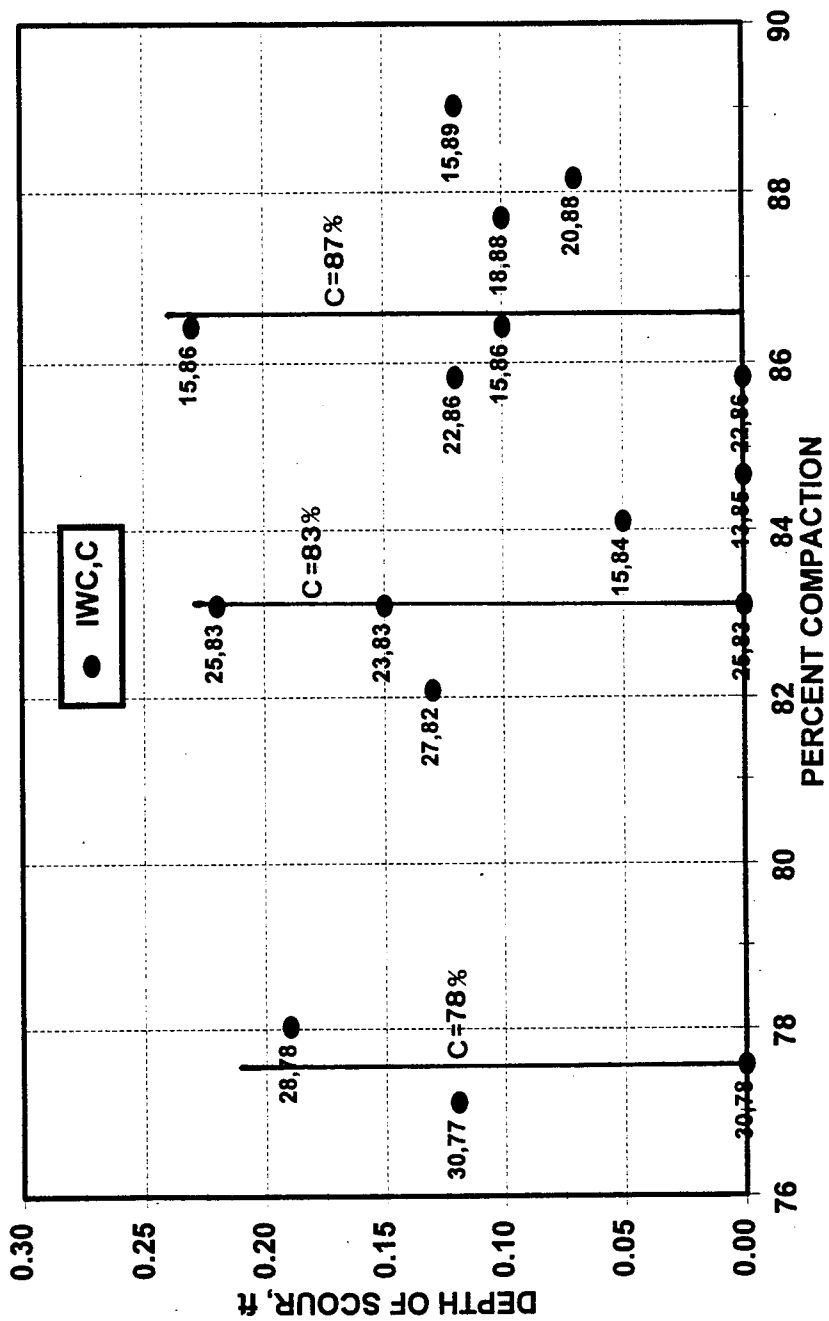


Figure (5.78) Effect of Compaction on Maximum Scour Depth for Kaolinite Clay.

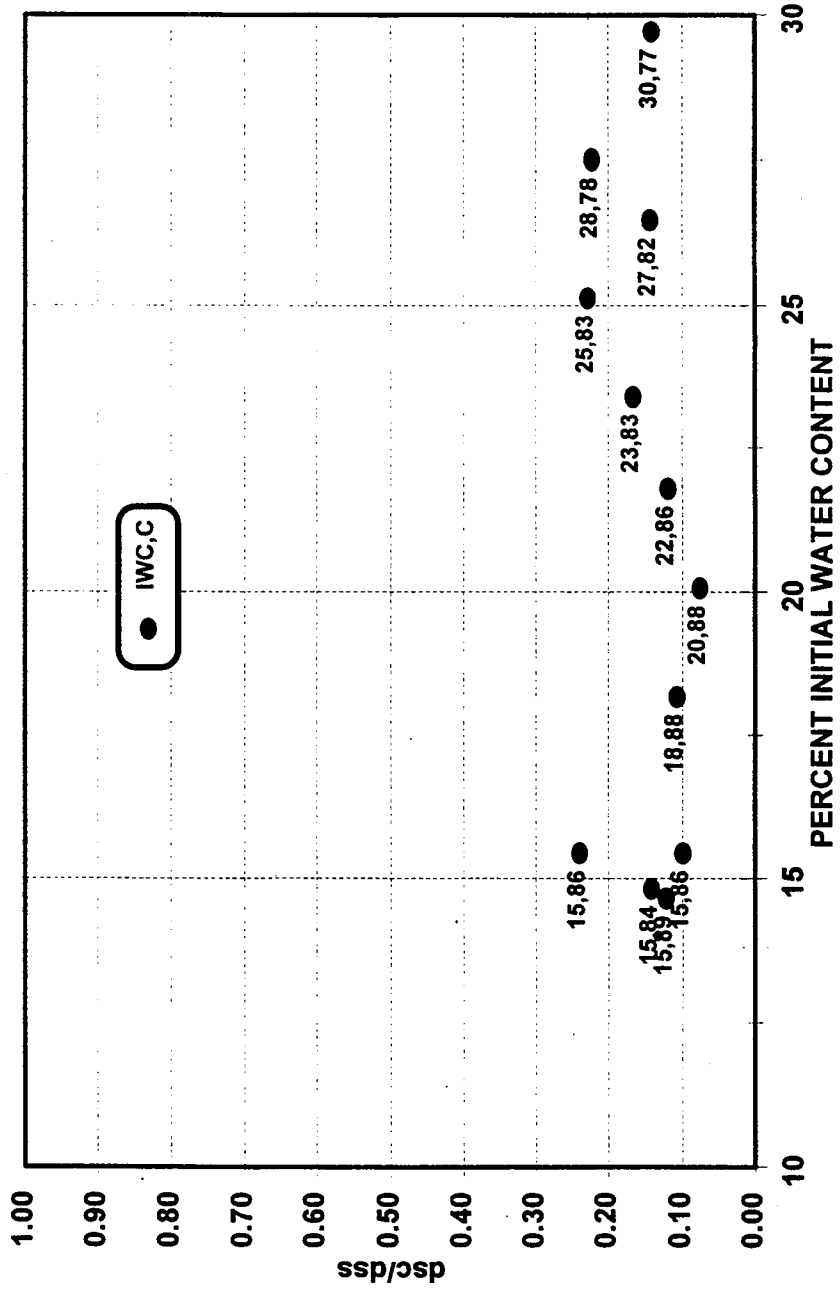


Figure (5.79) Effect of Initial Water Content on Normalized Scour Depth for Kaolinite Clay.

the effect of initial water content on normalized maximum depth of scour. For different percentages of initial water content, the normalized depth of scour varies in a narrow range from 0.09 to 0.23. This concludes that the effect of initial water content at the low clay content of 30 % is not applicable and should be considered only at higher percentages of clay content. However, the effect of Froude number on normalized maximum depth of scour still exists as shown in Figure 5.80 where normalized maximum depth of scour increases as the Froude number is increased. The relationship between normalized maximum depth of scour and Froude number is as follows ($R^2=68$ %):

$$d_{sc}/d_{ss} = 0.497 \cdot (Fr)^{2.46} \quad (5.11)$$

For higher clay contents, few experiments were conducted for 50 % Kaolinite clay content and there results are included in the analysis of clay content.

2. Clay Content Equation

The regression is performed on Kaolinite clay with different percentages of clay content varying from medium sand with 0 % clay up to 30 % clay. In this low clay content range, the percentage of sand in the soil mixture is high and makes the soil unable to retain water (no more than 10 %). The soil also does not respond to the compactive efforts. Therefore, in the prediction equation the initial water content and compaction will not be considered. Figure 5.64 is used to obtain the normalized depth of scour for different values of Froude number. These interpolated values is used in the final regression analysis and these values are shown in Table 5.18.

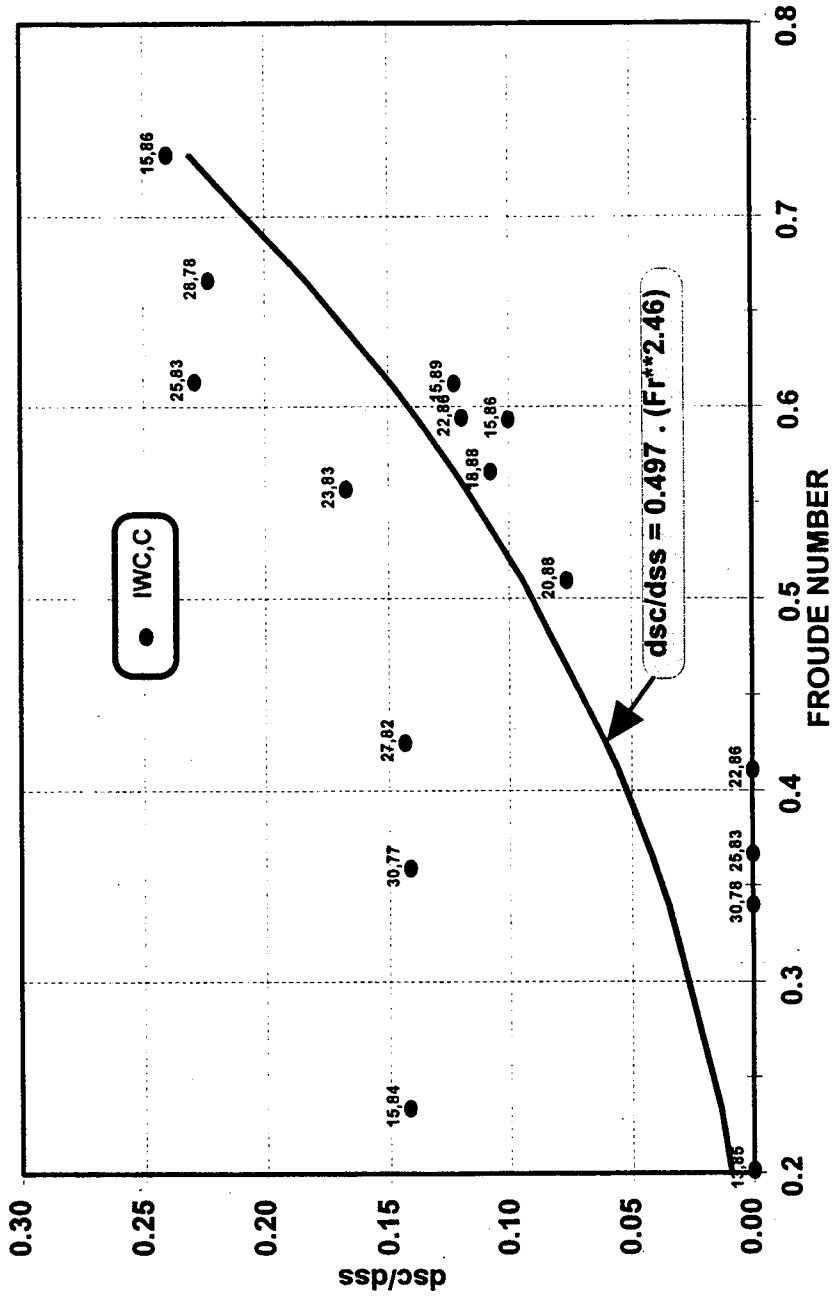


Figure (5.80) Variation of Normalized Scour Depth with Froude Number for Kaolinite Clay.

Table 5.18 Interpolated Values of Normalized Depth of Scour for different Percentages of Kaolinite Clay Content

Froude Number	Sand	5 % Clay	10 % Clay	15 % Clay	20 % Clay	25 % Clay	30 % Clay
0.45	1.00	0.99	0.94	0.81	0.49	0.19	0.09
0.40	1.00	0.99	0.90	0.68	0.31	0.14	0.09
0.30	1.00	0.98	0.89	0.61	0.20	0.10	0.09
0.20	1.00	0.95	0.71	0.43	0.16	0.05	0.00

From Table 5.18, the regression analysis between the normalized depth of scour and the percentage of clay content gives:

$$\frac{d_{sc}}{d_{sc}} = X_1 + (X_2 \cdot CC) + (X_3 \cdot CC^2) + (X_4 \cdot CC^3) \quad (5.12)$$

where

$$X_1 = 0.988;$$

$$X_2 = 2.788;$$

$$X_3 = -52.560;$$

$$X_4 = 110;$$

The non-linear least squares using the interpolated normalized scour depth resulted in the following summary statistics:

SOURCE	DF	SS	MS=SS/DF	R ²
REGRESSION	4	12.778	3.194	95.04
RESIDUAL	24	0.205	0.0085	
UNCORRECTED TOTAL	28	12.983		
CORRECTED TOTAL	27	4.078		

As seen from this table, there is a strong correlation between clay content and the normalized scour depth. Figure 5.81 shows the effect of the type of clay on the average normalized depth of scour. In this figure, as the percentage of clay content increases, the rate of scouring for Kaolinite clay gets faster than the rate of scouring for Montmorillonite clay.

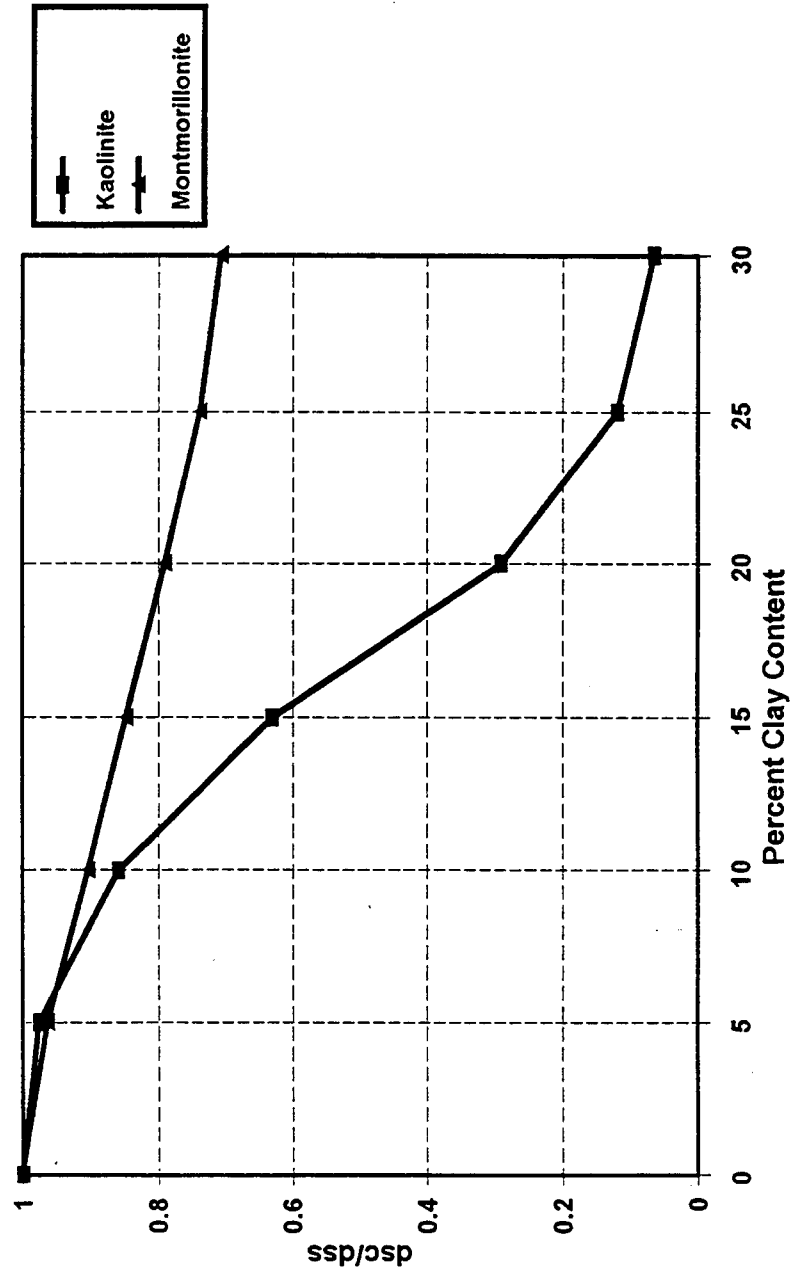


Figure (5.81) Effect of Clay Type on Normalized Scour Depth for Different Clay Contents.

CHAPTER 6

SUMMARY, CONCLUSIONS AND RECOMMENDATIONS

6.1 Summary

The main objective of this study is to investigate the effect of initial water content, clay content, and compaction for two types of clay, Montmorillonite and Kaolinite, on local abutment scour depth. Also, to study the effects of the initial water content, compaction, and clay content on the cross-sectional profile, the side slope, the longitudinal slope, and time rate of scour of the scour holes. To accomplish that, a series of experiments were conducted in the hydraulics laboratory flumes where most of the runs were in the clear water scour range. Several sets of experiments were conducted to cover all variables of cohesive materials one variable at a time.

In the first set, Montmorillonite clay was used with the same compaction range and changing initial water content to 15 %, 20 %, 28 %, 35 %, and 45 %.

In the second set, Montmorillonite clay were mixed with medium sand by the ratios of 0 %, 15 %, 30 %, and 40 % and with the same range of initial water content.

In the third set, Montmorillonite clay was used with the same range of initial water content and setting the mixture to low and high compaction.

In the fourth set, using a mixture of 30 % pure Kaolinite clay and 70 % medium sand and varying the initial water content to 15 %, 20 %, 25 %, and 30 % with the same

range of compaction.

In the fifth set, the Kaolinite clay were mixed with medium sand with the same range of initial water content and compaction. The Kaolinite clay ratios in the mixture were 10 %, 20 %, 30 %, and 50 %.

The analysis of all the data from the experiments were presented to discuss the changing effect of cohesive soil parameters on maximum depth of scour and the geometry of the scour hole. Also to study the slope angle of the scour hole and time rate of scour. The experimental data were used to develop equations that will help to predict maximum depth of scour based on initial water content, clay content and compaction for a different types of clay.

6.2 CONCLUSIONS

In this study, abutment scour experiments were conducted on two types of cohesion bed materials, Montmorillonite and Kaolinite clays, to investigate the effect of initial water content, clay content, and compaction on the abutment scour geometry for different flow conditions. The conclusions drawn from the previous analysis chapter are as follows:

1. For Montmorillonite clay with a given initial water content, the higher the compaction of the mixture, the less the scour depth will be.
2. For Montmorillonite clay with the same compaction, the mixture with 20 % initial water content will give less scour than the mixture with 12 % initial water content.
3. For Montmorillonite clay with the same range of mixture compaction, the scour depth

decreases as the initial water content increases from 12 % to 28 %. By increasing the initial water content from 28 % to 45 %, the depth of scour increases again.

4. For Montmorillonite clay, as the percentage of clay increases from 0 % to 30 % in the mixture, the scour depth decreases. By increasing the clay content from 30 % to 40 %, the scour depth stays almost the same. This is due to the influence of other parameters such as initial water content and compaction on the clay mixture beyond 30 % clay content.

5. In comparing compaction with Torvane shear strength in the case of Montmorillonite clay, Figure 5.48 shows three different curves depending on the initial water content. The first curve is for initial water contents of 12 % and 20 % where the Torvane shear increases as the compaction increases which is the case for unsaturated clay. The second curve is for the initial water contents of 28 % and 35 % where the Torvane shear increases as the compaction increases but changes very little. Finally, the third curve is for 45 % initial water content where there is no change in Torvane shear value and it is very small due to the high percentage of initial water content. The initial water contents from 28 % to 45 % are in the range of saturated clay and the measured values are too small to be used as an indicator of maximum depth of scour.

6. Also, in some experiments of Montmorillonite clay, at high initial water content of 28 %, the torvane shear strength was almost zero and the clay was erosion resistant at high Froude number which is another indication of the unreliability of Torvane shear test.

7. For both Montmorillonite and Kaolinite clays, with the change of any variable, the

maximum depth of scour increases as the Froude number is increased.

8. The scour holes takes the shape of partial inverted cones and the maximum depth of scour is located around the upstream corner of the abutment. The longitudinal slope angle is higher in the upstream direction than the downstream direction. The slope angle flatten out near the downstream end of the abutment.

9. The longitudinal slope in Montmorillonite clay follows the same trend of maximum depth of scour, where for both upstream and downstream directions, as the initial water content increases from 12 % to 28 %, the slope decreases and then increases again as the initial water content is increased from 28 % to 45 %. For compaction, as the compaction increases, the longitudinal slope angle is decreased. As the clay content in the mixture increases from 0 % to 15 %, the slope shows no change. By increasing the clay content from 15 % to 30 %, the slope is decreased. The slope shows little change by increasing clay content from 30 % to 40 % and this is due to the influence of other cohesion parameters such as initial water content and compaction. It is noticed also that the slope angles for the upstream direction are 1.5 to 2 times the downstream slope angles.

10. For time rate of scour, K value is used to determine the rate of scouring where as K increases, the time needed to reach equilibrium conditions is decreased. The K value gets higher as the initial water content increases from 12 % to 28 % and at 28 % initial water content, time to reach equilibrium is maximum (no scour case). Increasing the initial water content further from 28 % to 45 % decreases the time needed to reach equilibrium. The clay with lower compaction reaches equilibrium condition in less time

than the clay with higher compaction. The time needed to reach equilibrium condition decreases as the percentage of clay content is increased in the mixture.

11. For Kaolinite clay with the same range of mixture compaction and 30 % clay content, the normalized depth of scour shows little change as the initial water content is increased from 15 % to 30 %.

12. For Kaolinite clay, as the percentage of clay increases from 0 % to 30 % in the mixture, the scour depth is decreased. By increasing the percentage of clay from 30 % to 50 %, the scour depth is increased again. This is due to the influence of other cohesion parameters such as initial water content and compaction on clay mixtures beyond 30 % clay content.

13. For Kaolinite clay, both upstream and downstream directions, as the initial water content increases from 15 % to 20 %, the longitudinal slope increases. But by increasing the initial water content from 20 % to 30 %, the slope stays almost the same. Increasing the clay content from 0 % to 50 %, the slope is increased slightly in the upstream direction. It is noticed also that the slope angles for the upstream direction are 1.5 to 2 times the downstream slope angles.

14. For Kaolinite clay, as the initial water content increases, the scour hole reaches equilibrium much faster. As the clay contents increases from 0 % to 30 %, the K value decreases and the time needed to reach equilibrium condition increases. By increasing the clay content from 30 % to 50 %, the K value increases and it takes less time to reach the equilibrium condition.

15. In comparing compaction with torvane shear strength in the case of Kaolinite clay,

Figure 5.75 shows more than one torvane shear strength value for the same compaction which will result in the prediction of more than one scour depth for the same torvane shear strength and that makes torvane shear strength an unreliable indicator for predicting the scour depth.

16. It is noticed that Montmorillonite clay have similar behavior to Kaolinite clay in terms of percentage of clay content where in both clays, as the clay content increases from 0 % to 30 %, maximum scour depth is decreased for both clays. Beyond 30 %, the scour depth gets influenced by other cohesion parameters such as initial water content and compaction.

17. Montmorillonite clay prediction Equations 5.8 and 5.9 show that the initial water content, clay content and compaction are the most dominant factors in determining maximum depth of scour. In the saturated range, compaction is the most important parameters in determining the scour depth. while for saturated range, initial water content is more important than compaction. In Equation 5.10, percentage of clay content is the only recognized parameter for clay mixtures with less than 30 % clay content.

18. Kaolinite clay prediction Equation 5.12 show that the clay content is the dominant parameter in determining maximum depth of scour for clay mixtures with less than 30 % clay content. Because of the low percentage of clay content in the clay mixtures, initial water content and compaction did not have recognized effects on the scour depth.

19. These experiments were performed under laboratory conditions and for short term runs only (up to 16 hours) and the resulting curves and conclusions were based on that.

20. In the bridge site, the long term effects on the abutment scour such as freeze and

thaw, climatic changes, and dry and wet cycles are different than the controlled conditions and relatively short period of the experiments conducted in the laboratory for this study. These conditions could increase the depth of maximum scour over a long period of time. Also, this will change the behavior of time rate of scour where there will be a continuous increase of scour depth with a very slow time rate of scour over a long period of time which is in contrast to the present study which indicates reaching maximum depth of scour in relatively short period of time and stop scouring after that.

6.3 Recommendations for Future Research

On the basis of the results of this investigation, the following future researches is recommended:

1. The study should be extended to a wider variate of clay types such as Illite, Vermiculite, and Smectite.
2. A more reliable field data collection methods should be established to collect data from the bridge abutment sites to have more understanding of the effect of cohesion parameters on scour geometry compared to the collected data from the laboratory.
3. Higher percentages of clay content should be used to investigate the effect of initial water content and compaction for Kaolinite clay mixtures. This is because up to 30 % clay content, there was no apparent effect of initial water content and compaction on scour depth for both Montmorillonite and Kaolinite clays.
4. Analytical and numerical models to predict the Abutment local scour should be explored in conjunction with the data collected from the physical experiments to provide

more reliable numerical models.

5. Effect of clay layering with other types of soils such as sand, gravel, and silt should be investigated to study the layering effect on scour depth.
6. Comparison of laboratory data collected from this study with prototype size experiments should be conducted for both Montmorillonite and Kaolinite clays to study the scale effect on the resulting scour depth.
7. Investigate other clay parameters that might have an effect on scour depth such as SAR, salt concentration, and Atterberg limits.
8. Effect of abutment shapes on clay scour depth should be investigated.
9. Abrasive effects of sediment carried by the approach flows should be investigated.
10. Effect of viscosity on scour depth due to sediment concentration should be studied.

References

- Abt, S. R. and Ruff, J. F., 1982. Estimating Culvert Scour in Cohesive Material. *Journal of Hydraulics Division, ASCE*, Vol. 108, No. HY1, pp. 25-34.
- Alizadeh, A., 1974. Amount and Type of Clay and Pore Fluid Influences on the Critical Shear Stress and Swelling of Cohesive Soils. Ph.D. Dissertation, University of California, Davis.
- Ariathurai, R. and Arulanandan, K., 1978. Erosion Rates of Cohesive Soils. *Journal of the Hydraulics Division, ASCE*, Vol. 104, No. HY2, pp. 279-283.
- Arulanandan, K. 1975. Fundamental Aspects of Erosion of Cohesive Soils. *Journal of the Hydraulics Division, ASCE*, Vol. 101, No. HY5, pp. 635-639.
- Arulanandan, k., Gillogley, E., and Tully, R., 1980. Development of a Quantitative Method to Predict Critical Shear Stress and Rate of Erosion of Natural Undisturbed Cohesive Soils. Technical Report No. GL-80-5, U.S. Army Engineer Waterways Experiment Station, Vicksburg, Miss.
- Arulanandan, K., Loganathan, P., and Krone, R., 1975. Pore and Eroding Fluid Influences on Surface Erosion of Soil. *Journal of the Geotechnical Engineering Division, ASCE*, Vol. 101, No. GT1, pp. 51-65.
- Arulanandan, K., Sargunam, A., Loganathan, P., and Krone, R. B., 1973. Application of Chemical and Electrical Parameters to Prediction of Erodability. *Soil Erosion: Causes and Mechanisms; Prevention and Control. Special Report 135, Highway Research Board, National Research Council*, pp. 42-51.
- Barden, L. and G. R. Sides, 1970. Engineering Behavior and Structure of Compacted Clay. *Journal of the Soil Mechanics and Foundation Engineering Division, ASCE*, Vol. 96, No. SM4, pp. 1171-1200.
- Bowles, J. E., 1978. *Engineering Properties of Soils and Their Measurements*. 2nd edition, McGraw-Hill Book Company, New York.
- Chow, V. T., 1959. *Open-Channel Hydraulics*. McGraw-Hill, New York.
- Chapman, D. L. 1913. A contribution to the theory of electrocapillarity, *Philosophical Magazine*, Vol. 25, No. 6, pp. 475-481.

- Christensen, R. W. and B. M. Das (1973). Hydraulic Erosion of remolded Cohesive Soils, in *Soil Erosion: Causes and Mechanisms, Prevention and control*, Special Report No. 135. Highway Research Board, National Research Council, Washington, D.C., pp. 819.
- Cody R. P. and Smith J. K., 1987. *Applied Statistics and the SAS Programming Language*. North Holland.
- Collis, Goerge, N. and Smiles, D. E., 1963. An Examination of Cation Balance and Moisture Characteristic methods of Determining the Stability of Soil Aggregate. *Journal of Soil Science*, Vol. 14, p. 21.
- Dane, J. H. and Klute, A., 1977. Salt Effects on the Hydraulic Properties of a Swelling Soil. *Soil Science Society of America Journal*, Vol. 41, No. 6, pp. 1043-1049.
- Dunn, I. S., 1959. Tractive Resistance of Cohesive Channels. *Journal of the Soil Mechanics and foundation Engineering Division, ASCE*, Vol. 85, No. SM3, pp. 1-24.
- Froehlich, D.C., 1989, "Abutment Scour Prediction," Paper Presented at 68th TRB Annual Meeting, Washington, D.C.
- Gill, M.A., 1972, "Erosion of Sand Beds Around Spur Dikes," *Journal of Hydraulic Division, ASCE*, Vol. 98, No HY9, September, pp 1587-1602.
- Gouy, G. 1910. Sur la constitution de la charge electrique a la surface d'un electrolyte, *Annieue Physique (Paris)*, Serie 4, Vol. 9, pp. 457-468.
- Grim, R. E., 1962. *Applied Clay Mineralogy*. McGraw-Hill, New York.
- Grim, R. E., 1968. *Clay Mineralogy*, 2nd edition, McGraw-Hill, New York.
- Grissinger, E. G., 1966. Resistance of Selected Clay Systems of Erosion by Water. *Water Resources Research*, Vol. 2, No. 1, pp. 130-138.
- Heizen, R. T. and Arulanandan, K., 1977. Factors Influencing Dispersive Clays and Method of Identification. *Dispersive Clays, Related Piping, and Erosion in Geotechnical Projects*, ASTM STP623, J. L. Sherard and R. S. Decker, Eds., ASTM, pp. 202-217.
- Hodek, R. J. and Lovell, C. W., 1979. Soil Aggregates and Their Influence on Soil Compaction and Swelling. *Transportation Research Record 733*, National Research Council, pp. 94-99.

- Holtz, R. D. and Kovacs, W. D., 1981. *An Introduction to Geotechnical Engineering*, Prentice-Hall.
- Kamphuis, J. W. and Hall, K. R., 1983. *Cohesive Material Erosion by Unidirectional Current*. *Journal of Hydraulic Engineering*, ASCE, Vol. 109, No. 1, pp. 49-61.
- Kandiah, A., 1974. *Fundamental Aspects of Surface Erosion of Cohesive Soils*. Ph.D. Dissertation, University of California, Davis.
- Kandiah, A. and Arulanandan, K., 1974. *Hydraulic Erosion of Cohesive Soils*. *Transportation Research Record 497*, National Research Council, pp. 60-68.
- Kelly, W. E. and Gularte, R. C., 1981. *Erosion Resistance of Cohesive Soils*. *Journal of the Hydraulics Division*, ASCE, Vol. 107, No. HY10, pp. 1211-1224.
- Kwan, T. F., 1988. *A study of Abutment Scour*. Report No. 451, School of Engineering, University of Auckland, Auckland, New Zealand.
- Lambe, T. W., 1958. *The Structure of compacted Clay*. *Journal of the Soil Mechanics and Foundation Engineering Division*, ASCE, Vol. 84, No. SM2, pp. 682-706.
- Lambe, T. W., and Whitman, R. V., 1969. *Soil Mechanics*. John Wiley & Sons, Inc., New York.
- Laursen, E.M., 1980, General Report No. 3, "Predicting Scour At Bridge Piers and Abutments: A Study to Advance The Methodology of Assessing The Vulnerability of Bridges To Floods," Arizona Department of Transportation.
- Lewis, D. A. and Schmidt, N. O., 1977. *Erosion of Unsaturated Clay in a Pinhole Test, Dispersive Clays, Related Piping, and Erosion in Geotechnical Projects*, ASTM STP623, J. L. Sherard and R. S. Decker, Eds., ASTM, pp. 260-273.
- Liou, Y. D., 1970. *Hydraulic Erodability of Two Pure Clay Systems*. Ph.D. Dissertation, Colorado State University, Fort Collins, Colorado.
- Liu, M.K., F.M. Chang and M.M. Skinner, 1961, "Effect Of Bridge Construction On Scour and Backwater," Department of Civil Engineering, Colorado State University, Report No. CER60-HKL22, February.
- Marshall, C.E., 1964. *The Physical Chemistry and Mineralogy of Soils*. Vol. 1 - *Soil Materials*. Wiley, New York.
- McNeal, B. L., Norvell, W. A., and Coleman, N. T., 1966. *Effect of Solution Composition on the Swelling of extracted Soil Clays*. Soil Science Society of America,

Proceedings, Vol. 30, pp.313-317.

Mitchell, J. K., 1993. *Fundamentals of Soil Behavior*. John Wiley & Sons, Inc., New York.

Mitchell, J. K., Campanella, R. G., and Singh, A., 1968. Soil Creep as a Rate Process. *Journal of the Soil Mechanics and Foundation Engineering Division, ASCE*, Vol. 94, No. SM1, pp. 231-253.

Mitchell, J. K., Singh, A., and Campanella, R. G.. 1969. Bonding, Effective stresses, and Strength of Soils. *Journal of the Soil Mechanics and Foundation Engineering Division, ASCE*, Vol. 95, No. SM5, pp. 1219-1246.

Paaswell, R. E., 1973. Causes and Mechanisms of Cohesive Soil Erosion: The State of the Art. Special Report 135, Highway Research Board, National Research Council, pp. 52-74.

Parchure, T. M. and Mehta, A. J., 1985. Erosion of Soft Cohesive Sediment Deposits. *Journal of Hydraulic Engineering, ASCE*, Vol. 111, No. 10, pp. 1308-1326.

Partheniades, E., 1971. Erosion and Deposition of cohesive Materials. *River Mechanics*, Vol. II, Chapter 25. H. W. Shen, Editor.

Perry, E. B., 1975. Piping in Earth Dams Constructed of Dispersive Clay; Literature Review and Design of Laboratory Tests, Technical Report S-75-15 Soil and ~~Parent~~ Laboratory, U.S. Army Engineer Waterways Experimental Station, Vicksburg, Miss.

Preston, J. H., 1954. The Determination of Turbulent skin Friction by Means of Pilot Tubes. *Journal of the Royal Aeronautical Society*, Vol. 58, pp. 109-121.

Raudkivi, A. J., 1976. *Loose Boundary Hydraulics*, 2nd Edition, Pergamon Press.

Raudkivi, A. J. and Hutchison, D. L., 1974. Erosion of Kaolinite Clay by Flowing Water. *Proc. Royal Society London, Series A*, No. 337, pp. 537-554.

Raudkivi, A. J. and Tan, S. K., 1984. Erosion of Cohesive Soils. *Journal of Hydraulic Research, International Association for Hydraulic Research*, Vol. 22, No. 4, pp. 217-233.

Raussell-Colom, J. A., and Serratos, J. M. 1987. Reactions of clays with organic substances, Chap. 8. In: A. C. D. Newman (Ed.), *Chemistry of Clays and Clay Minerals*, Mineralogical Society Monograph No. 6, London, pp. 371-422.

Rowell, D. L., 1963. Effect of Electrolyte Concentration on the Swelling of Orientated

Aggregates of Montmorillonite. *Soil Science*, Vol. 96, pp. 368.

Sargunam, A., 1977. Concept of Critical Shear Stress in Relation to Characterization of dispersive Clays. *Dispersive Clays, Related Piping, and erosion in Geotechnical Projects*, ASTM STP623, J. I. Sherard and R. s. Decker, Eds., ASTM, pp. 390-397.

Sargunam, A., Riley, P., Arulanandan, K., and Krone, R. B., 1973. Physico-Chemical Factors in Erosion of Cohesive soils. *Journal of The Hydraulics Division, ASCE*, Vol. 99, No. Hy3, Proc. Paper 9609, Mar., pp. 555-558.

Schmehl, W. R., 1983. Ag 467 Class Notes, Department of Agronomy, Colorado State University, Fort Collins, Colorado.

Seed, H. B. and Chan, C. K., 1961. Compacted Clays: Structure and Strength Characteristics. *Transaction, ASCE*, Vol. 126, Paper No. 3426, pp. 1343-1425/

Shaikh, A., 1986. Surface Erosion of Compacted Clays. Ph.D. Dissertation, Colorado State University.

Sherard, J. L., 1975. Discussion of Paper "Pore and Eroding Fluid Influences on Surface Erosion of Soils." *Journal of the Geotechnical Engineering Division, ASCE*, Vol. 101, No. GT12, Dec., pp. 1299-1300.

Sherard, J. L. and Decker, R. S., editors, 1977. *Dispersive Clays, Related Piping, and Erosion in Geotechnical Projects*. American Society for Testing and Minerals.

Sherard, J. L., Decker, R. S., and Ryker, N. L., 1972. Piping in Earth Dams of Dispersive Clay. *Proceedings of the ASCE Specialty Conference on the Performance of Earth and Earth-supported Structures*, Vol. 1, Purdue University, Lafayette, Indiana, pp. 589-626.

Sherard, J. L., Dunning, L. p., Decker, R. S., and Steele, E. F., 1976a. Pinhole Test for Identifying Dispersive soils. *Journal of the Geotechnical Engineering Division, ASCE*, Vol. 102, No. GT1, pp. 69-85.

Sherard, J. L., Dunnigan, L. P., and Decker, R. S., 1976b. Identification and Nature of Dispersive Soils. *Journal of the Geotechnical Engineering Division, ASCE*, Vol. 102, No. GT4, pp. 287-301.

Simons, D. B. and Senturk, F., 1993. *Sediment Transport Technology*. Water Resources Publications, Fort Collins, Colorado.

Smerdon, E. T. and Beasley, R. P., 1961. Critical Tractive Force in Cohesive Soils. *Agricultural Engineering*, Vol. 42, pp. 26-29.

Sowers, G. F., 1979. *Introductory Soil Mechanics and Foundations: Geotechnical Engineering*, 4th edition, Macmillan Publishing Co., Inc., New York.

Sposito, G. 1989, The diffuse ion swarm near smectite particles suspended in 1:1 electrolyte solutions, *Clays and Clay Minerals*, Special Lecture, Volume No.4.

Terzaghi, K. and Peck, R. B., 1971. *Soil Mechanics in Engineering Practice*, 2nd Edition, John Wiley and Sons, Inc., New York.

Van Olphen, H., 1963. *An Introduction to Clay Colloid Chemistry*. Wiley Interscience, New York.

Verwey, E. J. W., and Overbeek, J. Th. G., 1948. *Theory of the Stability of Lyophobic Colloids*. Elsevier, Amsterdam, New York, London.

WinterKorn, H. F., 1973. *Experimental Study of the Attack of Water on Dry Cohesive Soil Systems. Soil Erosion: Causes and Mechanisms; Prevention and Control*, Special Report 135, Highway Research Board, National Research Council, pp. 1-7. Laursen E. M., "Observations on the Nature of Scour". *Proceedings of the fifth Hydraulic conference*, June 9-11, 1952.

